Validation et application de biomarqueurs lipidiques pour la reconstruction des changements environnementaux en Afrique de l'Est

Sarah Coffinet

Université Pierre et Marie Curie

Ecole doctorale Sciences de l'Environnement d'Ile-de-France

UMR 7619 METIS, Département de biogéochimie

Validation and application of lipid biomarkers to reconstruct past environmental changes in East Africa

Validation et application de biomarqueurs lipidiques pour la reconstruction des changements environnementaux en Afrique de l'Est

Par Sarah Coffinet

Thèse de doctorat de géochimie organique

Dirigée par Sylvie Derenne et Arnaud Huguet

Soutenue le 08 octobre 2015

Devant un jury composé de :

M. Vincent GROSSI	Directeur de Recherche CNRS	rapporteur
M. Rich D. PANCOST	Professeur	rapporteur
M. Jérémy JACOB	Chargé de Recherche CNRS	examinateur
M. André-Jean FRANCEZ	Maître de Conférence	examinateur
M. François BAUDIN	Professeur	examinateur
M. Amos E. MAJULE	Professeur	invité
Mme Sylvie DERENNE	Directeur de Recherche CNRS	directrice de thèse
M . Arnaud HUGUET	Chargé de Recherche CNRS	co-encadrant de thèse

A mes parents

A Arthur

A mes amis

Vous êtes ma force,

mon inspiration

Le but de la recherche de méthode n'est pas de trouver un principe unitaire de toute connaissance, mais d'indiquer les émergences d'une pensée complexe, qui ne se réduit ni à la science, ni à la philosophie, mais qui permet leur intercommunication en opérant des boucles dialogiques.

Edgar Morin, Science avec conscience (1982)

Remerciements

Je souhaite tout d'abord remercier (I would first like to thank) Vincent Grossi et Rich Pancost d'avoir accepté de rapporter ce travail de thèse, ainsi que Jean-Marie Mouchel, directeur de l'UMR Metis de m'avoir accueilli dans ses locaux. Je remercie également Hélène Budzinski et Alain Saliot d'avoir participé à mes comités de pilotage.

J'adresse ensuite mes profonds et sincères remerciements à mes deux encadrants de thèse, Arnaud Huguet et Sylvie Derenne. Je vous remercie pour votre patience, votre présence, votre soutien, votre confiance et pour toutes les opportunités que vous m'avez offertes. C'est une chance d'avoir pu travailler avec vous.

Au cours de cette thèse, j'ai eu la chance de collaborer avec de nombreux collègues et d'être accueillie dans plusieurs laboratoires, toujours très chaleureusement.

Je remercie donc les collègues de l'ISTO à Orléans pour leur accueil, et je citerai notamment Marielle Hatton pour son aide dans la préparation des échantillons et tout particulièrement Fatima Laggoun qui a suivi cette thèse dès les premiers mois et qui a toujours été de bon conseil.

I also thank our colleagues from the University of Krakow, Mariusz Gałka, Piotr and Monika Kołaczek for their collaboration on the Kyambangunguru project.

Je remercie également Hervé Rybarczyk de m'avoir introduit au monde des statistiques et à la joie du codage avec R !

I warmly thank Nikolai Pedentchouk for his collaboration. It was a great pleasure to work with you, and I have learnt so much! I also thank the Geosciences group at the Newcastle University, especially Tom Wagner for his kind welcome and Paul and Bernie for their technical assistance. Thanks to Charlotte, Darcy and Kate for the (night) tours in Newcastle! I am very glad to have been hosted by Dawn Dunn and will remember our late discussions! I have rarely been so well welcomed; so thank you all to have made my stay at Newcastle unforgettable.

Je remercie David Williamson de m'avoir donné l'opportunité de participer à une campagne de terrain à Masoko. Je le remercie aussi, ainsi que Laurent Bergonzini, pour tout ce qu'ils m'ont appris, et tout ce qu'ils leur restent à m'apprendre, en science comme ailleurs ! I have a special thought to my two field partners: Winne et Matokeo. Thanks for helping me in the field and thanks for all the culture sharing ☺. I also thank everyone at Masoko, for being so nice and helpful during my stay there. Thank you to Amos Majule and to the Institute of Resource Assessment (IRA) at Dar Es Salaam to have welcomed me in Tanzania.

Qu'aurait été ma thèse sans mes collègues … très fade sans aucun doute ! C'est pourquoi je pense aujourd'hui très fort à vous tous, stagiaires, doctorants, post-doctorants, permanents ou non permanents. J'ai passé de très bons moments avec vous et je vous souhaite à tous le meilleur. Je remercie aussi tous les stagiaires qui m'ont aidée, de près ou de loin, à préparer les échantillons nécessaires à cette thèse (ah que de colonnes …. !) : Manon, Fanny, Camille, Clara et tout particulièrement Michaël.

Merci à Charlotte Tardieu pour son aide dans la mise en forme (quelle que soit l'heure !) et à Patrick Coyac pour son (toujours) joli coup de crayon.

Pour finir, je voudrais adresser un remerciement particulier à Alain Saliot et à Kamal Boubekeur qui m'ont orientée et encouragée vers la recherche tout au long de mon cursus universitaire, ainsi qu'à Stéphane Bouchonnet qui m'a fait découvrir (et apprécier !) le monde de la spectrométrie de masse !

Contents

Introduction

As soon as societies have emerged, the understanding of climatic variations has been a key issue for the upholding and the prosperity of civilizations. The ability to predict climatic variability is essential to plan agricultural work but also to predict natural hazards. In the 20th century, the humankind realized that it was not only subjected to climatic variations but that it was also taking part in its variability. Since the emergence of the industrial era (19th century), the temperature rose by 0.85 °C as a result of increased greenhouse gas emissions. The consequences of this global warming will be devastating if no action is taken to reduce these emissions. This thesis happens at a critical time as in December 2015, the 21st Conference of Parties (COP21) will take place in Paris (France). This conference is one of the last chances for international political leaders to have the courage to take a constraining commitment on greenhouse gas emission limitations to avoid worldwide thermal runaway.

Global warming has been evidenced and monitored by an international consortium of scientists, the IPCC (Intergovernmental Panel on Climate Change). These researchers based their conclusions on observations and predictions of a wide range of environmental parameters. However, since the measurements of these parameters are only available for the 20th century, geological records have to be investigated to better understand past climatic changes. This is critical to refine model predictions of future climate changes. The first paleoclimatic reconstructions were made in ice and marine sediment cores, leading to a better understanding of the high contribution of the oceanic circulation in the global climate regulation. Today, the aim is to assess the climatic variability over the continents. This requires the development of adequate tools to reconstruct past environmental changes from continental archives which are more heterogeneous than marine ones.

The aim of this thesis is to validate the applicability of two families of lipid biomarkers, the glycerol dialkyl glycerol tetraethers (GDGTs) and mid and long chain *n*-alkanes (C_{23} – C_{31}), in a specific continental area: The Rungwe Volcanic Province (RVP) in the southwest of Tanzania. GDGTs are membrane spanning lipids produced by Archaea and some unidentified Bacteria while mid and long chain *n*-alkanes are major constituents of the epicuticular layer of vegetation external organs, especially their leaves. They are ubiquitous and were detected in numerous environmental settings, from marine sediments to paleosol sequences.

The RVP was chosen because of the existence of several types of continental archives - crater lakes, peatlands and a topoclimosequence (2960 m altitude) - in a delimited area, submitted to

the same external parameters (in terms of climate, tectonics, landuse and human impact). Moreover the RVP belongs to a multidisciplinary research consortium called RESON (Rungwe Environmental Science Obseratory Network). The hydrology, (Bergonzini et al., 2001; Delalande, 2008), geology (Williamson et al., 2014, 1999, 1998) and biogeochemistry functioning of the area (de Mesmay, 2008) are well known. In addition, climate variations over the last 45000 yrs (Barker et al., 2000; Garcin et al., 2006; Thevenon et al., 2003; Vincens et al., 2003) were also investigated using lacustrine archives (Lake Masoko). The infrastructures and previous results obtained in the framework of the RESON will be especially useful to investigate the validity of GDGTs and *n*-alkanes as environmental proxies in the region.

This work benefited from the funding of the project "*Study of complex lipids (glycerol dialkyl glycerol tetraethers) and of their source microorganisms in lacustrine settings: case of Lake Masoko (Tanzania)"* (PI: A. Huguet) by the national program EC2CO (2012-2013) of the CNRS National Institute for Earth Sciences and Astronomy (INSU). Three field campaigns (April and December 2012, July 2014) were achieved in the framework of this projet, during which surface soils and leaves were collected along the topoclimosequence, as well as a 4 m peat core in the Kyambangunguru crater marsh. In addition, surficial sediment and suspended particulate matter samples were collected at three depths in the Lake Masoko water column. The abundance and distribution of GDGTs and *n*-alkanes were determined in this wide range of samples. The hydrogen isotopic composition of individual long chain *n*-alkanes (δ^2H_{wax}) was also measured in Newcastle-upon-Tyne (United Kingdom) thanks to an EAOG (European Association of Organic Geochemists) travel scholarship.

This manuscript is divided into six chapters. The first chapter reviews the current state of knowledge on (i) Late Holocene climate variations and on (ii) GDGT and *n*-alkane origins, variability and application to environmental reconstructions in continental archives. The second chapter presents the environmental context of the RVP and of the two crater wetlands investigated in this thesis: the Kyambangunguru crater marsh and Lake Masoko. The third chapter describes the materials and methods used in this study. The three remaining chapters compile the results obtained during this three-year project. Chapter four is dedicated to the applicability of GDGTs and δ^2H_{wax} as environmental proxies in soils. It presents methodological studies using elevation gradients as "full-scale" *in situ* experiments to observe the response of GDGTs and *n*-alkanes to temperature changes in recent surface soils. Chapter five presents the study of a marsh/peatland site located at the center of a former volcanic crater: the Kyambangunguru marsh. This chapter combines a methodological study exploring

potential biosynthetic intermediates of GDGTs and a multi-proxy approach, including GDGTs and *n*-alkanes, to reveal the ecosystem changes of the Kyambangunguru marsh over the last 4000 yrs. The last chapter focuses on Lake Masoko. The sources of GDGTs in this lake were determined by analysing these compounds in the water column, sediment and surrounding soils. Then, both GDGTs and *n*-alkanes were applied to the reconstruction of climate variations over the last 4000 yrs.

Chapter 1.

State of the Art: Biomarkers and paleoclimate in East Africa during the Late Holocene

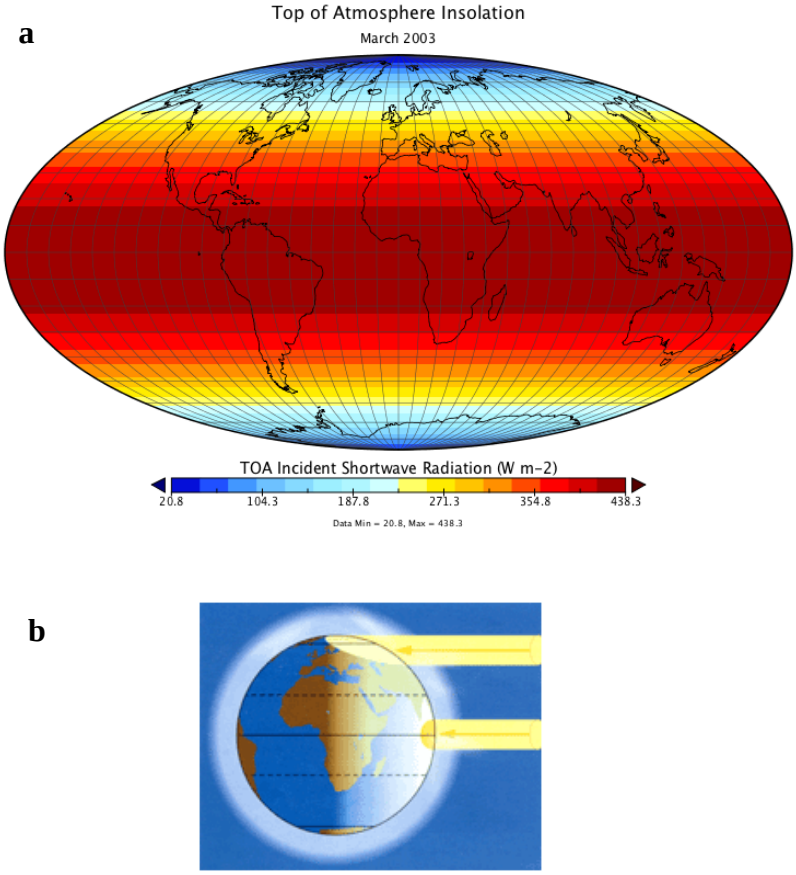

Figure 1: (a) World map of Atmosphere insolation showing the highest value at the equator (scale: fom 20.8 W/m² in blue to 438.3 W/m² in red). This is due to the Earth curvature as represented in (b). *Sources: Geosciences department of Penn State (2a) Amiens' regional education authority office (2b) websites*

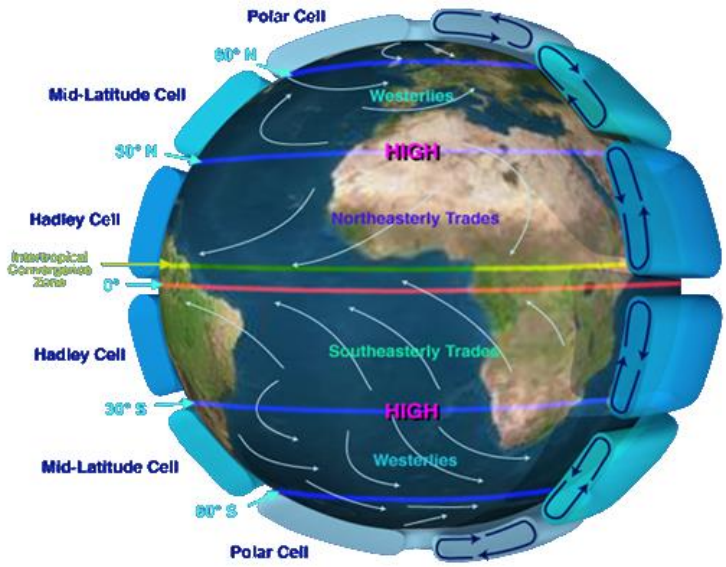

Figure 2: Meridional cells, ITCZ and main air currents responsible for part of the heat transportation from the equator to the poles. *Source: American university consortium for atmospheric research (UCAR) website*

1.1. General context

1.1.1 Late Holocene East African climate variations: why does it matter?

Tropical regions receive the highest degree of insolation from the Sun because of their location close to the equator and hence possess an excess in energy relative to the poles (Figure 1). As a result, coupled atmospheric and oceanic circulations create thermal gradients to compensate this disequilibrium and redistribute the energy from the tropics to the poles (Godard and Tabeaud, 2009). Atmospheric circulation is responsible for ca. 50% of this redistribution via the succession of meridional cells (Figure 2). In the tropics these cells are called the Hadley cells and correspond to the ascension of the hot air masses at the meteorological equator which is thus defined as a region of low air pressure, also called the intertropical convergence zone (ITCZ). These low pressures are compensated by surficial air fluxes (trade winds) converging from each hemisphere (Figure 2). When the trade winds pass above hot oceanic water masses they get saturated in water. As a result, the ascension of these hot water-saturated air masses above the continents is accompanied by high precipitation rates at these locations. On the other side of the Hadley cell, subsidence of the resulting dry air masses is notably responsible for the localization of deserts around the globe. Thus the position and the strength of the Hadley cells are highly important to understand the distribution of present and past climate at a global scale (McGregor and Nieuwolt, 1998).

Position of the ITCZ varied over geological times, principally because of orbital - induced changes in the location of maximum insolation which led to major climate perturbations (Gasse, 2000). It was notably the main driver of the Holocene climate variability at the millennial scale. The Holocene started ca. 11.7 kyr BP at the end of the last glacial event on Earth – the Younger Dryas (12.9 – 11.7 kyr BP; Figure 3) – and is characterized by a rapid warming and high amplitudes of tropical precipitations over the years (Mayewski et al., 2004). It can be divided into three temporal periods (Wanner et al., 2011): the early deglaciation phase (11.7 – 7 kyr BP), the Holocene Thermal Optimum (7 – 4.2 kyr BP) and the Neoglacial period (4.2 kyr BP to present). This last period has now ended due to the global warming induced by anthropogenic releases of greenhouse gases (IPCC, 2013). (Crutzen and Stoermer, 2000) proposed to define the

present epoch (since the latter part of the 18th century) as the "Anthropocene" to emphasize this increasing impact of human activities on the geobiosphere. In addition to gradual change towards weakening of the Northern Hemisphere monsoon (Braconnot et al., 2007), rapid and frequent temperature fluctuations were observed in numerous archives from the mid and late Holocene (Gasse, 2000; Wanner et al., 2011) of which the physical drivers are not yet well constrained. In tropical East Africa, these rapid changes appear sometimes out-of-phase from one site to another (Verschuren et al., 2000; Castañeda et al., 2009; Mills et al., 2014), highlighting the spatial complexity and heterogeneity of this area. These recent century-scale fluctuations are particularly interesting to study as they are more directly relevant to modern and future climate change. Moreover, in these areas, paleoclimatic reconstructions have long been hampered by two conjugated phenomena: (i) traditional hydrological proxies based on lake water budgets are additionally influenced by temperature changes, (ii) the temperature changes are poorly constrained because few proxies are sensitive enough to the typical moderate temperature variations experienced in the tropics (Verschuren et al., 2009).

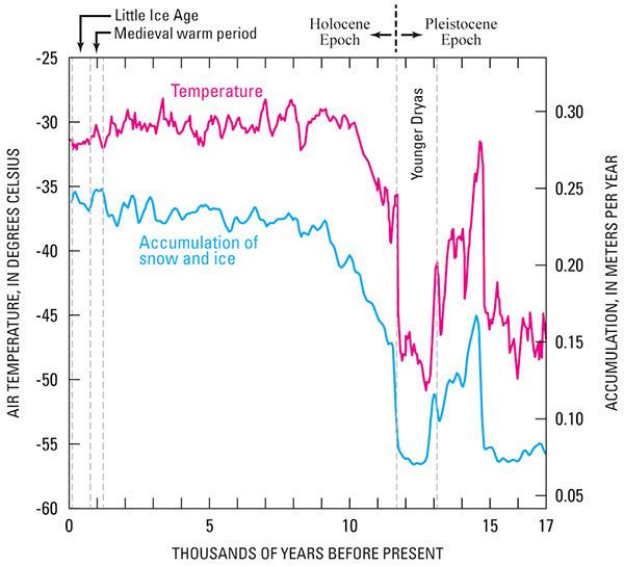

Figure 3: Temperature variations during the late Pleistocene Epoch and the Holocene Epoch, determined as proxy temperatures from ice cores extracted from the central part of the Greenland ice sheet. Modified from Alley (2000, p. 9, Fig. 12). *Source:* (Williams and Ferrigno, 2012).

Therefore, late Holocene climatic variations in East Africa need to be further investigated in order to (i) better distinguish regional (or even global) drivers (e.g. SST variations) from local ones (e.g. orographic effects), (ii) improve the mapping of local

climate responses in these sensitive areas and (iii) assess the impact of these various responses on global climate regulation.

1.1.2 The advantages and challenges of continental archives

Physical and biological indicators of climate variability were first investigated in ice cores and then in marine sediment cores collected during oceanographic cruises (Cortijo et al., 2013). Nevertheless, even though the oceans cover more than 71 % of the surface of the Earth, it is also crucial to examine continental archives to improve the spatial coverage of past climate records and to relate the climatic patterns observed over oceans. Continents comprise various and heterogeneous landscapes (mountains, valleys, lakes, forests, cities), making the atmospheric circulation and regional climates much more complex than over the oceans (Godard and Tabeaud, 2009). Below will be detailed three widespread types of continental archives: paleosols, peatlands and lakes. They correspond to the three archive types studied in this thesis.

Paleosols

Soil profiles can hardly be used as continental archives due to pedogenesis, which likely alter the signal recorded at the soil surface after burial. However, some terrestrial sites exhibit sequences of loess-paleosol (Figure 4), in which the initial climatic signal is preserved much more efficiently. A loess horizon is an aeolian sediment deposited over a soil surface and coming from adjacent deserts or previously frozen territories (after von Richthofen definition, Pécsi, 1990; Hatté and Rousseau, 2013). Deposition of such stratum occurs during arid and cold periods when winds are stronger. In contrast, when climate gets warmer and more humid, pedogenesis is favoured and a soil stratum develops above the loess sequence. This alternation carries *per se* a climatic signal. In addition, geochemical proxies can be analysed both in loess, with the same tool as in sediments, and in paleosols with adapted indicators (Hatté et al., 2001; Gocke et al., 2014).

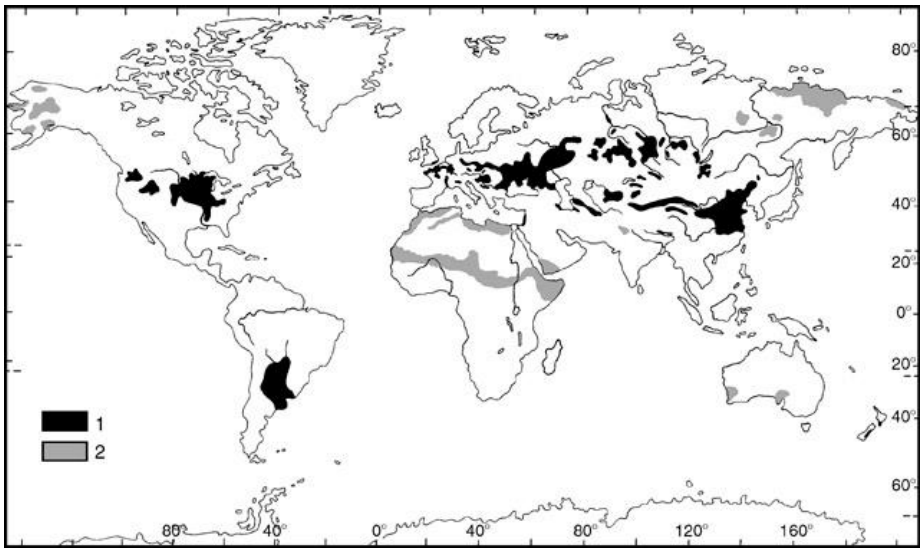

Figure 4: Distribution of loess and loess-like sediments. *1*: Loess and loess-like sediments; *2*: Loess derivates and loess-like sediments. *Source:* (Pécsi, 1990)

Peatlands

Peatlands are wetlands where the soil is saturated in water and are characterised by anoxic and acidic conditions, leading to reduced biological activity and accumulation of organic matter (Killops and Killops, 2005). The development of specific climate proxies is required in these environments with unique biodiversity and physicochemical conditions in comparison to soils and sediments. They are highly dynamic ecosystems and their vegetation and hydrology can be totally modified at a centennial-time scale (Loisel and Yu, 2013), which notably explains why they have not been extensively used as paleoclimate archives so far. A major challenge in using peat as climatic archive is to disentangle biological signals linked to peat dynamic changes in ecosystem from those linked to regional climate changes. Nevertheless, the chronological accumulation of organic matter, due to the growth of a new vegetation layer on the preceding one, confers to peatlands a high potential for past climate reconstructions, as confirmed by several studies (Blackford, 2000; Amesbury et al., 2012). The different proxies available for paleoreconstructions in peat were recently listed by Chambers et al. (2012) and include, for example, dendroclimatology, analysis of testate amoebae, molecular stratigraphy, bulk and compound-specific isotopic analysis.

Lakes

Among continental archives, lacustrine ones were extensively studied, as numerous proxies – notably those based on the distribution and composition of phytoplanctonic and micro-algal species – developed for marine environments are also applicable in

lakes based on the similarity of their formation (Castañeda and Schouten, 2011). Indeed, both lacustrine and marine sediments are formed by the accumulation of dead remains from the biosphere living in the water column. In lakes, this organic matter is mixed with inorganic (and to a lesser extent organic) material from the catchment area transported via surface runoff. Part of the material deposited in lakes may also come from aeolian transportation. Sediment deposition is a chronological process and its rate is usually high in lakes, so that paleoenvironmental reconstruction in lakes can encompass high-temporal resolution (Castañeda and Schouten, 2011). However, volcanic and tectonic activities and the presence of benthic microorganisms in sediments can disturb the linear accumulation of the latter. In the same way, during arid periods, tropical lacustrine sediments may be subjected to desiccation, thus disturbing their regular accumulation. Another difficulty for paleoenvironmental studies from lacustrine records is the determination of the sensitivity of each lake to small climatic variations. Climate-sensitive lakes are those where the water level fluctuations are principally regulated by climatic processes, *i.e.* precipitation and evaporation rates (Figure 5). Such lakes include (i) those where the only output is evaporation, (ii) those where surface and subsurface outflow (Qos and QosubS in Figure 5) is negligible when compared to evaporation output and (iii) amplifier ones where lake level variability is controlled by river inflow (Qis in Figure 5), itself governed by climate changes. Crater lakes, such as the one studied in this thesis, often display these characteristics and are thus ideal for paleoclimatic reconstructions. (Verschuren, 2003).

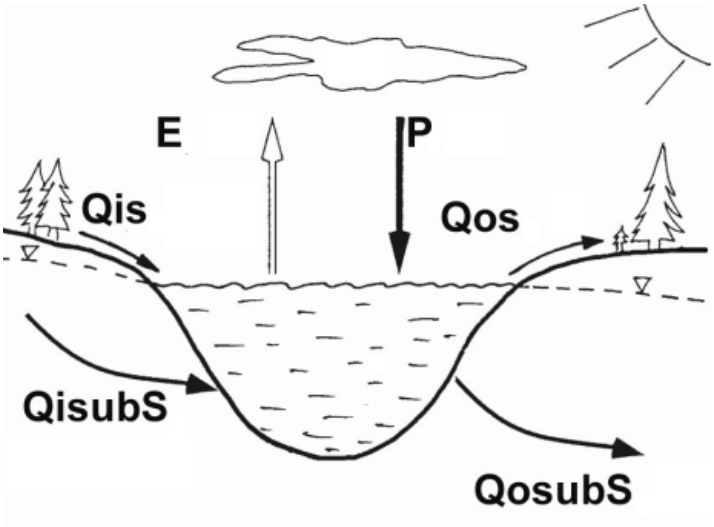

Figure 5: Hydrological budget of a lake. E: evaporation; P: precipitation; Qis: surface inflow; Qos: surface outflow; QisubS: subsurface inflow; QosubS: subsurface outflow. *Adapted from Delalande (2008)*

1.1.3 Tools to reconstruct past climate variations in continental archives

Past climate reconstructions from geological archives are based on the observation and/or analysis of preserved biological remains, either thick organic walls (e.g. algae such as *Botryoccocus* or *Scenedesmus*) or mineral exoskeletons (e.g. coccolithophors, corals, *Coleoptera*, diatoms …). Various organism remains, from the vertebrate and invertebrate animals to the unicellular plankton, or from vegetation (terrestrial, aquatic, algal) have been studied for their distribution (Gornitz, 2009). Indeed ecological diversity strongly depends on climatic factors. For example, the presence of specific micro-fossil assemblages of foraminifera, coccoliths or diatoms in aquatic sediments indicates that climatic conditions were favorable for the survival of the observed taxa (Ericson and Wollin, 1956; Barker et al., 2000). Similarly, vegetation remains (terrestrial and aquatic) are also preserved in humid archives: vegetation cover history can be tracked through pollen distributions (e.g. Davis and Moutoux, 1998) while charcoal abundance can be related to the frequency of fires (Thevenon et al., 2010). On the Holocene timescale, preserved organic tissues can be examined by light microscopy, informing on both the vegetation and planktonic taxa formerly present at the study site (e.g. van Geel, 1978) and on the physicochemical conditions at that time (based on the degradation degree of organic matter (OM); e.g. Zocatelli et al., 2012).

In addition to the presence/absence observation of organism remains, the chemistry of the geological archives encompasses signals of past environmental changes (Figure 6). At the bulk level, elemental (carbon, nitrogen, hydrogen) and isotopic ($\delta^{13}C$, $\delta^{15}N$) analyses of the organic fraction of the sediments provide information on their origin but also on the site primary productivity and on the degree of degradation of the OM (Meyers, 1997, 2003). At the fossil level, some elemental ratios such as the Mg/Ca ratio of Foraminifera tests (Nürnberg et al., 1996; Lear et al., 2000) or the Ca/Sr and Mg/Sr ratios of Ostracod carbonate carapaces (Cronin, 2009) have been related to temperature or salinity. Similarly, because these exoskeletons are formed in equilibrium with the surrounding water, their isotopic composition records the one of the water column which in turn depends on temperature-dependent fractionation processes. Investigation of the $^{18}O/^{16}O$ of these carbonated remains have been widely used to infer past temperature variation (Emiliani, 1955).

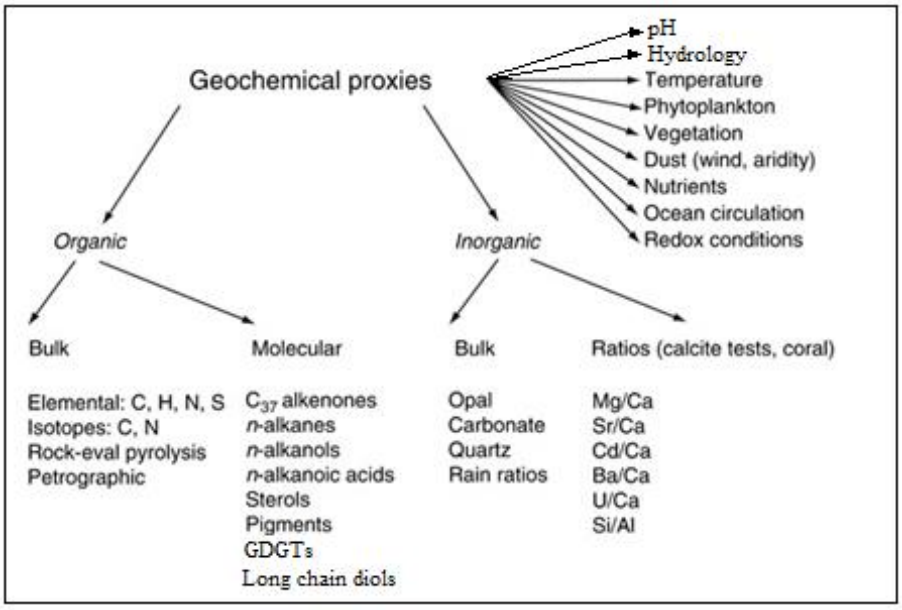

Figure 6: Summary of geochemical proxies investigated in geological archives and the main environmental parameters they can track. The molecular-based ones will be discussed in the following section. *Adapted from* (Gornitz, 2009).

Geological objects may also directly inform on the climatic conditions prevailing at the time of their formation. For example, paleo-shorelines record lake level fluctuations related to variations in precipitations and evaporation at the lake surface over time (Garcin et al., 2012a), while the presence of moraines indicates the past expansion of glaciers (Williamson, 2013). Polar ice core isotopic composition delivered the first detailed record of past temperature variations since the last ice age (Gow et al., 1968; Epstein et al., 1970; Dansgaard et al., 1971) and are also the only archives to contain direct atmospheric composition information, in the air bubbles trapped during the ice formation.

However these proxies (i) are not all ubiquitous and (ii) may contain biases. Notably interpretation from bulk analyses are often hampered because the recorded signal is a mix of different sources. Therefore, paleoclimatic studies are now more and more based on multi-proxy approaches, where some proxies can be used to constrain the signal sources while the combination of independent temperature proxies strengthens the paleoclimatic interpretation. In the past decades, highly sensitive analytical techniques were developed, allowing OM characterization at the molecular level and giving access to new tools – so-called biomarkers – for paleoclimate reconstructions. In the following section, the concept, applicability and limits of the latter will be detailed.

1.2. Biomarkers

1.2.1 Introduction: The concept of biomarkers

Biomarkers are molecules from living organisms which are preserved in geological archives due to their high chemical stability. Their structure and their isotopic signature can hold information about (i) their source and/or (ii) the environment they were produced in. Indeed, some molecules will be specifically produced by certain species or group of species, the biomarker being then more or less specific. For instance, triterpanes are specific biomarkers to a vegetation clade (angiosperms or gymnosperms; (Killops and Killops, 2005) while the millacin has been reported to be specific to a few vegetation species (Jacob et al., 2008; Bossard et al., 2013). In addition, some organisms are able to modulate the production of the biomolecules they synthesise in reaction to environmental changes, in order to maintain the viability of their cells (Gunstone et al., 1994). The monitoring of such biomolecules can therefore be used to track environmental changes with time and space.

In this respect, paleothermometers have been developed based on the distribution of some biomolecules such as GDGTs, alkenones and long chain diols. GDGTs will be described in more details in the following section. Alkenones are long chain unsaturated ketones produced by a few species of Haptophytes in the oceans (Volkman et al., 1980). First, Marlowe et al. (1984) observed a relationship between the degree of unsaturation in alkenones and temperature. Subsequently, Brassell et al. (1986) developed the $U^{K'}_{37}$ index to numerically express this degree of unsaturation and Prahl et al. (1988) established a transfer function to reconstruct absolute temperature from the $U^{K'}_{37}$. This proxy has since then been extensively used in paleoclimatic context (Herbert, 2003) but is restrained to aquatic environments where the corresponding haptophyte communities are present. More recently, another family of biomarkers, namely the long chain alkyl diols, was used to derive temperature in marine (Rampen et al., 2012) and lacustrine (Rampen et al., 2014) environments based on their distribution, as expressed by the LDI (long chain diol index). The long chain diols, which differ by the length of their alkyl chain and by the position of the hydroxyl groups, were first detected by (de Leeuw et al., 1981) and their origin remain unclear. They have notably found to be produced by eustigmatophyte algae (Volkman et al., 1992, 1999) but also some diatoms (Sinninghe Damsté et al., 2003) and dictyochophyte algae (Rampen et al., 2011)

The number of available biomarkers has considerably increased over the last 30 years following up the analytical improvements in the separation, detection and characterisation of organic compounds. The development of interfaces for coupling liquid chromatography and mass spectrometry allows the detection of higher molecular weight compounds than with gas chromatography, such as the glycerol dialkyl glycerol tetraethers or the bacteriohopanepolyols (Hopmans et al., 2000; Talbot et al., 2001). In addition, the isotopic signature of individual compounds can now be routinely determined using on-line compound-specific isotope analyses (Scrimgeour et al., 1999). This tool allowed to define new proxies for environmental parameters (e.g. hydrology) and can also be used to track the sources and origin of biomarkers.

The following sections will be focused on two families of biomarkers, the glycerol dialkyl glycerol tetraethers and the *n*-alkanes which are more extensively investigated in this thesis. The origin, strength and limits of application of these compounds will be assessed based on the available literature.

1.2.2 Glycerol dialkyl glycerol tetraethers:

1.2.2.1. Sources and biosynthesis

Glycerol dialkyl glycerol tetraethers (GDGTs) are membrane-spanning lipids (Figure 7) composed of long aliphatic carbon chains linked by an ether bond to a glycerol moiety at each extremity. They were first detected in 1972 in archaeal cultures of *Thermoplasma acidophilum* (Langworthy et al., 1972) and further characterized in 1977 (Langworthy, 1977). GDGTs were initially thought to be an adaptation to extreme conditions such as high growth temperature and acidity, under which many archaea thrive. Nevertheless, it has become clear over the last decade that they occur ubiquitously in a wide range of environments, such as marine and lacustrine sediments (Schouten et al., 2002; Liu et al., 2011) water columns (e.g. Schouten et al., 2012; Buckles et al., 2014; Loomis et al., 2014b), soils (Weijers et al., 2007; Peterse et al., 2012), peatlands (e.g. Damsté et al., 2000; Huguet et al., 2010), hot springs (Ward et al., 1985; Pancost et al., 2006) and speleothems (Yang et al., 2011).

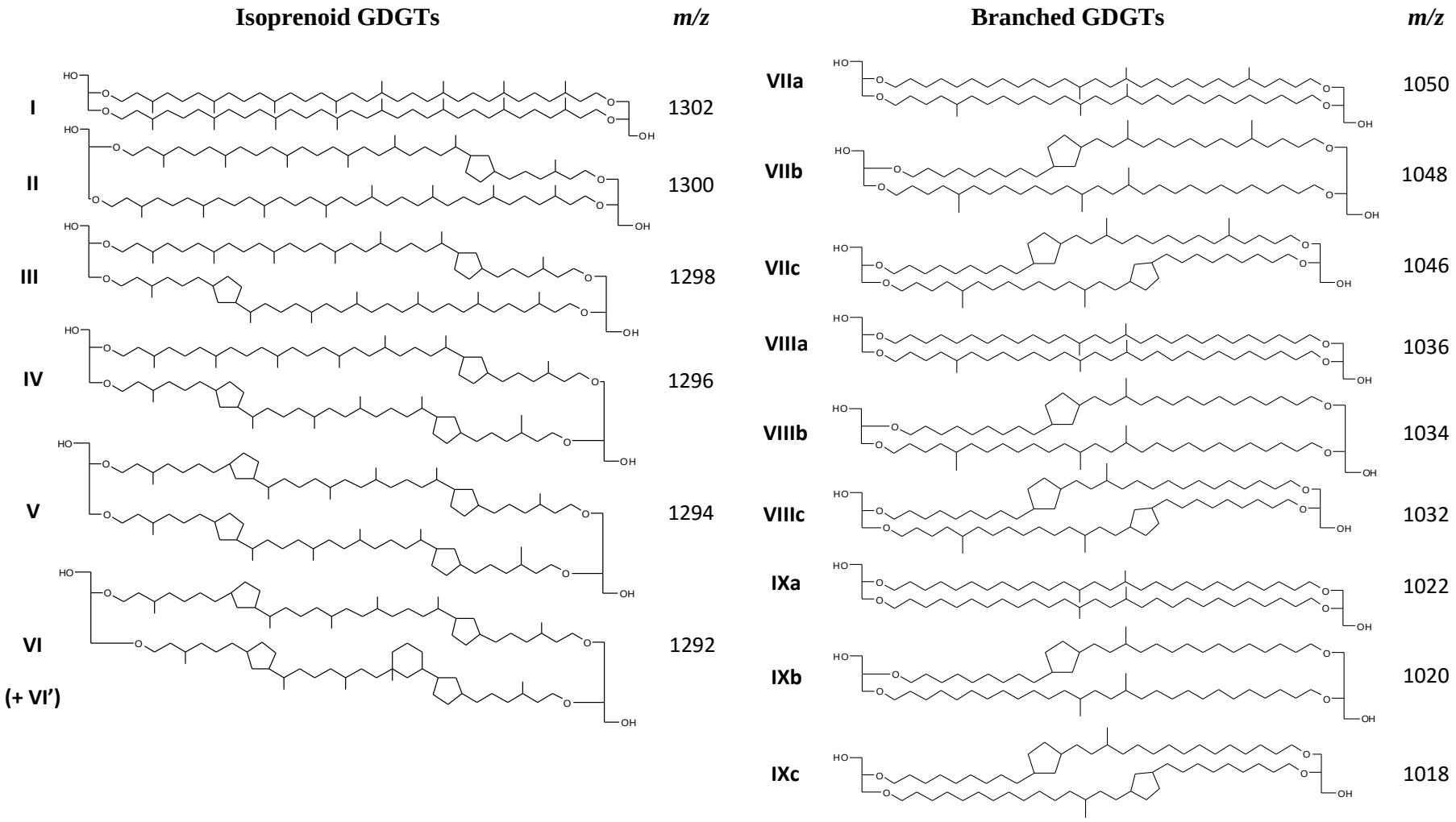

Figure 7: Structures of isoprenoid and branched glycerol dialkyl glycerol tetraethers (GDGTs).

GDGTs can be detected as core lipids (CLs; Figure 7) or intact polar lipids (IPLs) in the environment. IPLs are the predominant form of lipids in the living cells (Schouten et al., 2008; Pitcher et al., 2011; Elling et al., 2014) and correspond to CLs with polar head groups (sugar and/or phosphate units) attached to glycerol moieties (Figure 8; Nishihara et al., 1987). The polar extremities of the IPLs interact with the extra and intra cellular aqueous solutions, while their apolar chains ensure the sealed closing of the cells. The polar head group of the IPLs is thought to be rapidly lost after cell lysis (White et al., 1996), leading to the persistence of GDGTs as CLs in the environment. However, significant amounts of GDGTs in the IPL form were detected in deeply buried sediments (Lipp and Hinrichs, 2009), questioning this assumption.

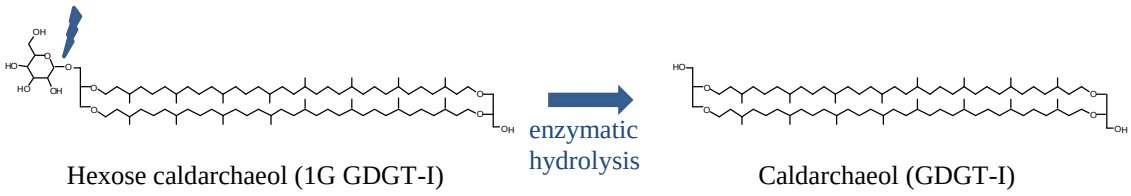

Figure 8: Enzymatic hydrolysis of IPL GDGT-I into CL GDGT-I at the lysis of the cell

GDGTs exhibit a large diversity in the composition of their carbon skeletons (Figure 7), but two main classes can be distinguished: isoprenoid GDGTs (iso GDGTs) and branched GDGTs (br GDGTs). Hereafter, current knowledge on the sources, and biosynthesis of each class is detailed, based on the review compiled by (Schouten et al., 2013) and on more recent literature.

Isoprenoid GDGTs:

Iso GDGTs are produced by Archaea, one of the three domains of life introduced by (Woese and Fox, 1977). Archaeal membrane lipids bear distinct structural features compared to most of the bacterial membrane lipids, with isoprenoid carbon skeletons being ether-bound to glycerol moieties (Figure 7). The structures of the main iso GDGTs (I-VI), differing by the number of cyclopentane moieties in their alkyl chains (from 0 to 4), are presented in Figure 7. GDGT VI, also called crenarchaeol, comprises a cyclohexane moiety in addition to the four cyclopentane moieties (Figure 7). This compound possesses a regio isomer (because of the asymmetric carbon in the cyclohexane moiety), called GDGT VI', which is found in significant amounts in

natural samples (Schouten et al., 2002). GDGT I, sometimes referred to as caldarcheol, is the most common iso GDGT, as it was detected in all the archaeal phyla (Figure 9; Pearson and Ingalls, 2013) while GDGT VI (and VI') is thought to be specific for the phylum Thaumarchaeota, even though it has been recently suggested that it could also be produced by Marine Group II Euryarchaeota (Lincoln et al., 2014). Iso GDGTs containing 1 to 4 cyclopentane rings (GDGTs II-V) are produced by Thaumarchaeota, Crenarchaeota and some Euryarchaeota (Figure 9; Pearson and Ingalls, 2013). Iso GDGTs have been detected in all types of environments, from marine settings (sediment and water column) to soils (Schouten et al., 2013)

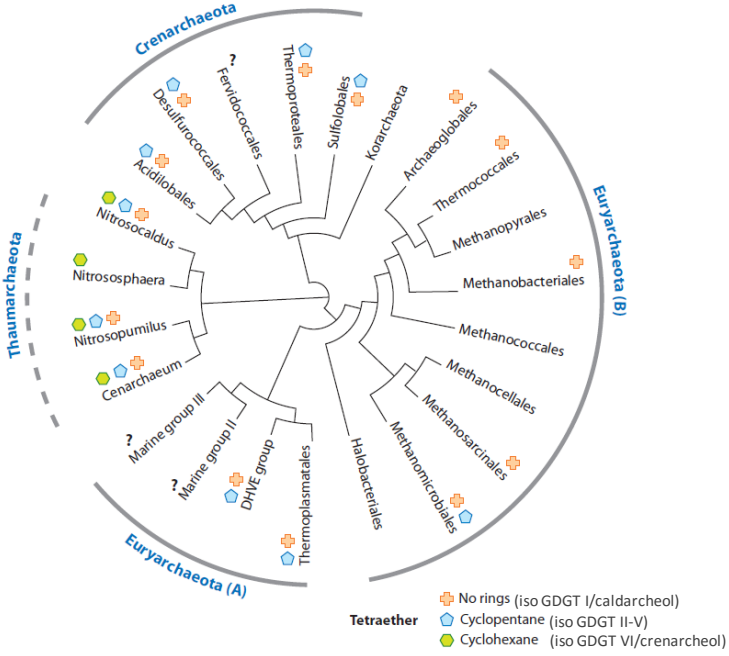

Figure 9: Phylogenetic tree showing the topology of relationships between orders of Archaea based on 16S rRNA sequences. The major kingdoms of Archaea are the Korarchaeota, Crenarchaeota, Thaumarchaeota and Euryarchaeota. The euryarchaeal group comprising Thermoplasmatales and their relatives (*A*), as well as all Thaumarchaeaota and Crenarchaeota studied to date, are known for synthesizing GDGTs containing cyclopentane rings. Only the Thaumarchaeota are known to produce crenarchaeol [GDGT VI]. Abbreviations: DHVE, deep-sea hydrothermal vent Euryarchaeota. *From Pearson and Ingalls, 2013*.

A biosynthetic route for iso GDGTs was proposed by (Koga and Morii, 2007) and involves isopentenyl diphosphate (IPP) and dimethyl allyl diphosphate (DMAPP) as building blocks, which are two products of the mevalonic acid pathway (Figure 10). Condensation of DMAPP with several IPPs leads to the production of geranyl geranyl diphosphate (GGPP). This step is followed by the linkage of two GPPs to a glycerol-1-phosphate (G-1-P) to form digeranyl geranyl glyceryl phosphate (DGGGP). The last step of this original pathway, which was never documented, is the head-to-head condensation of two saturated DGGGPs and internal cyclization. The iso GDGT biosynthetic pathway has been revisited very recently by (Villanueva et al., 2014) and it also involves elongation of DMAPP with IPP units. However, these authors suggested that the cyclopentane rings could be formed during the latter step and that the head-to-head condensation, catalysed by phytoene synthase, would occur between GGPPs rather than DGGGPs. The last step would consist in the attachment of two G-1-P at each extremity of the biphytane chains (Villanueva et al., 2014). Even though this new biosynthetic pathway partly fills the lack of the one proposed by (Koga and Morii, 2007), the biosynthesis of GDGT VI is still not completely elucidated.

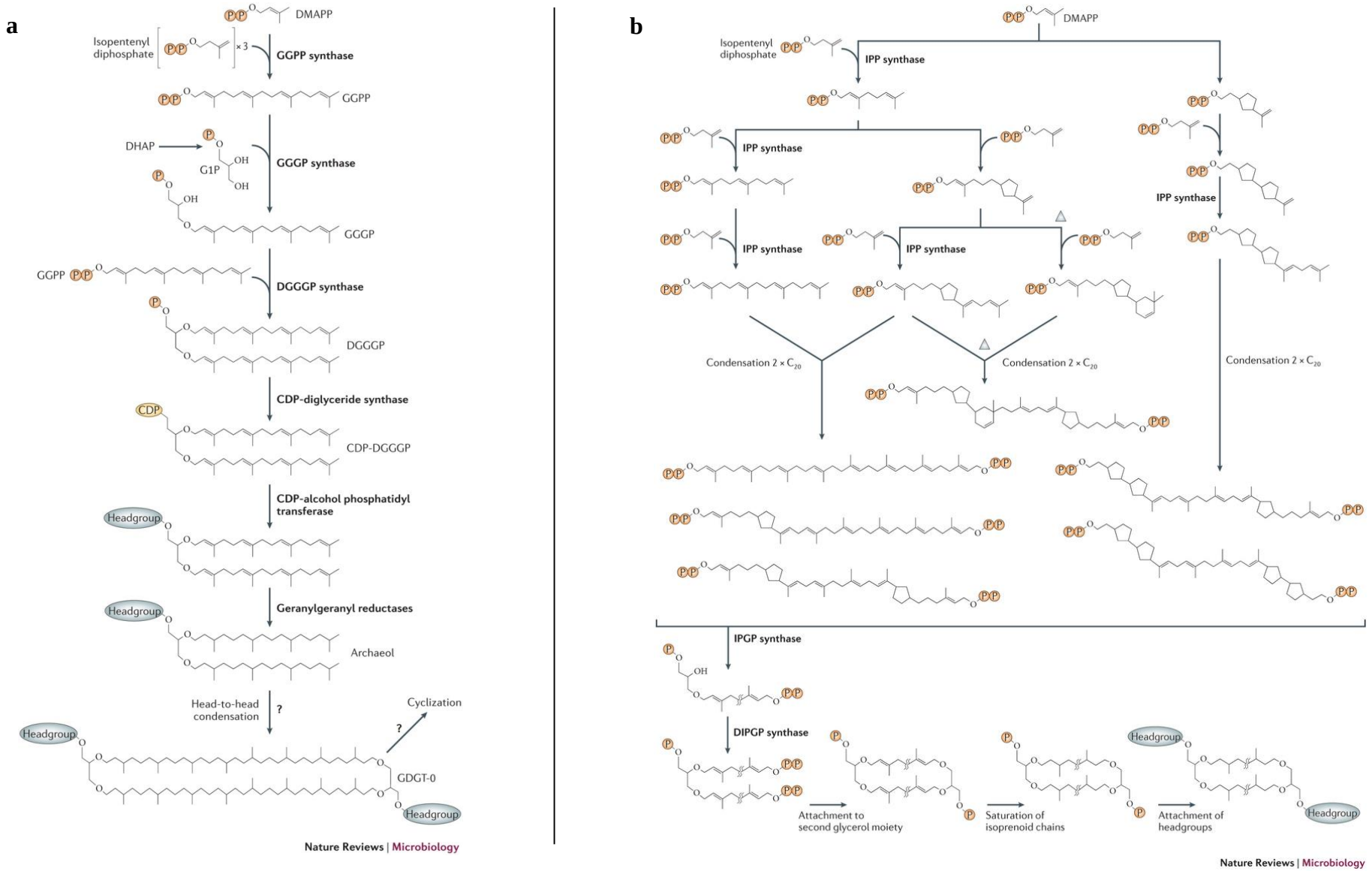

Figure 10: Iso GDGT biosynthtetic pathways as (a) proposed by Koga and Morii (2007) and (b) revisited by Villanueva et al. (2014). *Adapted from Villanueva et al. (2014)*

Branched GDGTs:

Br GDGTs were first detected in a peatland by Sinninghe Damsté et al. (2000). In contrast with iso GDGTs, they are characterised by branched instead of isoprenoid alkyl chains (Figure 7). NMR characterization of a purified br GDGT (br GDGT VIIIa; Weijers et al., 2006a) revealed that the stereoconfiguration of its glycerol moieties was opposite to the one of iso GDGTs, suggesting a bacterial origin of br GDGTs. Indeed, as a result of evolutionary difference (Koga et al., 1998), archaea use the *sn*-glycerol-1-phosphate (G-1-P) to form their lipids, while bacteria use the *sn*-glycerol-3-phosphate (G-3-P), leading to opposite configuration of the respective lipids.

Unlike iso GDGTs, little is known about the sources and biosynthesis of br GDGTs. The high abundance of these compounds in the waterlogged parts of peatlands suggests that they are produced by anaerobic bacteria, even though the exact group(s) of microorganisms biosynthesizing them are still unknown. (Weijers et al., 2009) suggested that *Acidobacteria* might be possible producers of br GDGTs, as both br GDGTs and *Acidobacteria* were observed to be highly abundant along a peat core from Sweden. In addition, br GDGT IXa was observed in small amounts in one cultured subdivision of *Acidobacteria* (SD 1; Sinninghe Damsté et al., 2011) and large amounts of *iso* diabolic acid ether-bound to a glycerol - a possible precursor of br GDGTs (Figure 11) - was recently detected in most of the investigated *Acidobacteria* subdivisions (Sinninghe Damsté et al., 2014). By analogy with the biosynthetic pathway of iso GDGTs and based on preliminary studies (Jung et al., 1993; Ring et al., 2006), it was proposed that the biosynthetic pathway of br GDGTs would include ω,ω' condensation of two C_{15} fatty acids followed by esterification with glycerol moieties and reduction into ether assemblages (Figure 11; Sinninghe Damsté et al., 2011). In any case, all these results hint towards *Acidobacteria* as possible producers of the br GDGTs. However further research is still necessary to better constrain the source microorganisms of br GDGTs, which are ubiquitously produced in terrestrial, marine, riverine and lacustrine environments (Schouten et al., 2013; Zell et al., 2014). This is all the more complex as the diversity of bacteria on Earth remains largely unknown and that culturing them represents a huge challenge.

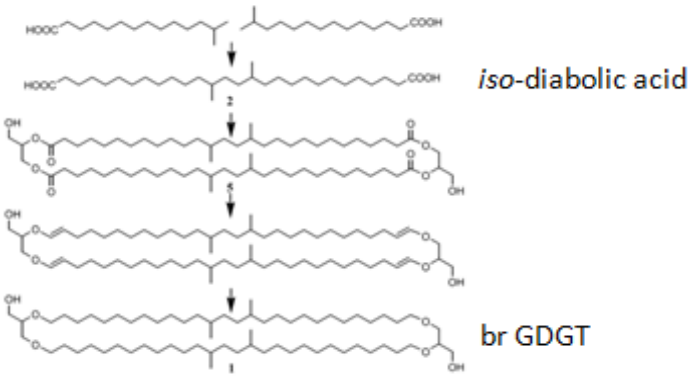

Figure 11: Br GDGT condensation pathway proposed by Sinninghe Damsté et al. (2011).

In the past few years, suites of novel glycerol-based alkyl ether lipids with structures apparently related to GDGTs were detected in the environment, especially in marine sediments (Liu et al., 2012a, 2012b, 2012c; Zhu et al., 2014a, 2014b). They include tetraethers and diethers whose skeletons bear additional hydroxyl, methyl groups or unsaturations (Figure 12). These newly discovered compounds can be (i) additional membrane lipids, (ii) biosynthetic intermediates or (iii) degradation products of GDGTs. In this thesis, we have investigated more deeply the abundance and distribution of one of these new glycerol ether lipid families: the glycerol dialkanol diethers (GDDs; Figure 12).

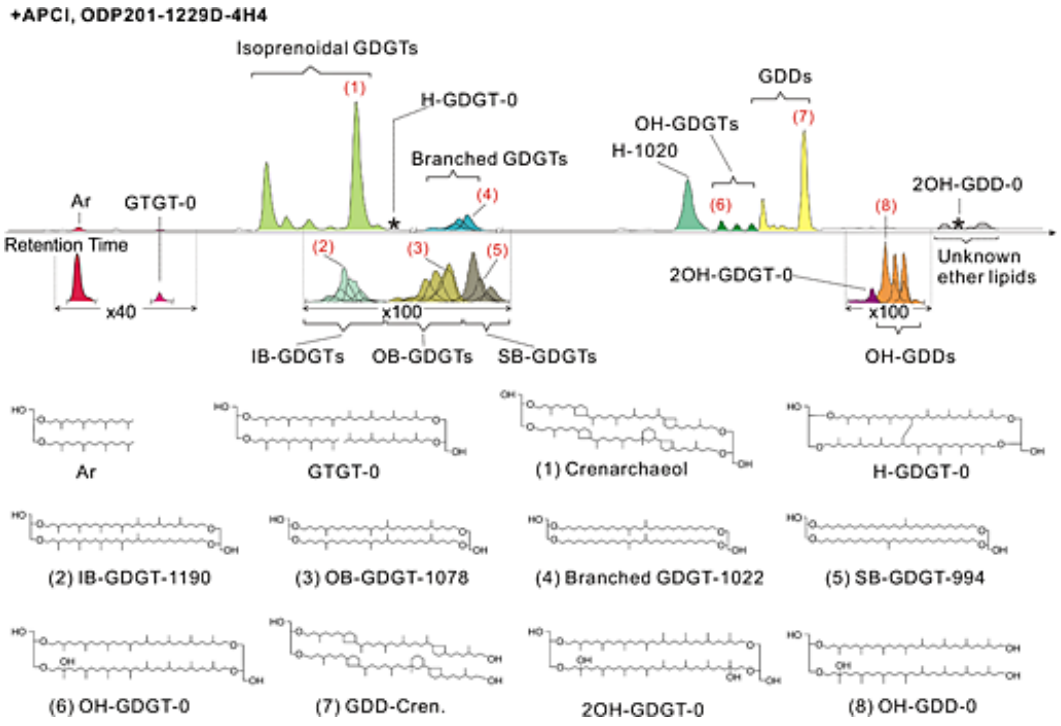

Figure 12: LC/APCI/MS chromatogram showing the distribution of glycerol ether lipids in sample ODP201-1229D-4H4, Peru Margin (Liu et al. 2012c) and their corresponding structures. From Liu et al. (2012c).

1.2.2.2. Proxy development

Membrane lipids protect cell content from the outside environment. They ensure the sealed closing of the cells but allow the entry of components essential for their survival. To do so, microorganisms are able to adapt their membrane composition to modulate its packing and fluidity according to the physical and chemical conditions of the medium (e.g. pressure, temperature and pH). Therefore, membrane lipids can be used as proxies for the environmental conditions under which the microorganisms grew.

This is especially the case for GDGTs. The number of cyclopentanes in iso GDGTs has been shown to increase with the temperature in several thermophilic archaeal cultures (Derosa and Gambacorta, 1988; Uda et al., 2001), corresponding to an adaptation of the thermal transition points of cell membranes (Gliozzi et al., 1983). Culture studies of br GDGT source microorganisms could not be performed, as the latter remain unknown (see previous section) but similar structural adaptations has been demonstrated in the composition of bacterial membrane lipids. For example bacteria change the degree of saturation, of branching or the chain lengths of their fatty acid alkyl chains according to changing environmental conditions (Reizer et al., 1985; Prado et al., 1988; Suutari and Laakso, 1992). Another critical aspect when developing proxies based on biomarkers is the conservation of the latter compounds through time (see section 1.2.1.). So far, the oldest iso and br GDGTs were detected in archives from the Jurassic (Carrillo-Hernandez and et al., 2003; Jenkyns et al., 2012) as far as 185 ± 5 Ma old (Tramoy, Huguet et al., personal communication). As a result, several proxies were developed to reconstruct past environmental parameters (especially temperature and pH) based on iso and br GDGT distribution. In the following, we will detail the development of the TEX_{86} based on iso GDGTs, the MBT/CBT indices based on br GDGTs and the BIT, based on the relative contribution of br GDGTs relative to iso GDGT VI (crenarchaeol).

TEX_{86}

Based on the experiments on archaeal cultures described above, (Schouten et al., 2002) investigated the relationship between the cyclisation degree of iso GDGTs and sea surface temperature (SST) in a set of 44 marine sediments globally distributed. They found a statistically significant correlation and proposed a new proxy to reconstruct SST based on the cyclisation degree of iso GDGTs: the TEX_{86} index (tetraether index of

tetraethers consisting of 86 carbons; equation 1). A linear correlation between TEX_{86} and SST was reported (Schouten et al., 2002; equation 2):

$$TEX_{86} = \frac{[III]+[IV]+[VI']}{[II]+[III]+[IV]+[VI']} \quad (1)$$

$$TEX_{86} = 0.015 \times SST + 0.28 \ (R^2 = 0.92) \quad (2)$$

This index is only valid if the iso GDGTs are predominantly produced by Thaumarchaeota (Schouten et al., 2002). Whereas Thaumarchaeota are highly abundant in the oceans, this condition may be an issue for the extension of the TEX_{86} proxy to continental settings, as we will discuss later in this section.

First applications of this proxy to reconstruct past SST were promising (e.g. Huguet et al., 2006; Castañeda et al., 2010; Shintani et al., 2011). However, a warm bias was observed when TEX_{86} temperatures were reconstructed from high latitude sediments, whereas an opposite trend was noticed at low latitudes. To improve the accuracy of temperature reconstruction, alternative calibrations were developed. (Kim et al., 2008) re-determined the linear calibration between SST and TEX_{86} (equation 3) after having analysed a more extensive and global set of marine sediments (containing 287 core-tops) than in the initial calibration by Schouten et al. (2002):

$$SST = 81.5 \times TEX_{86} - 26.6 \quad \text{(standard error (s.e.) = 1.7 °C)} \quad (3)$$

Then, Kim et al. (2010) developed two additional indices based on the distribution of iso GDGTs in sediments, the TEX^{L}_{86} (equation 4) and the TEX^{H}_{86} (equation 5) to overcome the biases in reconstructed temperatures observed with the TEX_{86} at low and high latitudes, respectively. They recommend using the TEX^{L}_{86} for regions where SST are below 15 °C and the TEX^{H}_{86} otherwise.

$$SST = 67.5 \times TEX^{L}_{86} + 46.9 \quad \text{(s. e.: 4.0 °C)} \quad (4)$$

$$SST = 68.4 \times TEX^{H}_{86} + 38.6 \quad \text{(s. e.: 2.5 °C)} \quad (5)$$

However several points are questionable about these calibrations based on new indices. Their standard error is higher than the one of the original TEX_{86} calibration. Thus, even if SST reconstructions are more accurate, they are less precise. Another drawback is that they are locally constrained. The scientific rationale of describing the linear relationship experimentally observed between microorganism growth temperature and iso GDGT

distribution with a non-linear model can also be questioned. (Tierney and Tingley, 2014) recently proposed an alternative way of calibrating the TEX_{86}: a spatially flexible Bayesian model, called BAYSPAR (see section 1.2.2.3. for details).

In addition, iso GDGTs were also found in lakes (Powers et al., 2004; Blaga et al., 2009). However, in many of the lakes, iso GDGTs were shown to be produced by Thaumarchaeota and by methanogenic Archaea. As pointed earlier, this additional production of iso GDGT would result in distorting the temperature signal derived from the TEX_{86} index. Thus Blaga et al. (2009) proposed to use the ratio of GDGT I (caldarchaeol) vs. GDGT VI (crenarchaeol) to determine if TEX_{86} was applicable in a particular setting, based on the assumption that crenarchaeol is only biosynthesized by Thaumarchaeota. If the GDGT I/GDGT VI ratio is lower than 2, then Thaumarchaeota can be considered as the predominant producer of iso GDGTs. Occurrence and application of iso GDGTs in continental settings will be detailed in section 1.2.4.

MBT/CBT

Similarly to iso GDGTs, the main br GDGTs exhibit a varying number of cyclopentanes (0 to 2) but also methyl groups (4 to 6) in their alkyl chains (Figure 7). The relationship between the br GDGT distribution in 130 soils distributed worldwide and different environmental parameters (air temperature, pH, summed cations, electronic conductivity, precipitations) was statistically tested (Weijers et al., 2007). The degree of cyclisation, expressed in the CBT index (cyclisation ratio of branched tetraéthers, equation 6) was shown to be significantly correlated to pH and the degree of methylation, expressed in the MBT index (methylation index of branched tetraethers; equation 7), was observed to be related to mean annual air temperature (MAAT) and, to a lesser extent, to pH (Weijers et al., 2007):

$$MBT = \frac{[IXa + IXb + IXc]}{[VIIa + VIIb + VIIc] + [VIIIa + VIIIb + VIIIc] + [IXa + IXb + IXc]} \quad (6)$$

$$CBT = -\log\left(\frac{[VIIIb] + [IXb]}{[VIIIa] + [IXa]}\right) \quad (7)$$

The temperature was hypothesised to have a direct effect on the membrane fluidity of br GDGT source microorganisms, while the variation of the number of cyclopentanes could permit to maintain the proton gradient - necessary for energy production - across

the membrane (Weijers et al., 2007). Based on MBT/CBT, calibrations were developed to reconstruct MAAT and pH (equations 8 and 9; Weijers et al., 2007):

$$MAAT = \frac{MBT - 0.122 - 0.187 \times CBT}{0.020} \quad (RMSE = 4.8\ °C) \quad (8)$$

$$pH = \frac{3.33 - CBT}{0.38} \quad (RMSE = 0.7) \quad (9)$$

Even though the correlation between MBT, CBT and MAAT is robust statistically ($p < 0.05$), it exhibits a large degree of scatter ($R^2 = 0.77$; Root mean square error (RMSE) = 4.8 °C), which may prevent accurate MAAT reconstruction.

Peterse et al. (2012) extended the br GDGT calibrations developed by Weijers et al. (2007) by adding 126 globally distributed soils. They proposed a simplified form of the MBT index, defined as the MBT' (equation 10), by excluding GDGTs VIIb and c (Figure 7) very often below or just over the detection threshold in soils.

$$MBT' = \frac{[IXa + IXb + IXc]}{[VIIa] + [VIIIa + VIIIb + VIIIc] + [IXa + IXb + IXc]} \quad (10)$$

New transfer functions between MBT', CBT and MAAT and/or soil pH were defined (equations 11 and 12; Peterse et al., 2012):

$$MAAT = 0.81 - 5.67 \times CBT + 31.0 \times MBT' \quad (RMSE = 5.0\ °C) \quad (11)$$

$$pH = 7.90 - 1.97 \times CBT \quad (RMSE = 1.1) \quad (12)$$

The correlation coefficient of this new transfer function for MAAT (R^2 0.59; Peterse et al., 2012) was lower than the one of the original calibration (Weijers et al., 2007) and the RMSE (5 °C; Peterse et al., 2012) was similar to the original one. The high scatter observed in this global soil calibration was suggested to be related to (i) the inherent heterogeneity of worldwide soils due to complexity of the pedogenesis processes, (ii) a potential offset between MAAT and mean annual soil temperature (where br GDGTs are actually produced; Peterse et al., 2012) and (iii) the fact that other environmental parameters than MAAT and pH, such as soil humidity/aridity, may also have an impact on br GDGT distribution (see details in the following section). The further observation that br GDGTs could also be produced in aquatic environments, notably in lakes (Tierney et al., 2012; Buckles et al., 2014; Loomis et al., 2014a, 2014b), led to the development of specific calibrations that will be detailed in section 1.2.4.3.

BIT

Based upon the assumption that on the one hand, br GDGTs are produced by soil bacteria and, on the other hand, GDGT VI (crenarchaeol; Figure 7) are produced by aquatic Thaumarchaeota (Pearson and Ingalls, 2013), Hopmans et al., (2004) developed an additional index, the BIT (branched and isoprenoid tetraether index; equation 13) to track terrigenous inputs into aquatic environments:

$$BIT = \frac{[VIIa]+[VIIIa]+[IXa]}{[VI]+[VIIa]+[VIIIa]+[IXa]} \qquad (13)$$

This proxy was used in different riverine systems and successfully tracked a decreasing relative contribution of soil OM in river fans with increasing distance from the coast (Herfort et al., 2006; Kim et al., 2012, 2006, 2007). However, recent studies highlighted that br GDGTs were also produced in aquatic environments (see section 1.2.4. for details) and GDGT VI (crenarchaeol) in soils (e.g. Liu et al., 2013; Weijers et al., 2006), challenging the applicability of the BIT.

1.2.2.3. Current limitations and perspectives for research

OPEN RESEARCH QUESTION: Understand the origin of scatter in GDGT-based calibrations and develop ways to reduce it.

Applications of GDGT-derived proxies to a wide range of modern settings and archives (marine and lacustrine sediments, peatlands, speleothems, loess-paelosoils sequences ….) globally distributed on Earth pointed out occasional mismatch between the reconstructed and expected temperatures (either MAAT or SST) or pH (e.g. Zachos et al., 2006; Tierney and Russell, 2009; Weijers et al., 2011). This shows that the calibrations described above cannot always be applied directly likely due to the analytical uncertainty and the influence of other environmental parameters or regional specificities. This is all the more true as, as specified above, these worldwide calibrations exhibit a large degree of scatter, especially the correlation between MAAT and br GDGT distribution (RMSE = 5 °C). In this section, we will review the most recent developments to reduce the scatter in GDGT calibrations and improve the accuracy of temperature reconstruction, while section 1.2.4. will detail the last

progresses made for paleoenvironmental reconstruction in continental archives (paleosols, peatlands and lakes).

Recently, additional isomers of br GDGTs - where the methyl groups are located in the 6th position rather than in the 5th one (Figure 13; De Jonge et al., 2013)- were detected by using improved LC-MS protocols with either two HILIC amide (Becker et al., 2013) or four silica columns (De Jonge et al., 2014) in tandem. These new isomers are labelled with a prime symbol. De Jonge et al. (2014) investigated the influence of these new isomers in the correlation between MBT'/CBT and MAAT by reanalysing the samples used by Peterse et al. (2012) and Weijers et al. (2007). They observed that the fractional abundances of the 6-methyl br GDGTs were highly correlated to pH and were the source of the pH dependence of the MBT'. Consequently, they proposed to (i) exclude these new isomers from the MBT' calculation to obtain a pH independent reconstruction of MAAT (equation 14) and to (ii) include them in the CBT calculation (equations 15 and 16):

$$MAAT = -8.57 + 31.45 \times MBT' \text{ (R² = 0.66; RMSE = 4.8 °C; n = 222)} \quad (14)$$

$$CBT' = \log_{10} \frac{VIIa' + VIIb' + VIIc' + VIIIa' + VIIIb' + VIIIc' + IXc}{IXa + VIIIa + VIIa} \quad (15)$$

$$pH = 7.15 + 1.59 \times CBT' \text{ (R² = 0.85; RMSE = 0.52 °C; n = 221)} \quad (16)$$

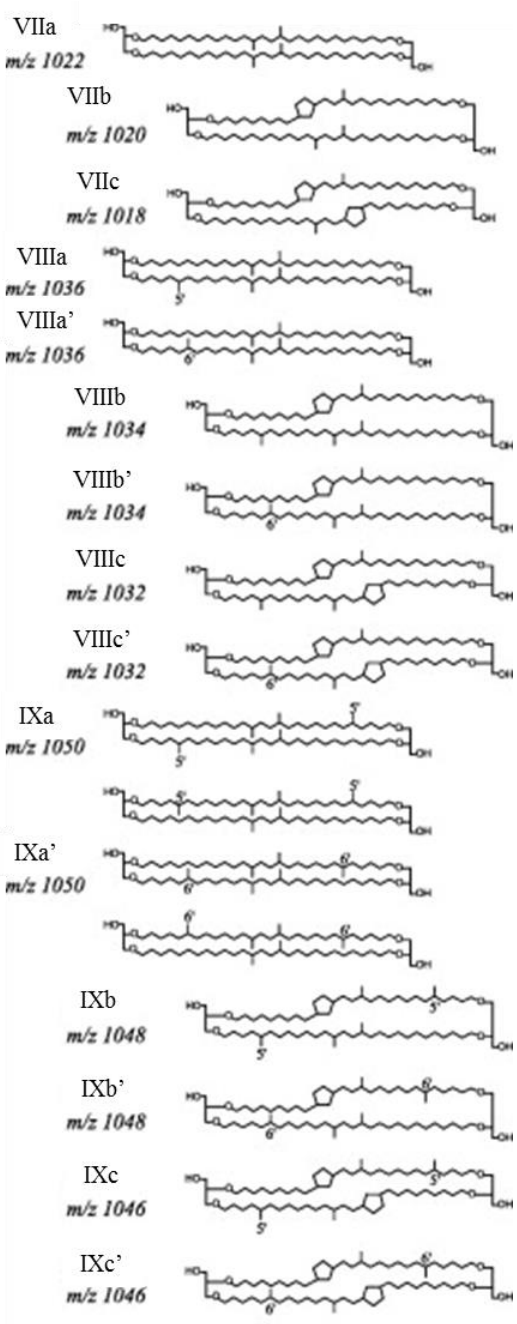

Figure 13: Chemical structures of br GDGTs including those containing one or two methyl groups at the α and/or ω-6 position (indicated with a prime symbol). Note that the numerotation is different from the rest of the thesis (GDGTs I are GDGTs IX series, II are the series VIII and III correspond to GDGTs VII). *From* (De Jonge et al., 2014).

Separation of the 5- and 6-methyl br GDGT isomers seems necessary to accurately assess the relationships between br GDGT distribution and environmental parameters. However, these methods were developed with ultra-high pressure liquid chromatography (UHPLC), a device still scarcely found in laboratories. This new methodology could be used with traditional HPLC chains, since it does not reach the

maximum pressure of most of the HPLC pumps (max. pressure during analysis = 200 bar; De Jonge et al., 2014). Nevertheless, few laboratories have set up this new methodology yet. Thus the impact of these new isomers on temperature and pH reconstructions in a wide range of environment types and locations remains putative. All the samples presented in the present thesis were analysed with the original method based on cyano columns (Schouten et al., 2013; details in Chapter 3) but we acknowledge for each presented study (see Chapters 4, 5, 6) the potential impact of the new methodology on our results. In any case, the discovery of these isomers is not sufficient to explain the temperature biases observed in many publications (see section 1.2.4) neither did it improve the accuracy of the global soil calibration (the RMSE is still around 5 °C).

Several authors pointed out the potential impact of other environmental parameters than temperature or pH on GDGT distribution. Indeed as the diversity of GDGT structures result from microorganism response to environmental factors, any biological stress (such as nutrient concentrations, water saturation of the medium, energy availability) could influence their distribution. For example, culture experiments and environmental studies stressed out that pH (Macalady et al., 2004), nutrient availability (Turich et al., 2007) or depth of the water column (Taylor et al., 2013) may have an impact on iso GDGT distribution. The fact that br GDGT source organisms are still unknown precludes any culture experiments. Thus, exploration of additional parameters potentially impacting br GDGT distribution can only be achieved in natural samples, even though it is sometimes difficult to constrain which parameter is driving a specific response. Despite this, the existing literature suggests that several factors may impact the br GDGT distribution. One of these factors is the soil water content. On the one hand, Huguet et al. (2010a, 2013a), Weijers et al. (2011) and Loomis et al. (2011) observed an offset between reconstructed and measured MAAT in peatlands and permanently water-logged soils. In addition, Peterse et al. (2009a) and Huguet et al. (2010a) observed lower MBT (*i.e.* indicative of a higher contribution of methylated compounds) in areas where precipitations are > 2000 mm and in the wettest area of a French peatland with constrasted hydrological regime, respectively. On the other hand, Dirghangi et al. (2013) found that soil aridity had a significant effect on the br GDGT distribution. This finding was confirmed by Menges et al. (2013), Yang et al. (2014a) and Zell et al. (2014) who demonstrated a systematic underestimation of soil pH in these arid environments. Seasonality is also suspected to impact the distribution in iso

and br GDGTs, as it could explain the warm bias in reconstructed temperatures observed in high latitudes (e.g. Wuchter et al., 2006; Pitcher et al., 2011b; De Jonge et al., 2014 and references therein) and is easily related to enhanced microbial activity during the warmer periods of the year.

The development of local calibrations (Tierney et al., 2010; Shevenell et al., 2011) which *de facto* integrate all the environmental parameters common to a specific region, notably those driven by climate, can be a powerful way to reduce the scatter and increase the accuracy of temperature reconstructions. However, one might wonder how much local these calibrations should be, *i.e.* at which scale they should they be developed? To a continental scale or within a geographically consistent part of a continent? To a country scale or to the one of a territory within a country? The more local the calibrations, the less relevant in explaining the dynamics of the environment they will be. Moreover, one might also wonder to which extent the results from two different local calibrations can be compared. Recently, Tierney and Tingley (2014) partly reconciled these two *a priori* antagonist goals (increasing the accuracy of the reconstructions while maintaining the universal character of the iso GDGT calibration) by developing a spatially flexible worldwide model for the TEX_{86} calibration called BAYSPAR. This model is based on the mathematical properties of Bayesian models, which allow the coefficients of the linear relationship between TEX_{86} and SST to smoothly change according to the geographical location of sampling. In a sense, it may be considered as combining all the regional calibrations into one. In our opinion, another major strength of this model is the fact that it is upgraded each time additional analyses of iso GDGTs in top sediment cores are made available, implying that the more data are added to the model, the more precise it should become.

1.2.3 Mid- and long-chain *n*-alkane distribution and hydrogen isotopic signature

1.2.3.1. Sources, biosynthesis and proxy development

Sources and biosynthesis

n-Alkanes are common lipids found in large quantities in all types of continental archives (Eglinton and Eglinton, 2008). Thorough studies of sediments, soils and living

organisms led to a classification of *n*-alkane producers based on the chain length of these compounds. It is commonly admitted that short even or odd numbered *n*-alkanes (< C_{21}) are mainly produced by aquatic micro- and macro-algae and cyanobacteria (Han et al., 1968; Gelpi et al., 1970), mid-chain odd numbered *n*-alkanes (C_{21} – C_{25}) by aquatic macrophytes (Ficken et al., 2000; Gao et al., 2001) and long odd numbered *n*-alkanes (> C_{25}) by terrestrial higher plants (Eglinton and Hamilton, 1967). In this document we will focus only on mid and long chain *n*-alkanes originating from plants. They are found in the epicuticular wax present at the surface of the aerial parts of the vegetation where they act as a protecting layer (Eglinton and Hamilton, 1967).

In photosynthetic organisms, *n*-alkanes are derived from the decarboxylation of *n*-alkanoic acids which are formed via the acetogenic biosynthetic pathway (Figure 14; Sachse et al., 2012 and references therein). This pathway consists in the conversion of the Acetyl-CoA precursor into a butyryl chain via multiple reactions mediated by the NADPH complex. The butyryl chain is further elongated to *n*-alkanoic acid by addition of C_2 units with a final step of decarboxylation leading to *n*-alkanes.

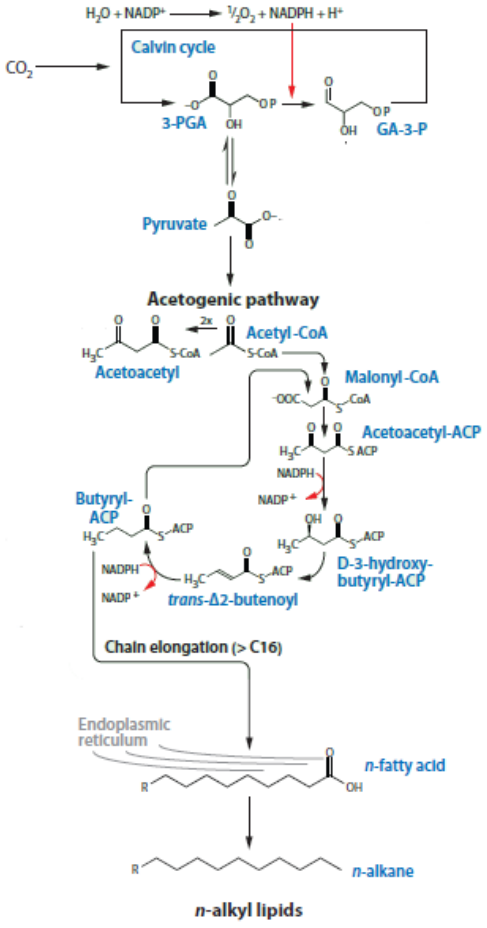

Figure 14: *n*-alkane biosynthetic pathway. *Adapted from Sachse et al. (2012)*

Proxies based on n-alkane distribution:

Based on (i) the biosynthetic pathway of *n*-alkanes and (ii) their distribution in living organisms, several proxies derived from their distribution in natural samples were developed. We will further describe the carbon preference index (CPI), the average chain length (ACL) and the P_{aq} index.

Carbon preference index (CPI)

The CPI index is a ratio assessing the relative importance of odd homologues over even ones (equation 17):

$$CPI = \frac{1}{2} \times \left(\frac{\sum C_{odd\ 25-33}}{\sum C_{even\ 24-32}} + \frac{\sum C_{odd\ 25-33}}{\sum C_{even\ 26-34}} \right) \qquad (17)$$

The almost exclusive presence of odd carbon numbered alkanes in plant waxes is the direct consequence of their biosynthetic pathway (see previous paragraph). Upon degradation, oxidation of alkanes result in the formation of the corresponding alkanoic acids which will then undergo decarboxylation yielding alkanes with one carbon less than in the initial chain, *i.e.* with even carbon number chain. As a result, CPI is supposed to be high (>> 1) in immature sediments and to decrease with increasing degradation processes (Killops and Killops, 2005). In recent sediments, unusually low CPI values can be due to petroleum pollution (Bray and Evans, 1961) or wood burning (Standley and Simoneit, 1987)

Average chain length (ACL):

Weighted average chain length of *n*-alkanes is usually calculated as follows (equation 18):

$$ACL = \frac{\sum C_i \times i}{\sum C_i} \qquad (18)$$

Several factors have been suggested to impact the ACL values. First of all, as described earlier (section 1.3.2.1), a change in vegetation will likely be reflected in ACL values, as aquatic macrophytes generally synthesise shorter *n*-alkanes than higher plants in average (e.g. Ficken et al., 2000). Similarly, *n*-alkanes in herbaceous species were found to be dominated by carbon chain length higher than 31 (Rommerskirchen et al., 2006) leading to rather high ACL values. In addition, some authors have observed a relationship between ACL and air temperature (Gagosian and Peltzer, 1986;

Rommerskirchen et al., 2003; Zhang et al., 2006). Rommerskirchen et al. (2003) suggested that higher ambient air temperature may lead to an increase in the *n*-alkane chain length, reflecting an increase in the melting point of the epicuticular waxes. Alternatively, some authors observed a relationship between ACL and aridity, with longer *n*-alkane chain length in arid environments (Schefuß et al., 2003; Liu and Huang, 2005). This relationship is in agreement with the accepted assumption that drier environments are generally characterised by an increased contribution of herbaceous species, resulting in an increased contribution of C_{31} *n*-alkane homologues. However the relationships between climate parameters and ACL remain putative, as they were never demonstrated in controlled experiments (like greenhouses).

P_{aq} index

As specified earlier (section 1.3.2.1), mid-chain *n*-alkanes (C_{21} - C_{25}) were observed to be more abundant in macrophytes than in higher terrestrial plants (Ficken et al., 2000; Gao et al., 2011). In order to track the potential colonization of freshwater bodies by vegetation, Ficken et al., (2000) proposed the P_{aq} index (equation 19):

$$P_{aq} = \frac{C_{23}+C_{25}}{C_{23}+C_{25}+C_{29}+C_{31}} \qquad (19)$$

When P_{aq} values are higher than 0.4, the contribution of submerged/floating macrophytes to the total *n*-alkane pool is supposed to be high, whereas it is supposed insignificant when P_{aq} values are below 0.1. Intermediate values, $0.1 < P_{aq} < 0.4$, correspond to a colonization of the lake edges by emergent macrophytes. This index could further be used to reconstruct past lake level fluctuations, if we assume that a shallow lake will be more prone to vegetation colonization.

Methodological improvements (Scrimgeour et al., 1999) allowed to determine the hydrogen isotopic composition (δ^2H) of individual compounds thanks to high temperature conversion interface. This led to the thorough investigation of the δ^2H of n-alkanes and of its potential as environmental proxy.

1.2.3.2. Origin and variability of the hydrogen isotopic signature of *n*-alkanes (δ^2H_{wax}) and proxies based on δ^2H_{wax}

Source water isotopic signature:

The initial source of hydrogen for plants is the closest source of meteoric water, either soil water (further taken up by roots) or continental water reservoirs (wetlands such as lakes, rivers, peatlands ...). The isotopic signature of these water bodies will mainly depend on that of precipitations, which varies of more than 400‰ (Sheppard, 1986). (Dansgaard, 1964) described the different processes impacting the isotopic signature of precipitations. Because of Rayleigh equilibria, the light ^1H isotope will always preferentially evaporate, whereas the heavier ^2H isotope will more easily precipitate. The variation in $^2H/^1H$ ratio in the water cycle from the oceans to the inland precipitations can be deduced from this assumption (Figure 15). Clouds formed from the evaporation of aquatic (essentially oceanic) masses will get progressively ^2H-depleted as they are pushed further inlands. This effect is known as the continental effect (Dansgaard, 1964) and was found to be the first one to rule the isotopic signature of meteoric water. The second effect ruled by Rayleigh equilibrium is the temperature effect: the colder the temperature, the more ^2H-depleted the water mass becomes. This effect controls the latitudinal isotopic composition of precipitations (Figure 15). Furthermore, when air masses circulate upwards along altitudinal transects, successive Rayleigh equilibria will lead to a progressive ^2H-depletion of the air masses as they rise up. This effect is called the altitudinal effect. The last effect is limited to tropical regions where rain falls abundantly. It is referred to as the amount effect and results in ^2H-depletion of the precipitations because of the wringing out of the light isotope.

^2H-enrichment of the soil water can occur if the area is submitted to high evapotranspiration rates, the latter phenomenon depending on the relative humidity and temperature of the site. As for the isotopic signature of lakes, it is related to its water budget, *i.e.* the sum of the inflow and outflow water. In the case of climate-sensitive lakes, such as those studied in this thesis, the main driver of the water is the difference between the precipitation and evaporation rates (P-E). Variations in this difference will directly impact the isotopic signature of the wetland as the light ^1H isotope will be preferentially evaporated, leading to a ^2H-enrichment of the water body, while in tropical areas the amount effect related to high precipitation rates may lead to ^2H-depletion of the water of the lake.

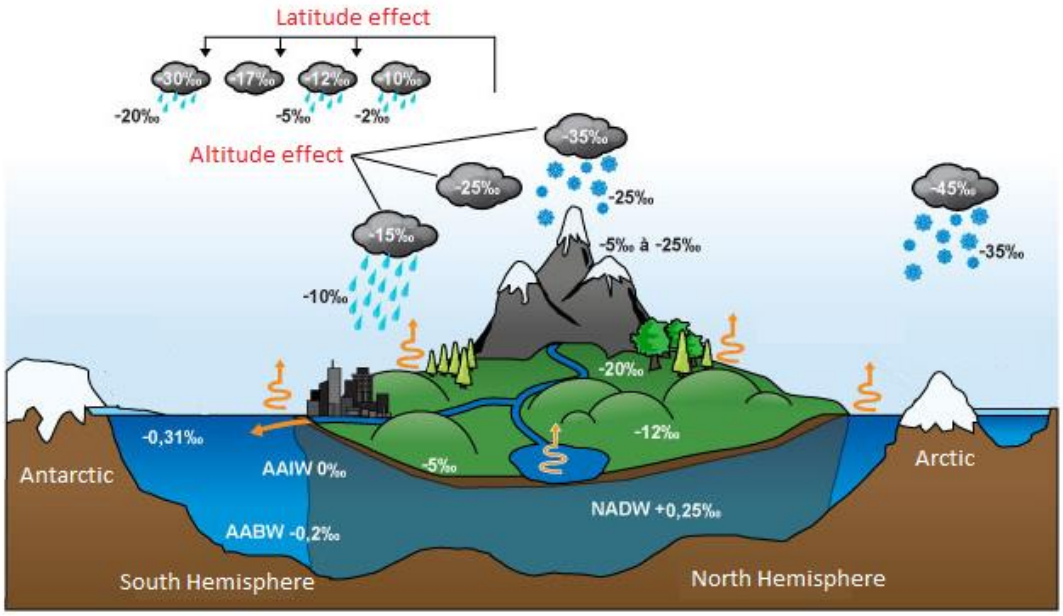

Figure 15: Hydrogen isotopic composition variations in the water cycle. Numbers must solely be considered as illustrations of the enrichment or depletion trend but not as measured values. *Adapted from La géochimie : Un outil pour l'étude de l'environnement (MOOC proposed by the French virtual university of environment and sustainable development).*

δ^2H of n-alkanes:

Several studies have shown that the δ^2H of *n*-alkanes produced by plants (δ^2H_{wax}) is directly correlated to the isotopic signature of their water source although systematically ^2H-depleted (e.g. Estep and Hoering, 1980; Sessions et al., 1999; Sauer et al., 2001). This ^2H-depletion is due to (i) fractionation occurring during *n*-alkane biosynthesis and (ii) physical processes, as detailed below. The δ^2H difference between these lipids and their source water is expressed by the apparent fractionation (equation 20):

$$\varepsilon_{l/w} = \frac{\delta^2H_{lipid} + 1}{\delta^2H_{water} + 1} - 1 \qquad (20)$$

Fractionation related to biosynthesis:

Any addition, elimination and exchange of hydrogen during the biosynthesis of *n*-alkanes can potentially cause hydrogen fractionation relative to the source water. First fractionation occurs during photosynthesis, *i.e.* during the production of 3-PGA (3-phosphoglyceric acid) and GA-3-P (glyceraldehyde-3-phosphate) in the Calvin cycle and is estimated to be ca. -171‰ (Yakir and DeNiro, 1990). Successive hydrogen fractionation is regulated by H additions in the acetogenic pathway via reaction with the

NADPH (nicotinamide adenine dinucleotide phosphate (reduced)) which is highly ^{2}H-depleted (ca. -200‰ relative to the cell water, Sachse et al., 2012). The relative impact of the NADPH – which depends on its biosynthetic pathway – on the δ^2H of lipids is poorly understood but could be significant (Sachse et al., 2012). Final fractionation occurs during the chain elongation by Acetyl-CoA units addition (Figure 14).

Fractionation related to evapotranspiration processes

As described above, biosynthesis of *n*-alkanes takes place in the leaf cells. Thus their isotopic signature will also depend on the fractionation of the leaf water. The latter will depend on the transpiration rates of the leaves as the lighter water (with the ^{1}H isotope) will evaporate faster than the heavier one. Transpiration of leaves will depend on several environmental factors including relative humidity, ambient temperature and partial pressure in CO_2 (P_{CO2}) (Sachse et al., 2012). Recently, Kahmen et al. (2013a, 2013b) demonstrated experimentally that the ^{2}H-enrichment due to evaporation has a significant effect on the isotopic signature of *n*-alkanes.

Proxy development

Because preliminary studies showed that δ^2H_{wax} was related to δ^2H of precipitations (e.g. Estep and Hoering, 1980; Sessions et al., 1999; Sauer et al., 2001), it was proposed as a proxy to reconstruct past hydrological regimes: humid climates should be characterized by ^{2}H-depletion of the *n*-alkane isotopic signature relative to arid climates (Sessions et al., 1999; Sauer et al., 2001). Successful applications of this proxy was notably shown in central Africa where it was investigated along riverine and lacustrine sediment cores (Schefuß et al., 2005; Tierney et al., 2011). Recently, Jia et al. (2008) proposed to use the δ^2H_{wax} to predict changes in meteoric water isotopic composition along a Chinese altitudinal gradient, the latter being related to temperature variations. They suggested that the δ^2H_{wax} could be applied as a proxy of paleoaltitude.

1.2.3.3. Current limitations and perspectives for research

OPEN RESEARCH QUESTION: Constrain the sources of variability of the n-alkane-derived proxies to improve their specificity

The widespread occurrence of *n*-alkanes can lead to misinterpretation of their distribution in the sedimentary record. Indeed, in addition to plants, several other organisms, such as microbes and fungi, have been observed to produce *n*-alkanes (Nguyen Tu et al., 2000) with similar chain length. Moreover, early diagenesis was also found to impact the *n*-alkane distribution in soils (e.g. Nguyen Tu et al., 2004). The sole application of *n*-alkane distribution-derived proxies can thus become hazardous and these proxies should rather be applied in combination with other proxies characterizing the OM such as light microscopy observations (pollen, macro-fossils, palynofacies), bulk elemental analysis (e.g. C/N ratio) and/or investigation of other plant biomarkers.
The aforementioned limitations in the application of *n*-alkane distribution-derived proxies also impact the δ^2H_{wax}-derived proxies. Indeed, it is difficult to quantify the relative contribution of the different potential sources of *n*-alkanes in sediment and soil archives. Thus, if we cannot identify which organisms produced the studied *n*-alkanes, it is challenging to interpret their observed isotopic signature. In addition, the apparent fractionation of *n*-alkanes was observed to differ from one species to another (Chikaraishi and Naraoka, 2007; Hou et al., 2007; Pedentchouk et al., 2008; Feakins and Sessions, 2010). Therefore, variations of the δ^2H of *n*-alkanes could result from changes in vegetation source instead of climatic changes. Preliminary study on early diagenesis of *n*-alkanes in soils observed that it also seemed to impact their δ^2H values (Zech et al., 2011). Therefore, additional studies in controlled experiments and different environmental settings are needed (i) to better track the variations of *n*-alkane isotopic signature, from their biosynthesis to their preservation in sedimentary archives and (ii) to quantify the relative importance of biological and climatically-driven effects on these variations.

1.2.4 Applicability in continental archives:

In this section, the applicability of proxies based on GDGTs and *n*-alkanes in continental settings (paleosols, peatlands and lakes) will be discussed, with a particular focus on the remaining questions and locks to tackle.

1.2.4.1. In loess-paleosol sequences:

GDGTs and δ^2H_{wax} have rarely been investigated in loess-paleosol sequences. One of the major studied site is the loess plateau in China. The latter exhibits loess-paleosol sequences over more than 640 000 km². Peterse et al. (2011, 2014), Gao et al. (2012) and Jia et al. (2013) successfully used br GDGTs in this site for the reconstruction of past MAAT in East Asia. They found that temperature was driven by variation of the Northern Hemisphere insolation and observed a lag between MAAT variation and the onset of monsoon precipitations. In addition, Zech et al. (2012) analysed br GDGTs along three loess-paleosol sequences in Serbia, Siberia and Tanzania. Relative variations in br GDGT-derived MAAT were consistent with those obtained from other proxies but absolute MAAT estimates were observed to be often unrealistically high. This warm offset could be due to post depositional production of br GDGTs in the loess-paleosol sequences, leading to an overprint of the initial br GDGT signal (Huguet et al., 2012, 2013b).

n-Alkane distribution in loess deposits was notably investigated by Zhang et al. (2006) and Bai et al. (2009) who both successfully reconstructed past vegetation successions in the Chinese Loess Plateau. Liu and Huang (2005) measured the δ^2H of *n*-alkanes in a loess-paleosol sequence covering the last 130 kyrs in the Chinese Loess Plateau and found its variations to be highly correlated to magnetic susceptibility measurements, which is an established proxy for monsoon circulation.

In parallel to the aforementioned studies in loess-paleosol archives, the applicability of GDGT- and *n*-alkane-based proxies was also tested in modern surface soils – considered as modern equivalent of the paleosols – and especially along altitudinal gradients. The latter have indeed the advantage of presenting natural variations in temperature and can therefore be used as *in situ* tests of the response of biomarkers to temperature changes. To the best of our knowledge, GDGTs have been investigated so

far along 7 mountains located all around the world, *i.e.* in (i) Asia (Mts. Meghalaya, Ernst et al., 2013 ; Jianfengling, Huan et al., 2012; Shennongjia, Yang et al., 2014c ; Gongga, Peterse et al., 2009b; Xiangpi, Liu et al., 2013), (ii) Africa (Mts. Kilimanjaro, Sinninghe Damsté et al., 2008) and (iii) South America (Mt. Andean, Anderson et al., 2014). Br GDGT-derived MAAT were found to correlate with altitude along all the gradients, even though a high degree of scatter was observed for some mountains (e.g. Mt. Gongga; Peterse et al., 2009b). In addition, a significant relationship between TEX_{86} and MAAT was observed along Mt. Xiangpi (Liu et al., 2013). This suggests that temperature may also have an influence on the distribution of iso GDGTs in soils and that, in certain circumstances, TEX_{86}, which was initially developed in aquatic environments, could be applied as a temperature proxy in soils as well.

δ^2H_{wax} was investigated along several mountains in Asia (Ernst et al., 2013; Jia et al., 2008; Luo et al., 2011) where it systematically exhibited a ^2H-depletion trend with altitude. However in Africa, Peterse et al. (2009b) did not find such a trend along Mt. Kilimanjaro (Tanzania). They postulated that the "amount effect" (cf. section 1.2.3.2.) overprinted the temperature effect. GDGTs and δ^2H_{wax} were jointly analysed along some altitudinal gradients (Peterse et al., 2009b; Ernst et al., 2013; Zhuang et al., 2015). It was argued that altitudinal changes could be assessed more reliably using two proxies by compensating the discrepancy of GDGTs and δ^2H_{wax} in certain settings (*i.e.* in arid soil for GDGTs or in tropical areas for $\delta^2H_{wax;}$ (Peterse et al., 2009b). Based on the previous studies which demonstrated a variation of δ^2H_{wax} with altitude, Polissar et al. (2009) and Hren et al. (2010) successfully applied δ^2H_{wax} to reveal the uplift history of the Sierra Nevada and the Tibetan plateau respectively. However, such applications are only possible if the compared paleosols have the same age and underwent similar climatic conditions.

1.2.4.2. In peatlands:

Br GDGTs were discovered for the first time in a peatland from the Netherlands (Sinninghe Damsté et al., 2000). These compounds were then analysed in several European peatlands, where they were always found to be highly abundant (Weijers et al., 2004, 2006a, 2009, 2011; Huguet et al., 2010a, 2013a, 2014; Liu et al., 2010) which led to suggest that br GDGT producers must be anaerobes (see details in section 1.2.2.1.). However, few studies reconstructed past temperature variations from brGDGT distribution in peatlands. Weijers et al. (2011) observed a warm bias when reconstructing past temperature from br GDGTs in a peat core from the Swiss Jura Mountains covering the last 13 000 yrs BP. Similarly, Huguet et al. (2013a) showed that MBT/CBT-derived MAAT estimates overestimated recorded MAAT in surficial peat samples from the French Jura Mountains. This may be due to additional parameters impacting br GDGT distribution, such as soil water content and vegetation cover, as already discussed (see section 1.2.2.3). In contrast, Ballantyne et al. (2010) reconstructed Pliocene MAAT with three independent proxies including br GDGTs, $\delta^{18}O$ and growth rings of tree fossils and vegetation macroremain taxa assemblages. They did not observe major differences between MAAT estimates obtained from br GDGTs. In addition, Weijers et al. (2011) observed that br GDGT-derived pH recorded the transition from a *Carex*-dominated fen to a *Sphagnum*-dominated bog, the latter being usually more acidic than the former, even though the pH amplitude reconstructed with the br GDGTs was probably overestimated. Combined together, the few results obtained in peatlands until now indicate the potential of br GDGTs as temperature and pH proxies in peatlands, but suggest that br GDGT calibrations specific to peatlands should be developed to take into account the unique environmental characteristics of these ecosystems.

Recently, Nichols et al. (2014) successfully used br GDGTs and *n*-alkane isotopic signature to track the impact of climate change on the vegetation assemblage in an Alaskan peatland. They combined br GDGT-derived pH and *n*-alkane distribution to monitor changes in vegetation along the peat core, and δ^2H_{wax} and MBT/CBT indices to record past changes in hydrology and temperature respectively. Although the absolute br GDGT-derived temperatures were warmer than expected, as previously observed by Weijers et al. (2011) and Huguet et al. (2013a), the reconstructed temperature variations

were highly consistent with nearby records of glacial ice extent variations (Nichols et al., 2014).

The use of *n*-alkanes in peatlands was directed towards the identification of biomarkers for *Sphagnum*. These mosses dominate the waterlogged peatlands and play an important role in maintaining the physical and chemical equilibrium necessary for the peatland preservation, notably due to the large amount of biomass they produce. It has been observed (Charman, 2002) that *Sphagnum* was more abundant during wet periods while peatlands tended to be colonized by sedge type species during dryer periods. Several studies showed that the C_{23} *n*-alkane was indicating *Sphagnum* presence (Nott et al., 2000; Baas et al., 2000; Pancost et al., 2002; Nichols et al., 2006). Nichols et al. (2006) successfully tracked hydrological variations in an American peatland by determining *Sphagnum* relative abundance from C_{23} *n*-alkane variations along the core. Alternatively, Zhou et al. (2005, 2010) used *n*-alkane distribution, notably ACL proxy, combined with pollen assemblage, C_{org} and fatty acid analyses to demonstrate vegetation changes associated with climatic changes over the studied period (late glacial and Holocene). Xie et al. (2000, 2004) investigated the δ^2H of individual *n*-alkanes in two British peat cores and observed higher variations for the δ^2H of C_{23} *n*-alkane than that of C_{29} *n*-alkane. They concluded that, in *Sphagnum*-dominated peatlands, the δ^2H of C_{23} *n*-alkane was a promising proxy for the reconstruction of hydrological variations. More recently, Seki et al. (2009) and Nichols et al. (2010) proposed to track the precipitation - evaporation balance (P-E) at the surface of the peatland by measuring the difference between (i) the δ^2H of the C_{29} *n*-alkane, representative of vascular plants taking up water in the deep layers of the peat, hence non-impacted by the evaporation, and (ii) the δ^2H of the C_{23} *n*-alkane produced by *Sphagnum* at the surface of the peat and hence impacted by evaporative processes. They successfully applied this approach to a 3000-year peat core from Minden Bog (Michigan, USA). To the best of our knowledge, the applicability of *n*-alkanes as vegetation and hydrological proxies in peatlands which are not dominated by *Sphagnum* remains poorly documented.

1.2.4.3. In lakes:

Iso GDGTs were detected not only in marine but also in lacustrine sediments (Powers et al., 2004), leading to the development of lacustrine calibrations between TEX_{86} and lake surface temperature (LST; Powers et al., 2005, 2010):

$$LST = 55.2 \times TEX_{86} - 14.0 \quad (R^2 = 0.86;\ n = 12) \quad (21)$$

However, as stressed in section 1.2.2.2., iso GDGT producers in lakes are not necessarily Thaumarchaeota. Contribution from methanogenic and methanotrophic archaea have been found to be dominant in some lakes (Powers et al., 2005; Blaga et al., 2009), which prevented the application of the TEX_{86} in those lakes (see section 1.2.2.2.). In order to determine when TEX_{86} could be applied to reconstruct LST, (Blaga et al., 2009) developed the I/VI ratio (see section 1.2.2.2.). It seems from these first observations that large lakes are more suitable for the use of TEX_{86} as paleothermometer than small ones (Powers et al., 2010).

Br GDGTs were also detected in lakes and sometimes in larger amount than iso GDGTs (Blaga et al., 2009; Sinninghe Damsté et al., 2009; Tierney and Russell, 2009; Bechtel et al., 2010; Powers et al., 2010; Loomis et al., 2011). As detailed in section 1.2.2.2., Hopmans et al. (2004) initially hypothesized that br GDGTs in lakes were derived from catchment soils. Nevertheless, it is now admitted that br GDGTs can also be produced *in situ* in lakes, in the water column and/or sediment. Two points were put forward to account for this production: (i) br GDGT distribution was observed to differ between the water column and surface sediment on the one hand and surrounding soils on the other hand, and (ii) br GDGTs were shown to be more abundant in lake sediments than in surrounding soils (Tierney et al., 2012; Buckles et al., 2014; Loomis et al., 2014a, 2014b). Depending on the investigated lake, br GDGT can derive either from soils or from lacustrine water column/sediment, or even from a mixture of both. *In situ* production of br GDGTs was further observed in river and marine sediments (Zell et al., 2014) generally leading to an underestimation of MAAT estimates when the soil calibrations by Weijers et al. (2007) or Peterse et al. (2012) are used for temperature reconstruction. Consequently, specific lacustrine calibrations were developed to take into account the *in situ* production of br GDGTs in lake. The development was made either at the global scale (Pearson et al., 2011) or at the regional one (Zink et al., 2010; Sun et al., 2011) and notably in East Africa (Tierney et al., 2010; Loomis et al., 2012).

Further research is now needed to assess the reliability of these recently developed lacustrine calibrations and to determine where br GDGTs are produced in aquatic ecosystems, *i.e.* at which depth(s) in the water column and in the sediment. In this thesis, the most recent lacustrine calibration for East Africa (equation 22; Loomis et al., 2012) was used when necessary:

$$MAAT = 22.77 - 33.58 \times f(VIIa) - 12.88 \times f(VIIIa) - 418.53 \times f(VIIIc) + 86.43 \times f(IXb) \quad \text{(RMSE = 1.9 °C)} \quad (22)$$

Where *f(x)* is the fractional abundance of the compound x relative to the total br GDGTs.

n-Alkane distribution and isotopic signature have been extensively studied in lake sediments where these compounds are largely abundant. Several studies (e.g. Schwark et al., 2002; Hanisch et al., 2003; Castañeda et al., 2009; Castañeda and Schouten, 2011) used *n*-alkanes to reconstruct the past vegetation changes of the catchment area to infer climatic variations from this vegetation succession. However, due to the limitations expressed earlier (section 1.2.3.3.), it is often difficult to draw clear conclusions from the sole *n*-alkane distributions. *n*-Alkane-derived proxies, such as ACL or P_{aq}, are rather used to support results obtained from other biomarkers or proxies. As for the analysis of *n*-alkane isotopic signature, it seems promising. Several studies indeed showed that, in lacustrine sediments, long chain *n*-alkanes (C_{27}, C_{29}, C_{31}) record the δ^2H signal of meteoric water (Sauer et al., 2001; Sachse et al., 2004; Mügler et al., 2008) while short and mid chain *n*-alkanes (C_{17}, C_{19}, C_{23}, C_{25}) seem to record δ^2H values of lake water (Sauer et al., 2001; Huang et al., 2004; Sachse et al., 2006; Hou et al., 2008). Based upon the assumption that the aquatic vegetation (algae, submerged/floating macrophytes) is not impacted by evapotranspiration processes, Sachse et al. (2004, 2006) proposed to use the difference between the C_{31} and the C_{17} *n*-alkanes isotopic signatures ($\Delta\delta^2H_{wax}$) as a proxy for terrestrial evapotranspiration. First applications of this proxy showed contrasted results (Mügler et al., 2008; Aichner et al., 2010; Rao et al., 2014), essentially because some macrophytes, and not only terrestrial plants, can also produce C_{31} *n*-alkanes, leading to biased δ^2H values of C_{31} *n*-alkanes. Recently, Garcin et al. (2012b) investigated δ^2H of *n*-alkanes in lacustrine sediments along a latitudinal transect in West Africa. They found that in this region, unlike in Europe (Sachse et al., 2004, 2006), the δ^2H of the C_{17} *n*-alkane was not correlated with the δ^2H

of lake water due to multiple sources for this compound. They also showed that the δ^2H of the C_{29} and C_{31} *n*-alkanes were correlated to different source waters suggesting that they were produced by different vegetation types. These findings highlight the necessity to carefully examine the vegetation of lake catchment area before using δ^2H_{wax} for paleohydrological reconstruction in these environments and the need for additional research on the applicability of the δ^2H_{wax} proxy in tropical areas.

1.3. Conclusions

This review of the literature highlighted lacks in the understanding of Late Holocene tropical continental records, especially, the spatial heterogeneity and the short-scale drivers of climatic variations are not well constrained. The use of ubiquitous biomarkers, such as GDGTs and *n*-alkanes, should help addressing these gaps in knowlege. However, as they are derived from living organisms, the signal they encompass is necessarily complex. There is therefore a need to determine the robustness of their link to environmental parameters (temperature, hydrology) before expanding their use to a broader paleoclimatic context. This work therefore combines methodological studies and multi-proxy applications to investigate the potential of these two promising biomarkers in a delimited and geologically well-constrained area of East Africa.

Chapter 2.

Study site: The Rungwe Volcanic Province

2.1. Geology, climate and vegetation of the region

The Rungwe volcanic province (RVP), located in the southwest of Tanzania, is a large volcanic mountain region (1,500 km²; Fontijn et al., 2012) in the western branch of the East African Rift System (EARS; Figure 16). The RVP is delimited by the Poroto mountains in the north, the Lake Malawi in the south and the Livingstone escarpment in the west (Figure 16). The region began being volcanically active in the late Miocene (9.2 Ma) and is still active today. The last eruption (Mt. Kiejo) was recorded at the end of the 19th century (Harkin, 1960). Several maar-type craters were created during the late Pleistocene phreatomagmatic explosions along the Mbaka fault system (Figure 16; Fontijn et al., 2012), which is now harbouring closed crater lakes.

The RVP belongs to the humid equatorial zone of Africa, mainly dependent on the migration of the intertropical convergence zone (ITCZ). The ITCZ is a zone of low pressure air masses accompanied by abundant precipitations (cf. details in section 1.1.1). In East Africa, the major source of moisture is the Indian Ocean, as the eastern trade winds get loaded in water vapour when they flow above the ocean and condensate when they converge in the ITCZ (van der Ent and Savenije, 2013). In January, the ITCZ reaches its southernmost position (centered at ca. 15°S) which results in the RVP in the alternation of a hot humid season from November to May and a relatively colder dry season from June to October (Figure 17). Precipitations reach 1980 mm/yr, with April being the most humid month (465 mm/yr) of the year and September the driest (11 mm/yr). Air temperature varies slightly along the year, from 19 °C in July to 25 °C in November, leading to a mean annual air temperature (MAAT) of 22.3°C (Figure 17). The RVP is among the most humid regions of Tanzania together with the coastal zone (Basalirwa et al., 1999), as moisture recycled over lake Malawi then condensates above the RVP because of the orographic effect of the Poroto mountains. Additional rainfalls in June and October maintain permanent wet conditions in the upper mountain (Williamson et al., 2014)

Vegetation of the region belongs to the Zambezian type (White, 1983). It comprises semi-deciduous humid Miombo forests below 1500 m, composed of *Caesalpiniaceae*, mainly *Brachystegia*, *Isoberlinia* and *Julbernardia*, and Afromontane

evergreen forest, bamboo forest and montane grassland above 1500 m (Vincens et al., 2003). Increasing cultivation of the lowland zone is altering this biota by (i) decreasing the tree cover and (ii) replacing endemic species by standardized crop species (Williamson et al., 2014).

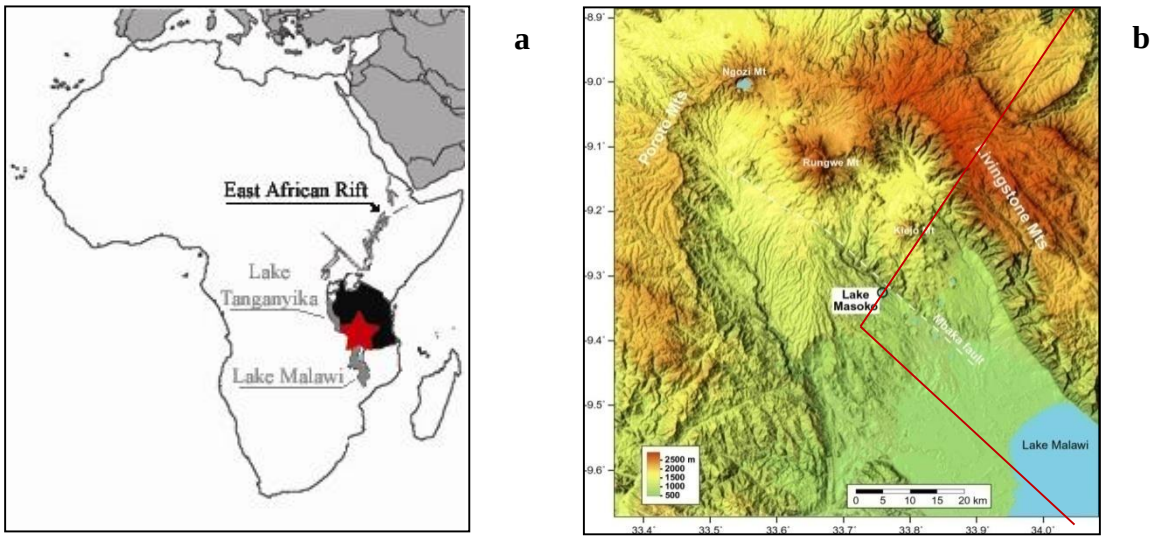

Figure 16: (a) Location map of the Rungwe Volcanic Province (RVP), at the extremity of the western branch of the East African Rift System (after Delalande, 2008). (b) Digital elevation model of the RVP, (after Garcin, 2006).

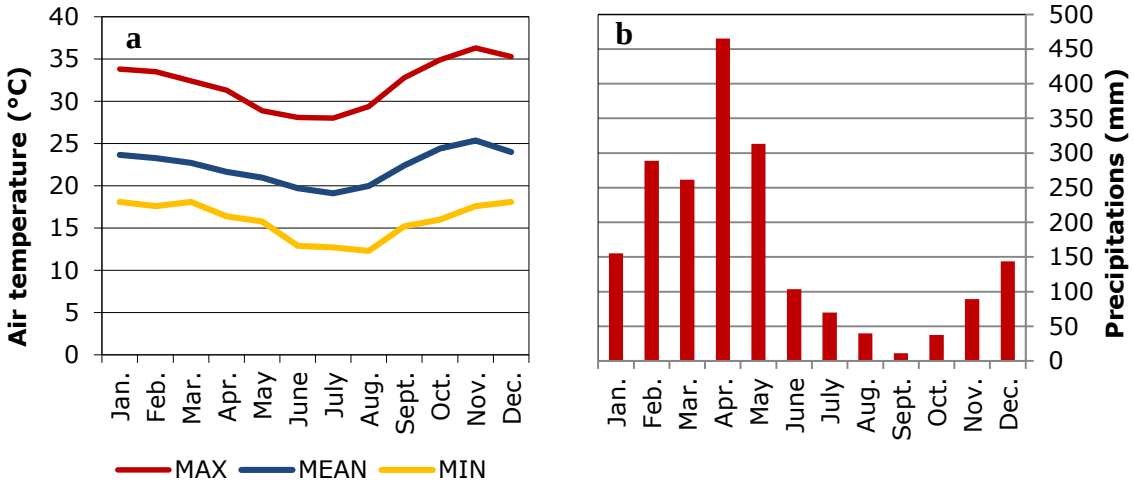

Figure 17: (a) 3-year mean (2010-2013) monthly mean, maximum and minimum air temperatures and (b) 8-year mean (2006-2014) monthly precipitations at Masoko weather station (840 m.a.s.l.).

2.2. The Kyambangunguru marsh

The Kyambangunguru marsh (9°22' S - 33°47' E, 660 m a.s.l.) is located in a maar crater. The inner marsh is ca. 0.04 km² and its catchment area, limited to the crater slopes, is relatively small (0.20 km²; Delalande, 2009). The slopes of the crater are steep and covered by typical humid Miombo forest, dominated by *Brachystegia*, *Uapaca* and *Acalypha* tree species (Figure 19a; A. Vincens and G. Buchet, unpublished results). Shrubs of *Rubiaceae* and *Myriaceae* families are present at the edge of the marsh. The inner marsh comprises peat mats and water holes (Figure 19b). The vegetation of the peat mats is dominated by *Cyperaceae* sedges (*Carex, Cyperus)* while floating (*Nymphaea*) and submerged macrophytes are abundant in the water holes. The marsh has a dual facies (Figure 18 and Figure 19), alternating between a water saturated peatland during the dry season and a small lake – 1.5 m maximal depth (Figure 18) – at the end of the wet season.

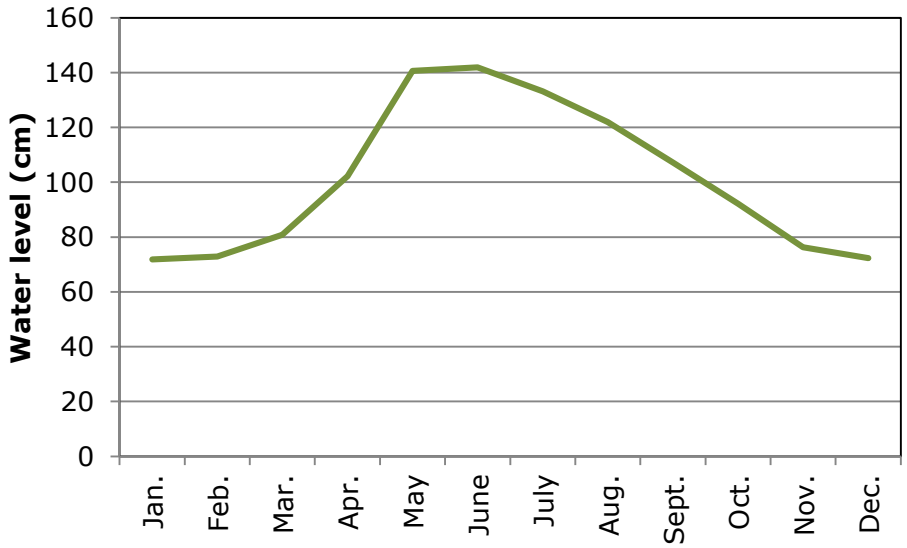

Figure 18: 6-year (2006-2014) mean monthly water level of Kyambangunguru marsh at the gauge (see Figure 19b)

Figure 19: Photographs of the Kyambangunguru crater marsh taken in July 2014 and highlighting the difference in vegetation cover between (a) the slopes and (b) the marsh.

Figure 20: Photograph of Lake Masoko bank (as of July 2014), illustrating its topography and vegetation cover.

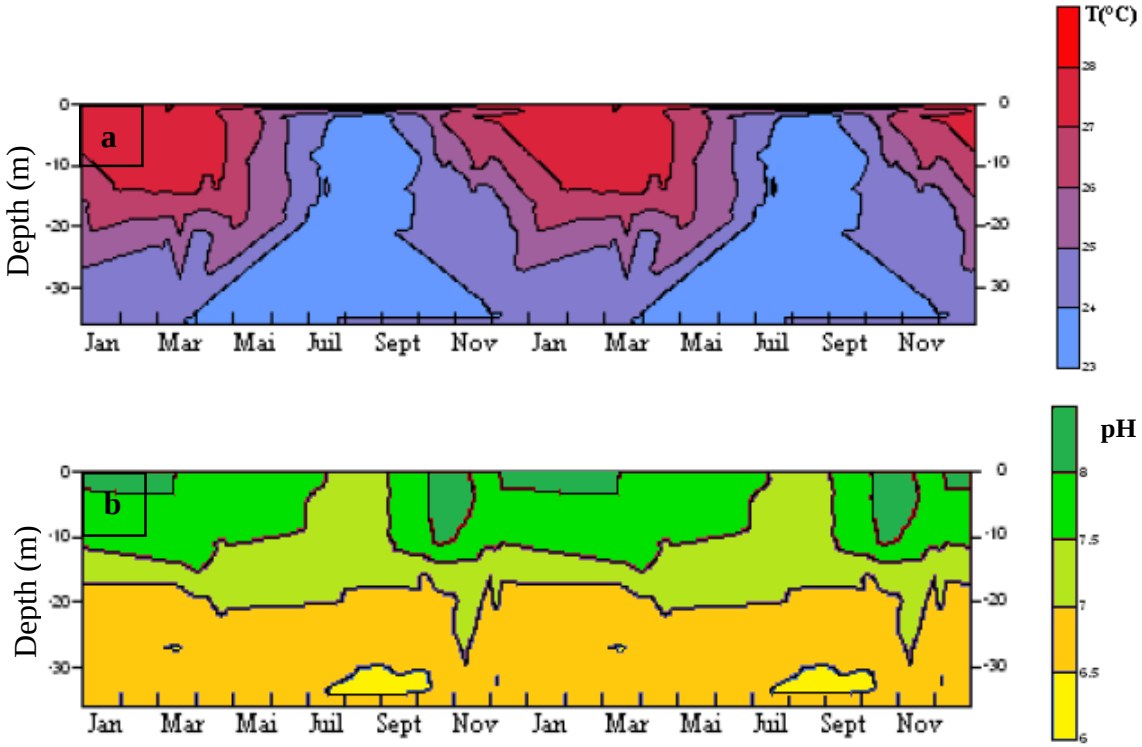

Figure 21: Monthly mean temperatures (a) and pH (b) of Lake Masoko water column. *Adapted from Kayvantash, 2012.*

2.3. Lake Masoko

Lake Masoko (9°20.0' S, 33°45.3 E) is a 39 m depth maar lake located at ca. 840 m.a.s.l. in the RVP (Figure 20). Its catchment area is small (0.57 km²) relative to its surface area (0.36 km²) and is covered by low altitude Miombo-like vegetation (see section 2.1). It is a monomictic-type lake, stratified from September to June. During the stratified season, mean surface temperature is 28.2 ± 0.2 °C and surface pH is ca. 8.5, while the mean temperature of the bottom layer is 23.5 ± 0.5 °C and its pH is 6.7 (Figure 21; Kayvantash, 2012). Mixing of the whole water column occurs once a year during the dry season (June-October), when air temperature is lower and winds at the lake surface are stronger. The water column temperature is then homogenized at ca. 23.0 °C, while surface pH decreases to 7.4 (Figure 21; Kayvantash, 2012). An oxycline is located between 16 and 24 m depth during the stratified season (Figure 22), with oxygenated water at the surface and anoxic ones at depth. During the dry season, this oxycline disappears and the whole water column is then well oxygenated. The lake is oligotrophic, *i.e.* its nutrient and mineral concentrations are low, as evidenced by the conductivity values which are stable at ca. 40 µS/cm all along the water column (Figure 22). As a result, its productivity is low.

Lake Masoko is mainly supplied by precipitations (75 %) and to a lower extent by a regional superficial groundwater reservoir. 60 % of the output is underground, the rest being due to evaporation processes (Bergonzini et al., 2001; Delalande et al., 2005).

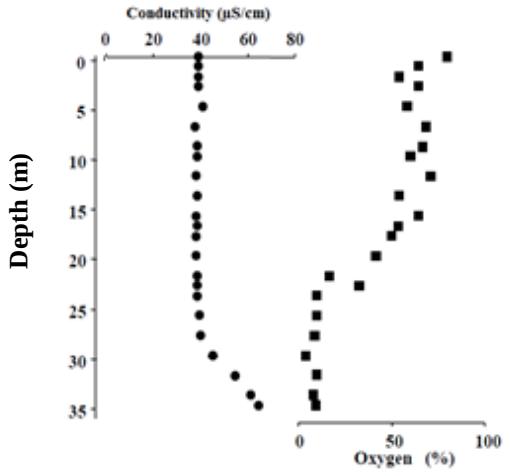

Figure 22: Conductivity and oxycline of Lake Masoko water column. *Adapted from Delalande, 2008 and de Mesmay, 2008.*

Chapter 3.

Materials & Methods

3.1. Sampling

Three field campaigns were carried out in the RVP in April 2012, December 2012 and July 2014. Most samples of this thesis were collected during these campaigns. The sample set includes 52 surface soils (0-5 cm) and vegetation leaves (from 78 specimens, details in Appendix 1) collected along Mt. Rungwe from 500 to 2800 m.a.s.l., 10 sediments collected at the edge of the Lake Masoko or at the bottom of the water column as well as 8 particulate organic matter (POM) samples collected at different depths (5, 18 or 33 m) in the water column of the Lake Masoko. Details about sampling are summarized in Appendix 1.

In addition, two cores were investigated in this thesis. First, a 4 m peat core was collected in December 2012 in the center of the Kyambangunguru crater marsh with a Wright piston corer and sampled in the field at 1 cm resolution. GDGTs and *n*-alkanes were analysed in 35 samples evenly distributed along this core. Second, a 2.70 m sediment core was collected in Lake Masoko in 2007 by David Williamson and the RESON team and then kept in a cold room (4 °C) at CEREGE (Aix-en-Provence, France). This core was sampled at a 1 cm resolution in June 2014. GDGTs and *n*-alkanes were analysed in 50 samples evenly distributed along this core.

Last, 20 surface soil samples were collected in 2013 along Mt. Kenya (Kenya) from 1900 to 3160 m by Tina Omuombo and David Williamson. The abundance and distribution of GDGTs and *n*-alkanes in soils from Mt. Kenya and Mt. Rungwe were compared (see section 4.2).

All samples were kept at -20 °C in Paris (France) and then freeze-dried, except for vegetation samples which were collected in paper envelopes, naturally dried under ambient conditions and then grinded before transportation to France. Note that for each specimen (see Appendix 1) several leaves were sampled and then pooled before grinding to get an averaged signal.

3.2. Extraction, separation and additional treatments of lipids

Three different protocols were used for lipid extraction according to the type of sample and the molecules investigated. Protocol 1 was used for samples where only GDGT core lipids (CLs) were investigated, *i.e.* soil samples from the altitudinal transects (results in Chapter 4) and from the Lake Masoko sediment core (results in Chapter 6). Indeed previous study showed that extraction with ASE could deteriorate part of intact polar lipids (IPLs; Huguet et al., 2010). In contrast, protocol 2, gentler, was used for simultaneous extraction of CL and IPL GDGTs, *i.e.* for the Kyambangunguru peat core, soils and sediments surrounding Lake Masoko and POM from its water column. An alternative protocol, protocol 3, was used for lipid extraction from leaves. Details of each protocol are summarized in Table 1.

3.2.1 Protocol 1: extraction with an automated solvent extractor (ASE) followed by alumina column

Samples were extracted (3 × 5 min) with dichloromethane (DCM): methanol (MeOH) (9:1, v:v) using an accelerated solvent extractor (ASE 100 – Dionex; 100°C, 10×10^6 Pa). The extract was separated into two fractions through a 2 cm diam. column of Al_2O_3 (activated overnight at 150°C) using heptane:DCM (9:1, v:v) and DCM:MeOH (1:1, v:v) respectively. The two fractions were then rotary evaporated, re-dissolved in 1 ml heptane and centrifuged using an Eppendorf Mini Spin centrifuge (1 min, 7000 rpm) prior to further analysis.

3.2.2 Protocol 2: modified Bligh-Dyer extraction followed by silica column

A modified Bligh-Dyer procedure (Bligh and Dyer, 1959) was used for samples where both CLs and IPLs were investigated. Samples were extracted with a solvent mixture of MeOH:DCM:phosphate buffer at pH 7.4 (2:1:0.8; v:v:v) in an ultrasonic bath (3 x 10 min). DCM and phosphate buffer were then added to give a new volume ratio (1:1:0.9, v:v:v). Each extraction was followed by centrifugation (10 min, 3500 rpm) and all extracts were collected in a separation funnel. The DCM layer was separated by decantation from the MeOH/phosphate buffer phase, which was then rinsed three times

with DCM. The resulting DCM phase containing the total lipid extract was dried over Na_2SO_4 and rotary evaporated under near vacuum.

Separation of this extract was performed on a 2 cm diameter column of silica (activated overnight at 130 °C). The first fraction, containing the apolar lipids, was eluted with 40 ml DCM. The second fraction, containing the CLs, was eluted with 48 ml of DCM:acetone (2:1, v:v), followed by 30 ml DCM:acetone (1:1, v:v) and the last fraction, containing the IPLs, was eluted with 40 ml DCM:MeOH (1:1, v:v) followed by 30 ml MeOH. This fraction was separated into 2 aliquots. About 80% of the fraction was subjected to acid methanolysis in 1 M HCl/MeOH during 24 h at 100 °C to cleave off the polar head groups of the GDGT IPLs and release the corresponding CLs. The mixture was then diluted in MeOH and rotary evaporated under near vacuum (3 ×) to neutralise the hydrolysed aliquot which was then dried under N_2, dissolved in 1 ml heptane and centrifuged using an Eppendorf Mini Spin centrifuger (1 min, 7000 rpm). The second aliquot of this fraction (ca. 20%) was kept for direct analysis to determine the carryover of CLs into the IPL fraction, which amounted to < 5% of the CLs detected after acid methanolysis of the third fraction. The two other fractions were directly rotary evaporated after fractionation over the silica column, dried under N_2, dissolved in 1 ml heptane and centrifuged using an Eppendorf Mini Spin centrifuger (1 min, 7000 rpm) before further analysis except for the first (apolar) fraction of the peat core samples which underwent further treatment (section 3.2.4).

3.2.3 Protocol 3: extraction and separation of lipids from vegetation samples

For each specimen, ca. 0.6 g of grinded leaves were sonicated with 30 ml of DCM:MeOH (9:1, v:v) during 15 min. The extract was separated into 2 fractions on silica columns following the procedure described by (Kahmen et al., 2013a). The first fraction containing the *n*-alkanes was eluted with heptane and the second one with DCM:MeOH (1:1, v:v).

Table 1: Protocol type, mass extracted and volume of solvent used for extraction for each type of sample analysed in this thesis. For the ASE protocol the volume of solvent is not chosen by the operator, and the size of the cell is provided instead.

Sample type	Protocol	Mass extracted (g)	Volume of solvent (ml) or size of the ASE cell
Soils of the altitudinal transects	ASE (protocol 1)	ca. 40 g	100 ml × 3
Soils (around Masoko and Kyambangunguru)	Bligh Dyer (protocol 2)	ca. 40 g	49 ml × 3
Peat (Kyambangunguru)	Bligh Dyer (protocol 2)	ca. 1 g	49 ml × 3
Sediments (Lake Masoko	Bligh Dyer (protocol 2)	ca. 5 g	49 ml × 3
POM (Lake Masoko)	Bligh Dyer (protocol 2)	ca. 0.6 g	49 ml × 3
Sediment core (Lake Masoko)	ASE (protocol 1)	ca. 1 g	10 ml × 3
Vegetation	Protocol 3	ca. 0.6 g	30 ml x 3

3.2.4 Additional treatment: separation of n-alkanes over AgNO3 impregnated columns

The apolar fraction of the peat core samples from Kyambangunguru was further separated on silver nitrate (10%, w:w) impregnated silica columns in Pasteur pipettes in order to isolate the *n*-alkanes for compound-specific δ^2H analysis. Heptane and DCM were successively used as eluents.

3.3. Lipid analysis

3.3.1 GDGT and GDD analysis

For most of samples, high pressure liquid chromatography coupled to a mass spectrometer with an atmospheric pressure chemical ionization source (HPLC-APCI-MS) was performed with a Shimadzu LCMS-2020. Separation was achieved with a Prevail Cyano column (2.1 mm x 150 mm, 3 µm; Alltech, Deerfield, IL, USA) at 30°C, using a mixture of A and B (A= hexane and B= isopropanol) at 0.2 ml/min. Elution began at 99% A/1% B for 5 min followed by a linear gradient to 98% A/2% B in 45 min. A second linear gradient led to a mixture of 90 % A/10 % B in 10 min, maintained for 10 min and returned to the initial conditions (99 % A/1 % B) in 14 min, maintained for 10 min. Injection volume was 10 µl. Single ion monitoring (SIM) of the $[M+H]^+$ ions (Figure 7) was used to detect GDGTs and GDDs.

Soil samples collected along Mt. Rungwe in April 2012 were analysed at the Service d'analyse de spectrométrie de masse at Chimie ParisTech (Paris, France) with an Agilent 1100 series HPLC instrument equipped with an automatic injector and coupled to a PE Sciex API 3000 mass spectrometer. The column specified above was used for the GDGT separation. Injection volume was 10 µl. GDGTs were first eluted isocratically with 99% A/1% B for 5 min. The following linear gradient was subsequently used: 99% A/1% B to 98% A/2% B in 45 min, maintained for 5 min, followed by 98% A/2% B to 90% A/10% B in 1 min, maintained for 10 min and then back to 99% A/1% B in 1 min, maintained for 10 min. The flow rate was set at 0.2 ml/min. Ion scanning was performed in pseudo single ion monitoring (SIM) mode, i.e. scanning was from m/z 1015 to 1025, 1030 to 1040, 1044 to 1054 and 1290 to 1310 for the detection of the [M+H]+ ions of br GDGTs VII, VIII IX and iso GDGTs respectively (Figure 7).

Semi-quantification of the GDGTs was performed by comparing the integrated signal of the respective compound with the signal of a C_{46} synthesised internal standard (Figure 23) assuming the response factors to be identical. This standard (concentration 0.011 µg/µl) was added at the end of the sample preparation with a known amount. Typical MS chromatogram is displayed in Figure 24.

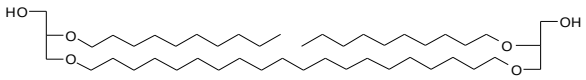

Figure 23: Internal standard used for semi-quantification of GDGTs.

Fractional abundances *f* of the major br GDGTs and iso GDGTs were calculated as follows:

$$f(i) = \frac{i}{\sum(br\ GDGTs)} \qquad (23)$$

$$f(i) = \frac{i}{\sum(iso\ GDGTs)} \qquad (24)$$

i corresponds to the concentration of the corresponding br or iso GDGT, and roman numerals refer to the structures in Figure 7.

It should be noted that in Section 5.1. br GDGT fractional abundances were compared to fractional abundance of their br GDD analogues. Since cyclic br GDGTs were not detected or were present at very low concentrations, fractional abundances of br GDGTs and br GDDs were calculated by taking into account only the straight compounds, as specified below:

$$f(i) = i/(VIIa + VIIIa + IXa) \quad (25)$$

In contrast, iso GDD fractional abundances were calculated in the same way as for iso GDGTs:

$$f(i) = \frac{i}{\sum(iso\ GDDs)} \qquad (26)$$

The ratio of iso vs. br GDGTs, denoted $R_{i/b}$, was calculated by dividing the total concentration of iso GDGTs by the one of br GDGTs, as proposed by (Xie et al., 2012). Similarly, the ratio $R_{i/b}$ was determined for GDDs (cf. Section 5.1).

Based on triplicate injections, the maximal analytical error for the different indices was: 0.09 for MBT and MBT', 0.03 for CBT, 0.07 for TEX_{86} and 0.01 for BIT, respectively.

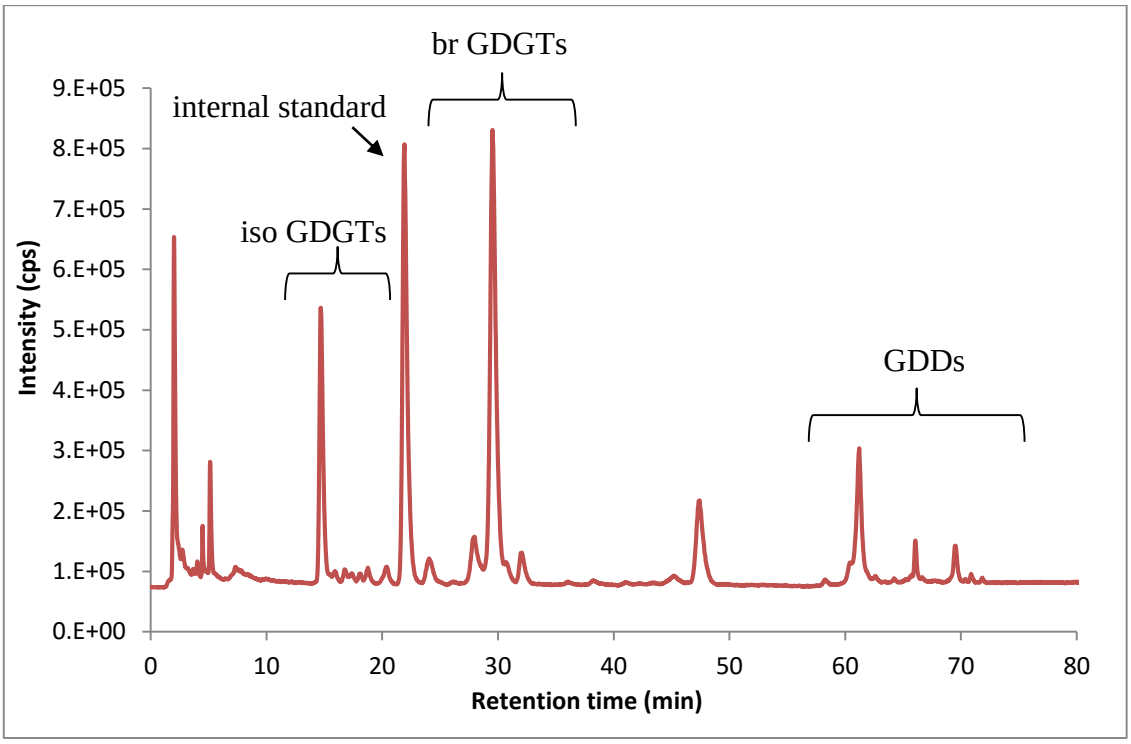

Figure 24: Typical HPLC-APCI-MS chromatogram obtained after GDGT – GDD analysis of a peat core sample (Kyambangunguru; 165 cm depth).

3.3.2 *n*-alkane analyses

n-Alkanes were analyzed by gas chromatography coupled to a mass spectrometer (GC-MS) using an Agilent Network 6890 GC System coupled with a 5973 Mass Selective Detector, with electron impact at 70eV. 1 µl was injected and the separation was achieved using a Restek RXI-5 Sil MS silica capillary column (30 m × 0.25 mm i.d., 0.50 µm film thickness) with He as the carrier gas at 1 ml/min flow rate. Initial temperature was set to 50 °C and increased up to 320 °C at a 4 °C/min lapse rate. Samples were injected in splitless mode and the injector temperature was 280 °C.

n-Alkane hydrogen isotopic composition was measured at Newcastle University (Newcastle-upon-Tyne, UK) using a Delta V+ isotope-ratio mass spectrometer (IRMS, ThermoFisher) connected to a GC Ultra Trace (ThermoFisher), a Finnigan GC Combustion III (ThermoFisher) and a high temperature conversion (HTC) system set up at 1400 °C. The GC temperature was set to start at 50 °C and then to raise to 250 °C at a lapse rate of 15 °C/min and from 250 °C to 320 °C at a lapse rate of 5 °C/min. Temperature was then hold at 320 °C for 15 min. Every sample was analysed in duplicate and the $^{2}H/^{1}H$ ratio was reported on the VSMOW (Vienna standard mean

ocean water) scale. A mixture of *n*-C_{16} to *n*-C_{30} alkane standard and 5α androstane standard was run at the beginning and at the end of each sequence to adjust the reference gaz. In the following, we will refer to the individual *n*-alkane hydrogen isotopic composition as δ^2H_{Cn} which is calculated according to the following equation:

$$\delta^2H_{alc} = \frac{\left({}^2H/{}^1H\right)_{alc}}{\left({}^2H/{}^1H\right)_{VSMOW}-1} \times 1000 \qquad (27)$$

3.4. pH and elemental analysis

The pH of the soils was measured in ultrapure water (Milli-Q, Millipore) with a 1:2.5 soil:water ratio.

Total organic carbon (C_{org}) and nitrogen (N) contents of most of the samples were determined by elemental analysis performed at the Service Central d'Analyse du CNRS, Villeurbanne, France. Soils, POM and sediments collected in and around Lake Masoko were analysed at the Laboratoire d'Analyse des Sols of INRA, Arras, France.

3.5. Analyses of the Kyambangunguru peat core

3.5.1 Core chronology

To assess the age model of the Kyambangunguru peat core, 11 radiocarbon dates were obtained from bulk organic matter (OM) and 4 from wood macroremains, respectively (Table 2). All measurements were conducted at the Artemis Accelerator Mass Spectrometry (AMS) facility of Saclay.

Table 2: AMS dated sample information and estimated age calibrated with OxCal software (Bronk Ramsey, 2008)

Sample ID	Depth	Material	14C date (yrBP)	Age error (yr)	Cal. age (cal. yrBP)	Cal age range BP (95.4%)
SacA40073	1.5	OM	post 1950	-	modern	-
SacA36759	8	OM	255	35	231	435 - 143
SacA40074	54	OM	890	30	753	800 - 682
SacA40075	54	wood	825	30	704	742 - 666
SacA36761	116.5	OM	1590	45	1441	1536 - 1324
SacA40076	116.5	wood	1745	30	1619	1701 - 1539
SacA36760	173.5	OM	2215	40	2196	2318 - 2059
SacA36747	190.5	OM	2240	35	2223	2328 - 2103
SacA40077	190.5	wood	2515	30	2560	2719 - 2365
SacA36758	267.5	OM	2785	40	2841	2945 - 2759
SacA40078	267.5	wood	2880	30	2947	3062 - 2857
SacA40079	319	OM	3170	30	3335	3445 - 3236
SacA36748	371.5	OM	3395	35	3589	3692 - 3478
SacA40080	417.5	OM tephra	3745	30	4042	4151 - 3926
SacA38523	420.5	OM tephra	3160	50	3320	3450 - 3182

3.5.2 Quantitative palynofacies analysis

Palynofacies was performed at the Institut des Sciences de la Terre d'Orléans (ISTO, Orléans, France) on 12 fresh samples evenly collected along the core. Preparation of the samples includes treatment with 50 ml of fluorhydric acid (HF) overnight at 40° C followed by 50 ml of HCl for 30 min to get rid of the mineral components of the samples. Samples were then rinsed until neutralisation of the pH. Quantification of the different types of OM is based on the methodology developed by (Graz et al., 2010) by incorporation of a standard solution of *Cupressus* pollen at 10 $mg.ml^{-1}$ in each sample. Samples are prepared in thin sections before optical investigations, performed with a microscope in transmitted light with a 50× objective. Particle identification was performed using the methodology described by (Boussafir et al., 2012; Graz et al., 2010). Particles were classified into 6 types: (i) 4 corresponding to those described by (Graz et al., 2010), i.e. granular amorphous OM (gAOM), reddish amorphous OM (rAOM), translucent ligno cellulosic fragments (tLC), mycelium fragments (myc), and (ii) 2 corresponding to those described by (Boussafir et al., 2012), i.e. slightly amorphised OM (saLC) and algal organic matter (algOM) (Figure 25). Whenever necessary, identification of the particle was further checked

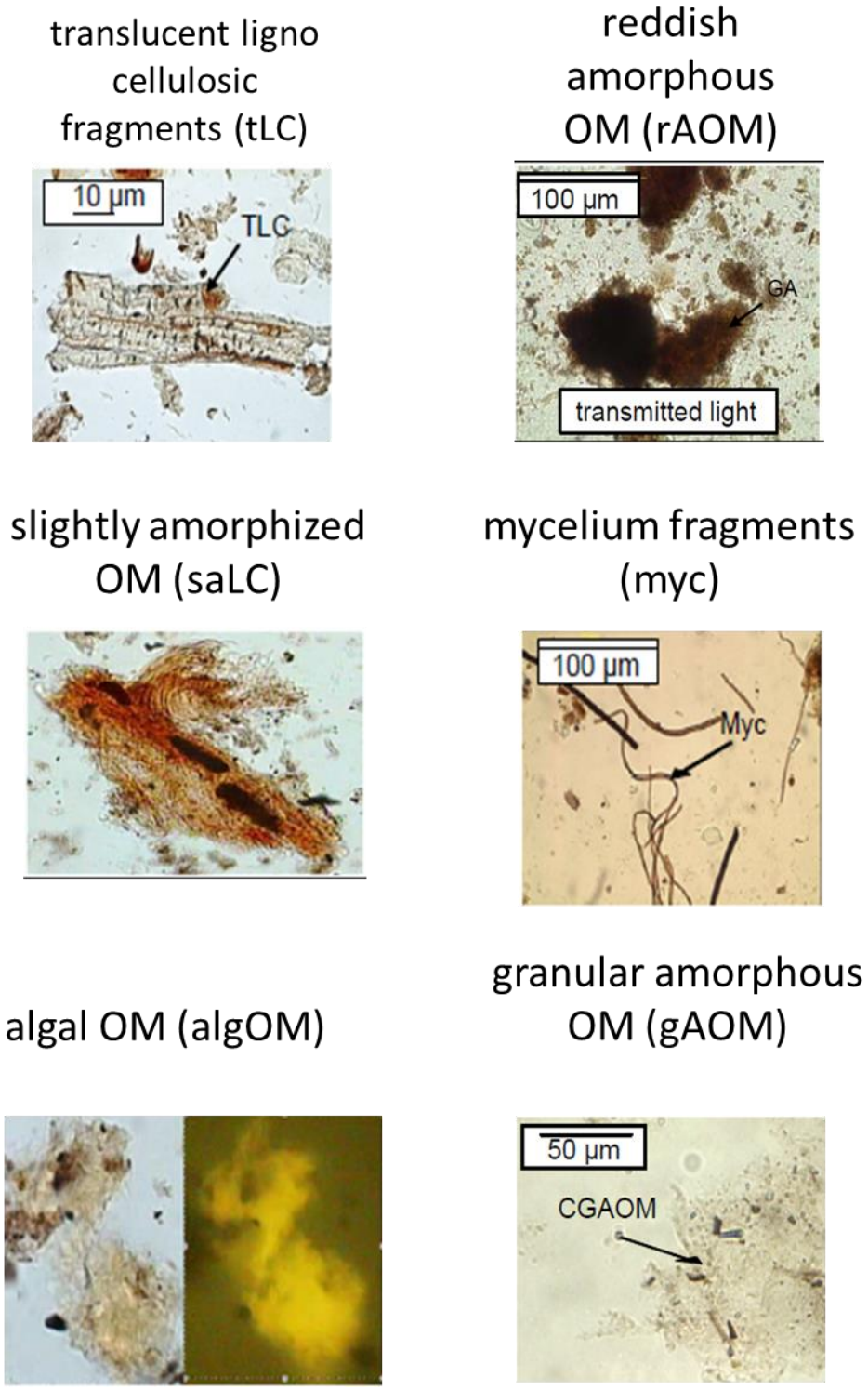

Figure 25: Photographs of palynofacies fractions used for OM characterization along the core. *From Graz et al., 2010 and Boussafir et al., 2012.*

under UV excitation. Mass of each particle type was determined after 40 countings according to eq. 28:

$$m_{part} = \frac{m_{std} \times A_{part}}{A_{std}} \times \frac{d_{part}}{d_{std}} \qquad (28)$$

m_{part}: mass of the particle; m_{std}: mass of the standard; A_{part}: counted surface of the particle; A_{std}: counted surface of the standard; d_{part}: density of the particle; d_{std}: density of the standard. Densities used for the calculation were determined by (Graz et al., 2010). In section 5.2., results from the palynofacies are expressed as relative abundance (in terms of mass) of each particle to the total.

3.5.3 Macroremain analysis:

Plant macroremains were analysed in 105 samples (8-10 cm^3) along the core. These analyses were performed by Mariusz Gałka (Adam Mickiewicz University, Poznań, Poland). Samples were rinsed with warm water and sieved at 0.25 mm. Macrofossils of the selected plants were studied in transmitted light with a Nikon SMZ800 stereoscopic microscope at a magnification of 10 to 200. Species determination of individual plant macrofossils was performed based on data from (Velichkevich and Zastawniak, 2006, 2009). Plant macroremain diagrams (cf. section 5.2.1.4.) were prepared with the C2 graphics software (Juggins, 2007).

3.5.4 Pollen and non-pollen palynomorphs

Pollen and non-pollen palynormorph analyses were carried out by Piotr and Monika Kołaczek (Adam Mickiewicz University, Poznań, Poland). 44 samples (each of 2 cm^3) were prepared using standard laboratory procedures: adding 10% HCl to dissolve carbonates, heating in 10% KOH to remove humic compounds and at least 24-hour treatment with HF to remove the mineral fraction followed by Erdtman's acetolysis (Berglund and Ralska-Jasiewiczowa, 1986). Lycopodium tablet of known number of spores (n=20848, produced by University of Lund) was added to each sample for calculation of microfossil concentration (Stockmarr, 1971). Pollen and spores were counted with a biological microscope under 400× and 1000× magnification until the number of at least 500 pollen grains was obtained (e.g. Vincens et al., 2003, 2007). Pollen grains were identified using atlases (Gosling et al., 2013), databases available at websites such as African Pollen Database (http://apd.sedoo.fr/) and Universal Pollen

Collection (Institut des Sciences de l'Évolution Montpellier; http://www.palyno.org/). Non pollen palynomorphs (NPPs) were identified using publications (Gelorini et al., 2011; van Geel et al., 2011; Miola, 2012). The NPP type numbers follow the convention of 'HdV-number' and 'UG-number', in which acronym 'HdV' means Hugo de Vries Laboratory of the University of Amsterdam (The Netherlands), whereas 'UG' is Universiteit Gent (Belgium; Miola, 2012). Percentages of pollen grains, spores and NPPs were calculated as the ratio of an individual taxon to the TPS (total pollen sum), i.e. the sum of AP (arboreal pollen) and NAP (non-arboreal pollen spores and NPPs excluding aquatic and wetland plants such as *Cyperaceae*).

3.6. Statistical treatment

MBT', CBT and br GDGT-derived temperatures in the surficial core samples and soils surrounding the Kyambangunguru crater marsh (Chapter 5) and Lake Masoko (Chapter 6) were compared with Mann-Whitney test on the median.

Potential correlations in Chapters 4, 5 and 6 were tested by calculating the correlation coefficient. Whenever each of the 2 elements were normally distributed, the Pearson correlation coefficient was calculated; otherwise, we determined the Spearman correlation coefficient instead. Correlations and results of the tests were considered as significant when the *p*-value was < 0.05.

Regional calibration in Chapter 4 was obtained by performing a multiple linear regression on measured MAAT, MBT' and CBT.

Outliers in Chapter 5 (in black in the different graphs) were defined by plotting the corresponding residuals vs. leverage graph for each correlation. Whenever a data point was outside the Cook's distance, it was considered as an outlier. Data analysis was performed using the R software (R Core Team, 2013).

Chapter 4.

Assessment of the potential of GDGTs and δ^2H_{wax} as paleoenvironmental proxies in East Africa from altitudinal gradient studies

In this Chapter, we present methodological studies assessing the potential of GDGTs and δ^2H_{wax} to record MAAT variation in soils, based on the analysis of surface soils along East African altitudinal transects. The first part displays preliminary results on the distribution of br and iso GDGTs in surface soils along Mt. Rungwe in the Rungwe Volcanic Province. This study was published in *Organic Geochemistry* (Coffinet et al., 2014). The second part of this chapter synthesizes all published results of br GDGTs and δ^2H_{wax} along East African altitudinal transects so far as well as additional data we obtained during a second sampling campaign along Mt. Rungwe and along Mt. Kenya (Kenya). It led to the development of the first East African regional calibration of br GDGTs in soils. This study is to be submitted to *Earth and Planetary Science Letters.*

4.1. Potential of GDGTs as a temperature proxy along an altitudinal transect in Mount Rungwe (Tanzania)

For this study, 21 surface soil samples (0-5 cm depth) were collected in 2012 along Mt. Rungwe from 520 m to 2800 m. Lipid were extracted according to Protocol 1 (see section 3.2.1) before br and iso GDGT analysis. The goal of this study was to investigate the applicability of the MBT/CBT and TEX_{86} indices as two complementary and independent paleoelevation proxies in the RVP. Br GDGTs were previously investigated along only one altitudinal transect in East Africa (Mt. Kilimanjaro; Sinninghe Damsté et al., 2008).

4.1.1 GDGT distribution and concentration

Br GDGTs and iso GDGTs were detected in all the soils, as shown for example in the HPLC/MS base peak chromatogram of a sample collected at 1680 m altitude (Figure 26). Compounds VIIIa, IXa and IXb were predominant among the br GDGTs, representing all together 74 to 95% of total br GDGTs (cf. Appendix 2). Compounds VIIb and VIIIc were detected in only a few samples, where they were present at low concentration (each representing < 4% of total br GDGTs) and GDGT VIIc was not detected in any of the samples. GDGTs I and VI were the most abundant iso GDGTs in all samples except No. 21, representing respectively up to ca. 62 % and 74 % of total iso GDGTs (cf. Appendix 2). There was no correlation between the individual br GDGT and iso GDGT concentrations on one hand and altitude on the other hand.

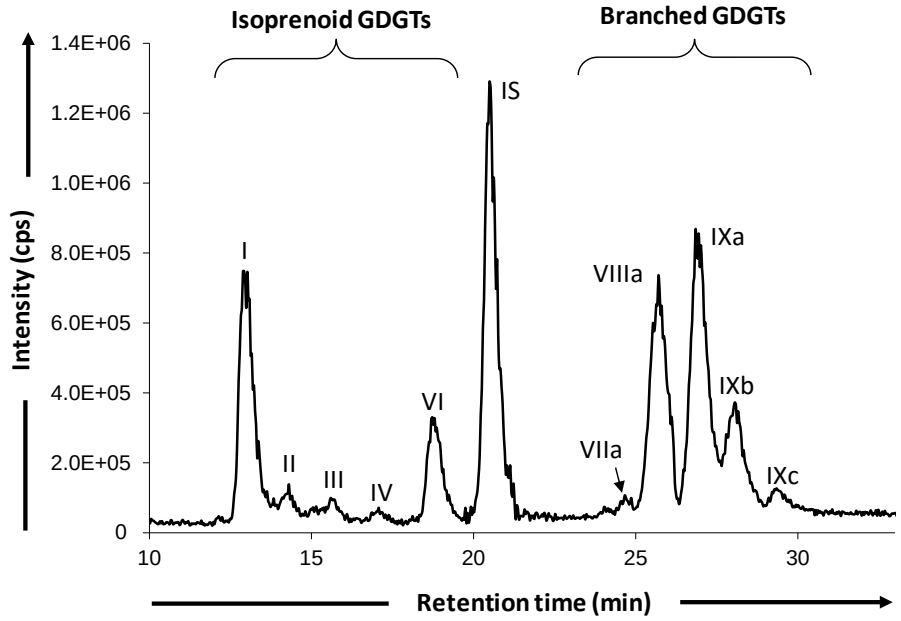

Figure 26: HPLC/MS base peak chromatogram of sample 14 collected at 1680 m altitude.

The concentration of br GDGTs was between 1.1 and 8.3 µg/g C_{org} (mean 3.3µg/g C_{org}; Table 3), in agreement with that in soils from Africa and China (Loomis et al., 2011; Yang et al., 2012) but substantially lower than for a recent study in India (Ernst et al., 2013). In the same way, iso GDGT concentration ranged between 0.05 and 1.5 µg/g C_{org} (mean 0.5 µg/g C_{org}), consistent with the range generally observed in soils (Weijers et al., 2006; Huguet et al., 2010b). Br GDGT and iso GDGT concentrations were not correlated with altitude ($R^2 < 0.03$). The br GDGTs were largely preponderant among the total GDGTs (*i.e.* iso and br), as classically observed for soils. The iso GDGTs represented on average 14% of the total GDGTs, in agreement with other studies reporting relative abundances around 10% (Weijers et al., 2006) or even lower (around 2% in US eastern coast soils; Dirghangi et al., 2013). Consequently, the BIT values were high in all soils from Mt. Rungwe (0.90 ± 0.06; Table 4), as previously observed in most soils (e.g. Loomis et al., 2011). Nevertheless, it should be noted that the iso GDGT relative abundance with respect to total GDGTs can sometimes be high (up to 71%) as recently found, for example, in two sets of dry soils from the Tibetan Plateau in China and from a western US transect (Liu et al., 2013 and Dirghangi et al., 2013). This could indicate that the growth of Archaea, such as Thaumarchaeota, is favoured by dry and alkaline soils rather than by wet and acidic soils, as recently suggested (Wang et al., 2013; Yang et al., 2014c). In contrast, humid conditions may favour the development of anoxic microenvironments in soils and therefore the growth of br GDGT source microorganisms, suggested to be anaerobic (Weijers et al., 2006).

Table 3: General properties (altitude, coordinates, sampling dates, organic carbon (C_{org}) concentration) and abundance of iso GDGTs and br GDGTs normalised to C_{org} for soil samples

Sample	Altitude (m)	Coordinates	Sampling dates	C_{org} (%)	Total brGDGTs (µg/g C_{org})	Total iGDGTs (µg/g C_{org})	rel. iGDGTs (%)[a]	I/VI[b]
1	520	S 09.40492° E 33.90782°	04/29/2012	4.9	5.0	0.8	14	0.5
2	520	S 09.40492° E 33.90782°	04/29/2012	5.3	2.7	0.5	15	0.4
3	529	S 09.40842° E 33.917284°	04/29/2012	3.2	2.1	0.1	9	0.3
4	640	S 09.37025° E33.79949°	04/28/2012	6.2	2.6	0.8	23	0.2
5	692	S 09.35699° E 33.79721°	04/27/2012	2.6	4.6	1.3	22	0.2
6	826	S 09.35270° E 33.82296°	04/27/2012	5.8	2.5	0.9	26	2.5
7	869	S 09.33008° E 33.75884°	04/25/2012	4.8	2.1	0.1	16	0.4
8	869	S 09.33008° E 33.75884°	04/25/2012	4.4	1.2	0.2	3	0.2
9	994	S 09.33470° E 33.81031°	04/27/2012	3.6	3.3	0.7	17	0.1
10	1092	S 09.32068° E 33.80958°	04/27/2012	2.3	6.6	0.6	9	0.1
11	1211	S 09.30013° E 33.80783°	04/27/2012	8.0	1.2	0.03	3	0.3
12	1374	S 09.28262° E 33.81349°	04/27/2012	6.3	1.1	0.3	26	0.1
13	1550	S 09.26021 E 33.820295°	04/27/2012	4.9	3.0	0.4	12	0.2
14	1680	S 09.23784° E 33.81677°	04/27/2012	4.0	2.4	0.8	35	0.5
15	1702	S 09.35993° E 33.81637°	04/27/2012	2.9	4.5	0.4	10	0.1
16	1846	S 09.22716° E 33.81249°	04/25/2012	3.2	2.9	0.4	14	0.1
17	2020	S 09.02202° E 33.56576°	04/30/2012	2.5	5.9	0.6	9	0.1
18	2055	S 09.02124° E 33.56478°	04/30/2012	5.3	4.3	0.4	9	0.1
19	2080	S 09.07322° E 33.40782°	04/29/2012	0.8	8.3	1.5	16	0.4
20	2200	S 09.15288° E 33.43117°	12/07/2012	5.4	1.9	0.2	8	0.1
21	2800	S 09.13715° E 33.94668°	11/30/2012	10.0	1.9	0.05	2	n.d.[c]

4.1.2 Br GDGT-derived proxies

MBT, MBT' and CBT indices were calculated for all the soils from the altitudinal transect (Table 4). CBT was between 0.08 and 1.01 (Table 4) and correlated with measured pH in the soils (R^2 0.60, data not shown), as observed in previous studies (Weijers et al., 2007; Peterse et al., 2012), confirming that pH is the main environmental parameter controlling the cyclisation degree of br GDGTs .pH estimates based on the calibration of Peterse et al. (2012) were higher than measured pH by, on average, 0.8 units (Table 4). They were closer to measured values than those based on the calibration of Weijers et al. (2007), suggesting that the revised calibration could be more suitable than the original to reconstruct soil pH in the region, in contrast with preliminary comparisons made for central Africa by Peterse et al. (2012). CBT also correlated moderately with altitude (R^2 0.48; data not shown). Such a relationship has not been described before and cannot be the result of interrelation between pH and altitude since measured pH and altitude were poorly correlated (R^2 0.20; data not

shown). Therefore, the CBT might be influenced by parameters other than pH and which change with altitude. This should be investigated along other altitudinal transects.

MBT values were always identical to MBT' ones except for samples 17 and 18 and were between 0.58 and 0.82 (Table 4). A trend was observed between MBT and altitude (R^2 0.39, data not shown). This relationship is weaker than that found by Liu et al. (2013; R^2 0.69) for soils from Mt. Xiangpi (China), which may be partly due to the differences in pH of Mt. Xiangpi (7.7 ± 0.2) and Mt. Rungwe soils (6.0 ± 0.5; Table 4). Indeed, the relationship between MBT and pH for Mt. Xiangpi alkalescent soils (R^2 0.18; Liu et al., 2013) was observed to be not as significant as in global soils (R^2 0.37; Weijers et al., 2007). Therefore, the alkalescency of Mt. Xiangpi soils may lead to a lower influence of pH on MBT values (Liu et al., 2013) and in turn to a lower scattering in the MBT-altitude relationship than in acid soils, such as Mt. Rungwe ones. Nevertheless, further studies are necessary to confirm the potential correlation between MBT and altitude and the applicability of MBT as a paleoelevation proxy.

Table 4: Br GDGT and iso GDGT-derived proxies and estimated pH and temperature along Mt. Rungwe transect.

Sample	Altitude (m)	brGDGT-derived proxies						Measured pH	iGDGT-derived proxies			BIT
		MBT[b]	CBT	T (Weijers)	T (Peterse)	pH (Weijers)	pH (Peterse)		TEX_{86}	T (Kim)	T (Powers)	
1	520	0.69	0.08	27.4	21.6	8.6	7.7	6.5	n.d.[c]	n.d.	n.d.	0.85
2	520	0.74	0.22	28.6	22.4	8.2	7.5	6.3	n.d.	n.d.	n.d.	0.85
3	529	0.72	0.09	28.9	22.5	8.5	7.7	5.6	n.d.	n.d.	n.d.	0.92
4	640	0.63	0.29	22.7	18.7	8.0	7.3	6.4	0.88	45.1	34.6	0.79
5	692	0.69	0.16	26.9	21.3	8.3	7.6	6.3	0.87	44.1	33.9	0.76
6	826	0.61	0.46	20.3	17.3	7.6	7.0	5.9	0.75	34.8	27.6	0.89
7	869	0.69	0.48	24.1	19.6	7.0	6.6	7.3	n.d.	n.d.	n.d.	0.99
8	869	0.79	0.68	27.0	21.4	7.5	7.0	6.1	0.79	37.4	29.4	0.90
9	994	0.66	0.33	23.9	19.5	7.9	7.3	6.4	0.86	43.3	33.4	0.85
10	1092	0.66	0.59	21.3	17.9	7.2	7.2	6.1	0.70	30.6	24.7	0.94
11	1211	0.75	0.73	24.8	20.1	6.8	6.5	5.7	n.d.	n.d.	n.d.	0.97
12	1374	0.82	0.78	27.5	21.7	6.7	6.4	5.6	0.63	24.7	20.8	0.93
13	1550	0.65	1.01	17.1	15.4	6.1	5.9	5.5	0.72	32.5	26.0	0.92
14	1680	0.57	0.53	17.5	15.5	7.4	6.9	6.0	0.71	31.3	25.2	0.81
15	1702	0.65	0.68	20.2	17.2	7.0	6.6	5.7	0.71	31.2	25.1	0.94
16	1846	0.58	0.57	17.5	15.5	7.3	6.8	5.6	0.61	22.9	19.6	0.92
17	2020	0.48 (0.49)	0.57	12.8	12.8	7.3	6.8	5.9	0.71	31.6	25.4	0.94
18	2055	0.42 (0.43)	0.34	11.8	12.2	7.9	7.2	6.2	0.78	36.8	28.9	0.92
19	2080	0.61	0.84	16.3	14.8	6.5	6.2	6.3	0.58	21.2	18.4	0.93
20	2200	0.58	0.90	14.4	13.6	6.4	6.1	5.5	0.68	28.8	23.5	0.94
21	2800	0.58	0.85	14.0	14.0	6.5	6.2	5.5	n.d.	n.d.	n.d.	n.d.

MAAT was reconstructed from the MBT, MBT' and CBT indices (Figure 27; Table 4) using the calibrations developed by (Weijers et al., 2007; Peterse et al., 2012).The differences between the temperature estimates based on the two calibrations were not constant with altitude, the greatest difference being at lower altitudes (up to 6.5 °C; Figure 27).

Nevertheless, temperature estimates based on the calibration of (Weijers et al., 2007; Peterse et al., 2012) were generally more consistent with instrumental data than those based on the calibration of (Weijers et al., 2007; Peterse et al., 2012).The difference between temperature estimates and instrumental data was ca. + 1.5 °C and up to – 4 °C when using the calibrations of Weijers et al. (2007) and Peterse et al. (2012), respectively. This shows that in the Mt. Rungwe region, the original soil calibration by Weijers et al. (2007) yields accurate temperatures and that MBT/CBT is a valid temperature proxy for East Africa, in agreement with previous studies in the region (Sinninghe Damsté et al., 2008, 2012a; Loomis et al., 2011).

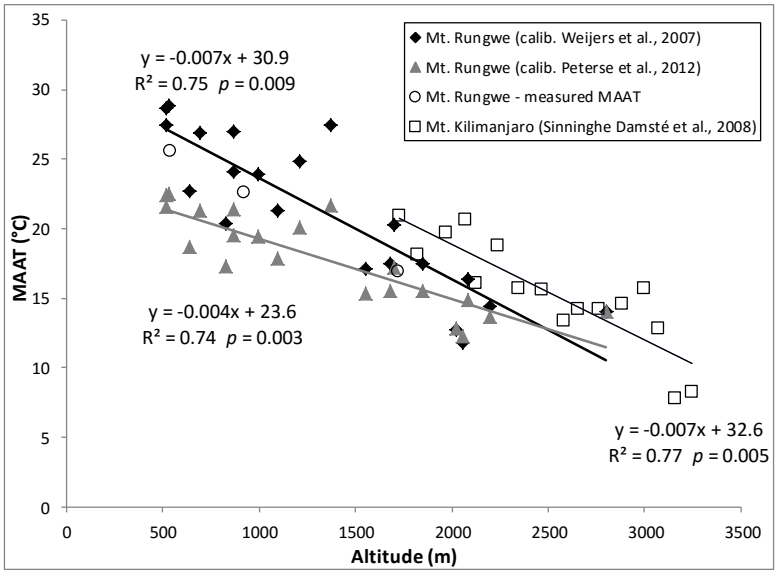

Figure 27: Relationship between altitude and MBT/CBT-derived MAAT estimates based on original soil calibration (Weijers et al., 2007a) and extended calibration (Peterse et al., 2012) along Mt. Rungwe altitudinal transect. MAAT calculated using the calibration by Weijers et al. (2007a) for an altitudinal gradient along Mt. Kilimanjaro, Tanzania (Sinninghe Damsté et al., 2008) is shown for comparison.

The br GDGT-derived MAAT decreased linearly with altitude Figure 27), as previously observed for every altitudinal gradient (Sinninghe Damsté et al., 2008; Peterse et al., 2009a; Hren et al., 2010; Ernst et al., 2013; Liu et al., 2013). MBT/CBT-derived temperature lapse rate (0.7 °C/100 m) calculated with the calibration by Weijers et al. (2007) fitted the one determined from in situ measurements (0.7 °C/100 m) better than the lapse rate (0.4 °C/100 m) calculated with the calibration of Peterse et al. (2012), in contrast with recent results reported by Ernst et al. (2013) for an Indian altitudinal transect. The MBT/CBT-derived temperature lapse rate of 0.7 °C/100 m along Mt. Rungwe is also consistent with the one obtained by Sinninghe Damsté et al. (2008) for an altitudinal transect in the same area (Mt. Kilimanjaro). The relationship between MBT/CBT-derived MAAT and altitude observed in

the two transects is similar, even though the y-intercept for the Mt. Kilimanjaro transect is 1.7°C higher than for the Mt Rungwe transect (Figure 27). The difference lies within the uncertainty range (± 5 °C, Weijers et al., 2007) of the br GDGT calibration and can therefore be neglected. When combined, the altitudinal gradients for Mt. Kilimanjaro and Mt. Rungwe provide a correlation of MBT/CBT with air temperature along a large East African transect (520-3893 m), ensuring the applicability of the MBT/CBT as a paleoelevation proxy in the region, Mt. Kilimanjaro being the highest mountain of Africa.

4.1.3 Iso GDGT-derived proxies

TEX_{86} index was determined for 15 of the 21 samples. It could not be calculated for the samples from 520, 529, 869, 1220 and 2800m (samples 1, 2, 3, 7, 11 and 21) because one or several of the iso GDGTs necessary for the TEX_{86} calculation were not detected (cf. Appendix 2). TEX_{86} values ranged between 0.63 and 0.88 (Table 4). A proper application of the TEX_{86} requires that all iso GDGTs are derived from Thaumarchaeota (Schouten et al., 2013). Unlike marine sediments, care has to be taken prior to applying the TEX_{86} index to soils. Indeed, in marine sediments, the phylum Thaumarchaeota is often predominant (Karner et al., 2001; Herndl et al., 2005) and is therefore the main producer of iso GDGTs. This is not the case for soils, where iso GDGTs, except crenarchaeol, may have several origins, *i.e.* Thaumarchaeota and Euryarchaeota (Pesaro and Widmer, 2002; Weijers et al., 2006), which may lead to biased TEX_{86} values. This bias can be avoided by assessing the origin of iso GDGTs via the calculation of the ratio of caldarchaeol (GDGT I) to crenarchaeol (GDGT VI), which was initially developed for lacustrine environments (Blaga et al., 2009). A ratio of GDGTs I/VI> 2 is considered as indicating a predominance of Euryarchaeota among the archaeal community. In almost all our samples, except 6 and 21, the ratio was much lower than 2 ranging from 0.10 to 0.54 (mean 0.23; Table 3). This suggests (i) that in Mt. Rungwe soils, iso GDGTs were mainly derived from Thaumarchaeota, as previously observed for several other locations: Mt. Xiangpi soils (Liu et al., 2013), soils from a western US transect (Dirghangi et al., 2013) and 35 soils distributed over the world (Weijers et al., 2006) and that (ii) the calculation of the TEX_{86} is meaningful.

A linear relationship (R^2 0.50) between TEX_{86} and altitude was observed for Mt. Rungwe soils (Figure 28a). Such a relationship (R^2 0.68) was also recently obtained by Liu et al. (2013) for soils collected along a small altitudinal gradient (3250-4100 m) at Mt. Xiangpi, China. The correlations between TEX_{86} and altitude were comparable for the two altitudinal

transects (slopes of -0.00011 for Mt. Rungwe and -0.00015 for Mt. Xiangpi; Figure 28a). Based on the results, it appears that TEX_{86}– when the conditions for its proper application are present, *i.e.* Thaumarchaeota are the predominant source of iso GDGTs – could be used as a paleoelevation proxy, as recently hypothesized by Liu et al. (2013). Nevertheless, the applicability of the index as a universal paleoelevation proxy may be questioned by the fact that a given TEX_{86} value corresponds to a much higher altitude (ca. 1800 m higher) for Mt. Xiangpi soils than for Mt. Rungwe samples.

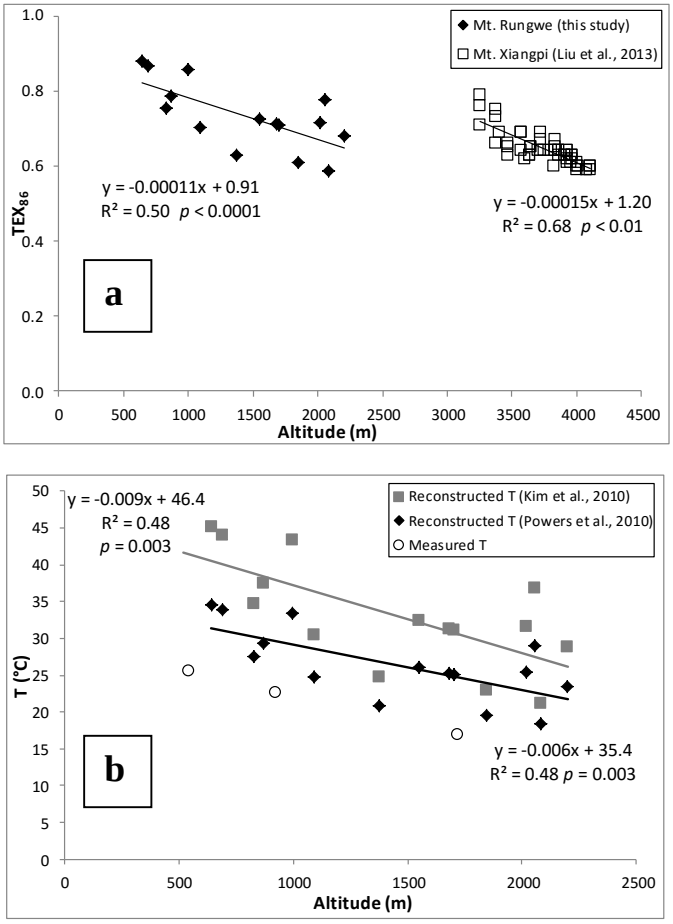

Figure 28: (a) Relationship between altitude and TEX_{86} along Mt. Rungwe altitudinal transect and along an altitudinal gradient at Mt. Xiangpi, China (Liu et al., 2013). (b)Relationship between altitude and TEX_{86}-derived temperature based on marine calibration by Kim et al. (2008) and lacustrine calibration by Powers et al. (2010) along Mt. Rungwe transect [temperatures measured in situ are also presented (white circles)].

Different factors could explain such a difference. First, the location of the sampling site and thus the geographical origin of the soils might have an impact on the relationship between altitude and TEX_{86}. Indeed, the absolute temperature at 800m is not the same in Tanzania and in the Tibetan Plateau in China (9.3 °C in Tanzania at 3017 m vs. -0.7 °C for Mt. Xiangpi at 3200 m; see Hemp, 2006 and Wang et al., 2012 respectively) because of their different

distance from the equator (9.20°S and 36.7-36.8°N respectively). Therefore, if we assume that TEX_{86} correlates mainly with temperature, as observed in marine (Kim et al., 2010) and lacustrine (Powers et al., 2010) sediments, then the difference in temperature for a given altitude could in turn explain the shift between the TEX_{86} vs. altitude relationship for soils from contrasting sampling sites. Further application of the index to different altitudinal transects globally distributed is needed to investigate this hypothesis. If the latter is confirmed, regional calibrations may be more appropriate to use TEX_{86} index as a paleoelevation proxy. Additionally, it cannot be excluded that environmental parameters other than temperature, such as vegetation cover or soil humidity have an effect on the relative distribution of iso GDGTs and thus on the TEX_{86} values in soils. Soil humidity was notably shown to have an influence on br GDGT (Huguet et al., 2010a; Peterse et al., 2012; Dirghangi et al., 2013) and iso GDGT (Wang et al., 2013; Yang et al., 2014c) distributions. In the case of Mt. Rungwe, the annual amount of precipitation does not change significantly with altitude (Bergonzini, 1998). Therefore, temperature can be considered as the main factor responsible for the changes in iso GDGT and br GDGT distribution occurring with altitude, precipitation having only a minor effect. In any case, more studies are necessary to better understand and constrain the environmental factors impacting the iso GDGT distributions and consequently the TEX_{86}index in soils.

Temperatures were estimated from TEX_{86} values (Table 4) using the calibrations developed for marine sediments by Kim et al., (2010) and lacustrine sediments by Powers et al., (2010). TEX_{86} derived temperature values based on the marine and lacustrine calibrations were higher than instrumentally measured values by on average 18 °C and 7 °C, respectively (Figure 28b). The data from the lacustrine calibration developed by Powers et al. (2010) fitted with instrumental ones (Figure 28b) better in terms of absolute temperature and temperature lapse rate (0.7 °C/100m, which is equal to the one determined from in situ measurements) than those based on the marine calibration of Kim et al. (2010). Similarly, Liu et al. (2013) observed that TEX_{86}-derived temperature estimates for Mt. Xiangpi soils (25.5 ± 3.2 °C based on the marine calibration of Kim et al. (2010) overestimated actual temperature in the region by up to 15 °C. These results show that TEX_{86} lacustrine and marine calibrations cannot be directly applied to soils, as suggested by Liu et al. (2013). According to Liu et al. (2013), the temperature overestimation of the two aquatic-based calibrations could be explained by a difference in iso GDGT relative distributions between soils and sediments. Indeed, the relative abundance of the crenarchaeol regio isomer (GDGT VI') with respect to total crenarchaeol abundance seems particularly different between these two environments. The

relative abundance of GDGT VI' was around 8% in Mt. Rungwe samples (Appendix 2), similar to the values in soils reported by Liu et al., (2013) (between 6 and 9%) and largely above the usual abundance in lake sediments (ca. 1%; see Liu et al., 2013 and references therein). Based on soil cultures of Thaumarchaeota (Sinninghe Damsté et al., 2012b) and environmental observations (Timonen and Bomberg, 2009), this over representation of the crenarchaeol regio isomer may suggest that group I.1b Thaumarchaeota dominates among the archaeal communities at Mt. Rungwe and Mt. Xiangpi surface soils, while group I.1a is usually dominant in aquatic systems (Pearson and Ingalls, 2013). This hypothesis needs to be confirmed from microbiological analysis. In any case, additional studies are required to improve the understanding of the iso GDGTs sources in soil and assessing the applicability of TEX_{86} as a temperature proxy in these environments.

4.1.4 Conclusions

The abundance and distribution of br GDGTs and iso GDGTs were determined in surface soils collected along an altitudinal gradient at Mt. Rungwe, Tanzania. The br GDGTs were much more abundant than iso GDGTs, as observed in most of the soils investigated so far (Schouten et al., 2013 and references therein); br GDGT distribution was shown to vary with altitude, which was reflected in the decrease in MBT/CBT-derived MAAT with higher elevation. The MBT/CBT-derived temperature lapse rate (0.7 °C/100 m) calculated using the calibration by (Weijers et al., 2007) was similar to the in situ measured one and was also consistent with results obtained by (Sinninghe Damsté et al., 2008) for an altitudinal gradient in the same area (Mt. Kilimanjaro), at higher altitude. These results confirm the robustness of the MBT/CBT as a temperature proxy in East Africa for a large range of altitude. In addition, TEX_{86} varied linearly with altitude, with lower TEX_{86} values at higher elevation. As suggested for the MBT/CBT, the adiabatic cooling of air with altitude could explain the TEX_{86} variation along Mt. Rungwe. Such a relationship between TEX_{86} and altitude has also been recently noticed for Mt. Xiangpi, China (Liu et al., 2013). However, a large degree of scatter between these two independent altitudinal gradients was observed. More studies are needed to fully understand the environmental factors impacting the distribution of iso GDGTs in soils and to investigate the potential use of the TEX_{86} as a paleoelevation proxy.

4.2. Applicability of GDGTs and δ^2H of *n*-alkanes as environmental proxies in East Africa

The objective of the present study was to examine the effect of altitudinal changes on br GDGT distribution and δ^2H_{wax} at a regional scale in East Africa. It is based on a data comparison of previously investigated br GDGT distribution along East African altitudinal transects, *i.e.* Mt. Rwenzori (Uganda; Loomis et al., 2011), Mt Rungwe (Tanzania; Coffinet et al., 2014) and Mt. Kilimanjaro (Tanzania; Sinninghe Damsté et al., 2008). Along the latter, δ^2H_{wax} analysis was also performed (Peterse et al., 2009b), standing for the only δ^2H_{wax} analysis in East Africa so far. We extended these published datasets with additional measurements of both br GDGT distribution and δ^2H_{wax} in 60 surface soils along Mt. Rungwe and Mt. Kenya (Kenya). We first assessed whether the measured temperature altitudinal gradient was constant at a regional scale, as it is a prerequisite for this data synthesis. Then we address how the altitudinal effect in the δ^2H of precipitations (see section 1.2.3.2) is recorded in δ^2H_{wax} and if br GDGTs can accurately track temperature changes with altitude at a regional scale.

4.2.1 Measured temperature variation with altitude in East Africa:

To date, altitudinal gradients of measured mean annual air temperatures (MAAT) were observed along all the East African mountains investigated (Sinninghe Damsté et al., 2008; Loomis et al., 2011; Coffinet et al., 2014 and WorldClim derived MAAT along Mt. Kenya), but they were individually considered. In the present study, measured MAAT data from all these transects were combined to evaluate the possibility of determining a regional temperature lapse rate (Figure 29). The latter was determined as 0.6°C/100 m, with 93% of the MAAT variance being explained by altitude variations (Figure 29). This strong relationship implies that adiabatic cooling of air with altitude is the predominant driver of MAAT in East Africa and thus that the data obtained on individual mountains can be combined to assess, at a regional scale, the effect of altitudinal-derived temperature changes on br GDGTs.

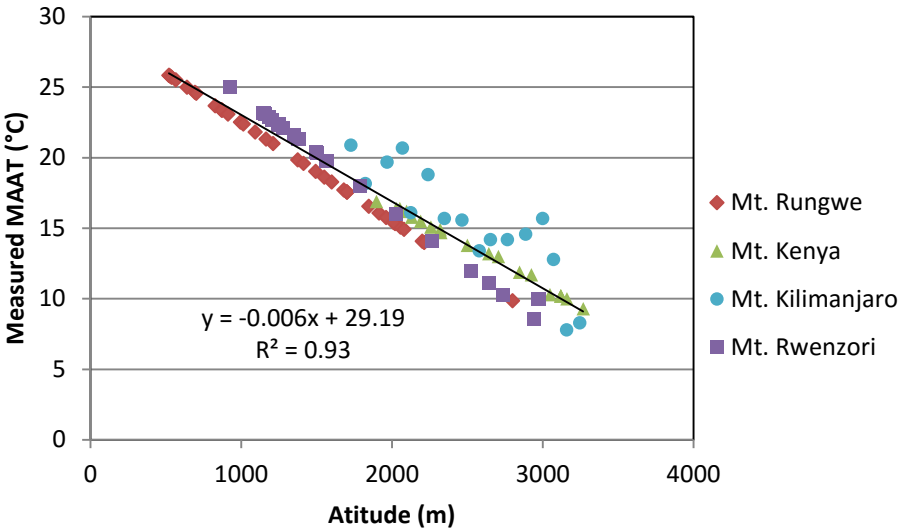

Figure 29: Measured mean annual air temperature (MAAT) along altitudinal gradients in East Africa

4.2.2 δ^2H of *n*-alkanes along Mt. Kenya and Mt. Rungwe

n-Alkanes were analysed in 40 surface soil samples collected between 500 and 2800 m along Mt. Rungwe, and in 20 samples collected between 1900 to 3160 m along Mt. Kenya. Parameters relative to their distribution (C_n range, C_{max}, ACL and CPI) are summarized in Table 5. None were correlated with altitude. Along the 2 transects, CPI values were all > 1, indicating a predominance of odd-over-even *n*-alkanes predominance (Table 5), and ACL values remained comparable (28 ± 2; Table 5). These results suggest that *n*-alkanes present in the surface soils originate predominantly from the higher plants covering the slopes of the 2 mountains (Eglinton and Hamilton, 1967) as it was expected. δ^2H of the major odd *n*-alkanes (C_{27}, C_{29},C_{31}) was comprised between-109‰ and-177‰ in Mt. Rungwe, and between-116‰ and -167‰ in Mt. Kenya (Table 5). These values are in the same range as those previously determined (-114‰ − -156‰) along Mt. Kilimanjaro by Peterse et al., (2009b).

The concentration-weighted mean values of δ^2H C_{27} – C_{31} alkanes (δ^2H_{wax}, Table 5) were plotted against altitude for Mt. Kenya and Mt. Rungwe (Figure 30a-b) in order to determine if the isotopic composition of *n*-alkanes reflected the isotopic depletion of precipitations related to air cooling with increasing altitude (Dansgaard, 1964). A statistically significant, though scattered, depletion trend was observed along Mt. Kenya (Figure 30a, $p < 0.05$) supporting this hypothesis, as it was observed in several Mts. in Asia (Jia et al., 2008; Luo et al., 2011; Ernst et al., 2013). In contrast, no trend was noticed along Mt. Rungwe (Figure 30b, $p > 0.05$) just like along Mt. Kilimanjaro (Peterse et al., 2009b). Peterse et al., (2009b) hypothesized that the "amount effect", *i.e.* the more depleted δ^2H values in precipitation with increasing

rainfall amount and intensity (see section 1.2.3.2.) – supposedly important in tropical regions – was able to cancel the altitude effect in Mt. Kilimanjaro. This explanation does not hold for Mt. Kenya where a depletion trend was noticed with altitude. Moreover, δ^2H of the mean annual precipitations (δ^2Hp; Bergonzini, personal communication) was determined from rainfall collected at three weather stations along Mt. Rungwe (540, 920 and 1720 ma.s.l.) and a linear decrease in δ^2Hp with altitude was observed (lapse rate of -0.5 ‰/100 m; Bergonzini, personal communication) in contrast to what was observed in soils from the same Mt. It must be noted however, that this D-depletion trend is small compared to other montaneous settings where it usually ranges between -1 and -4‰ (Araguás-Araguás et al., 2000). This suggests that the lack of trend observed along Mts. Rungwe and Kilimanjaro may rather be related to (i) the effect of plant physiological processes such as species-specific biochemical fractionation and/or (ii) local physical processes such as changes in relative humidity (RH) along the transect impacting water evaporation from the soil and the leaves. Consequently, when combining data from the 3 transects (Figure 30c), no trend is apparent at a regional scale. This highlights the complexity of the signal recorded by δ^2H_{wax} which encompasses a biological signal in addition to the environmental one, each of them being not well constrained yet (Sachse et al., 2012). This multi-source signal restrains δ^2H_{wax} applications to site-specific studies and prevents its generalization at a regional scale in East Africa.

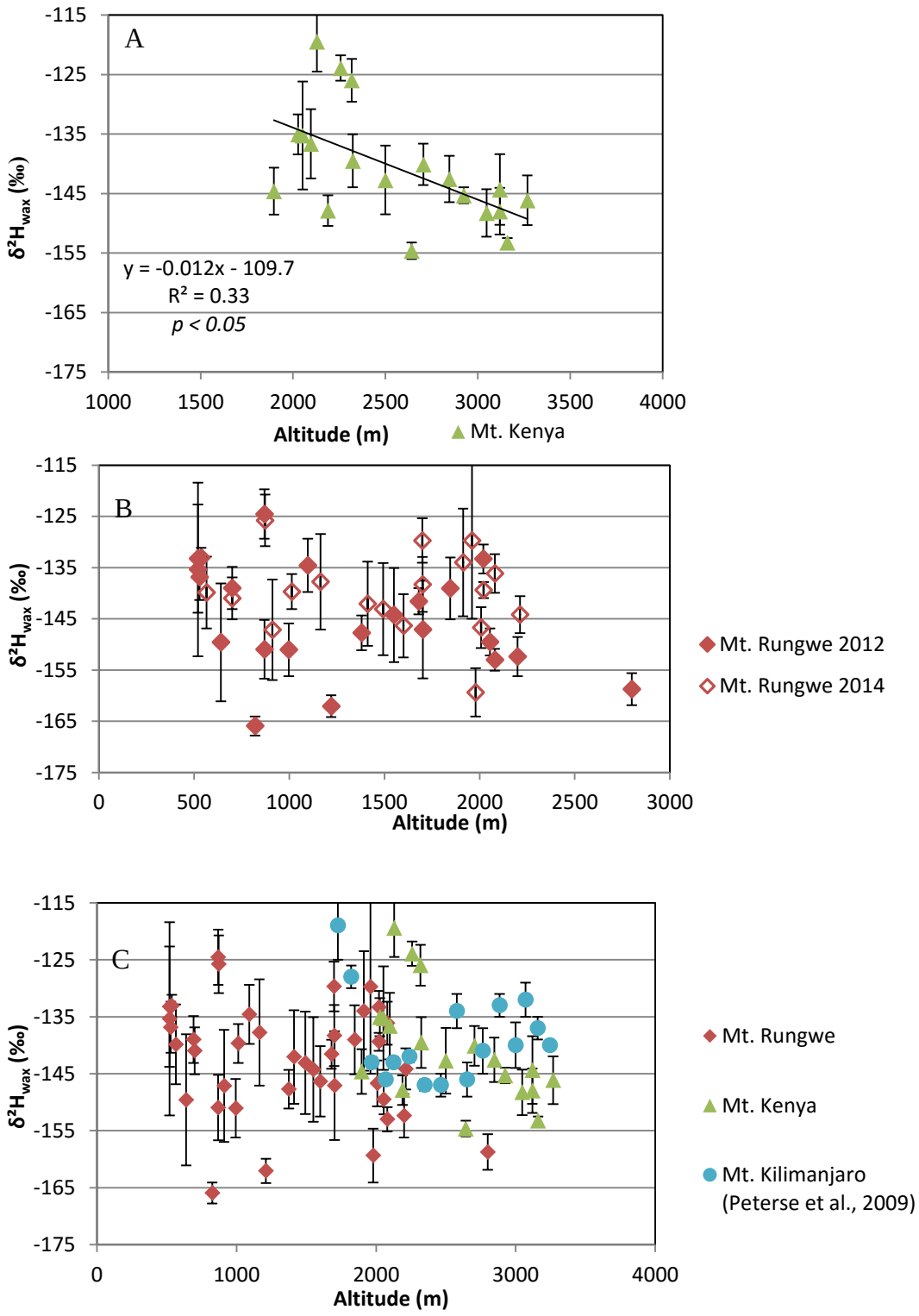

Figure 30: δ^2H_{wax} values variations (A) along Mt. Kenya, Kenya; (B) along Mt Rungwe, Tanzania; (soils sampled in 2012 (solid symbols) and in 2014 (open symbols) are distinguished) and (C) at a regional scale: combination of measurements along Mt. Rungwe (2012 and 2014; red diamonds), Mt. Kenya (green triangles) and Mt. Kilimanjaro, Tanzania (Peterse et al., 2009b; blue circles)

In order to get some insights on the potential physiological factors occurring during *n*-alkane biosynthesis, leaves from Bamboo (*Arundinaria tesselata*) and Avocado (*Persea Americana*) were collected along Mt. Rungwe and their δ^2H of individual *n*-alkanes measured. These two species were chosen because (i) they are representative of the vegetation and (ii) they are found all along the altitudinal gradient (500 – 2800 m.a.s.l.). The apparent fractionation ($\varepsilon_{l/p}$; equation 20 in section 1.2.3.2.) between the isotopic composition of precipitations (Bergonzini, personal communication) and of the C_{29} *n*-alkanes of each species was calculated (Figure 31). Indeed species-specific $\varepsilon_{l/p}$ was already reported in several studies (Chikaraishi and Naraoka, 2007; Hou et al., 2007; Eley et al., 2014) and could partly explain the lack of trend observed along the 2 mountains. As the *n*-alkanes detected in soil are derived from a mix of vegetation, their apparent fractionation will be a weighted average of the apparent fractionation of each plant. Thus, if the vegetation cover changes along the gradient, the *n*-alkane isotopic signature may record changes in vegetation rather than changes in δ^2Hp due to the altitudinal effect. These two plants exhibit different $\varepsilon_{l/p}$ which both generally increased with altitude (Figure 31; except for Bamboo around 2000 m altitude, potentially because these plants were sampled in a montane forest environment). This trend suggests that *n*-alkanes biosynthesised at high altitude were more ^2H-enriched (*i.e.* resulting in an increase in δ^2H_{wax} with altitude) than those biosynthesised at lower altitudes which would have eased or cancelled the expected depletion related to altitude. This phenomenon could be explained by increasing water evaporation from the soil and/or from the leaves at higher altitudes. *n*-Alkane isotopic signature sensitivity to evapotranspiration processes was indeed demonstrated by Kahmen et al. (2013a, 2013b). However, as no environmental parameters apart from temperature and δ^2Hp were carefully monitored along Mt. Rungwe, it is difficult to determine the causes of the lack of record of the altitudinal effect in the δ^2H_{wax}.

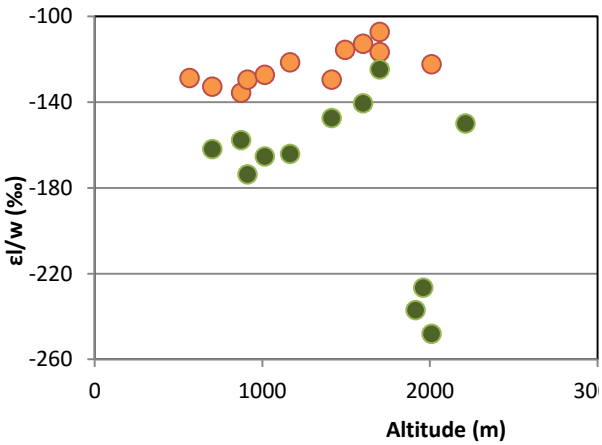

Figure 31: Variation with altitude of apparent fractionation (εl/w) of C_{29} alkane of two plant species, Bamboo (green cirles) and Avocado (orange circles), sampled along Mt. Rungwe.

Table 5. GDGT (MBT, CBT, calculation details are presented in section 1.2.2.2.) and *n*-alkane (ACL, CPI, calculation details are presented in section 1.2.3.2) distribution parameters, together with the δ^2H of the most abundant *n*-alkanes (C_{27}, C_{29} and C_{31}) and the average δ^2H of these *n*-alkanes (denoted δ^2H_{wax}). *These samples exhibit UCM located at the mid-chain *n*-alkanes elution time, suggesting contamination. This does not impact long chain *n*-alkane distribution nor hydrogen isotopic signature. Therefore these samples were kept in the dataset.

campaign	Sample n°	altitude	MBT	CBT	C_n range	C_{max}	ACL	CPI	δ^2H_{C27}	δ^2H_{C29}	δ^2H_{C31}	δ^2H_{wax}
Mt. Rungwe (2012)	1	520	0.69	0.08	17-33	31	30	12	-118	-127	-141	-132
	2	520	0.74	0.22	14-33	29	28	12	-109	-138	-147	-132
	3	529	0.72	0.09	16-33	29	28	9	-119	-140	-139	-136
	4	640	0.63	0.29	14-33	29	28	15	-122	-149	-157	-146
	5	700	0.69	0.16	14-33	29	27	9	-133	-139	-144	-137
	6	820	0.61	0.46	14-33	31	29	11	-146	-163	-177	-163
	7	869	0.69	0.48	14-33	29	27	11	-140	-154	-156	-150
	8	869	0.79	0.68	14-33	31	27	8	-112	-125	-127	-123
	9	997	0.66	0.33	14-33	29	27	10	-136	-158	-152	-150
	10	1097	0.66	0.59	14-33	31	27	13	-131	-136	-135	-137
	11	1220	0.75	0.73	20-33	31	28	15	-152	-166	-163	-162
	12	1380	0.82	0.78	20-33	31	28	13	-145	-147	-149	-149
	13	1550	0.65	1.01	16-33	31	27	11	-136	-145	-146	-147
	14	1680	0.57	0.53	18-33	31	29	12	-130	-138	-149	-142
	15	1702	0.65	0.68	17-33	31	29	10	-133	-138	-155	-146
	16	1846	0.58	0.57	20-33	31	28	11	-131	-139	-142	-138
	17	2020	0.48	0.57	14-33	29	26	10	-135	-133	-133	-133
	18	2055	0.42	0.34	14-33	29	28	18	-134	-152	-145	-149
	19	2080	0.61	0.84	*	*	21	*	-134	-156	-158	-139
	20	2200	0.58	0.90	14-33	31	25	8	-156	-149	-153	-127
	21	2800	0.58	0.85	14-33	27	24	4	-156	-163	-160	-122
Mt. Rungwe (2014)	22	537	0.78	0.53	16-35	31	29	13	-114	-138	-136	-130
	23	565	0.83	1.16	16-35	29	29	10	-120	-140	-149	-137
	24	700	0.71	0.15	15-35	31	30	9	-133	-139	-144	-140
	25	873	0.78	0.87	15-35	31	30	7	-109	-125	-130	-125
	26	911	0.84	1.06	17-33	31	29	4	-123	-152	-154	-146
	27	1013	0.78	0.82	16-35	31	30	7	-121	-140	-146	-141
	28	1164	0.82	1.21	18-35	31	29	10	-144	-122	-152	-136
	29	1412	0.61	0.65	14-35	31	30	9	-110	-135	-157	-141
	30	1493	0.70	0.96	16-35	31	29	10	-133	-143	-148	-142
	31	1600	0.66	0.85	13-35	31	29	6	-145	-142	-150	-147
	32	1699	0.69	0.96	16-35	31	30	7	-115	-128	-135	-130
	33	1700	0.64	0.89	16-35	31	30	10	-111	-140	-148	-139
	34	1913	0.45	0.39	18-35	29	29	16	-131	-133	-138	-134
	35	1960	0.48	0.46	16-35	29	29	9	-161	-120	-131	-132
	36	2008	0.46	0.46	16-35	33	31	12	-119	-143	-152	-146
	37	2212	0.64	1.28	19-37	31	29	16	-114	-149	-141	-144
	38	2080	-	-	15-35	31	30	9	-132	-129	-140	-136
	39	2021	-	-	15-35	29	29	14	-130	-141	-144	-138
	40	1979	-	-	15-35	29	29	10	-158	-170	-149	-159
Mt. Kenya (2013)	41	3160	0.46	1.37	*	*	25	*	-158	-155	-143	-149
	42	3119	0.49	1.48	12-35	31	30	6	-141	-148	-149	-147
	43	3119	0.40	1.28	12-35	31	30	5	-121	-164	-167	-157
	44	3119	0.45	1.53	12-35	31	31	5	-135	-141	-149	-141
	45	3268	0.47	1.52	12-33	31	27	3	-156	-154	-132	-146
	46	3047	0.36	0.53	14-35	31	30	5	-136	-150	-151	-147

	47	2924	0.29	0.58	14-35	31	30	6	-158	-148	-141	-145
	48	2846	0.40	0.55	14-35	29	30	4	-136	-143	-145	-143
	49	2705	0.36	0.61	14-35	33	31	6	-134	-136	-144	-139
	50	2642	0.32	0.38	14-35	31	29	3	-149	-156	-156	-154
	51	2500	0.52	0.81	14-35	33	27	5	-144	-137	-144	-142
	52	2323	0.68	1.05	12-35	31	24	3	-135	-139	-141	-136
	53	2189	0.43	0.93	12-35	31	25	4	-143	-147	-150	-147
	54	2097	0.64	1.17	*	*	23	*	-134	-133	-139	-136
	55	2052	0.49	0.87	12-35	33	25	3	-135	-124	-141	-135
	56	1897	0.69	1.32	12-35	33	27	5	-146	-143	-145	-144
	57	2027	0.71	1.06	12-35	33	26	4	-127	-125	-141	-134
	58	2130	0.51	0.86	12-35	31	26	6	-108	-116	-122	-120
	59	2258	0.63	0.67	*	*	23	*	-123	-123	-126	-123
	60	2318	0.61	0.78	12-35	31	26	4	-120	-124	-130	-126

4.2.3 East African regional br GDGT calibration:

Br GDGTs were analysed in the same surface soils along Mt. Kenya and along Mt. Rungwe as for *n*-alkane analyses. Br GDGT proxies and corresponding temperature estimates were previously determined in 20 surface soils collected along Mt. Rungwe in 2012 and already published (see section 4.1., Coffinet et al., 2014). Here, 16 additional soil samples, collected in the RVP in 2014, were analysed for their br GDGT content and distribution. Br GDGT concentrations were similar in these soils (2.6 ± 2.1 µg/g dry wt. soil, Appendix 3) and in those analysed in 2012 (2.1 ± 1.2 µg/g dry wt. soil; section 4.1., Coffinet et al., 2014). In addition, the ranges of MBT' and CBT values were comparable for soils collected in 2014 (0.45 - 0.85 and 0.15 - 1.28 , respectively; Table 5), and those collected in 2012 (0.42 - 0.82,and 0.08 - 1.01, respectively; section 4.1., Coffinet et al., 2014). In Mt. Kenya, MBT' and CBT varied between 0.29 and 0.71, and 0.38 and 1.53, respectively (Table 5).

Br GDGT distribution was previously investigated in two additional East African mountains: Mt. Rwenzori (Uganda; Loomis et al., 2011) and Mt. Kilimanjaro (Tanzania, Sinninghe Damsté et al., 2008). Br GDGT-derived MAATs were determined using the global soil calibrations (Weijers et al., 2007; Peterse et al., 2012) and were found to successfully record the decrease in MAAT with altitude along these two mountains. Br GDGT-derived MAATs calculated using the soil calibration by Peterse et al. (2012) were also shown to decrease linearly with altitude along Mts. Rungwe and Kenya (R^2 0.79 and 0.67 respectively; data not shown). Combined together, these four studies highlight the robustness of br GDGTs as a temperature proxy in East Africa. However, the application of the global soil calibration still leads to substantial uncertainty in the temperature reconstruction (Root Mean Square Error (RMSE) = 5°C, Peterse et al., 2012 and R^2 0.61, Figure 32).

All together, when considering the present data and those already published (Sinninghe Damsté et al., 2008; Loomis et al., 2011; Coffinet et al., 2014), br GDGTs were analysed in 105 East African surface soils. Based on this large amount of samples (n=105), a least square multiple linear regression was performed between the MBT', CBT and the measured MAAT available for these 4 mountains (see section 4.2.1.). The following equation was obtained:

$$MAAT = -8.17 \times CBT + 25.39 \times MBT + 9.14 \quad (R^2 = 0.75, \text{RMSE} = 2.4\ °C) \qquad (29)$$

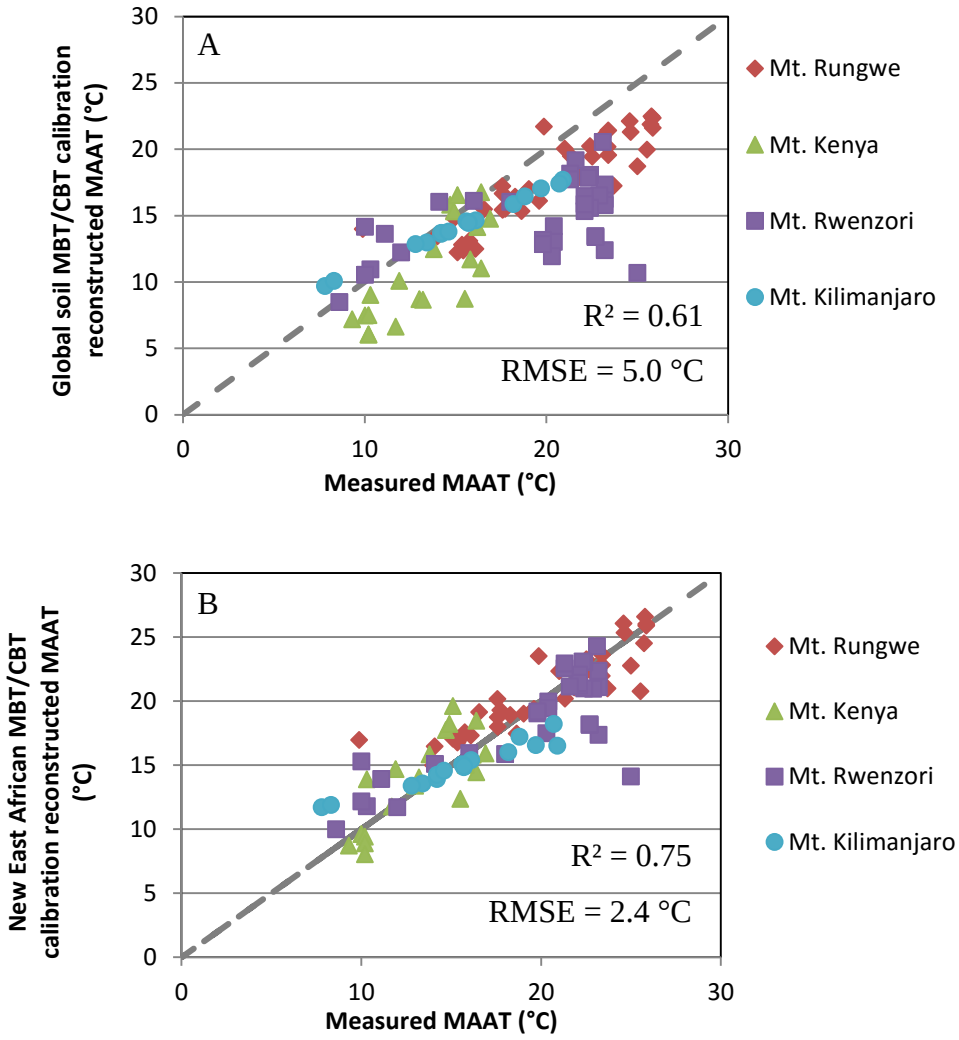

Figure 32 : Comparison of the accuracy and precision of (A) the global soil MBT/CBT calibration (Peterse et al., 2012) and (B) the new East African regional calibration developed in this study. Colours correspond to each mountain studied in the region: Mt Rungwe (red diamonds; Mt. Rungwe, this study and Coffinet et al., 2014); Mt. Kenya (green triangles; this study); Mt. Rwenzori (purple squares; Loomis et al., 2011); Mt. Kilimanjaro (blue circles; Sinninghe Damsté et al., 2008). The 1:1 line is represented in dashed grey as a reference.

This East African soil calibration (Figure 32) improves both the R^2 and RMSE of br GDGT-reconstructed MAAT over the global soil calibration (Figure 32, Peterse et al., 2012). The latter was developed based on the br GDGT distribution analysis of more than 250 surface soil samples globally distributed (see section 1.2.2.2). Regional calibrations were already developed in East African lakes (Tierney et al., 2010; Loomis et al., 2012) and also improved the robustness of the relationship between br GDGT distribution and temperature. This East African soil calibration was applied to the MAAT reconstruction along all the altitudinal transects (Figure 33). Br GDGT-derived MAAT lapse rate (0.05 °C/100 m; Figure 33) was

consistent with the measured one (0.06 °C/100 m; Figure 27). In addition, reconstructed MAAT was as dependent to altitude (R^2 0.80; Figure 33) as measured one (R^2 0.93; Figure 27).

The higher performance of the present regional soil calibration for MAAT reconstruction compared to the global one (Peterse et al., 2012) highlights the fact that other environmental parameters, such as hydrological regimes or soil physical and chemical properties (Dirghangi et al., 2013), may also impact br GDGT distribution in soils. This may partly explain the global soil calibration scatter (Peterse et al., 2012). Recently, the improvement of the br GDGT separation using silica columns led to the detection of additional GDGT isomers, which may represent up to 24% of the total br GDGTs (*i.e.* 5- and 6-methyl br GDGTs; De Jonge et al., 2014; Figure 13). These isomers were observed to be responsible for the correlation of the MBT' to both temperature and pH. Exclusion of the 6-methyl br GDGTs from the MBT' showed that it is no longer related to pH and allowed to slightly reduce the scatter of the global soil calibration (De Jonge et al., 2014). However no East African soils were included in this new global soil calibration. The relative abundance of 5- and 6-methyl isomers should thus be explored in East African soils as it might further improve the accuracy of the East African soil calibration. Another avenue for research is to test the applicability of the regional calibration developed in this study to other tropical areas to determine if common environmental parameters (such as soil water content) are controlling GDGT distributions in tropical areas.

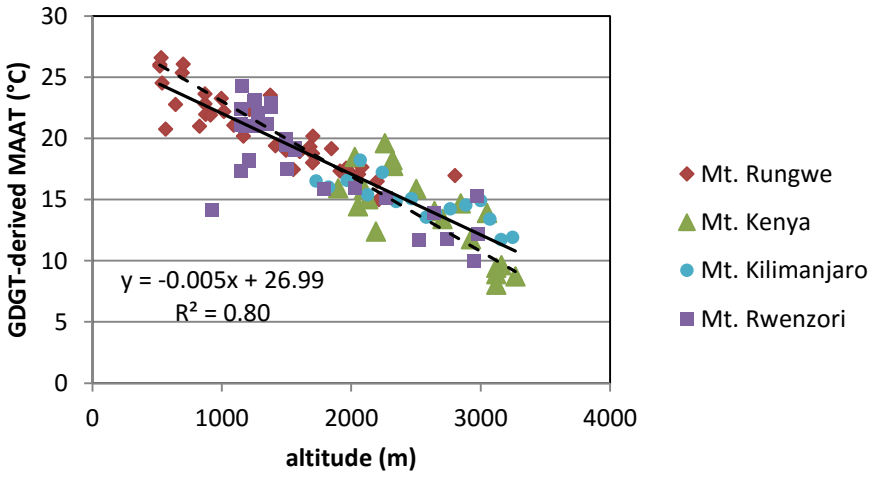

Figure 33: br GDGT-derived MAAT variation with altitude in East Africa according to the new East African regional calibration. The black solid line is the derived linear regression obtained from br GDGT-derived MAAT while the dashed black line is the measured MAAT altitudinal gradient (as presented in Figure 27).

4.2.4 Conclusion and implications:

δ^2H_{wax} and br GDGT distribution were determined in surface soils collected along two East African mountains (Mt. Rungwe in Tanzania and Mt. Kenya in Kenya). The values obtained in the present study were combined with data from altitudinal gradients previously investigated in the region to assess the applicability of δ^2H_{wax} and br GDGT as climatic proxies in East Africa. Br GDGTs appear to be less influenced by local environmental factors than $\delta^2H_{wax.}$ Indeed, δ^2H_{wax} variations did not systematically reflect altitudinal changes: a linear relationship between δ^2H_{wax} and altitude was observed for only one of the three investigated East African mountains. This study stresses the remaining gaps in the understanding of the environmental parameters driving the δ^2H values of *n*-alkanes. This calls for caution about the use of δ^2H_{wax} as a precipitation proxy in (paleo) soil archives. In contrast, br GDGT-derived MAAT were shown to record measured MAAT gradient along the four studied mountains. A regional East African calibration between br GDGTs and MAAT was developed. This improved both the accuracy and precision of MAAT reconstruction in the region compared to the global soil calibrations.

Conclusions of the chapter:

- Iso GDGTs could be used as paleoelevation proxy in the RVP.
- δ^2H_{wax} applicability to track the δ^2H of precipitations is hampered by additional physiological and/or environmental parameters.
- Br GDGTs are robust temperature proxies (i) in the RVP and (ii) regionally in East Africa.
- A new soil calibration was developed at the regional scale for East Africa to improve the precision and accuracy of br GDGT-derived MAAT reconstructions.

Chapter 5.

The Kyambangunguru marsh: Investigation of the biosynthesis of GDGTs and multi-proxy reconstruction of past environmental changes

This chapter combines analyses made on a 4 m peat core collected in December 2012 in the marsh at the centre of the Kyambangunguru crater (see section 2.2.). The first part is a methodological study investigating GDGTs and related molecules, the glycerol dialkanol diethers (GDDs), to attempt to understand the relationships between them. This study was published in *Organic Geochemistry* (Coffinet et al., 2015). The second part proposes a reonstruction of the ecological history of the site and of the potential drivers of the ecological transition over the last 4000 yrs, based on a multi-proxy approach. The latter involves GDGT and *n*-alkane analyses along with elemental analysis and light microscopy observations.This second part is to be submitted to *Quaternary Science Reviews.*

5.1. Occurrence and distribution of glycerol dialkanol diethers and glycerol dialkyl glycerol tetraethers in a peatcore from SW Tanzania

5.1.1 Introduction

Recently, a range of new glycerol ether lipids were detected (Liu et al., 2012c) including glycerol dialkanol diethers (GDDs) which resemble GDGTs, in that the alkyl chains are attached to a glycerol at one end and to hydroxyl groups at the other end (Figure 34). Like GDGTs, both GDDs with isoprenoid alkyl chains (iso GDDs; e.g. Liu et al., 2012a) and with branched alkyl chains (br GDDs; Yang et al., 2014b) have been detected, suggesting a dual archaeal and bacterial origin for these lipids. They were found in sediment (Knappy and Keely, 2011; Liu et al., 2012a, 2012c; Becker et al., 2013; Meador et al., 2014), soil (Yang et al., 2014b) and peat (Liu et al., 2012a). The iso GDDs were also found in pure archaeal cultures (Liu et al., 2012a, 2012c; Meador et al., 2014). Yet neither their source, function nor association with GDGTs have been clearly determined. Two hypotheses were proposed (Liu et al., 2012a; Meador et al., 2014; Yang et al., 2014b): GDDs could be (i) degradation products of GDGTs or (ii) biosynthetic compounds, either as structural membrane compounds or as GDGT intermediates. Meador et al. (2014) characterised for the first time a series of iso GDD IPLs with a glycosidic head group in estuarine and hot spring sediments as well as in a pure archaeal culture (*Nitrosopumilus maritimus*). This suggests that at least part of the iso GDD pool is of biosynthetic origin. Indeed, in living cells, membrane lipids are bound to a polar head group (sugar and/or phosphate units; Nishihara and Koga, 1987). In contrast, the

majority of the lipids found in natural environments have lost this head group upon cell death or lysis (White et al., 1979; Harvey et al., 1986; Logemann et al., 2011) and are detected as core lipids (structures in Figure 34).

In order to investigate the presence and the origin of GDDs in terrestrial environments, we analysed iso and br GDGTs and GDDs - either as core lipids (CLs) or derived from intact polar lipids (IPLs) - along a 4 m peat core from Tanzania, where GDGTs and GDDs were expected to be abundant. Indeed, the organic carbon content is high in peat, as a result of a low biodegradation activity (Laggoun-Défarge et al., 2008a). In addition, previous studies have shown that anaerobic peat bogs are enriched in br GDGTs, either due to an increase in source microorganisms or preservation (Weijers et al., 2006; Huguet et al., 2010a). The objectives of this work were to (i) compare the variation in GDGT and GDD abundance and distribution with depth and (ii) test for the presence of GDD IPLs in the core. To the best of our knowledge, the detection of br GDDs in the IPL form has not been reported.

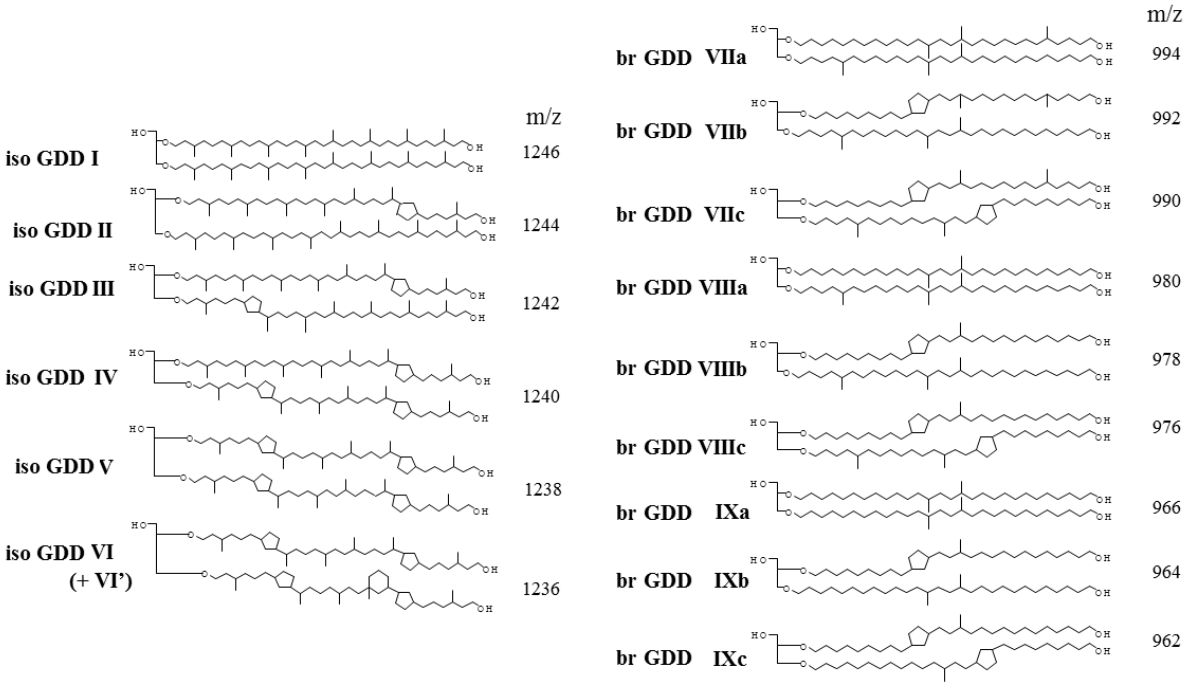

Figure 34: Structures of isoprenoid (on the left) and branched (on the right) glycerol dialkanol diethers (GDDs) and their m/z ratio related to their molar mass.

5.1.2 Variation in GDGT and GDD concentration with depth

Br GDGTs and iso GDGTs were detected in every sample, both in the CL and IPL fractions. In the CL fraction, total br GDGT concentration varied between 61.4 and 633.0 µg/g $C_{org,}$ and total iso GDGT concentration between 18.3 and 235.5 µg/g C_{org} (Figure 35a, b and Appendix 4). Br GDGT CL concentrations (2.4-354.5 µg/g dry wt. peat) in the Kyambangunguru swamp are in the lower end range of those found in a 1 m core from a Swiss peatland (20-1700 µg/g dry wt. peat; (Weijers et al., 2011) and comparable to those observed in a 50 cm German peat core (140-370 µg/g dry wt. peat; Liu et al., 2010). Similarly, iso GDGT CL concentrations in Kyambangunguru (0.7-131.6 µg/g dry wt. peat) are generally lower than those observed in the Swiss peat core mentioned above (10-700 µg/g dry wt. peat; Weijers et al., 2011) but higher than those found in a German peat core (2-17 µg/g dry wt. peat; Liu et al., 2010). Both br and iso GDGT CL concentrations in the Kyambangunguru swamp are also much higher than those in surficial soils from the Mt. Rungwe area (1.1-8.3 µg/g C_{org} and 0.05-1.5 µg/g C_{org} for br GDGTs and iso GDGTs respectively; Coffinet et al., 2014). This is consistent with observations that br GDGTs and iso GDGTs are especially abundant in peat deposits, suggesting that the anaerobic and acidic conditions there are favourable for the growth of GDGT source microorganisms and/or GDGT preservation (Pancost et al., 2000; Weijers et al., 2006; Huguet et al., 2010a).

In addition to GDGTs, br GDDs and iso GDDs were also detected in the CL and IPL fractions of all samples (Figure 35a, b, d, e). This is the first indication of br GDD IPLs in natural samples. GDD CL concentration ranged between 0.5 and 26.2 µg/g C_{org}, while the GDD IPL concentration was between 0.2 and 1.3 µg/g C_{org} (Figure 35a, b, d, e and Appendix 4). The proportion of GDDs relative to the total lipid pool (GDDs + GDGTs) ranged between 1 and 6% for br GDDs and iso GDDs in the CL fraction, and between 1 and 8% for br GDDs and iso GDDs in the IPL fraction, which is in the same range as in previous studies (3.5-17% for iso GDD CLs in marine sediments, Liu et al., 2012a; 2-15% for br GDD CLs and 6-16% for iso GDD CLs in soils, Yang et al., 2014b; 7-10% for iso GDD CLs and 3-4% for iso GDD IPLs in estuarine sediments, Meador et al., 2014).

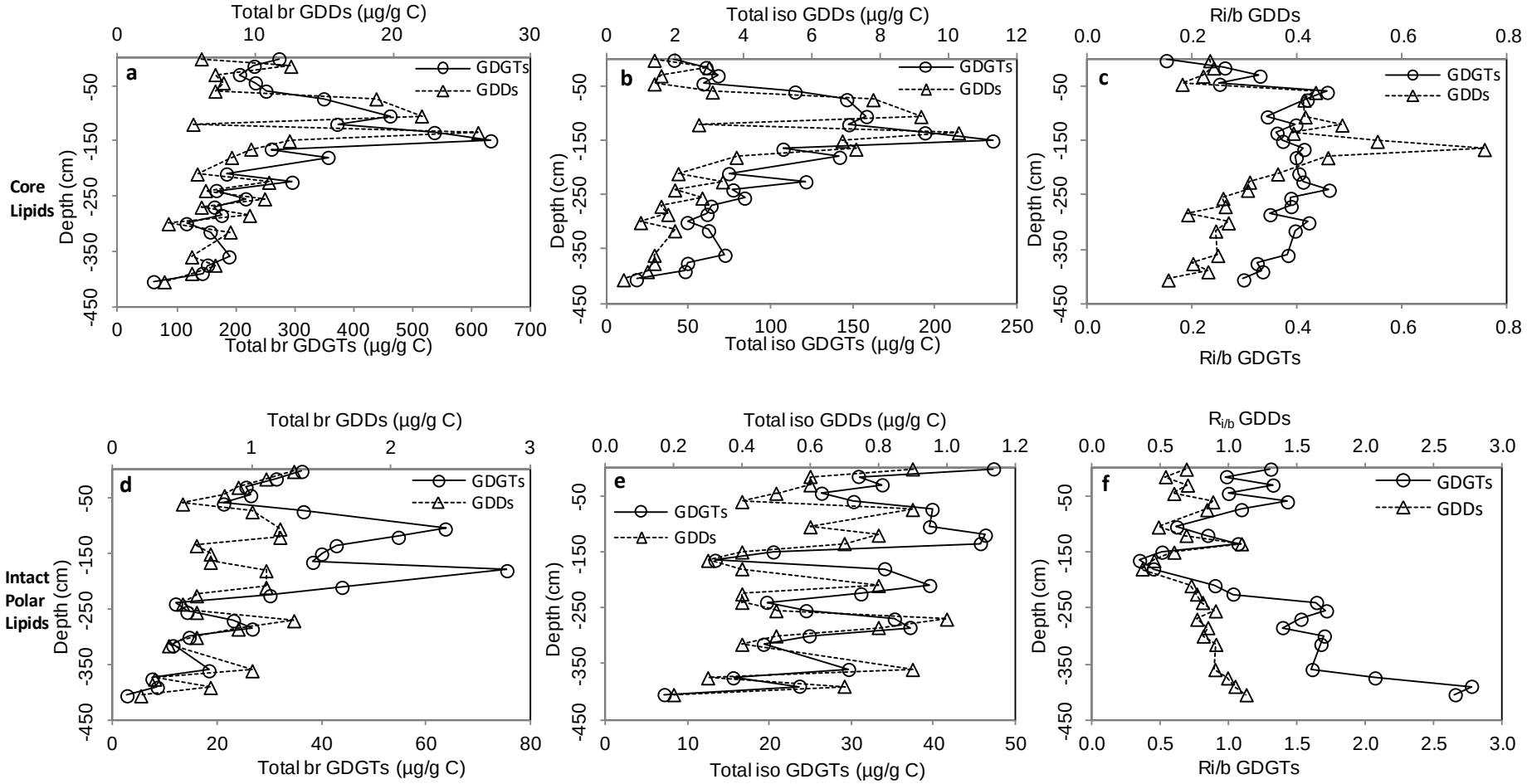

Figure 35: Depth profiles of GDD and GDGT concentration and of the ratio of isoprenoid over branched (Ri/b) ether lipids in CL (a-c) and IPL (d-f) fractions.

Depth profiles of iso GDGT and iso GDD concentration were comparable (Figure 35b, e) and correlated significantly in both lipid pools (R^2 0.56 and 0.58 for the CL and IPL fractions, respectively; $p < 0.05$; n=24), as previously observed by Meador et al. (2014) in estuarine sediments. Br GDGT and br GDD concentrations along the core were also found to correlate significantly ($p < 0.05$) in both the CL (R^2 0.42; Figure 35a) and IPL (R^2 0.47; Figure 35d) pools. In addition, the proportion of iso GDGTs vs.br GDGTs ($R_{i/b}$ ratio; Xie et al., 2012) co-varied significantly ($p < 0.05$) with the $R_{i/b}$ for GDDs, both in the CL (R^2 0.49; Figure 35c) and IPL fractions ($R^2$0.58; Figure 35f). A similar trend was observed by Yang et al. (2014b) for $R_{i/b}$ of GDD and GDGT CLs in Chinese soils and in a loess-paleosol sequence. Taken together, the consistent correlations between GDDs and GDGTs argue for a close relationship between these two types of molecules, either in their source, preservation or degradation processes.

In the CL fraction, the concentrations of br and iso GDGTs on the one hand, and br and iso GDDs on the other hand, showed comparable variation with depth (R^2 0.90 and 0.76 for GDGTs and GDDs, respectively; $p < 0.05$; Appendix 5A). Similarly, Weijers et al. (2009) observed a co-variation between iso GDGT and br GDGT CL concentration in a peat core from Sweden. This co-variation may be due to favourable environmental growth conditions in peat –such as anaerobic conditions (Pancost et al., 2000; Weijers et al., 2011) – shared by both archaea- and bacteria-producing GDGTs. Alternatively and/or complementarily, this might indicate that branched and isoprenoid compounds (either GDDs or GDGTs) have similar turnover in peat.

The concentration of br and iso GDGT and GDD CLs in Kyambangunguru peat core increased from the surface to 150 cm, where they reached a maximum and then decreased to a minimum at the bottom of the core (405 cm depth; Figure 35a, b). These depth profiles are similar to those observed for br and iso GDGTs by Weijers et al. (2006; 2011) in three peat cores from Switzerland, Sweden and the UK. This may be due to (i) the high accumulation rate of peat and (ii) the high preservation of organic matter (OM), and especially GDGTs (and GDDs), at these depths, as suggested by Weijers et al. (2006). It should be noted that we are here comparing a tropical peatland with 3 temperate ones. Additional peat cores from contrasting climatic environments need to be studied to confirm the generality of this trend.

GDGTs and GDDs in the IPL form were abundant all along the core, especially between ca. 1 and 2 m depth for br GDGTs (Figure 35d, e). This suggests the presence of GDGT-producing microorganisms all along the core. However, Xie et al. (2013) found the half-life of bacterial IPLs to be 100-1000 years at 1 m depth in marine sediments, suggesting that fossil IPLs may be preserved in particular environments. Such a phenomenon could also occur in peatlands, due to the very low degradation rate of OM in peat. This has to be taken into account when interpreting the IPL data in such settings.

5.1.3 Potential origin of GDDs

5.1.3.1. Relationship between GDGT and GDD distributions

GDGT distributions were similar in the IPL and CL fractions for both iso GDGTs and br GDGTs (Appendix 4), as observed in other peatlands (e.g. Huguet et al., 2010a). Compound I was the most abundant iso GDGT in both CL and IPL fractions, with a fractional abundance between 55 and 84% (Figure 36). Previous studies of peatlands support a dominant methanogenic origin for GDGT I in peat, as both methanogenic Euryarchaeota and GDGT I are relatively abundant in this setting (e.g. Pancost et al., 2000; Kotsyurbenko et al., 2004; Weijers et al., 2009). In contrast, compound VI was only detected in 11 of the 24 samples, with a fractional abundance < 6.5% (cf. Appendix 4). Fractional abundances of iso GDGTs II, III and IV were variable depending on the sample, but were systematically < 19.3% in both CL and IPL fractions (Figure 36b-d, f-h). GDGT IXa was largely predominant among the br GDGTs, with a fractional abundance in the CL and IPL fractions between 65 and 91% for GDGT IXa (Figure 37). Fractional abundance of GDGT VIIIa was between 9 and 31%, while that of GDGT VIIa was ≤ 4%, whatever the lipid pool (Figure 37a, b, d,e).

The relative distributions of the individual GDDs (either iso or br) were similar to those of the corresponding GDGTs, both in the CL and in the IPL fraction (Figure 36 and Figure 37). Fractional abundances of each iso GDD showed significant correlation ($p < 0.05$) with those of the corresponding iso GDGT (R^2 0.33 - 0.85) except for III in the CL fraction (Figure 36c). The correlation between iso GDGT and iso GDD VI was significant only in the CL

pool (R^2 0.54; $p < 0.05$; data not shown) and was less robust as these compounds were only detected in 10 out of 24 samples. Like the isoprenoid compounds, a significant correlation (R^2 0.83 - 0.97; $p < 2.6\times10^{-6}$) was observed between the fractional abundance of non-cyclic br GDDs and that of the corresponding br GDGTs, whatever the lipid pool (Figure 37). Cyclic br GDDs were tentatively assigned on the basis of their retention time and $[M+H]^+$ values. Nevertheless, since their relative abundance was very low (< 1%) and no structural elucidation was performed, they were not considered further in this study. Yang et al. (2014b) observed similar correlations between fractional abundances of GDGT and GDD CLs in Chinese surface soil samples and terrestrial sediments. Our results confirm and extend their finding, as correlation between fractional abundances of both iso and br GDGTs and GDDs are found for the first time in the IPL pool. It strongly suggests that these two groups of compounds are closely related and share common metabolic and/or degradation pathways (Liu et al., 2012a; Meador et al., 2014; Yang et al., 2014b), whatever their origin – archaeal or bacterial.

The correlations between individual br GDGT and br GDD relative abundances are close to the 1:1 line in both CL and IPL pools (Figure 37), suggesting that the two types of compounds share common sources. It should be noted that the regression line for *f*(br GDGT VIIIa) vs. *f*(br GDD VIIIa) is slightly below the 1:1 line, indicating the relative accumulation of GDD VIIIa vs. GDGT VIIIa (Figure 37b-e). An opposite trend was observed for GDGT IXa vs. GDD IXa (Figure 37c-f).The correlations between individual iso IPL GDGT and iso IPL GDD relative abundances also fall near the 1:1 line (Figure 36e-h), indicating potential common sources for iso GDGTs and iso GDDs. In the CL pool, a selective enrichment in iso GDGT I vs. iso GDD I on the one hand (Figure 36a) and in iso GDDs III and IV vs. iso GDGTs III and IV on the other hand (Figure 36c and d) was observed for samples from the 74-180 cm horizon, which correspond to most of the statistically defined outliers. The selective accumulation of iso GDDs III vs. the corresponding GDGT analogue in this horizon may also explain the lack of correlation observed between *f*(GDGT III) and *f*(GDD III).Preliminary results of organic matter analysis (Coffinet et al., see section 5.2) showed a clear shift from a lake to a peatland ecosystem in the 74-180 cm horizon. This may have led to changes in the composition of archaeal communities and also in the relative distribution of iso GDGTs and iso GDDs at these depths.

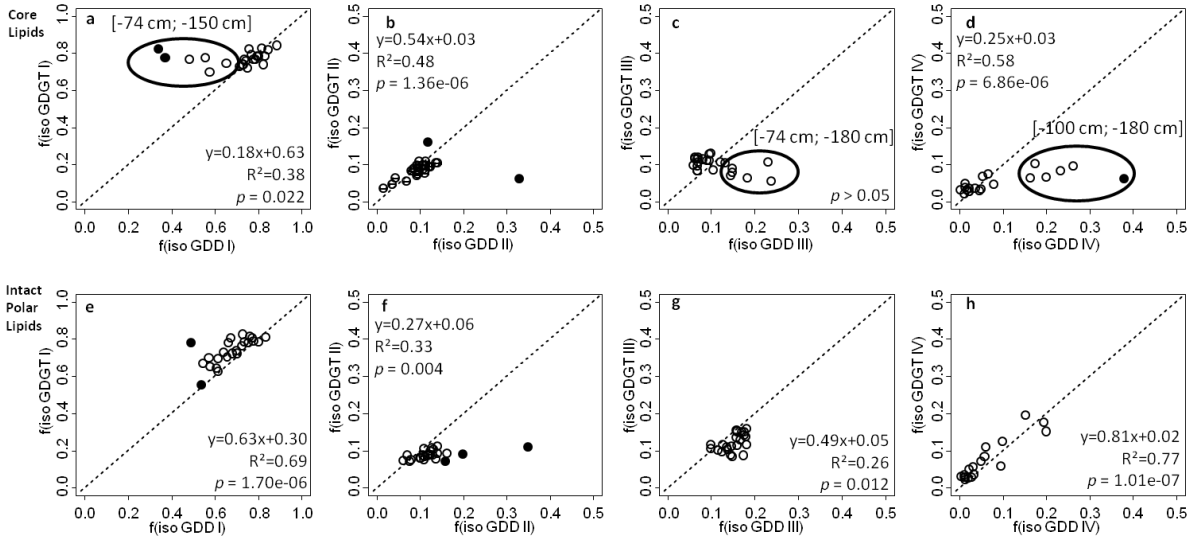

Figure 36: Correlations between fractional abundances of individual iso GDGTs and iso GDDs. The dotted line represents the 1:1 line. The black points were considered as outliers and were not included in the correlations. Encircled data points correspond to samples from the 74 cm -180 cm depth horizon.

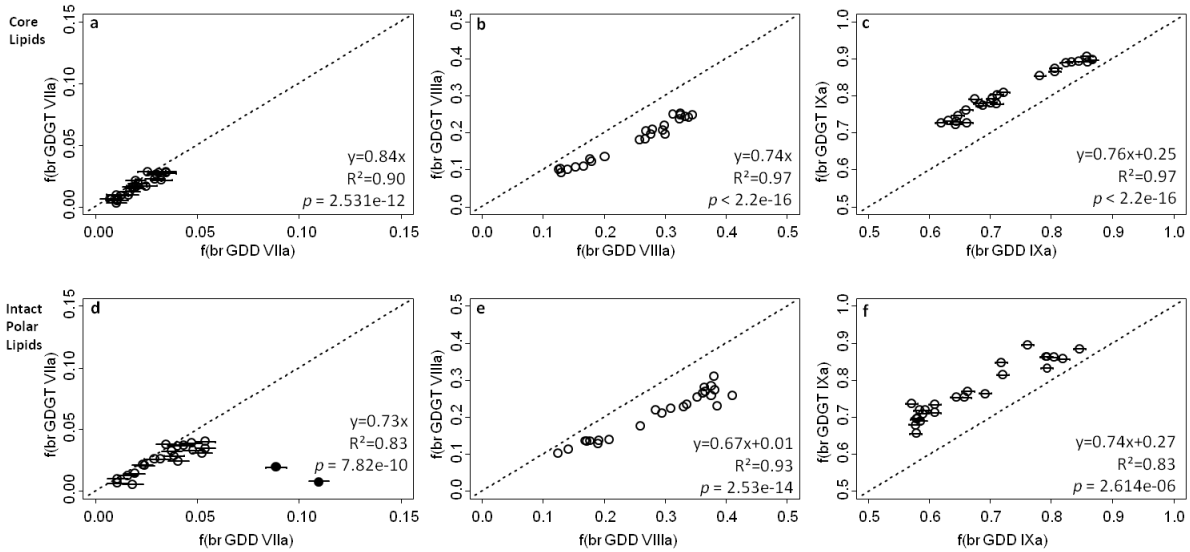

Figure 37: Correlation between fractional abundances of individual br GDGTs and br GDDs.The dotted line represents the 1:1 line. The black points were considered as outliers and were not considered in the correlations. Error bars were added when they were larger than the symbols.

5.1.3.2. Implications for origin of GDDs

The occurrence of iso GDD IPLs in the Kyambangunguru peatland confirms the observation of Meador et al. (2014) in sediments and archaeal cultures and their proposition that these compounds are - at least partly - of biosynthetic origin, based on the hypothesis that IPLs are markers of living viable organisms. It is assumed that the first step in the degradation of GDGT IPLs would be loss of the polar head group bound to core GDGTs, via enzymatic hydrolysis (White et al., 1996; Meador et al., 2014) rather than the cleavage of the 2 glycerol ether bonds of GDGT IPLs to yield GDD IPLs. The detection, for the first time, of br GDDs in the IPL form argues that br GDDs could, as well, have a biosynthetic origin based on the same rationales. Strong correlations were especially found between each br GDD IPL and its CL counterpart (R^2 0.31-0.93; $p < 0.05$; Appendix 5B) implying that, similarly to br GDGTs, br GDD CLs may derive from GDD IPLs. In addition, strong relationships between iso GDGT and GDD concentrations (Figure 35) on the one hand and br GDGT and GDD concentrations (Figure 35) on the other hand, were observed along the peat core. As also discussed above, some iso and br GDDs were noticed to be selectively enriched relative to their GDGT counterparts between 74 and 180 cm depth (compounds III and IV; Figure 36c-d) or over the whole core (compound VIIIa; Figure 37), suggesting a biosynthetic production of GDDs. Taken together, these observations support the idea that GDGTs and GDDs take part in similar or joint biosynthetic processes. However, the current hypotheses on the biosynthetic routes leading to the formation of GDGTs do not include GDD IPLs as biosynthetic intermediates of GDGTs. Indeed in the biosynthetic pathway of iso GDGTs, formation of the tetraether was described to occur via ω,ω' coupling of two diethers (Koga and Morii, 2007), and the biosynthetic pathway for br GDGTs proposed so far rather involves a dicarboxylic acid, *iso*-diabolic acid (Sinninghe Damsté et al., 2011). Nevertheless, other unknown pathways for GDGT biosynthesis, in which GDDs would be involved, may exist.

Alternatively, GDDs could be both an intermediate and a degradation product of GDGTs. Takano et al. (2010) proposed a recycling pathway for the synthesis of iso GDGTs in extreme environments with very low energy input, such as deep sea sediments. This pathway involves the potential recycling of biphytane diols derived from the degradation of ancient GDGTs, which would be further linked to newly synthesized glycerol. Liu et al.

(2012a) and Meador et al. (2014) proposed that iso GDDs may be involved in this pathway through glycerol addition or cleavage. Similar pathways are conceivable for br GDGTs. Further studies combining microbiology and geochemistry, notably in continental environments such as peatlands, are necessary to fully understand the role of GDDs in the environment. Nevertheless, the exact group(s) of bacteria biosynthesizing br GDGTs remain(s) unknown, even though some might belong to the phylum *Acidobacteria* (Weijers et al., 2009; Sinninghe Damsté et al., 2011). As long as the br GDGT source microorganisms are unknown, hypotheses on the origin and function of GDDs relative to GDGTs in bacterial membranes can only be speculative.

5.1.4 Conclusions

Br GDGTs, br GDDs, iso GDGTs and iso GDDs were detected in both the CL and IPL form along a 4 m peat core from SW Tanzania. It must be noted that it is the first report of br GDDs in the IPL form. Br GDD and iso GDD concentrations were found to co-vary significantly with br GDGT and iso GDGT abundances in both CL and IPL pools. Moreover, the relative abundance of each GDD was found to correlate significantly with its GDGT counterpart, the regression lines for GDGTs vs GDDs approximately being close to the 1:1 line for most of the compounds. Taken together, these results suggest a very close link between GDGTs and GDDs either of archaeal or bacterial origin. The detection of iso GDDs and br GDDs in the IPL-derived fraction of the peat core combined with the occurrence of iso GDD IPLs in sediments and in a pure archaeal culture (Meador et al., 2014) and the enrichment of some GDDs relative to their GDGT counterparts strongly argues in favor of a biosynthetic origin for at least part of the GDD pool, even though the hypothesis of GDDs being degradation products of GDGTs cannot be totally excluded. Additional studies are needed to fully understand the sources and fate of GDDs in natural environments.

5.2. Multi-proxy reconstruction of the environmental changes of a crater marsh in SW Tanzania (the Kyambangunguru marsh) over the last 4000 yrs

Light microscopy observations (palynofacies, palynology and macro remains), elemental (C_{org} and TN), molecular (GDGTs and *n*-alkanes) and isotopic analyses were combined to determine the environmental changes underwent by the Kyambangunguru marsh over the last 4000 yrs. In addition a model age was obtained based on AMS ^{14}C dating. In this part, we will first describe the results obtained for each type of analysis and then discuss the environmental changes along the core and their potential drivers.

5.2.1 Results

5.2.1.1. Lithology and chronostratigraphy

Dates were calibrated using the Bayesian approach of OxCal v. 4.2 software (Ramsey, 2008) with the ShCal13 atmospheric curve (Hogg et al., 2013) as the calibration set. Age obtained for the sample at 416 cm depth appears as outlier, potentially because of the low organic carbon (C_{org}) content in the sample, and was therefore rejected. A polynomial age model was derived from the 10 remaining ages obtained from bulk material (Figure 38).

The base of the core, at 4 m depth, consisted in a tephra layer. The following layers were a mixture of peat, gyttja and mineral layers (clay and sand, Figure 39). At ca. 200 cm an ash layer was observed. Above this layer, the core was predominantly constituted of peat at diverse stages of decay according to the depth: many vegetation remains were observed at the 175 – 75 cm interval while the decay was more pronounced from 75 cm to the top of the core. From 61 to 40 cm, a mineral layer was observed composed of two tephra layers at 60-61 and at 50-55 cm depths and clay otherwise (Figure 39).

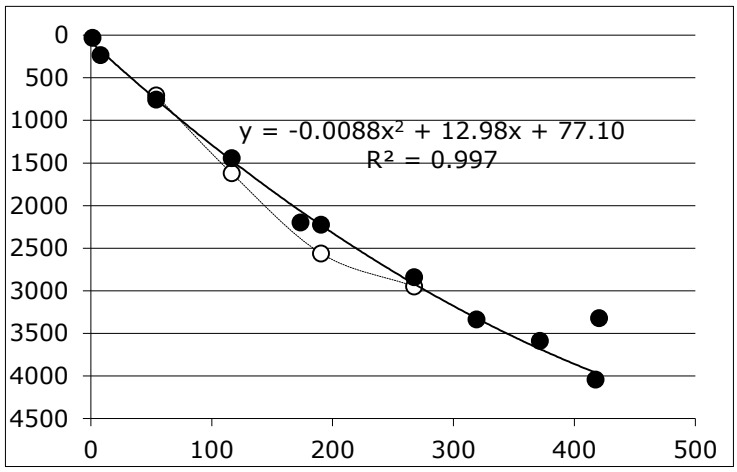

Figure 38: model age based on 14 ^{14}C AMS dates of bulk OM (black points). ^{14}C AMS dates of wood remains (white dots) are also represented.

5.2.1.2. Bulk carbon and nitrogen analyses

C_{org} content was high throughout the core (51.02 % ± 6.18, Table 6 and Figure 39), except in the tephra layer at the base of the core (ca. 4-5 %; Table 6 and Figure 39). Total nitrogen (TN) varied from 1.49 to 3.56 except for the tephra layer (0.24 %). Slightly lower TN values were observed in the 100 – 200 cm interval (ca. 2 %, Table 6 and Figure 39). As a result, the C/N ratio was higher in this interval (ranging from 16 to 38; Table 6 and Figure 45) while it was stable around 15 in the other parts of the core.

5.2.1.3. Palynofacies

The Kyambangunguru core is largely dominated (ca. 80% of the OM throughout the core) by ligno-cellulosic tissues (LC) deriving from vascular plants (Figure 39). These LC are found at 3 stages of degradation: (i) well-preserved tissues detected as translucent LC (tLC) in microscopy, (ii) slightly degraded/amorphised LC (saLC) in which cell structures are still partially recognisable and (iii) totally degraded/amorphised LC characterised by red aggregates of amorphous OM (rAOM). On average, tLC represent 19 % of total OM (Figure 39) while saLC particles are the most abundant type of OM (ca. 39 % on average) along the core. rAOM represents ca. 11 % of the total LC OM but increased to 20 % in the 300 - 63 cm depth horizon. In addition to this LC, mycelium from terrestrial fungi was observed between 240 cm and 60 cm depth. Grey membranes (algOM) and granular amorphous OM (gAOM; Figure 39), related to planktonic material, were mainly present at the base (until 330 cm) and at the surface (from 90 cm) of the core.

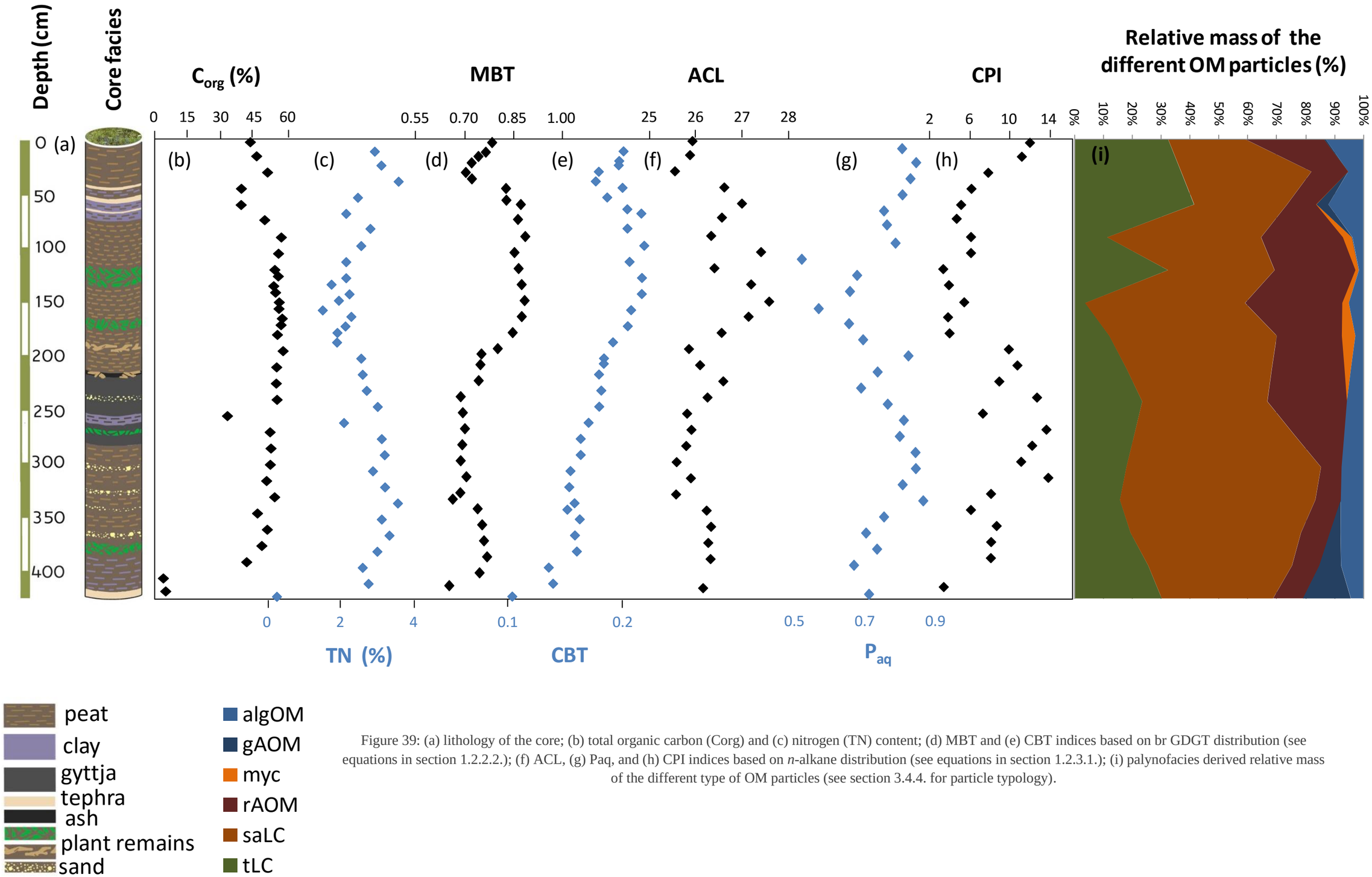

Figure 39: (a) lithology of the core; (b) total organic carbon (Corg) and (c) nitrogen (TN) content; (d) MBT and (e) CBT indices based on br GDGT distribution (see equations in section 1.2.2.2.); (f) ACL, (g) Paq, and (h) CPI indices based on *n*-alkane distribution (see equations in section 1.2.3.1.); (i) palynofacies derived relative mass of the different type of OM particles (see section 3.4.4. for particle typology).

5.2.1.4. Macroremain analysis

Macrofossils (Figure 40) are dominated by macrophytes (sedges, submerged/floating plants and algae) and wood remains. *Eleocharis sp.* (sedge) is present all along the core as well as *Nymphaea sp.* (floating macrophyte) which temporarily disappeared from 160 cm to 100 cm (Figure 40). In addition, from the base of the core until 280 cm, macrofossils are composed of remains of algae (*Nitella sp*, Figure 40) and submerged/floating plants (*Potamogeton sp.* and *Caldesia parnassiflora;* Figure 40). These species are replaced by *Juncus sp.* from 240 cm to 140 cm where more wood remains are also noticed in the profile. Eventually, from 140 cm to the surface, *Nitella sp.* reappeared together with *Carex sp.* and *Chara sp* (Figure 40).

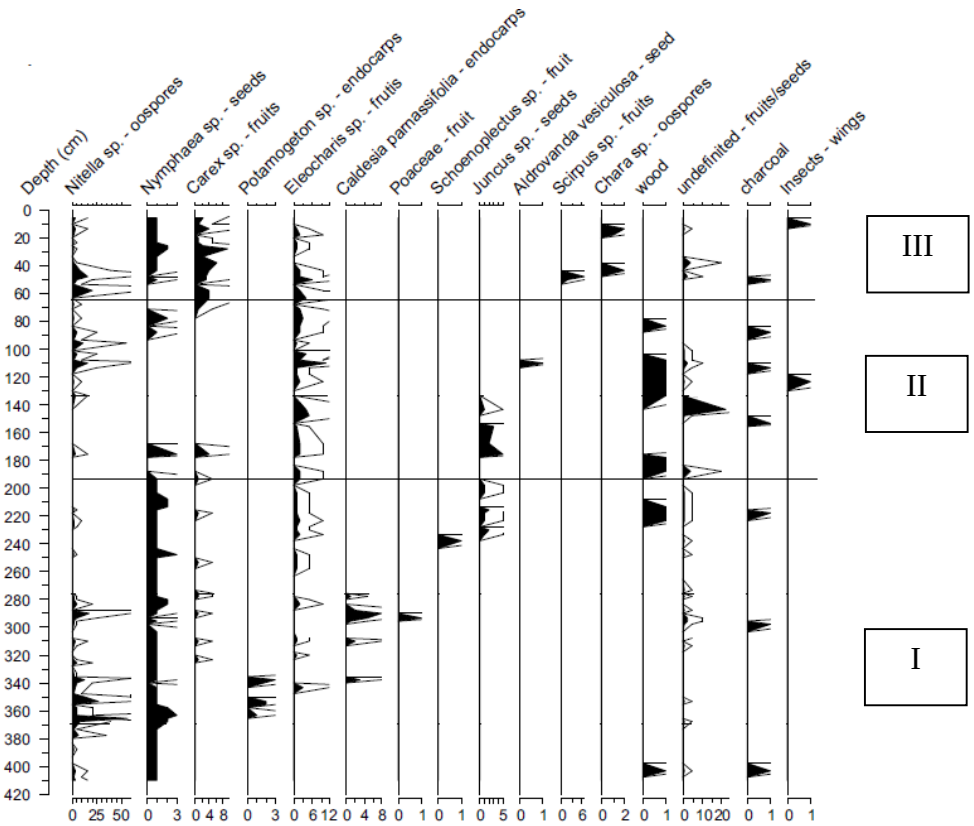

Figure 40: Macroremain diagrams. Results are given in absolute numbers. Roman numbers indicate the 3 ecological phases detected along the core (see section 5.2.2.1.)

5.2.1.5. Palynology:

Palynological analysis revealed the presence of 265 taxa of pollen and spores as well as non-pollen palynomorphs (NPPs). The results of palynological analysis are separated into two groups: (i) indicators of terrestrial vegetation, *i.e.* vegetation surrounding the marsh and (ii) indicators of marsh changes, *i.e.* those originated from taxa occurring in the marsh (Figure 41). Only the latter will be presented because they were saturating the archive making the interpretation of terrestrial taxa more hazardous. Note that fungal microremains (HdV and UG non pollen palynomorphs) were observed as well.

The lower part of the core (416–193 cm) is characterized by the predominance of (i) aquatic taxa such as pollen of Nymphaeaceae (*Nymphaea* type), (ii) epidermis of UG-1241 representatives and (iii) algae such as *Scenedesmus*, *Tetraedron minimum*, *Pediastrum* undiff., *Pediastrum angulosum* and *Botryococcus*. At the very base of the core, *Tetraedron trigonum* type, *Tetraedron incus/caudatum*, *Coelastraum reticulatum* and *Potamogeton* are highly abundant. All the aforementioned algae and submerged macrophytes rapidly decline from 393 to 363 cm. A linear decrease of Alismataceae (from 6.5% to 0.8%) is observed between 383 cm and 195 cm. At 303 cm, Cyperaceae spore percentages started increasing followed (at 253 cm) by an increase in monolete spores relative abundance.

The 193–93 cm depth interval is characterized by a prominent increase in Cyperaceae percentages (12–77%). From 193 cm to 113 cm, spores of *Lycopodiella caroliniana* (0.2–18%) as well as remains of testate amoeba *Assulina muscorum* are present. Monolete spores reach their highest values (64–69%) between 143 cm and 123 cm depth. In the meantime, relative percentage of fungal derived NPPs increased distinctly. UG-1077 and UG-1197 are predominant in the bottom part of the 193 – 93 cm depth interval whereas in its upper part, HdV-176, UG-1176, UG-1107 and *Entorrhiza* increase. At 113 cm and above, algae such as *Pediastrum angulosum*, *Botryococcus* and *Scenedesmus* together with *Nymphea* type become more frequent.

The upper part of the core (93–5 cm) has bipartite characters in terms of palynological patterns. From 93 to 46.5 cm, Cyperaceae pollen dominates (54–77%) together with spores of *Entorrhiza* fungi. In this section, optimum of Hallorrhagaceae pollen is detected (1.5–24%). From 54 cm and above, *Nymphaea* type percentages increases rapidly (up to 55%) and a subsequent rise of UG-1241, Alismataceae, *Potamogeton*, algae *Scenedesmus*, *T. minimum*, *Botryococcus*, and *Pediastrum* undiff. is observed.

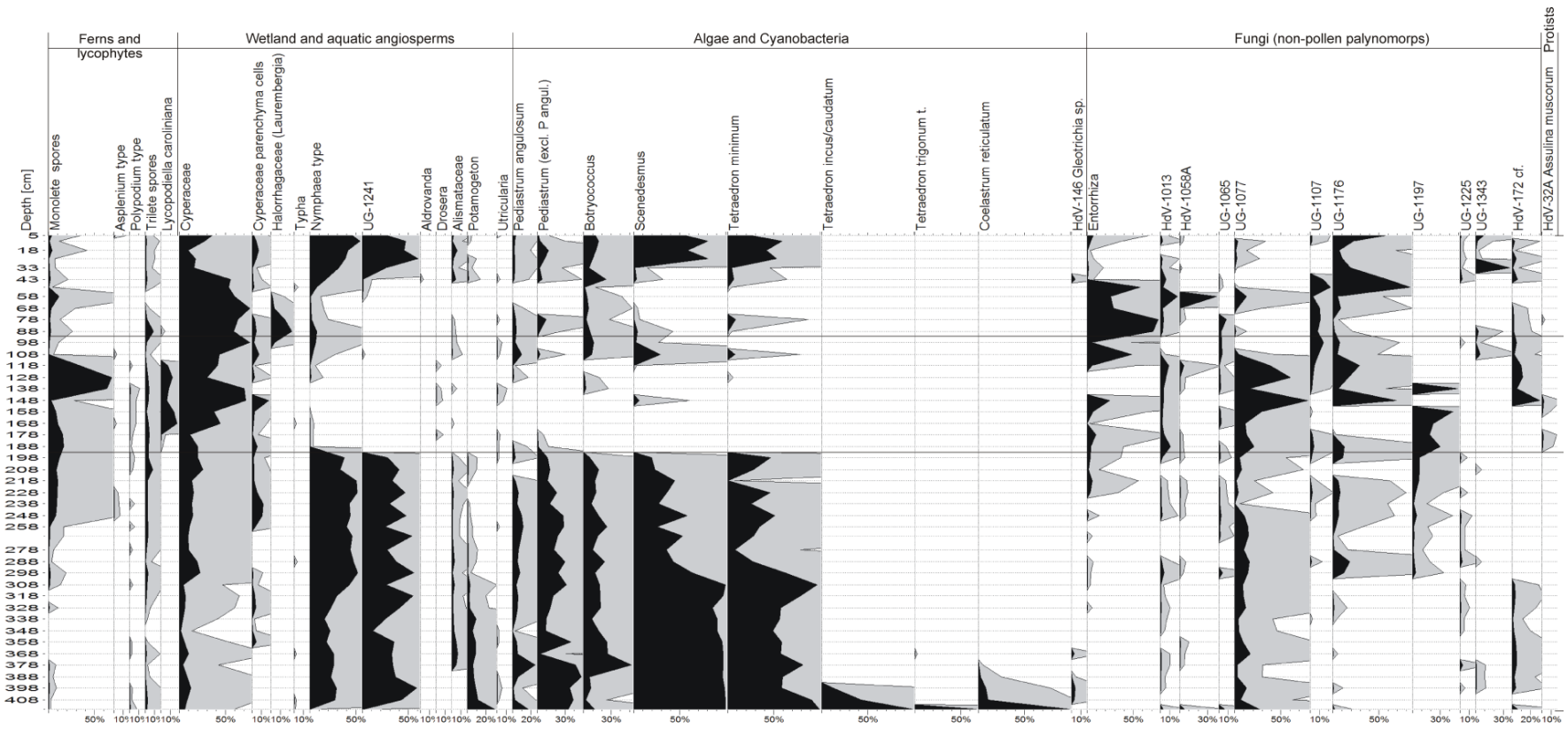

Figure 41: Ferns, aquatic pollen and NPP diagram for the Kyambangunguru marsh showing relative percentages of the selected taxa. They grey pattern shows a 10x magnification.

5.2.1.6. Br GDGT abundance and distribution:

For this multi-proxy study, only br GDGT core lipid variation was considered. Br GDGTs were abundant along the peat core (mean 121.5 ± 81.3 µg/g of dry wt. peat), with maximal concentration observed around ca. 150 cm depth. Br GDGT IXa was predominant among br GDGTs (mean fractional abundance 74%; Appendix 6). In contrast, cyclic brGDGTs were present at very low abundance, with average fractional abundances of compounds IXb and IXc being 4% and 2% (Appendix 6), respectively and other cyclic compounds (VII-VIIIb and VII-VIIIc) being detected in trace amounts (fractional abundance <0.2 %; Appendix 6). GDGT distribution and concentration of the 3 samples related to the tephra layer at the base of the core were different from the rest of the core, potentially because of input from non *in situ* material. Therefore they were discarded from the pH and temperature reconstructions. In the rest of the core, CBT varied from 0.53 to 2.01 with a mean value of 1.31 and was higher in the first 180 cm (1.41 – 2.01; Table 6 and Figure 39) than below (0.53 – 1.33; Table 6 and Figure 39). MBT was comprised between 0.65 and 0.89 with a mean value of 0.77 (Table 6 and Figure 39). The highest MBT values (>0.80) were encountered between 45 and 195 cm depth.

In order to determine the main source of br GDGTs in the Kyambangunguru marsh, the concentration and distribution of these compounds were examined in surficial peat samples and nearby soils (taken along the crater slopes and around the marsh). Both br GDGT abundance and distribution differed between surficial peat samples and soil samples collected near the marsh. In the soil samples, mean br GDGT concentration was 36.5 ± 14.7 µg/g C_{org} soil, *i.e.* ca. 7 times less than at the surface of the peat core (259.0 ± 27.6 µg/g C_{org}). In addition, the fractional abundance of GDGT IXb was much higher in the watershed soils (mean 13 %) than in the peat samples (mean 4 %). As a result the CBT ratio was significantly different between the surrounded soils (mean 0.79 ± 0.46) and the surficial peat (mean 1.49 ± 0.27; $p<0.05$, Mann-Whitney test on the means of the 5 soils and 5 first samples of the core; Figure 42). The MBT was higher in the watershed soils (mean 0.81 ± 0.08) than in the surficial peat samples (mean 0.74 ± 0.03) but this difference was not statistically significant ($p>0.05$; Figure 42).

Table 6: elemental analysis (organic carbon and total nitrogen), MBT index and CBT ratio derived from br GDGT distribution and br GDGT derived MAAT from the global soil calibration (Peterse et al., 2012) and the East African lacustrine calibration (Loomis et al., 2012).

Depth (cm)	TOC (%)	TN (%)	C/N	MBT	CBT	GDGT derived MAAT (°C) *Peterse et al. (2012)*	GDGT derived MAAT (°C) *Loomis et al. (2012)*
Soil A	-	-	-	0.90	0.80	24.3	27.5
Soil B	-	-	-	0.67	0.07	21.3	38.3
Soil C	-	-	-	0.82	0.61	22.7	31.9
Soil D	-	-	-	0.86	1.48	19.0	23.3
Soil E	-	-	-	0.80	0.98	20.1	26.7
2	43.1	2.9	14.8	0.77	2.01	13.4	16.1
12	-	-	-	0.77	1.46	16.3	21.0
15	45.9	3.1	14.9	0.74	1.46	15.6	20.3
22	-	-	-	0.72	1.29	16.0	21.0
30	50.8	3.6	14.3	0.71	1.26	15.5	20.2
37	-	-	-	0.72	1.49	14.8	20.1
45	39.1	2.5	15.9	0.83	1.36	18.8	22.2
57	-	-	-	0.83	1.53	17.9	21.5
60	39.0	2.1	18.3	0.87	1.66	18.6	21.5
73	49.5	2.8	17.8	0.87	1.53	19.0	21.8
90	57.0	2.5	22.4	0.89	1.68	18.8	21.8
105	55.7	2.1	26.2	0.86	1.55	18.5	21.5
120	54.1	2.1	25.4	0.87	1.66	18.3	21.3
127	55.6	1.7	32.1	-	-	-	-
135	53.6	2.2	24.1	0.88	1.66	18.6	21.7
142	54.4	1.9	28.2	-	-	-	-
150	56.0	1.5	37.6	0.89	1.57	19.4	22.0
157	55.9	2.3	24.6	-	-	-	-
165	57.4	2.1	27.2	0.88	1.54	19.3	21.9
172	56.9	1.9	30.1	-	-	-	-
180	55.2	1.9	29.4	0.85	1.41	19.2	21.6
195	57.8	2.5	22.7	0.80	1.33	18.2	21.1
201	-	-	-	0.75	1.33	16.7	20.5
210	54.9	2.6	21.3	0.75	1.29	16.8	20.4
225	54.7	2.7	20.3	0.74	1.31	16.5	20.5
240	55.1	3.0	18.4	0.69	1.29	14.9	19.7
255	32.8	2.1	15.9	0.70	1.20	15.6	20.6
270	51.9	3.1	16.8	0.70	1.13	16.2	20.8
285	52.3	3.2	16.5	0.69	1.13	15.9	21.1
300	52.0	2.9	18.2	0.69	1.04	16.3	21.8
315	50.4	3.2	15.8	0.71	1.03	17.0	22.1
330	54.0	3.5	15.3	0.69	1.07	16.1	21.3
337	-	-	-	0.66	1.01	15.7	22.0
345	46.3	3.1	14.9	0.74	1.12	17.5	22.3

360	50.7	3.3	15.3	0.76	1.08	18.1	22.8
375	48.2	3.0	16.2	0.76	1.09	18.2	22.8
390	41.4	2.6	16.1	0.77	0.85	19.9	26.2
405	4.1	2.7	1.5	0.75	0.89	19.0	24.7
417	5.1	0.2	21.3	0.65	0.53	18.1	27.6

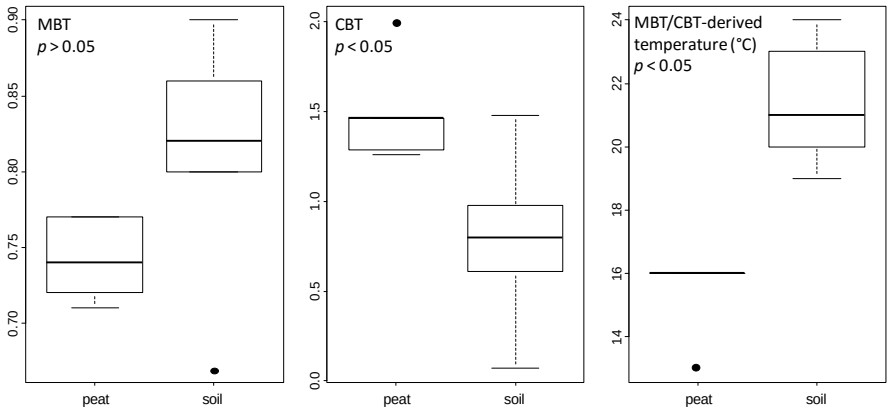

Figure 42: Comparison of MBT and CBT indices and br GDGT-derived temperatures (using the calibration by Peterse et al., 2012) in the Kyambangunguru marsh and in the surrounding soils.

5.2.1.7. *n*-alkane distribution and hydrogen isotopic composition:

Mid to long chain *n*-alkanes (> C_{21}) dominated most of the samples with C_{23} and C_{25} being the most abundant (23% and 21% on average respectively; Figure 43). Three typical *n*-alkane distributions patterns were encountered along the core (Figure 43) and defined as profiles A, B and C. Profile A (Figure 43) corresponds to the *n*-alkane distribution of the 0-30 cm and 195-375 cm depth intervals: it is dominated by odd numbered *n*-alkanes, the most abundant one being C_{23}, and presents a decreasing trend in relative abundance from C_{23} to C_{31}. Profile B (Figure 43) describes the *n*-alkane distribution from 180 cm to 45 cm. This distribution is characterized by a relative increase of the > C_{29} *n*-alkanes (sometimes up to C_{35}) and < C_{23}, especially C_{19}, *n*-alkanes together with a relative decrease of C_{23}, C_{25}, C_{27}; in comparison with profile A. C_{23} and C_{25} remain the most abundant *n*-alkanes. In this profile, even *n*-alkanes are also found in larger amount compared to profile A. Profile C (Figure 43) corresponds to the base of the core (390-417 cm). Even *n*-alkanes are slightly more abundant than in the other profiles and C_{23}, C_{25}, C_{27} are dominant. The CPI index indicates a clear odd-over-even preference throughout

the core (mean 8.1; Table 7 and Figure 39) while the ACL index only slightly varied (between ca. 25 and 27; Table 7 and Figure 39). The P_{aq} index was systematically lower than 1, ranging between 0.50 and 0.85 (Table 7 and Figure 44).

δ^2H composition of odd mid to long chain *n*-alkanes (C_{23}-C_{31}) varied between -96 ‰ and -172 ‰ (Table 7 and Figure 44) and was systematically enriched in the tephra layer (between -71‰ and -122‰; Table 7 and Figure 44), either because of exogenous sources of *n*-alkanes or fractionation during tephra deposition. Therefore, the isotopic composition of *n*-alkanes in the tephra will not be taken into consideration in the discussion section. Long chain *n*-alkanes (C_{29} and C_{31}) were more ^2H-enriched (-130 ‰ on average; Table 7 and Figure 44) than mid chains (C_{23} and C_{25}; -150 ‰ on average; Table 7 and Figure 44) compounds. δ^2H for individual *n*-alkanes significantly co-vary along the core ($p<0.05$; Table 4), except for the C_{31} *n*-alkane. No clear trend in the variation of the δ^2H composition of the individual *n*-alkanes was present with depth (Figure 44).

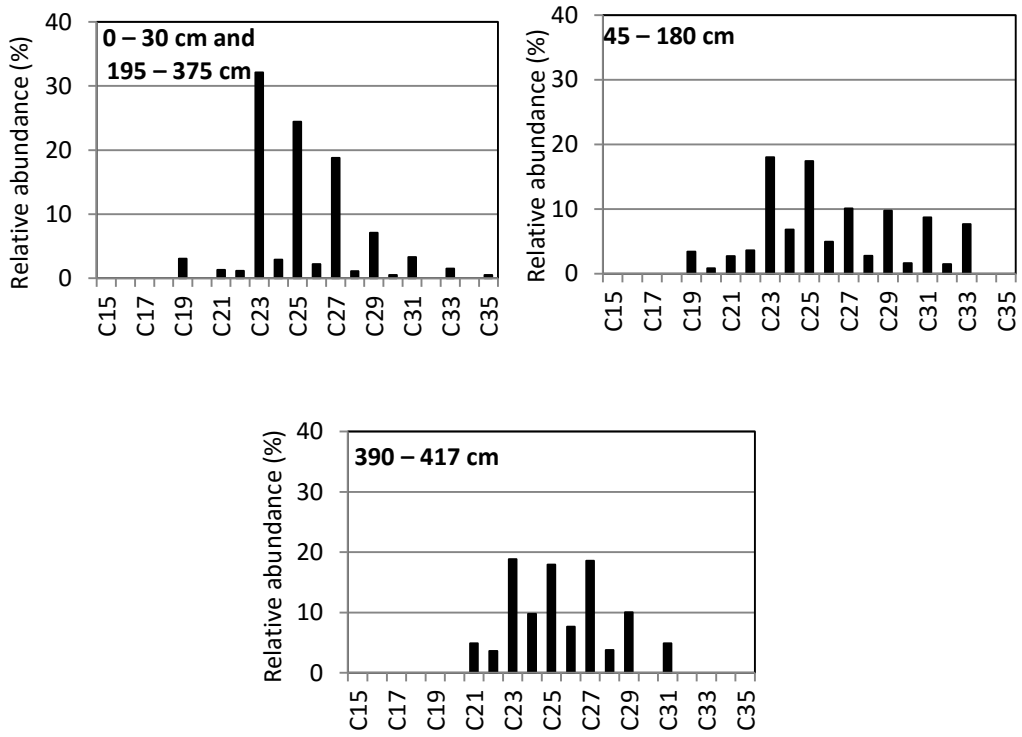

Figure 43: Typical *n*-alkane distributions observed along the core. The 3 profiles correspond to those described in the text.

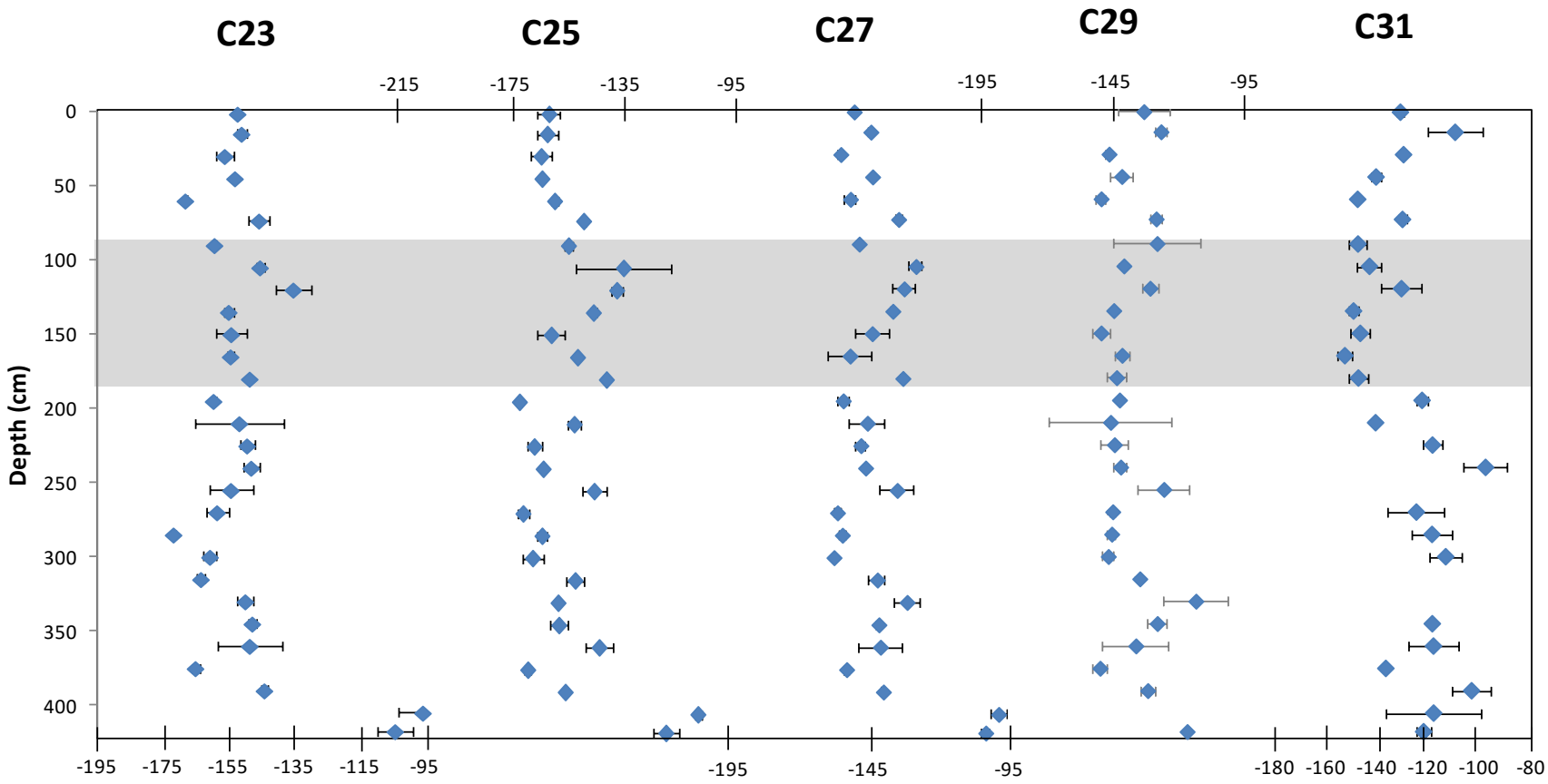

Figure 44: δ^2H composition (‰) of individual *n*-alkanes (from C_{23} to C_{31}) along the core. Analytical error is represented with error bars.

Table 7: *n*-alkane distribution parameters (ACL, CPI and P_{aq} calculation details are presented in section 1.2.3.1.) and hydrogen isotopic composition of the major odd-carbon-number long chain *n*-alkanes.

Depth	C_n range	C_{max}	ACL	CPI	P_{aq}	δ^2H_{C23}	δ^2H_{C25}	δ^2H_{C27}	δ^2H_{C29}	δ^2H_{C31}
2	16-33	23	25	12	0.80	-152	-161	-150	-133	-131
15	19-35	23	25	11	0.84	-151	-162	-144	-126	-109
30	16-32	23	25	8	0.83	-156	-164	-155	-146	-130
45	19-35	23	26	6	0.81	-153	-164	-144	-141	-140
60	19-35	23	26	5	0.75	-168	-159	-152	-149	-148
73	19-35	23	26	5	0.76	-146	-149	-134	-128	-130
90	16-35	25	26	6	0.79	-159	-154	-148	-128	-147
105	19-33	23	27	6	0.52	-145	-134	-128	-140	-143
120	15-33	25	26	3	0.68	-135	-137	-132	-130	-130
135	19-33	23	27	4	0.66	-155	-145	-136	-144	-149
150	15-33	25	27	6	0.57	-154	-160	-144	-149	-147
165	19-33	25	27	4	0.65	-154	-151	-152	-141	-153
180	16-35	23	26	4	0.69	-148	-140	-133	-143	-147
195	19-33	23	25	10	0.82	-159	-172	-154	-142	-122
210	15-33	23	26	11	0.74	-152	-152	-146	-145	-141
225	19-33	23	26	9	0.69	-149	-166	-148	-144	-118
240	19-33	23	26	13	0.76	-148	-163	-146	-141	-97
255	21-31	23	25	7	0.81	-154	-145	-135	-125	n.d.
270	16-31	23	25	14	0.80	-158	-171	-156	-144	-125
285	19-31	23	25	12	0.84	-172	-164	-154	-145	-118
300	16-31	23	25	11	0.84	-160	-167	-157	-146	-113
315	19-31	23	25	14	0.81	-163	-152	-142	-134	n.d.
330	22-29	23	25	8	0.86	-150	-158	-131	-113	n.d.
345	19-31	23	26	6	0.75	-148	-158	-141	-128	-118
360	16-33	25	26	9	0.70	-148	-143	-141	-136	-118
375	23-31	23	26	8	0.73	-165	-169	-153	-149	-137
390	16-33	27	26	8	0.67	-144	-155	-140	-131	-103
405	17-31	25	26	2	0.60	-96	-107	-99	n.d.	n.d.
417	21-31	23	26	3	0.71	-104	-119	-103	-116	-122

5.2.2 Discussion

5.2.2.1. Ecological history of the Kyambangunguru crater marsh:

Combination of microscopic observations, elemental and molecular analyses allowed reconstructing the ecological history of the Kyambangunguru wetland (Figure 45). Three units (Figure 45), representing the major ecosystem changes over the last 4000 yrs, were distinguished. While macro- and micro-fossils indicated the main biotic communities inhabiting the wetland and its surroundings, the palynofacies profile coupled with the C/N ratio revealed the origin of the OM and its degree of preservation (Bourdon et al., 2000). Furthermore, distribution of br GDGTs gave access to the pH of the site (Weijers et al., 2007; Tierney et al., 2010).

Unit I starts at the base of the core (4050 cal. yr BP) until 2150 cal. yr BP (193 cm) and is characterized by a relative stability of all the measured parameters and derived proxies (Figure 45), suggesting persistent lacustrine conditions. C/N values (ca. 15; Figure 45) indicate a mixed aquatic and terrestrial source of the OM (Meyers, 1997), which is confirmed by the presence of planktonic remains in the palynofacies (gAOM and algOM, Figure 45) and in the palynomorph profile (Figure 40). GDGT derived-pH is ca. 7 (Figure 45), which is consistent with current pH values of the RVP crater lakes (Delalande, 2008) further supporting the occurrence of a lake at this time. The high abundance of macro- (Figure 40) and micro-remains (Figure 41) from algae (*Nitella* sp.) and submerged/floating (*Potamogeton* sp., *Nymphaea* sp.) macrophytes suggests that this lake was relatively shallow and that its water column likely harboured abundant macrophyte vegetation. This is further supported by the low P_{aq} (Table 7 and Figure 39), the high C_{org} values (Table 6 and Figure 39) and the predominance of LC-derived OM (Figure 39) partly originating from *Cyperus* (according to microscopic observation; Laggoun-Défarge et al., 2008b).

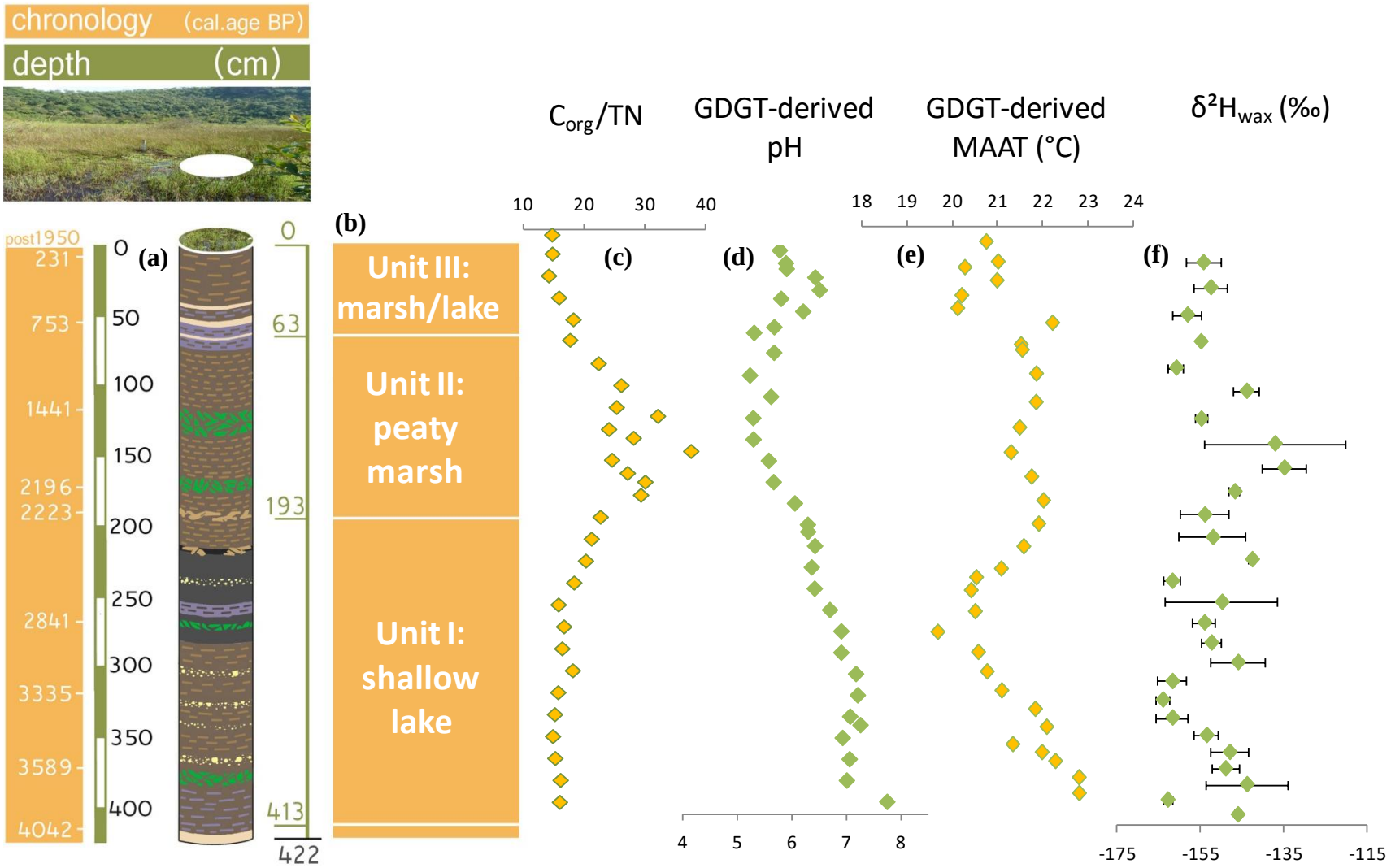

Figure 45: (a) Core chronology and lithography, (b) ecological phase unit combined with the variation of (c) C/N ratio, (d) br GDGT-derived pH (based on Tierney et al. (2010) calibration) (e) br GDGT-derived MAAT (based on Loomis et al. (2012) calibration) and (f) δ^2H_{wax} along the core.

All the aforementioned parameters exhibit a shift at 2500 cal. yr BP which set the beginning of a rapid environmental change, leading to unit II environmental conditions (Figure 45). This phase contains several traits of a peaty marsh environment. The C/N ratio strongly increases (up to ca. 40), which is consistent with the disappearance of planktonic remains in the micro-fossil and palynofacies record (Meyers, 1997; Figure 45) and evidences the formation of peat. Indeed, high C/N ratios (usually > 30 and sometimes up to 100) are common in peatlands, due to the high preservation of the OM in relation with the prevailing acidic and anoxic conditions (Laggoun-Défarge et al., 2008a). The increase in rAOM and the apparition of mycelium at that time (Figure 45) also suggests the accumulation of peat and start of terrestrialisation (Bourdon et al., 2000). Moreover, more wood remains are observed in the macrofossil profile. This can be related to development of trees and shrubs at the edges of the marsh. The shift towards more acidic pH (Figure 45) and the apparition of plant taxa specific to peatlands (Figure 40 and Figure 41) are additional elements supporting the hypothesis of a transition to a peaty marsh environment in unit II. It should be noted that all the planktonic species and *Nymphaea spp.* totally disappeared during unit II (Figure 40), which may reflect the decrease of the water table at that time.

Unit III describes environmental conditions which prevailed from 860 cal. yr BP (63 cm) to nowadays. Present monitoring of the site concludes to the presence of a dual ecosystem, *i.e.* (i) a shallow lake colonized by large sedge mats during the rainy season and (ii) a marsh-like facies at the end of the dry season due to high evaporation rates. This dual ecosystem is revealed by the microscopic observation of both lake and marsh markers, such as planktonic and *Carex* remains (Figure 40). In addition, GDGT distribution records fluctuation of pH (from 5.2 to 7.8), potentially due to large variations of the water table level.

5.2.2.2. Climate change reconstruction based on biomarkers

Application of biomarkers to palaeoenvironmental reconstruction requires to carefully constrain the factors impacting the distribution and isotopic composition of these compounds. This section will discuss the potential sources of GDGTs and *n*-alkanes in the Kyambangunguru marsh before using these molecules for the reconstruction of past temperature and hydrological changes.

Br GDGT-derived temperature reconstruction

Aquatic br GDGTs can have two main sources. They can be produced in soils (e.g. Weijers et al., 2007), and then transported by runoff to aquatic ecosystems. Nevertheless, recent studies in several lakes in the world (e.g. Blaga et al., 2010; Zink et al., 2010; Sun et al., 2011), and especially in East Africa (Tierney et al., 2010; Loomis et al., 2012), evidenced *in situ* production of br GDGTs in the water column and potentially in the sediments as well (Tierney et al., 2012; Buckles et al., 2014). On the one hand, due to geological specificities of the Kyambangunguru marsh at the centre of a steep crater (Figure 19), slope runoff can be expected to be an important potential source of GDGTs; on the other hand, the core is predominantly composed of peat and several studies showed that anoxic and acidic conditions prevailing in peat environments seem to favour the development of br GDGT-producing bacteria (e.g. Huguet et al., 2010a, 2013a). The much higher concentration of br GDGTs in the Kyambangunguru marsh than in the watershed soils, combined with the significant differences in br GDGT distribution between the two types of environments (especially cyclisation degree reflected by CBT values, Figure 42), support a predominant *in situ* production of these compounds in the marsh. As a result, MAAT reconstructed with the global soil calibration (Peterse et al., 2012) was observed to significantly differ between watershed soils and surface peat samples ($p < 0.05$; Figure 42), with a cold bias for MAAT reconstructed in the peat samples compared to current MAAT values (ca. 22.6 °C). Similar bias towards cold temperatures was also observed in East African lakes (Tierney and Russell, 2009; Tierney et al., 2010; Loomis et al., 2012) and led to the establishment of East African specific lacustrine calibrations (Tierney et al., 2010; Loomis et al., 2012) to take into account the *in situ* production of br GDGTs in these lakes. As no peat-specific calibration exists yet, and as the Kyambangunguru marsh derives from a lake, the most recent East African lacustrine calibration was applied to reconstruct temperature variations along the core (SFS calibration; Loomis et al., 2012; equation 22; Table 6 and Figure 46).

Br GDGT-derived MAAT varied from 19.7 to 22.8 °C, with MAAT estimate at the surface of the peat (20.7 °C; Figure 46) being close to measured MAAT in the area (22.6 °C). Unit III was marked by a MAAT decrease of more than 2 °C until 2730 cal. yr BP, followed by an increase of ca. 1 °C until 2150 cal. yr BP, *i.e.* at the onset of unit II. Then, MAAT remained high, comprised between 21 and 22 °C until 640 cal. yr BP before decreasing to reach current values (Figure 46). These MAAT variations are

consistent with those already published for the area (Powers et al., 2005; Tierney et al., 2008; Sinninghe Damsté et al., 2012a), although these studies cover a wider time span (starting 60 000 yrs BP (Tierney et al., 2008) or 25 000 yrs BP (Powers et al., 2005; Sinninghe Damsté et al., 2012a) ago), these three lacustrine archives displaying a temperature optimum centered at 1000 yr BP similarly to the Kyambangunguru record.

Hydrological variations using n-alkane isotopic signature:

n-Alkane sources have to be constrained before using the δ^2H composition of these molecules for the reconstruction of palaeohydrology. Indeed, *n*-alkane δ^2H composition can be impacted by numerous factors (Sachse et al., 2012), from source water isotopic composition to evaporative isotopic enrichment and taxa-specific physiological processes. Recent studies (e.g. Kahmen et al., 2013a, 2013b; Eley et al., 2014) notably showed that *n*-alkane δ^2H values differed depending on vegetation type. In contrast, (Tierney et al., 2010, 2011) successfully used average *n*-alkane δ^2H variation to infer past changes in the hydrological regime of two East African lakes, lake Tanganyika and lake Challa (Mt. Kilimanjaro, Tanzania), arguing against significant effects of vegetation change on *n*-alkane δ^2H composition.

In the Kyambangunguru marsh, *n*-alkanes probably originate from both the abundant macrophyte vegetation taking up their water in the marsh and higher terrestrial plants covering the crater slopes, taking up their water in the soil. Water isotopic monitoring of the region (Delalande, 2008; Bergonzini, personal communication) showed that, in the present days, these two water pools have different hydrogen isotopic composition ($\delta^2H_{soils} \approx \delta^2H_{precipitations}$ = -23 ‰, $\delta^2H_{marsh\ water}$ = 0 ‰). This difference in ^2H-enrichment seems to be recorded by the vegetation based on a rapid survey of the *n*-alkane hydrogen isotopic composition of a few plants in the marsh and along the slopes (Appendix 7). This may introduce an additional bias in the *n*-alkane δ^2H values if macrophytes and terrestrial plants both contribute in large amounts to the *n*-alkanes deposited in the sediment. The potential large contribution of *n*-alkanes derived from macrophytes in the Kyambangunguru marsh is supported by the core observation in light microscopy (see section 5.2.2.1.) and may complicate the interpretation of the *n*-alkane δ^2H signal. Therefore, individual *n*-alkane δ^2H variations were considered separately and accordingly to their potential vegetation sources.

It is generally assumed that short chain *n*-alkanes are dominantly produced by algae and bacteria (< C_{21}; Cranwell et al., 1987), mid-chain ones by macrophytes ($C_{23\text{-}25}$; Ficken

et al., 2000; Gao et al., 2011) and longer chain ones by terrestrial plants (> C_{25}; Eglinton and Hamilton, 1967). However, studies (Diefendorf et al., 2011; Nguyen Tu et al., 2011; Zech et al., 2011; Bush and McInerney, 2013) have shown that the distribution of *n*-alkanes could (i) considerably vary within and among species and (ii) be biased by exogenous *n*-alkane production, such as fungi or microbial production. Therefore, the δ^2H variations of individual *n*-alkanes along the core were statistically compared to evidence any differences in their respective hydrogen sources (Rao et al., 2014).

The δ^2H variations of C_{23}, C_{25}, C_{27} and C_{29} alkanes were shown to be significantly correlated to each other ($p<0.05$; Table 8), in contrast with C_{31} alkane δ^2H variation, which was not correlated to any of the other *n*-alkane δ^2H variation ($p > 0.05$;Table 8). This suggests that C_{31} *n*-alkane likely has different hydrogen source and/or fractionation processes (Rao et al., 2014) than other *n*-alkanes. C_{23}-C_{29} *n*-alkanes may be predominantly derived from macrophytes in the marsh. Although only C_{23} – C_{25} *n*-alkanes are usually cited as the main *n*-alkanes produced by macrophytes, a similar origin can be put forward for longer *n*-alkanes (C_{27} – C_{29}) in the Kyambangunguru site (Appendix 7) and in other sites (Ficken et al., 2000; Gao et al., 2011). In contrast, it is difficult to assess the origin of the C_{31} *n*-alkane. It could be assumed to be mainly produced by higher terrestrial plants covering the crater slopes of the Kyambangunguru marsh, but we cannot exclude a change in vegetation source with time. Therefore δ^2H composition of C_{31} *n*-alkane was neglected and those of C_{23} to C_{29} *n*-alkanes were averaged (written $\delta^2H_{C23\text{-}C29}$) and considered to track the water budget of the marsh, in terms of precipitation (P) and evaporation (E) variations, as determined by variation of the P-E difference.

When the evaporation rate at the surface of the marsh increases, its hydrogen isotopic composition gets ^2H-enriched because the light ^1H evaporates preferentially, while the isotopic signature of strong precipitations and long rains is ^2H-depleted because of the amount effect (Dansgaard, 1964). Thus, the hydrogen isotopic composition of the water marsh gets depleted (enriched) when P-E increases (decreases). Only slight variations in $\delta^2H_{C23\text{-}C29}$ (< 20 ‰) were observed over the last 4 000 years (Figure 46), suggesting that, the P-E excess (P-E>0) conditions observed today were already established 4000 yrs ago and that the climate remained humid during the whole period in agreement with other δ^2H records of the region (Tierney et al., 2010, 2011). Moreover, these authors also reported low amplitude fluctuations in the δ^2H record similar to those observed in Kyambangunguru (Figure 46). $\delta^2H_{C23\text{-}C29}$ values in the Kyambangunguru core were

observed to be slightly ²H-enriched during unit II (2150-860 cal. yrs BP), probably due to higher water evaporation at the surface of the marsh in agreement with the synchronous warming reported in the br GDGT-derived MAAT record. Low precipitations at this period are also plausible, as a major drought event around 2000 yr BP was noticed in many records of the region (e.g. Gasse, 2000; Russell and Johnson, 2005). Moreover, Thevenon et al. (2003) observed higher frequency of fires from 1800 yr BP to 1500 yr BP in a sedimentary record from Lake Masoko nearby, which could either be related to a drought period or to an increase in human activity in the RVP region.

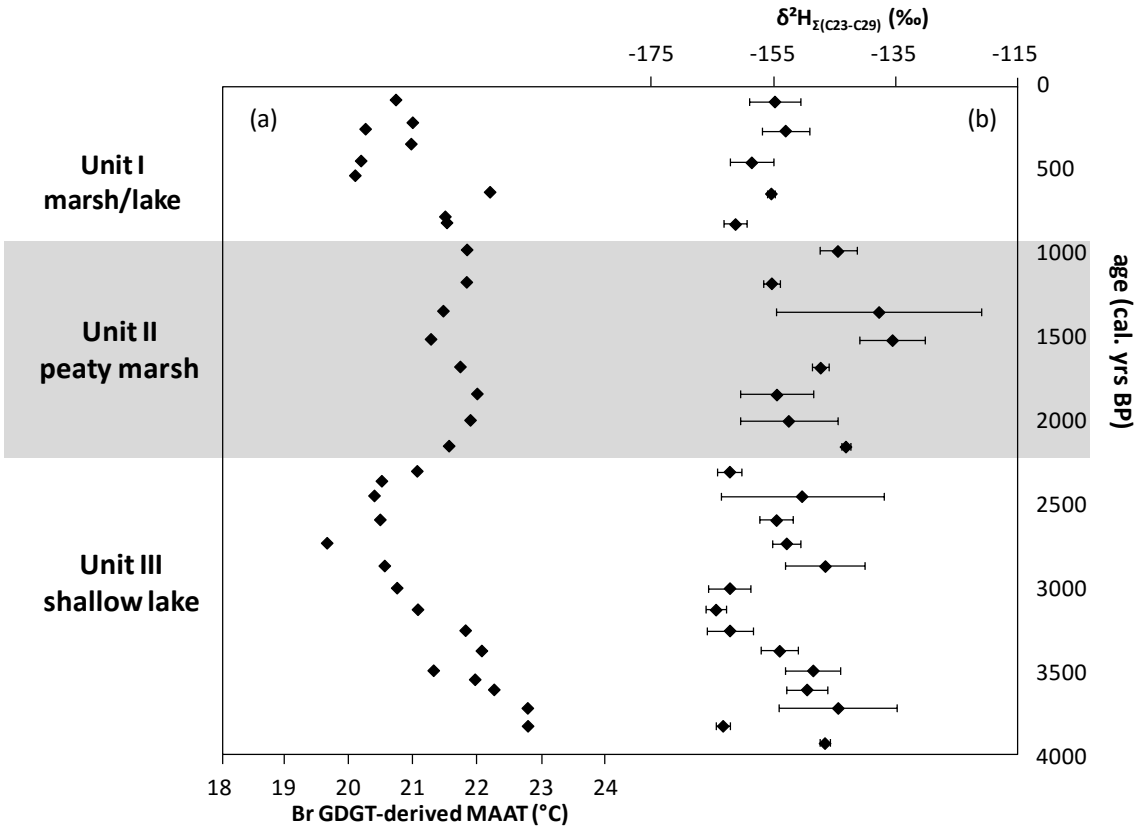

Figure 46: Variation in (a) br GDGT-derived temperature reconstructed with the SFS calibration by Loomis et al. (2012) and (b) average δ²H composition of C_{23} to C_{29} alkanes.

Table 8: correlation coefficient between individual *n*-alkane hydrogen compositions along the core. Bold numbers corresponds to statistically significant correlations ($p < 0.05$).

C23				
C25	***0.62***			
C27	***0.77***	***0.84***		
C29	***0.62***	***0.54***	***0.69***	
C31	*0.29*	*-0.26*	*-0.03*	*0.32*
	C23	C25	C27	C29

5.2.2.3. Internal vs. external drivers of ecosystem change?

The hydroseral succession describes a natural phenomenon of progressive colonisation of a freshwater body by different types of vegetation leading to its conversion to a swamp and eventually to a forest. Such conversion similar to the one recorded in Kyambangunguru could be due to the combination of several factors including allogenic, such as climate, and autogenic ones, notably vegetation infilling of the lake (Charman, 2002). The palynological record (Figure 41) exhibits an abrupt change in living communities at 2150 cal. yr BP. Planktonic and *Nymphaea* communities completely disappeared, while *Cyperus* spp. overrode the site in only a century (Figure 41). This behaviour suggests a threshold effect, which may reflect an autogenic hydroseral development effect rather than gradual climate change. Previous studies have shown the ability of *Nymphaea* spp. to form sudds floating at the surface of the water (Ellery et al., 1990; Charman, 2002) and pointed it out as a common step in the hydroseral succession leading to the conversion of a freshwater body to a swamp (Swan and Gill, 1970; Kratz and DeWitt, 1986). Developments of sudds and floating mats can be very quick in the tropics, as the warm temperatures hold up high vegetation productivity rates (Talling et al., 1998). The warming recorded at this period (see br GDGT-derived MAAT record; Figure 46) could then have acted as a positive feedback in promoting high rates of vegetation productivity. Consequences of this fast development of buoyant sudds are (i) large inputs of OM in the sediment, which progressively infilled the lake, (ii) vertical expansion of the mats by peat accumulation, and (iii) horizontal expansion and partial covering of the surface of the lake. The opposite evolution of plankton and *Nymphaea* from 3300 to 2300 cal. yr BP (Figure 41) supports this assumption: the more *Nymphaea* sudds would cover the lake surface, the

less light would penetrate the water column. This lake infilling may have been coupled with a decrease in the water level due to a drought event occurring around 2000 cal. yr BP. As explained above, this event was noticed in the Kyambangunguru $\delta^2H_{C23\text{-}C29}$ record as well as in several other lakes of the region (Gasse, 2000; Russell and Johnson, 2005).

At some point of the infilling, the lake could have become too shallow to allow the reproduction of the *Nymphaea*. In contrast, the sedges, which already inhabited the edges of the lake, could have been able to start colonizing the inner part of the marsh. Colonization of sedges at 2150 cal. yr BP marked the beginning of terrestrialisation of the marsh through peat accumulation and is evidenced by mycelium development (Figure 39). Permanent waterlogged conditions, characteristic of peat ecosystems, allowed the establishment of specific plant communities such as *Drosera* and *Lycopodiella Caroliniana* (Figure 41).

The end of unit II, from 1215 to 863 cal. yr BP, was marked by large fluctuations in the water table identified by the presence of *Enthorriza* in the micro-fossil record (Figure 41). *Enthorriza* is a fungi parasiting the roots of Cyperaceae when they are seasonnaly not submerged by water (Almeida-Leñero et al., 2005). This transition may have been triggered by the combination of internal and climatic factors. On the one hand, br GDGT-derived MAAT remained high during this period, suggesting high evaporation potential during the dry seasons which, combined with high water uptake from Cyperaceae (Nichols et al., 2014), may lead to seasonal complete dry-out of the marsh. This dry-out may explain the decay of waterlogged-restricted plants such as *Drosera* or *Lycopodiella caroliniana* and part of the *Cyperus* species (Diggs et al., 2006), as observed in the palynological profile (Figure 41). On the other hand, the water balance (P-E), recorded by the δ^2H isotopic composition, tended to increase over this period, suggesting that the rainy season is characterised by an increase in precipitations or longer depleted rain events. This may re-flood the marsh and create patches of free water, where phytoplankton, followed by *Nymphaea*, could re-establish. This corresponds to the present observations of seasonal high fluctuations of the water level in Kyambangunguru (Delalande, 2008 and Figure 18 in section 2.2.).

5.2.3 Conclusions

Multi-proxy investigation of the Kyambangunguru tropical crater wetland exhibited the transition from a shallow lake to a peaty marsh ca. 2000 yrs ago. This transition was principally driven by autogenic factors, through lake infilling as evidenced by microscopic observations of organic remains. Analysis of br GDGTs showed a cooling trend which last until ca. 2500 yr BP. Then, temperatures increased until 1800 cal. yr BP and remained high until ca. 1000 yr BP. Warming climate probably had a back-up role, supporting the hydroseral conversion by increasing the vegetation productivity and the water evaporation at the surface of the marsh. ^{2}H-enrichment of *n*-alkanes was observed when the wetland turned out to a peaty marsh, consistent with enhanced evaporation during this period. Current conditions of the wetland exhibit alternation of a shallow lake during strong rainy seasons and marsh subjected to high evaporation rates during dry seasons. This study highlights that the signal recorded in geological archives can be dominated by local ecological dynamics and that cores from different sites should be combined to infer robust paleoclimatic reconstructions.

Conclusions of the chapter:

- IPL br GDDs were detected for the first time along a peat core.
- Comparison between the distribution patterns of GDGTs and GDDs along with the presence of IPL derived GDDs suggest that at least part of GDDs is biosynthetically produced.
- Multi-proxy analysis revealed ecological transition from a shallow lake to a peaty marsh environment in Kyambangunguru ca. 2000 yrs ago.
- This transition seemed rather driven by hydroseral succession processes rather than climatic ones.

Chapter 6.

Lake Masoko : GDGT sources and Late Holocene climatic variation reconstruction

This chapter presents preliminary results from the investigation of GDGT and *n*-alkanes in Lake Masoko. The first part is dedicated to a methodological study of the occurrence and distribution of br and iso GDGTs, in their core lipid (CL) and intact polar lipid (IPL) forms. The second part presents paleoenvironmental reconstruction based on the analysis of iso, br GDGTs and *n*-alkanes along a 2.70 m long sediment core collected in 2007 in the centre of Lake Masoko. The aim was to reconstruct Late Holocene climatic changes from the latter.

6.1. Origin of GDGTs in Lake Masoko

6.1.1 Br and iso GDGT concentrations

Sediment traps were installed at three depths – 5, 18 and 33 m – in the center of Lake Masoko in April 2012. Br and iso GDGTs in the CL and IPL forms were analysed in the particulate organic matter (POM) collected from each depth of the trap in Dec. 2012, April 2013 and Dec 2013. It should be noted that the POM dataset was limited to 3 temporal series, which was not sufficient to investigate any seasonal trend. Therefore, the GDGT data from the 3 POM sample sets were combined for each depth. In addition to POM, GDGTs were also analysed (i) in 4 soils collected around the lake and (ii) in 6 surficial sediments collected at the edge of the lake and at the bottom of the water column (36 m depth).

The abundance of CL br GDGTs was much higher than the one of IPL-derived br GDGTs in all samples (representing ca. 90% of the total br GDGT pool in most of the samples; Table 9), suggesting that br GDGTs are predominantly of fossil origin. In the same way, CL iso GDGTs represented between 73% and 83% of the total iso GDGTs in POM collected along the water column. In contrast, the concentration of IPL-derived iso GDGTs was higher than the CL one in soils and sediments collected around the lake (Table 9), which suggests that a higher proportion of iso GDGTs is derived from recently active archaea in the latter settings. Whatever the type of samples, the proportion of IPL-derived GDGTs with respect to the total pool of GDGTs (i.e. CL + IPLs) was higher for iso than for br GDGTs, as previously observed in peat (e.g. Huguet et al., 2010a), soils (e.g. Huguet et al., 2010b) or sediments (e.g. Tierney et al., 2010). This might be due to the enhanced lability of IPL br GDGTs, assumed to be mainly

present as phospholipids and the more refactory nature of IPL iso GDGTs, assumed to be mainly present as glycolipids, as noticed by Tierney et al. (2012) in soils and sediments from Sand Pond Lake (USA).

Whatever the lipid pool, iso and br GDGT concentrations in the POM increased with water column depth (Table 9) with a ca. 10-fold increase for IPL and CL br GDGTs, 20-fold increase for CL iso GDGTs and 30-fold increase for IPL iso GDGTs. Such an increase with depth was already observed in other lacustrine water columns for br GDGTs and might be due to enhanced microbial activity in the deep anoxic layer of the lakes considering that br GDGT producers were suggested to be anaerobic organisms (e.g. Buckles et al., 2013, 2014; Loomis et al., 2014b).

Whatever the lipid pool, br and iso GDGT concentrations (normalized to C_{org}) were higher in sediments collected at the bottom of the water column than from the edges of the lakes (Table 9). In addition, GDGTs were much less abundant in soils than in sediments (Table 9). Such a trend was previously observed in several studies (Tierney and Russell, 2009; Blaga et al., 2010).

Table 9: GDGT concentrations, MBT' and CBT values, br GDGT-derived MAAT estimates based on Peterse et al. (2012) and Loomis et al. (2012) calibrations, GDGT I/GDGT VI ratio and TEX_{86} values for both core (CL) and intact polar (IPL) lipids.

	Concentration (µg/g C_{org})				MBT'		CBT		MAAT Peterse	MAAT Loomis	I/VI ratio		TEX_{86}	
	Br CL	Br IPL	Iso CL	Iso IPL	CL	IPL	CL	IPL			CL	IPL	CL	IPL
Soils	49.0 ± 34.3	4.0 ± 4.0	0.7 ± 0.3	4.1 ± 4.1	0.90± 0.05	0.67± 0.10	1.10± 0.29	1.00 ± 0.15	22.4 ± 0.8	27.2 ± 2.5	4.7	2.8	0.76 ± 0.13	0.13 ± 0.08
edge sed.	377.2 ± 145.4	18.9 ± 8.3	9.3 ± 5.7	19.5 ± 8.3	0.84 ± 0.01	1.77 ± 1.8	1.23 ± 0.22	1.31 ± 0.22	19.7 ± 1.5	24.5 ± 2.3	22.8	5.5	0.66 ± 0.05	0.07 ± 0.02
bottom sed.	771.6 ± 6.5	162.1 ± 21.2	265.2 ± 2.0	132.5 ± 15.5	0.48 ± 0.04	0.42 ± 0.01	0.51 ± 0.07	0.67 ± 0.01	12.1 ± 0.5	20.2 ± 0.4	0.4	0.4	0.70 ± 0.04	0.19 ± 0.02
POM 5 m	28.9 ± 13.5	3.8 ± 2.3	11.4 ± 5.3	2.8 ± 1.4	0.65 ± 0.07	0.61 ± 0.11	0.63 ± 0.15	0.57 ± 0.3	17.4 ± 1.3	27.7 ± 0.9	5.7	22.7	0.75 ± 0.05	0.78 ± 0.08
POM 18 m	200.5 ± 196.8	14.8 ± 13.5	84.3 ± 84	17.0 ± 12.4	0.54 ± 0.08	0.54 ± 0.09	0.52 ± 0.03	0.71 ± 0.2	14.6 ± 2.5	23.9 ± 4.6	0.5	6.1	0.72 ± 0.01	0.46 ± 0.14
POM 33 m	274.9 ± 185.2	27.8 ± 23.9	220.6 ± 144.9	83.1 ± 73.7	0.48 ± 0.03	0.49 ± 0.03	0.60 ± 0.03	0.65 ± 0.04	12.3 ± 1.2	21.1 ± 3.2	0.4	2.8	0.76 ± 0.02	0.58 ± 0.22

6.1.2 Br GDGT distribution and implications for the application of the MBT'/CBT

The distribution of br GDGTs in soils and sediments was compared through the calculation of the MBT' and CBT indices. Both MBT and CBT were found to be lower in the bottom sediment in comparison with soils and sediments at the edge of the lake (Figure 47 and Table 9). This result combined with the higher concentrations of br GDGTs observed in the bottom sediments in comparison with the soils and edge sediments support *in situ* production of br GDGTs in Lake Masoko. Br GDGTs can be produced in the sediment as well as in the water column, as indicated by the increase of the br GDGT concentrations in the POM with depth (Table 9). In addition, MBT' and CBT values of the POM samples were observed to be similar in the CL and in the IPL pool, except at 18 m depth for the CBT (Figure 48) which would further confirm *in situ* origin of the br GDGTs in the water column.

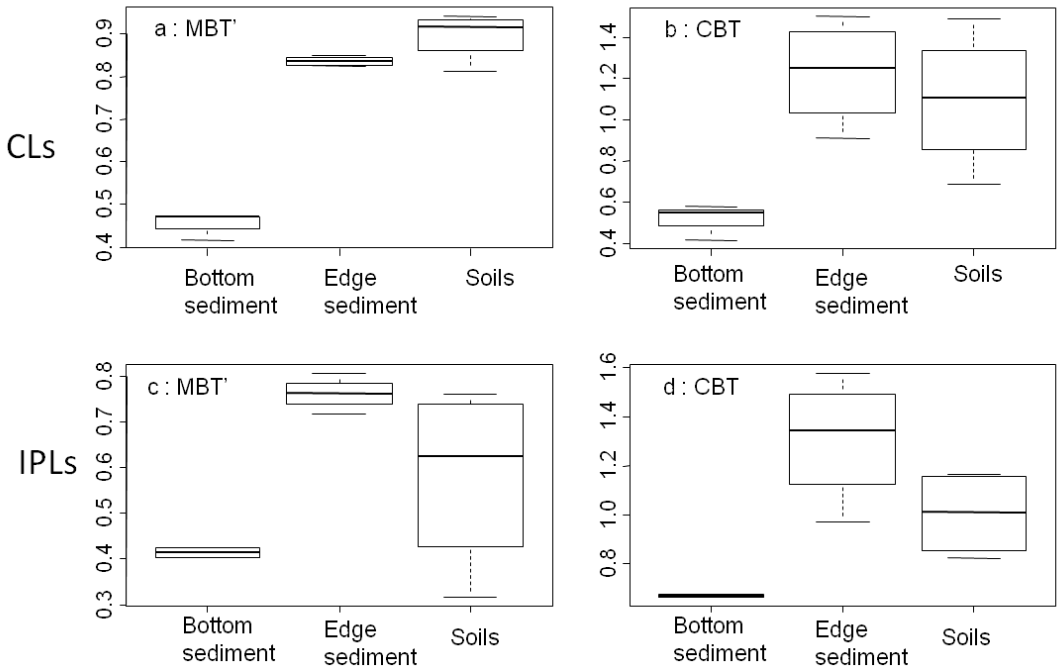

Figure 47: Comparison of (a) MBT' and (b) CBT between soils collected around the lake and sediments collected at the bottom of the water column and at the edge of the lake.

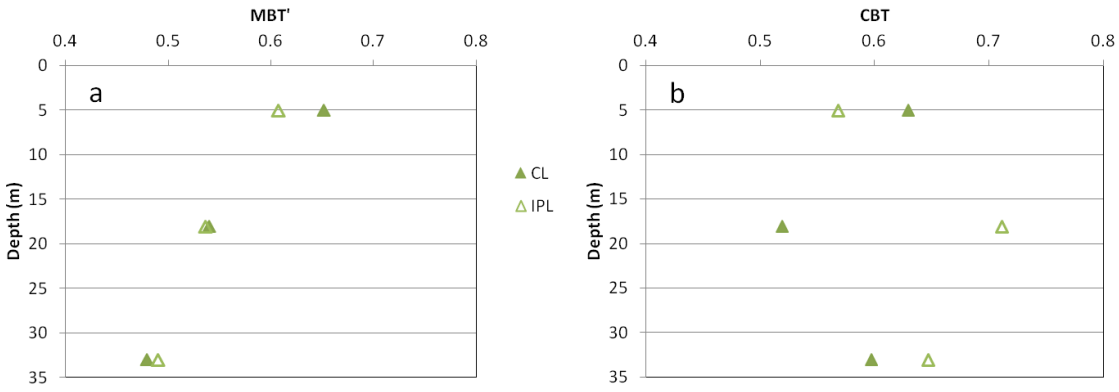

Figure 48: (a) MBT' and (b) CBT variations along the water column for CLs (solid symbols) and IPLs (open symbols).

MAAT was reconstructed from the MBT'/CBT using the global soil calibration by Peterse et al. (2012) and appeared to be significantly different between the sample types (Table 9). MAAT estimates from soils (22.4 °C ± 0.8) were consistent with the temperature recorded in the area (22.3 °C). In contrast, MAAT obtained from the POM and sediment samples were lower than expected. This cold bias in MAAT estimates was reported in previous studies in lakes (Tyler et al., 2010; Blaga et al., 2010; Sinninghe Damsté et al., 2012a; Shanahan et al., 2013) and is related to the *in situ* production of br GDGTs in these settings. Specific lacustrine calibrations have to be applied to MAAT reconstruction to take into account the latter phenomenon. The East African lacustrine calibration by (Loomis et al., 2012) was thus applied to sediments from the Lake Masoko and yielded reliable temperature estimates (24.5 °C at the edge and 20.2 °C at the bottom; Table 9) when considering the RMSE of this calibration (2.1 °C). The application of the aforementioned lacustrine calibration to POM samples showed a decrease of the temperature estimates with depth, consistent with the recorded temperature profile along the water column (cf. Chapter 2 and Figure 49). Br GDGTs from the POM samples thus seemed to have recorded the lake water column temperatures rather than the MAAT, which is another argument for br GDGT *in situ* production.

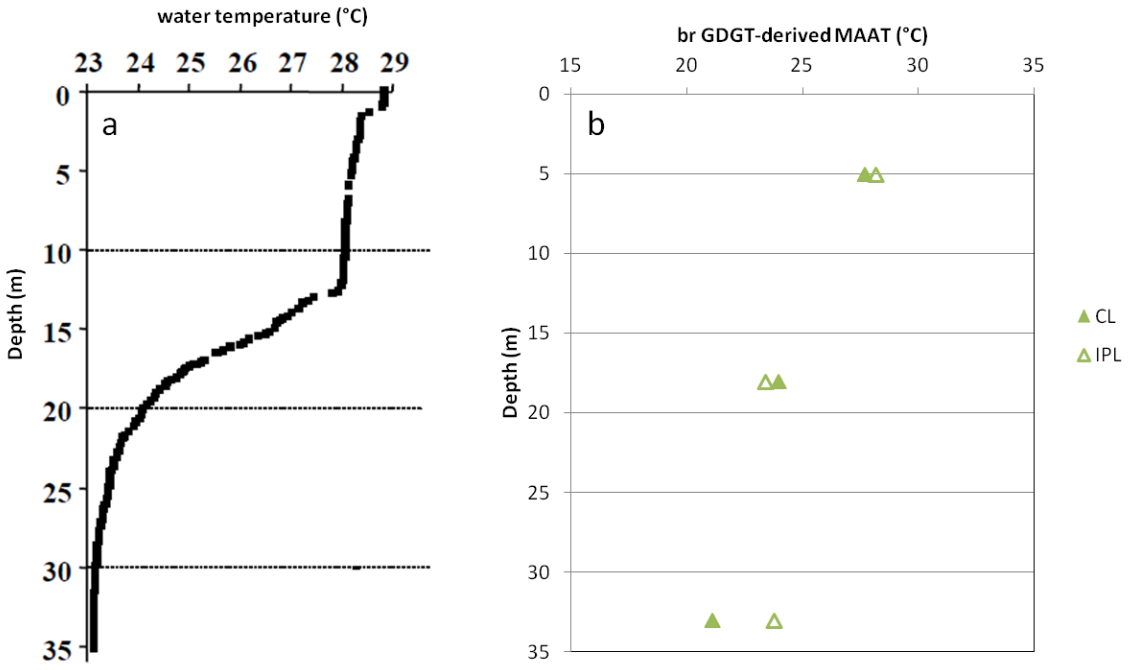

Figure 49: Comparison between (a) Lake Masoko thermocline and (b) br GDGT-derived MAAT (based on East African lacustrine calibration; Loomis et al., 2012) for the POM samples collected at 5, 18 and 33 m depth. MAAT was estimated from CL (solid symbols) and IPL (open symbols) br GDGTs

6.1.3 Iso GDGT distribution and implications for the application of the TEX_{86}

The TEX_{86} relationship with water surface temperature was developed in aquatic settings where iso GDGTs are predominantly produced by Thaumarchaeota (see discussions in Chapters 1 and 4) and is thus only valid if Thaumarchaeota are the main producers of iso GDGTs. The differences in iso GDGT sources can be distinguished by using the ratio of GDGT I vs. GDGT VI, which was initially developed by (Blaga et al., 2009) in lacustrine environments. Methanogenic archaea produce GDGT I but not GDGT VI, which is specific to Thaumarchaeota. A GDGT I/GDGT VI ratio lower than 2 indicates that iso GDGTs are predominantly produced by Thaumarchaeota and that the TEX_{86} can be properly applied to the reconstruction of water surface temperatures. Whatever the lipid pool, this condition was not fulfilled in soil and sediments collected around the lake and in POM collected at 5 m depth (Table 9), showing that iso GDGTs are produced by all major groups of archaea in these samples (Pearson and Ingalls, 2013). In contrast, the GDGT I/GDGT VI ratio was < 2 in the CL fraction of the POM

collected at 18 and 33 m depth and of the bottom sediments, indicating that Thaumarchaeota predominate among the archaeal communities in these samples and that TEX_{86} can be used for lake surface temperature (LST) reconstruction. However, this does not hold for the IPL fraction of the latter samples.

More generally, the iso GDGT distribution varied between the two lipid fractions of the POM samples collected at 18 and 33 m depth, with a higher relative abundance of GDGTs I and II and lower abundance of other iso GDGTs in the IPL than in the CL pool (Table 9 and Figure 50). This was reflected in the TEX_{86} values, which were lower in the IPL than in the CL fraction of these samples (Table 9). The high relative abundance of GDGT I, especially in the IPL pool – where it reached up to 66 % of the total IPL iso GDGTs (Figure 50) – was observed all along the water column, as also noticed by Buckles et al. (2013) in Lake Challa. This was related to an active and abundant methanogenic community in the water column. The iso GDGT distribution varied along the water column of the Masoko Lake, with a decrease in the relative abundance of GDGT I and a concurrent increase in the one of GDGT VI with depth (Figure 50). Lake Masoko is oligotrophic, with an oxycline at 18 m depth separating the oxygenated surface water layer from the deep anoxic one (see Chapter 2). Previous studies in stratified lakes observed a thaumarchaeotal bloom at the oxycline transition (Pouliot et al., 2009; Lliros et al., 2010; Auguet et al., 2011; Blaga et al., 2011; Schouten et al., 2012; Woltering et al., 2012) and consequently an increase in GDGT VI concentration at these depths (Schouten et al., 2012; Buckles et al., 2013). Such an increase was noticed at 18 m depth, but only in the CL pool (Figure 50), which might suggest that it is not directly related to a microbial bloom

In conclusion, TEX_{86}-derived temperatures in the sedimentary archive from Lake Masoko should be carefully interpreted as the archaeal communities vary widely in the water column.

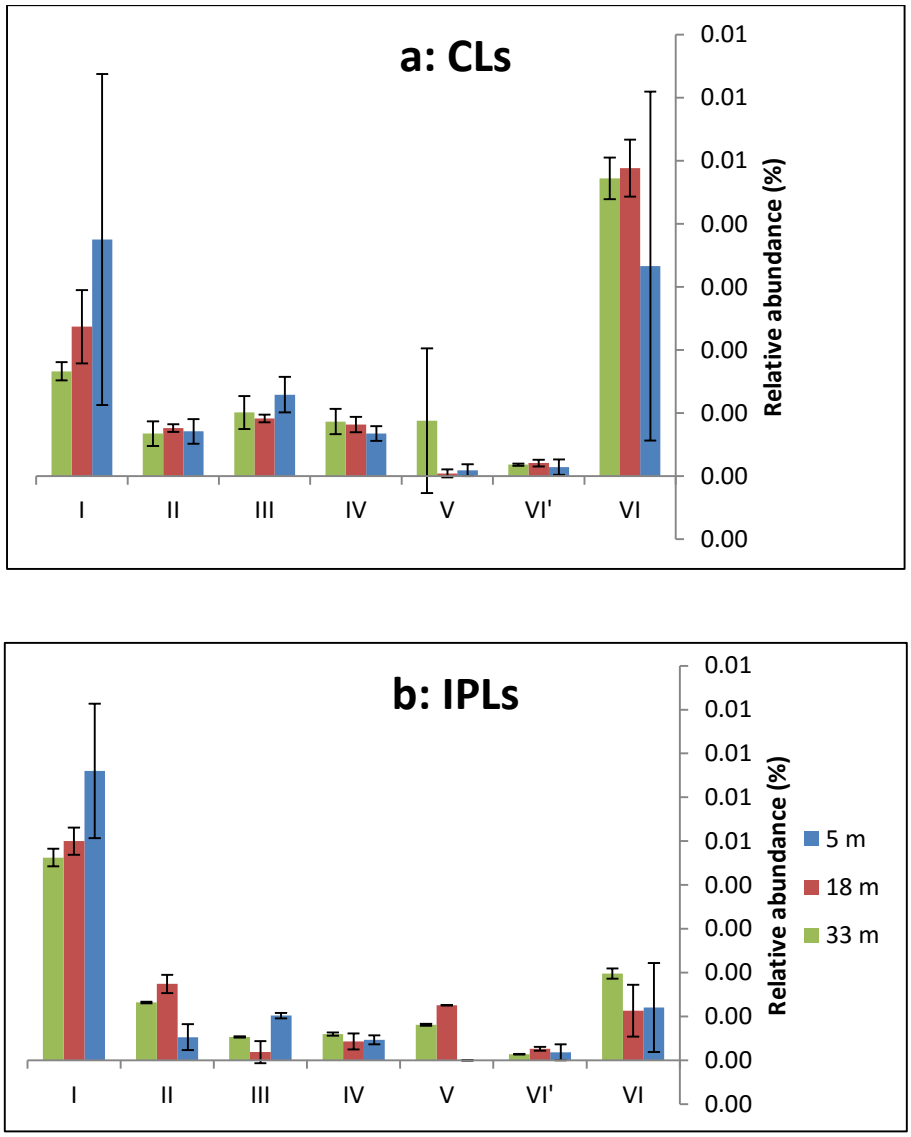

Figure 50: Relative abundance of individual iso GDGTs in the (a) CL and (b) IPL fractions at 5 (blue), 18 (red) and 33 (green) m depth (POM samples).

6.2. Late Holocene temperature reconstruction in Lake Masoko

The investigated 2.70 m sediment core from Lake Masoko comprises a thick tephra at its bottom and another one from 1.20 to 80 m depth, as already observed in sediment cores previously collected in Lake Masoko and in lakes nearby (Garcin et al., 2007). These tephra layers allow synchronizing data to well-defined time boundaries: the 1st tephra at the bottom of the lake was deposited 4000 yr BP and the 2nd one 1100 yr BP based on ^{14}C dating (Garcin et al., 2006). Robust chronology of the Late Holocene events in Lake Masoko was previously established (Garcin et al., 2006; de Mesmay, 2008). The following section presents the preliminary results obtained from the analysis of CL GDGTs and *n*-alkanes in 50 samples along the core. The objective of this study is to realise a high resolution (every 2 cm) analysis of biomarker-derived temperature proxies for the Late Holocene in East Africa. The C_{org} and N contents as well as $\delta^{13}C$ and $\delta^{15}N$ of these sediments will be determined in the near future. ^{14}C dating of some of the samples will also be performed allowing the comparison of the present data with those obtained from previous cores.

6.2.1 Temperature reconstructions based on br and iso GDGTs

Br and iso GDGTs were detected in all the samples along the core. Br GDGTs were systematically more abundant than iso GDGTs, as previoulsy observed in small crater lake sediments (e.g. Sinninge Damsté et al., 2009). In contrast, iso GDGTs are present at high concentrations in large lakes like Lake Malawi (Powers et al., 2011, 2005; Schouten et al., 2012). In the sediment core of the Lake Masoko, GDGT VI was the most abundant iso GDGT (mean 39.5 ± 3%) followed by GDGT I (mean 33.0 ± 2%). GDGTs VIIa, VIIIa and IXa are the predominant br GDGTs, with average relative abundances of 44.7 ± 2%, 27.4 ± 1% and 8.88 ± 1% respectively (Appendix. 8)

Br and iso GDGT-derived indices were calculated (Figure 51). TEX_{86}, varied from 0.61 to 0.75 along the core, with highest values at the top of the core (from 80 cm to the surface; Figure 51) indicating a higher proportion of cyclic iso GDGTs at these depths. High scattering of the TEX_{86} values below the first tephra layer (*i.e.* 120 cm depth) is observed. The range of TEX_{86} values is in good agreement with the one observed in previous studies of iso GDGTs in East African lakes (Powers et al., 2010, 2011). The

MBT' and CBT values varied between 0.51 and 0.64 and 0.55 and 0.73, respectively, consistent with previous studies of br GDGTs in nearby lakes (e.g. Tierney et al., 2010). The MBT', and to a lower extent the CBT, decreased between 270 cm and 120 cm depth, and the MBT' and TEX_{86} only slightly varied in the last 80 cm of the core (Figure 51), indicating rather stable conditions over the last 1000 yrs BP.

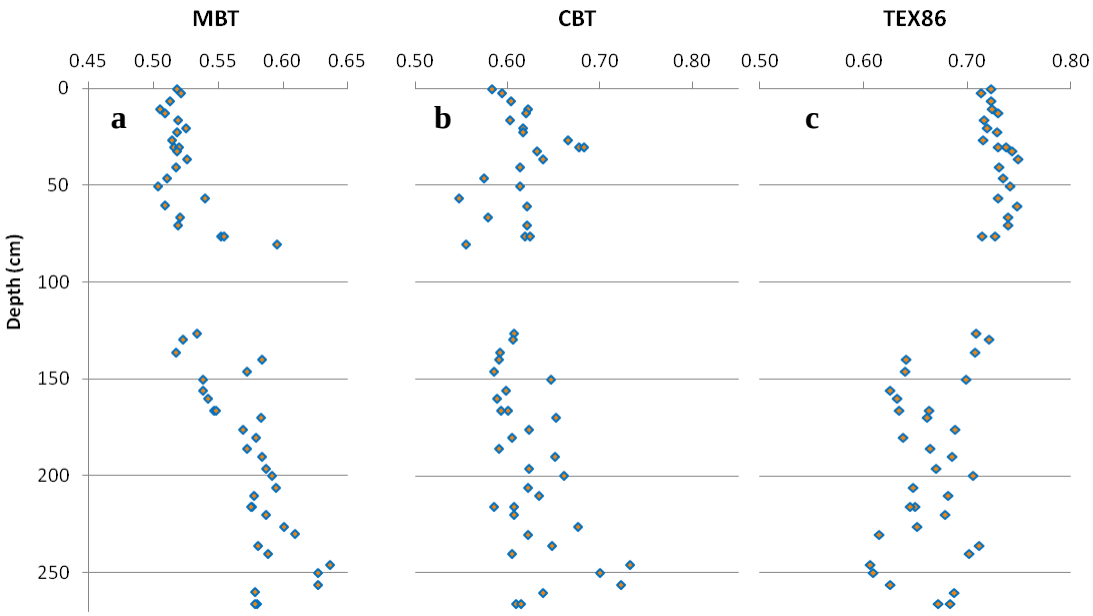

Figure 51: (a) MBT, (b) CBT and (c) TEX_{86} evolution with depth. The discontinuity between 80 et 120 cm corresponds to the first tephra.

The GDGT I/GDGT VI ratio was predominantly below 2 enabling to use the iso GDGT distribution as a paleothermometer. TEX_{86} index was thus converted into lake surface temperature (LST) using the transfer function developed by (Powers et al., 2010). Reconstructed LST for surficial sediments (first 10 cm) were ca. 26 ± 0.4 °C, in agreement with the actual mean LST at the bottom of the lake (25.6 °C, Kayvantash, 2012). Variation in LST along the core showed a global warming of the lake water from ca. 22 °C 4000 yr BP to 26 °C today (Figure 52). Nevertheless, TEX_{86}-derived temperatures from the deeper part of the core (from 270 cm to 120 cm) are very scattered. Bioturbation and/or turbidites created after the abrupt falling of the sediments forming the edge of the lake could have occasionally brought younger microbial material than the one present in the sediment at the time of its deposit, resulting in scattered LST estimates. Such phenomena were indeed pointed out at these depth

intervals in previously investigated cores from Lake Masoko (Garcin et al., 2006). Alternatively and/or complementarily, the scattering could be due to current colonization of the deep sediments by living archaeal communities, as observed in the deep biosphere of the ocean (Lipp and Hinrichs, 2009). These benthic archaea are also producing iso GDGTs (Xie et al., 2013). Nevertheless, it is not clear why these perturbations did not impact the br GDGT signal (Figure 52).

Mean annual air temperature (MAAT) was reconstructed based on fractional abundance of br GDGTs, according to the regional lacustrine calibration developed by Loomis et al. (2012). MAAT reconstructed from the top samples (first 10 cm) of the core (21 ± 0.4 °C) was consistent with the current MAAT of the site (22.3 °C). Reconstructed MAAT showed a decreasing trend in the deeper part of the core (from 4000 yr to 1100 yr BP; Figure 52), even though a slight increase was noticed just below the tephra layer (ca. 1100 yr BP). Above the tephra layer (from 1100 yr to present BP), MAAT decreased from 22 °C to 21 °C (Figure 52).

The MAAT record from the Lake Masoko strongly resembles the one obtained from br GDGT analysis along a peat core collected in the nearby Kyambangunguru marsh (see Chapter 5). Along the two cores covering the last 4000 yrs BP, MAAT varies between ca. 20 and 23-24 °C, with a peak in MAAT apparently occurring synchronously (centered at 1100 yr BP; Figure 52). ^{14}C dating of several samples along the core from Lake Masoko should allow refining the comparison of the two temperature records. Such a trend is opposite to the one observed in the LST record derived from the TEX_{86} index (Figure 52). This opposition questions the assumption that iso GDGTs record the LST. In addition, taking into consideration that complex archaeal dynamics was evidenced in Lake Masoko water column, one can hypothetize that iso GDGTs may rather record deeper temperatures. Analysis of additional biomarker-derived temperature proxies, such as $U^{K'}_{37}$ or LDI (cf. section 1.2.1.) would bring valuable information in this respect. However, a previous study of the biogeochemistry of the lake has shown that alkenones were absent from its sedimentary record (de Mesmay et al., 2007) and that long chain diols were only present in low abundance (de Mesmay, 2008).

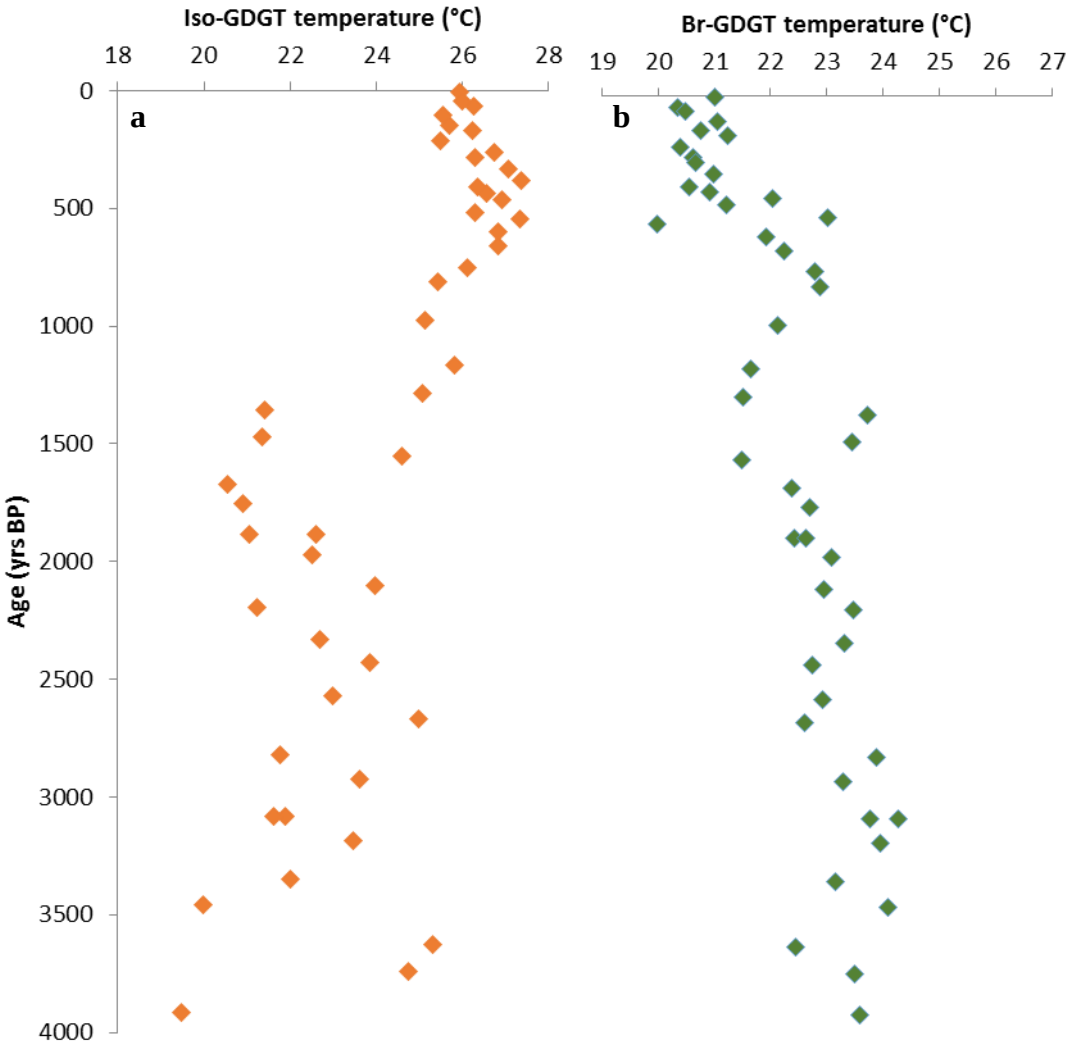

Figure 52: (a) iso GDGT-derived and (b) br GDGT-derived temperature variation with time.

6.2.2 Vegetation reconstruction based on *n*-alkane distribution

n-Alkanes were detected in all sediment samples, with the C_{27}, C_{29}, C_{31} homologues being predominant, as displayed in Figure 53, highlighting the three typical *n*-alkane distributions observed along the core. The predominance of long chain odd *n*-alkanes along the core suggests that these compounds are mainly derived from the higher terrestrial plants encountered along the slopes of the catchment area (Eglinton and Hamilton, 1967), as expected from the actual configuration of the site (see Chapter 2). The *n*-alkane distribution is reflected in the ACL, CPI, and P_{aq} indices which describe the average chain length, odd-over-even carbon number preference and relative contribution of terrestrial plants vs. macrophytes, respectively. The latter indices were

calculated according to equations 17, 18 and 19 and were plotted against depth (Figure 54). The ACL varied between 28 and 30, in agreement with the predominance of long chain *n*-alkanes all along the core (Figure 53). In the same way, CPI values were much higher than 1 in almost all samples, indicating an odd carbon number preference for *n*-alkanes as observed in higher terrestrial plants, thus confirming the low degradation stage of the studied sediment. Nevertheless, the CPI was much lower (≈ 1) above and below the first tephra layer, consistent with values observed in sedimentary rocks. P_{aq} values were generally lower than or equal to 0.4, suggesting that *n*-alkanes are predominantly derived from a mix of terrestrial plants and emergent macrophytes present at the edges of the lake rather than of floating/submerged macrophytes (Ficken et al., 2000).

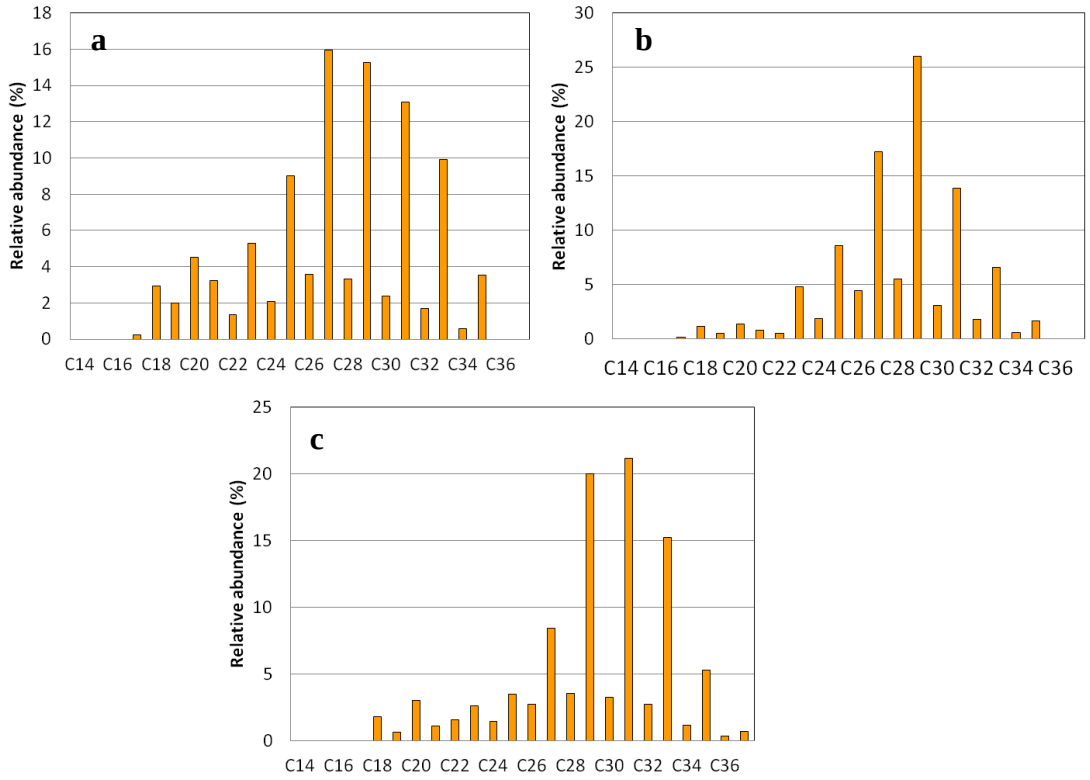

Figure 53: typical distributions of *n*-alkanes along the core: (a) at 6.5 cm depth, (b) at 176 cm depth and (c) at 256 cm depth.

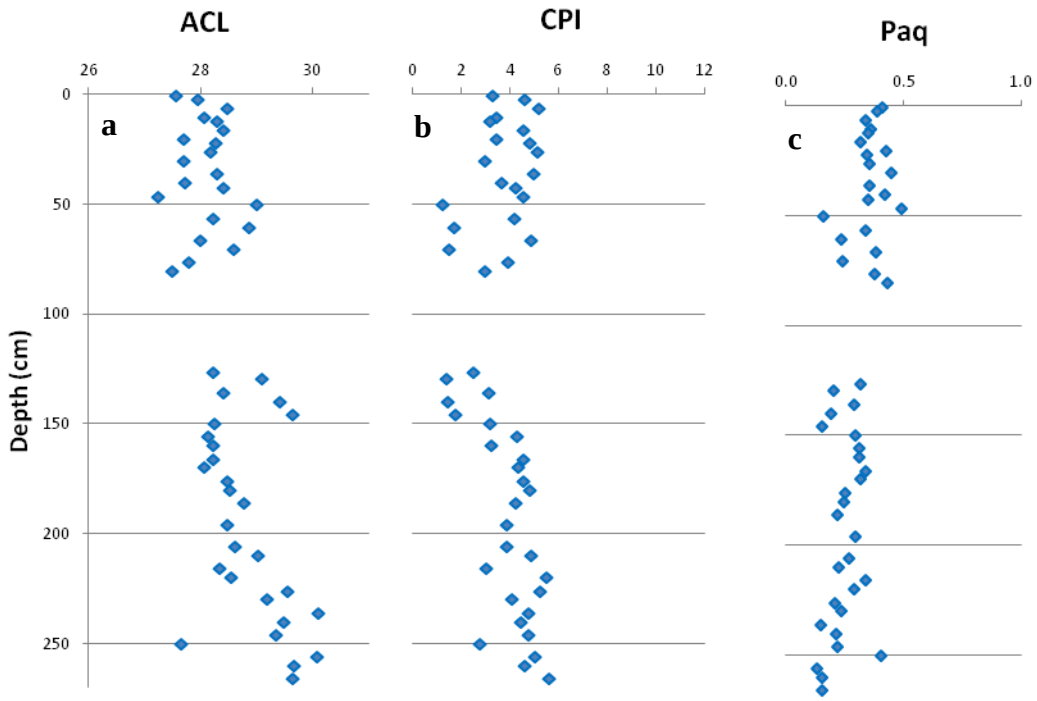

Figure 54: (a) ACL, (b) CPI and (c) P_{aq} variation with depth.

The ACL was observed to decrease in the deepest part of the core (270 - 120 cm depth), which could indicate a vegetation change from an open grassy environment to a closed canopy between 4000 and 1100 yrs BP. Indeed, grasses were suggested to predominantly produce *n*-alkanes with 31 or more carbons, while trees and shrubs frequently produce C_{27} and C_{29} *n*-alkanes predominantly (Rommerskirchen et al., 2006). The decrease in the ACL between the two tephra layers could therefore be related to a decreasing contribution of grass-derived *n*-alkanes and an increasing one of tree-derived *n*-alkanes in Lake Masoko sediments. Such a trend is consistent with observations from a previous pollen record in the lake (Vincens et al., 2003). Alternatively and/or complementarily, Rommerskirchen et al. (2003) proposed that an increase in the *n*-alkane chain length could reflect a protective adaptation of plants to warmer temperatures, with longer *n*-alkanes increasing the wax melting point. The decrease in the ACL over the 4000 – 1100 yr BP period would therefore indicate a cooling of the climate, which is consistent with the br GDGT-derived MAAT variations. However, the changes in *n*-alkane distribution have to be interpreted with care, due to the high variability of the latter in plants, as already discussed previously in this thesis (cf. Chapters 1 and 5).

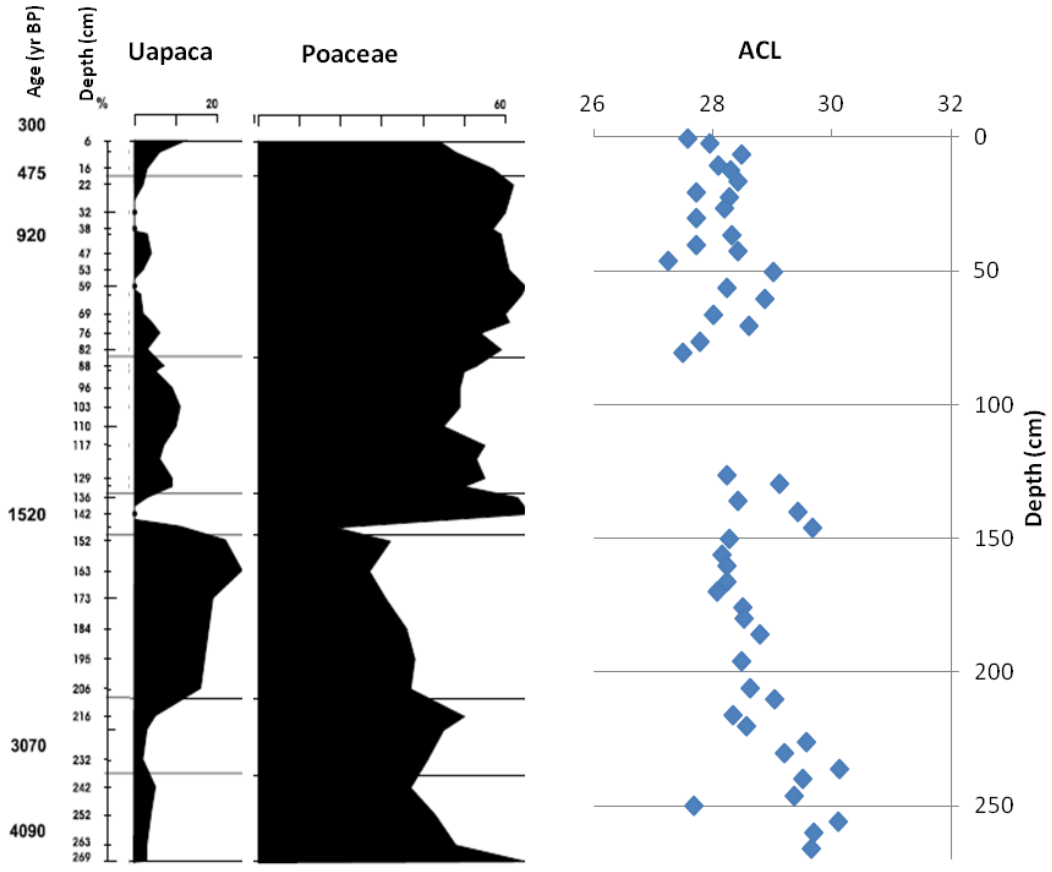

Figure 55: Comparison of the ACL variation with depth with previous pollen abundance as determined in a previous core of the lake spanning the same time period (Vincens et al., 2003).

6.2.3 Comparison with other regional records:

Previous paleoreconstructions of Lake Masoko have mainly dealt with lake level fluctuations (Barker et al., 2000; Bergonzini et al., 2001; Thevenon et al., 2003; Garcin et al., 2007; de Mesmay, 2008) and vegetation changes (Vincens et al., 2003). Combination of Lake Masoko and Kyambangunguru marsh (details in the precedent chapter) temperature records give a reliable estimation of past air temperature variation over the last 4000 yrs in the RVP (Figure 46 and Figure 52) and constitutes the first one to reconstruct past MAAT in the RVP. Nevertheless, the age model of the sediment core and the sedimentation rate of Lake Masoko are needed to accurately correlate these two records.

GDGT records from several other East African lakes are available, even though they span a much larger timescale than the core from the present study (e.g. 22-25 kyrs for Lakes Malawi and Challa, Powers et al., 2005; Sinninghe Damsté et al., 2012, respectively; 60 krs for Lake Tanganyika, (Tierney et al., 2008) and thus display a

weaker resolution. Br GDGT-derived MAAT estimates from Lake Challa vary between 19 and 22 °C (Sinninghe Damsté et al., 2012a), and are in the same range as those obtained for the RVP (19-22 °C; Figure 46 and Figure 52). In addition, similarly to our record from the RVP, a cooling trend followed by a warming one (ca. 1 °C) is observed, leading to a MAAT optimum centered at 1000 yrs BP (Figure 56), followed by a decrease in MAAT (ca. 2 °C) over the last 500 yrs. However, a 1000 yr offset in MAAT minimum - observed at 4000 yrs in Lake Challa and at 2500-3000 yr BP in the RVP - exists between the two records (Figure 46, Figure 52 and Figure 56a).

In addition, LST variation of the two major lakes surrounding the RVP – Lakes Tanganyika and Malawi – were reconstructed by Powers et al. (2005) and Tierney et al. (2008) using TEX_{86}. The range of reconstructed LST from these two archives is similar to the one observed in Lake Masoko (26-28 °C; Figure 52 and Figure 56b). In records of both Lakes Tanganyika and Malawi, a cooling trend from 4000 yr BP to 2500 yr BP followed by a warming of ca. 2 °C from 2500 yr BP to 1500 yr BP was observed, which is highly consistent with the RVP record (Figure 52 and Figure 56b). The time lag of the cooling trend observed in Lake Challa may reflect its northernmost position compared to the three other lakes.

Conclusions of the chapter:

- Distribution of CL and IPL-derived iso GDGTs in the water column of Lake Masoko suggests that diverse archaea, including Thaumarchaeota and methanogens, are present in the lake and contribute to the iso GDGT pool.
- However iso GDGTs detected in the sediment core predominantly originate from *Thaumarchaeota* thus enabling the application of the TEX_{86} paleothermometer. A global warming during the last 4000 yrs BP is observed although some scatter at the bottom of the core hamper further reliable interpretation.
- Investigation of CL and IPL br GDGT concentration and distribution in soils, surface sediments surrounding the lake and in the water column demonstrated *in situ* production of these compounds. A lacustrine specific calibration must therefore be used for MAAT reconstruction along the sediment core.
- MAAT reconstructed along the sediment core are in agreement with the Kyambangunguru record presented in Chapter 5 and other lacustrine records in East Africa.

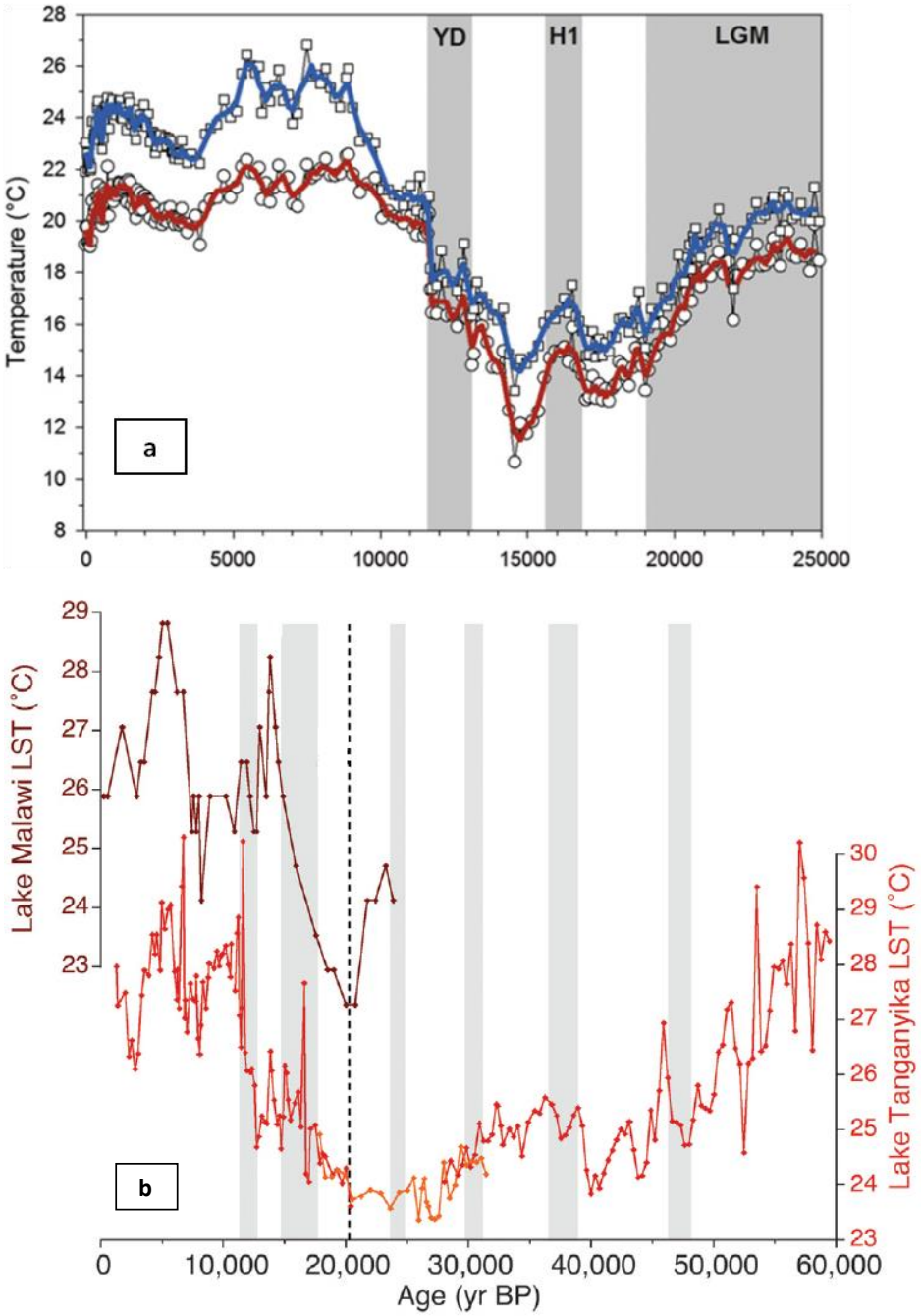

Figure 56: (a) GDGT-derived MAAT in Lake Challa (Sinninghe Damsté et al., 2012a) and (b) GDGT-derived LST in Lake Malawi (Powers et al., 2005) and in Lake Tanganyika (Tierney et al. 2008). Adapted from Sinninghe-Damsté et al. (2012a) and Tierney et al. (2008).

Conclusion

This work dealt with the applicability of two types of lipid biomarkers, GDGTs and *n*-alkanes, to reconstruct past environmental changes in East Africa. It combined methodological studies and applications in three types of continental archives: soil, peatland and lake. In addition, the hydrogen isotopic composition of individual *n*-alkanes was assessed in soils, leaves and peat samples.

Elevation gradients were used to assess the response of GDGTs and *n*-alkanes to temperature changes in surficial soils from East Africa. Br GDGTs were found to reliably record temperature changes in this area. A regional calibration was developed, combining all the br GDGT results from East African soils published so far. This new regional calibration could be applied to (i) paleosols of the region and (ii) surficial soils from other tropical regions (such as South America or South East Asia) to assess if common environmental parameters are controlling GDGT distributions in tropical areas. In contrast, δ^2H_{wax} was correlated with elevation-related temperature changes along Mt. Kenya, but not along Mt. Rungwe. These contrasting results highlight the complexity of the signal recorded by δ^2H_{wax} and call for more research on the physical and biological parameters impacting the hydrogen isotopic fractionation in *n*-alkanes.

A 4 m peat core was collected in a crater marsh (Kyambangunguru). Because of the high abundance of GDGTs in peat, this core was used to investigate the relationship between newly detected compounds, the glycerol dialkanol diethers (GDDs), and GDGTs. Observation of br and iso GDDs in the intact polar lipid form all along the core and selective enrichment of iso GDDs compared to the respective GDGTs at some depths strongly suggest that (at least part of) GDDs are biosynthetically produced. In parallel, a multi-proxy approach, involving molecular, isotopic and elemental analyses together with observation of biological remains in light microscopy, was conducted along the peat core. AMS ^{14}C analysis of several samples along the core allowed the development of an age model of the latter. All together these analyses showed that over the Late Holocene (i.e. the last 4000 yrs), the ecosystem changed from a shallow lake to a peatland and, more recently, to a dual marsh/peatland depending on the season. Based on br GDGT and δ^2H_{wax} variations along the core, we suggest that hydroseral succession

was the main driver of these conversions and that temperature warming probably had a positive feedback effect on this process, while hydrological regime fluctuations had only a minor effect.

In addition to the Kyambangunguru peat core, GDGTs and *n*-alkanes were also analysed along a 2.70 m sediment core collected in Lake Masoko. GDGT sources in this lake were investigated prior to any temperature reconstruction based on these compounds. Both Thaumarchaeota and methanogenic archaea were found to be contributors of the iso GDGT pool. Nevertheless, sedimentary iso GDGTs seemed to derive predominantly from Thaumarchaeota, enabling the use of TEX_{86} to determine the lake surface temperature. Br GDGTs were shown to be predominantly produced *in situ* in the lake, leading to the application of lacustrine calibrations for the temperature reconstructions. Preliminary results showed that a warming of air temperature occurred ca. 1500 yr BP, synchronously with the Kyambangunguru record. These results need to be completed by elemental and isotopic analyses (C, $\delta^{13}C$, N, $\delta^{15}N$). Long chain diols, which are newly developed temperature proxies, may also be analysed along the core if sensitive techniques are employed. So far, climatic reconstructions from the Kyambangunguru and Masoko cores show that the Rungwe Volcanic Province (RVP) has a coherent regional response to global climate change.

All together these results demonstrate the high potential of GDGTs and *n*-alkanes to reconstruct past environmental changes in the RVP region. They appear to be sensitive to small-amplitude climatic fluctuations and present the advantage to be ubiquitous in all continental settings. However, a good knowledge of the sampling site is required to accurately interpret the variations of these proxies

The perspectives of this work are numerous. First, in terms of biomarker applications for past reconstructions, there is a need for more controlled experiments. Too much incertitude remains in the environmental parameters potentially impacting their signal. The extensive understanding of br GDGTs is hampered by the fact that their source microorganisms remain unknown. This weakens the climatic reconstructions derived from these compounds. Controlled *in vitro* experiments would be necessary to investigate the impact of other environmental parameters than temperature and pH on br GDGT distribution. Determining br GDGT source microorganism remains a major challenge to address in the next years. Additionally, as peat samples from the

Kyambangunguru marsh and sediment ones from Lake Masoko both contain relatively large amount of GDGTs, stable isotope probing experiments could be implemented. These assays could constrain (i) the turnover of GDGTs, (ii) the metabolism of their source organisms in these two sites. Notably, insights in the dynamics of the benthic archaeal communities within Lake Masoko sediment could give clues to explain why the TEX_{86} signal is scattered downcore. In parallel, this work showed how the signal recorded by the δ^2H_{wax} was impacted by multiple factors. The RVP possesses a wide diversity in vegetation which the IRA and the University of Dar Es Salaam are putting efforts in mapping. We could take advantage of this inventory to study in depth the impact of soil water content, species types, location (in a primary forest, in an anthropized area, along the mountain slopes or downhill / uphill) in the δ^2H_{wax} signal.

One major scientific challenge today is to understand the reaction of ecosystems to the climate change to come. In this framework, it would be interesting to extend, and even to systematize, the approach we developed in the study of the Kyambangunguru marsh. Indeed, by combining independent proxies recording the ecological status changes on the one hand and integrating climatic changes on the other hand, we were able to distinguish the relative impact of internal changes, *i.e.* intrinsically related to the ecological dynamics of the site, to the one relative to regional climate changes. This may contribute to current key research topics. (i) If we extend this approach to other, previously studied, sites in East Africa we may be able to better understand the mismatch previously observed between East African Holocene records. (ii) Moreover, it could permit to develop, besides the history of climate, a history of ecological changes in the region. Assessing how the ecosystems reacted in the past to climatic change at the century scale will help in anticipating how they could react in the future. This issue is of utmost importance as the rise and fall of many civilisations in the past were related to dramatic changes in their surrounding environment.

Bibliography

Aichner, B., Herzschuh, U., Wilkes, H., Vieth, A., Böhner, J., 2010. δD values of n-alkanes in Tibetan lake sediments and aquatic macrophytes – A surface sediment study and application to a 16 ka record from Lake Koucha. Org. Geochem. 41, 779–790.

Almeida-Leñero, L., Ludlow-Wiechers, B., Geel, B. van, Gonzalez, M.C., Aptroot, A., 2005. Records of mid-Holocene fungi from Lake Zempoala, Central Mexico. Hyphal bridges over the Pacific: Advancing mycology. Hilo, Hawaii, U.S.A.

Amesbury, M.J., Barber, K.E., Hughes, P.D.M., 2012. Can rapidly accumulating Holocene peat profiles provide sub-decadal resolution proxy climate data? J. Quat. Sci. 27, 757–770.

Anderson, V.J., Shanahan, T.M., Saylor, J.E., Horton, B.K., Mora, A.R., 2014. Sources of local and regional variability in the MBT′/CBT paleotemperature proxy: Insights from a modern elevation transect across the Eastern Cordillera of Colombia. Org. Geochem. 69, 42–51.

Araguás-Araguás, L., Froehlich, K., Rozanski, K., 2000. Deuterium and oxygen-18 isotope composition of precipitation and atmospheric moisture. Hydrol. Process. 14, 1341–1355.

Auguet, J.-C., Nomokonova, N., Camarero, L., Casamayor, E.O., 2011. Seasonal Changes of Freshwater Ammonia-Oxidizing Archaeal Assemblages and Nitrogen Species in Oligotrophic Alpine Lakes. Appl. Environ. Microbiol. 77, 1937–1945.

Baas, M., Pancost, R., van Geel, B., Sinninghe Damsté, J.S., 2000. A comparative study of lipids in Sphagnum species. Org. Geochem. 31, 535–541.

Bai, Y., Fang, X., Nie, J., Wang, Y., Wu, F., 2009. A preliminary reconstruction of the paleoecological and paleoclimatic history of the Chinese Loess Plateau from the application of biomarkers. Palaeogeogr. Palaeoclimatol. Palaeoecol. 271, 161–169.

Ballantyne, A.P., Greenwood, D.R., Damsté, J.S.S., Csank, A.Z., Eberle, J.J., Rybczynski, N., 2010. Significantly warmer Arctic surface temperatures during the Pliocene indicated by multiple independent proxies. Geology 38, 603–606.

Barker, P., Telford, R., Merdaci, O., Williamson, D., Taieb, M., Vincens, A., Gibert, E., 2000. The sensitivity of a Tanzanian crater lake to catastrophic tephra input and four millennia of climate change. The Holocene 10, 303–310.

Barker, P., Gasse, F., 2003. New evidence for a reduced water balance in East Africa during the Last Glacial Maximum: implication for model-data comparison. Quat. Sci. Rev. 22, 823–837.

Basalirwa, C. P. K., Odiyo, J. O., Mngodo, R. J., Mpeta, E. J., 1999. The climatological regions of Tanzania based on the rainfall characteristics. Int. J. Climatol. 19, 69–80.

Bechtel, A., Smittenberg, R.H., Bernasconi, S.M., Schubert, C.J., 2010. Distribution of branched and isoprenoid tetraether lipids in an oligotrophic and a eutrophic Swiss lake: Insights into sources and GDGT-based proxies. Org. Geochem. 41, 822–832.

Becker, K.W., Lipp, J.S., Zhu, C., Liu, X.-L., Hinrichs, K.-U., 2013. An improved method for the analysis of archaeal and bacterial ether core lipids. Org. Geochem. 61, 34–44.

Berglund, B.E., Ralska-Jasiewiczowa, M., 1986. Handbook of Holocene Palaeoecology and Palaeohydrology, J. Wiley & Sons Ltd. ed. Berglund, B.E., Ralska-Jasiewiczowa, M., Chichester-Toronto.

Bergonzini, L., 1998. Bilans hydrologiques de lacs (Kivu, Tanganyika, Rukwa et Nyassa) du Rift Est-Africain. Mus. R. L'Afrique Cent. Tervuren Belg. Ann. Sér. Sci. Géologiques 103, 183.

Bergonzini, L., Gibert, E., Winckel, A., Merdaci, O., 2001. Bilans hydrologique et isotopiques (18O et 2H) du lac Massoko, Tanzanie. Quantification des échanges lac–eaux souterraines. Comptes Rendus Académie Sci. - Ser. IIA - Earth Planet. Sci. 333, 617–623.

Blackford, J., 2000. Palaeoclimatic records from peat bogs. Trends Ecol. Evol. 15, 193–198.

Blaga, C.I., Reichart, G.-J., Heiri, O., Damsté, J.S.S., 2009. Tetraether membrane lipid distributions in water-column particulate matter and sediments: a study of 47 European lakes along a north–south transect. J. Paleolimnol. 41, 523–540.

Blaga, C.I., Reichart, G.-J., Schouten, S., Lotter, A.F., Werne, J.P., Kosten, S., Mazzeo, N., Lacerot, G., Sinninghe Damsté, J.S., 2010. Branched glycerol dialkyl glycerol tetraethers in lake sediments: Can they be used as temperature and pH proxies? Org. Geochem. 41, 1225–1234.

Blaga, C.I., Reichart, G.-J., Vissers, E.W., Lotter, A.F., Anselmetti, F.S., Damste, J.S.S., 2011. Seasonal changes in glycerol dialkyl glycerol tetraether concentrations and fluxes in a perialpine lake: Implications for the use of the TEX_{86} and BIT proxies. Geochim. Cosmochim. Acta 75, 6416–6428.

Bligh, E.G., Dyer, W.J., 1959. A simple method of total lipid extraction and purification. Can. J. Biochem. Physiol. 37, 911–917.

Bossard, N., Jacob, J., Le Milbeau, C., Sauze, J., Terwilliger, V., Poissonnier, B., Vergès, E., 2013. Distribution of miliacin (olean-18-en-3β-ol methyl ether) and related compounds in broomcorn millet (Panicum miliaceum) and other reputed sources: Implications for the use of sedimentary miliacin as a tracer of millet. Org. Geochem. 63, 48–55.

Bourdon, S., Laggoun-Défarge, F., Disnar, J.-R., Maman, O., Guillet, B., Derenne, S., Largeau, C., 2000. Organic matter sources and early diagenetic degradation in a tropical peaty marsh (Tritrivakely, Madagascar). Implications for environmental reconstruction during the Sub-Atlantic. Org. Geochem. 31, 421–438.

Boussafir, M., Sifeddine, A., Jacob, J., Foudi, M., Cordeiro, R.C., Albuquerque, A.L.S., Abrao, J.J., Turcq, B., 2012. Petrographical and geochemical study of modern lacustrine sedimentary organic matter (Lagoa do Caçò, Maranão, Brazil): Relationship between early diagenesis, organic sedimentation and lacustrine filling. Org. Geochem. 47, 88–98.

Braconnot, P., Otto-Bliesner, B., Harrison, S., Joussaume, S., Peterchmitt, J.-Y., Abe-Ouchi, A., Crucifix, M., Driesschaert, E., Fichefet, T., Hewitt, C.D., Kageyama, M., Kitoh, A., Loutre, M.-F., Marti, O., Merkel, U., Ramstein, G., Valdes, P., Weber, L., Yu, Y., Zhao, Y., 2007. Results of PMIP2 coupled simulations of the Mid-Holocene and Last Glacial Maximum - Part 2: feedbacks with emphasis on the location of the ITCZ and mid- and high latitudes heat budget. Clim. Past 3, 279–296.

Brassell, S.C., Eglinton, G., Marlowe, I.T., Pflaumann, U., Sarnthein, M., 1986. Molecular stratigraphy: a new tool for climatic assessment. Nature 320, 129–133.

Bray, E.E., Evans, E.D., 1961. Distribution of *n*-paraffins as a clue to recognition of source beds. Geochim. Cosmochim. Acta 22, 2–15.

Buckles, L.K., Villanueva, L., Weijers, J.W.H., Verschuren, D., Damsté, J.S.S., 2013. Linking isoprenoidal GDGT membrane lipid distributions with gene abundances of ammonia-oxidizing Thaumarchaeota and uncultured crenarchaeotal groups in the water column of a tropical lake (Lake Challa, East Africa). Environ. Microbiol. 15, 2445–2462.

Buckles, L.K., H. Weijers, J.W., Verschuren, D., Sinninghe Damsté, J.S., 2014. Sources of core and intact branched tetraether membrane lipids in the lacustrine environment: anatomy of Lake Challa and its catchment, Equatorial East Africa. Geochim. Cosmochim. Acta 140, 106-126.

Bush, R.T., McInerney, F.A., 2013. Leaf wax n-alkane distributions in and across modern plants: Implications for paleoecology and chemotaxonomy. Geochim. Cosmochim. Acta 117, 161–179.

Carrillo-Hernandez, T., et al., 2003. Remarkably well-preserved archaeal and bacterial membrane lipids in 140 million year old sediments from the Russian platform (Kashpir Oil Shales Upper Jurrassic).

Castañeda, I.S., Werne, J.P., Johnson, T.C., Filley, T.R., 2009. Late Quaternary vegetation history of southeast Africa: The molecular isotopic record from Lake Malawi. Palaeogeogr. Palaeoclimatol. Palaeoecol. 275, 100–112.

Castañeda, I.S., Schefuß, E., Pätzold, J., Sinninghe Damsté, J.S., Weldeab, S., Schouten, S., 2010. Millennial-scale sea surface temperature changes in the eastern Mediterranean (Nile River Delta region) over the last 27,000 years. Paleoceanography 25, PA1208.

Castañeda, I.S., Schouten, S., 2011. A review of molecular organic proxies for examining modern and ancient lacustrine environments. Quat. Sci. Rev. 30, 2851–2891.

Charman, D., 2002. Peatlands and Environmental Change, John Wiley & Sons. ed. England.

Chikaraishi, Y., Naraoka, H., 2007. $\delta^{13}C$ and δD relationships among three n-alkyl compound classes (n-alkanoic acid, n-alkane and n-alkanol) of terrestrial higher plants. Org. Geochem. 38, 198–215.

Coffinet, S., Huguet, A., Williamson, D., Fosse, C., Derenne, S., 2014. Potential of GDGTs as a temperature proxy along an altitudinal transect at Mount Rungwe (Tanzania). Org. Geochem. 68, 82–89.

Coffinet, S., Huguet, A., Williamson, D., Bergonzini, L., Anquetil, C., Majule, A., Derenne, S., 2015. Occurrence and distribution of glycerol dialkanol diethers and glycerol dialkyl glycerol tetraethers in a peat core from SW Tanzania. Org. Geochem. 83–84, 170–177.

Cortijo, E., Labeyrie, L., Dulessy, J.-C., 2013. L'évolution de l'océan et du climat, les données de la paléocéanographie, in: Paleoclimatologie Trouver, Dater et Interpréter Les Indices (Tome I). Les Ulis et Paris (France).

Cranwell, P.A., Eglinton, G., Robinson, N., 1987. Lipids of aquatic organisms as potential contributors to lacustrine sediments—II. Org. Geochem. 11, 513–527.

Cronin, T.M., 2009. Ostracodes, in: Gornitz, V. (Ed.), Encyclopedia of Paleoclimatology and Ancient Environments, Encyclopedia of Earth Sciences Series. Springer Netherlands, pp. 663–665.

Crutzen, P.J., Stoermer, E.F., 2000. The "Anthropocene." IGBP Newsl. 41, 17–18.

Dansgaard, 1964. Stable isotopes in precipitation Dansgaard 1964.pdf.

Dansgaard, W., Johnsen, S.J., Clausen, H.B., Langway Jr., C.C., 1971. Climatic record revealed by the camp century ice core, in: The Late Cenozoic Glacial Ages. Turekian , K.K., New Haven, London, pp. 37–56.

Davis, O.K., Moutoux, T.E., 1998. Tertiary and Quaternary vegetation history of the Great Salt Lake, Utah, USA. J. Paleolimnol. 19, 417–427.

De Jonge, C., Hopmans, E.C., Stadnitskaia, A., Rijpstra, W.I.C., Hofland, R., Tegelaar, E., Sinninghe Damsté, J.S., 2013. Identification of novel penta- and hexamethylated branched glycerol dialkyl glycerol tetraethers in peat using HPLC–MS2, GC–MS and GC–SMB-MS. Org. Geochem. 54, 78–82.

De Jonge, C., Hopmans, E.C., Zell, C.I., Kim, J.-H., Schouten, S., Sinninghe Damsté, J.S., 2014. Occurrence and abundance of 6-methyl branched glycerol dialkyl glycerol tetraethers in soils: Implications for palaeoclimate reconstruction. Geochim. Cosmochim. Acta 141, 97–112.

Delalande, M., Bergonzini, L., Beal, F., Garcin, Y., Majule, A., Williamson, D., 2005. Contribution to the detection of Lake Masoko (Tanzania) groundwater outflow: isotopic evidence (^{18}O, D) / Contribution à la détection des pertes souterraines du Lac Masoko (Tanzanie): évidences isotopiques (^{18}O, D). Hydrol. Sci. J. 50.

Delalande, D., 2008. Hydrologie et géochimie isotopique du lac Masoko et de lacs volcaniques de la province active du Rungwe (sud-ouest Tanzanie). Université Paris Sud-Paris XI.

de Leeuw, J.W., Irene, W., Rijpstra, C., Schenck, P.A., 1981. The occurrence and identification of C30, C31 and C32 alkan-1, 15-diols and alkan-15-one-1-ols in Unit I and Unit II Black Sea sediments. Geochim. Cosmochim. Acta 45, 2281–2285.

de Mesmay, R., Grossi, V., Williamson, D., Kajula, S., Derenne, S., 2007. Novel mono-, di- and tri-unsaturated very long chain (C37–C43) n-alkenes in alkenone-free lacustrine sediments (Lake Masoko, Tanzania). Org. Geochem. 38, 323–333.

de Mesmay, R., 2008. Fonctionnement biogéochimique du lac Masoko (Tanzanie), approche par les biomarqueurs lipidiques sédimentaires.

Derosa, M., Gambacorta, A., 1988. The Lipids of Archaebacteria. Prog. Lipid Res. 27, 153–175.

Diefendorf, A.F., Freeman, K.H., Wing, S.L., Graham, H.V., 2011. Production of *n*-alkyl lipids in living plants and implications for the geologic past. Geochim. Cosmochim. Acta 75, 7472–7485.

Diggs Jr., G.M., Lipscomb, B.L., Reed, M.D., O'Kennon, R.J., 2006. Illustrated flora of East Texas. Botanical Research Institute of Texas.

Dirghangi, S.S., Pagani, M., Hren, M.T., Tipple, B.J., 2013. Distribution of glycerol dialkyl glycerol tetraethers in soils from two environmental transects in the USA. Org. Geochem. 59, 49–60.

Eglinton, G., Hamilton, R.J., 1967. Leaf Epicuticular Waxes. Science, New Series 156, 1322–1335.

Eglinton, T.I., Eglinton, G., 2008. Molecular proxies for paleoclimatology. Earth Planet. Sci. Lett. 275, 1–16.

Eley, Y., Dawson, L., Black, S., Andrews, J., Pedentchouk, N., 2014. Understanding ^{2}H/^{1}H systematics of leaf wax *n*-alkanes in coastal plants at Stiffkey saltmarsh, Norfolk, UK. Geochim. Cosmochim. Acta 128, 13–28.

Ellery, K., Ellery, W.N., Rogers, K.H., Walker, B.H., 1990. Formation, colonization and fate of floating sudds in the Maunachira river system of the Okavango Delta, Botswana. Aquat. Bot. 38, 315–329.

Elling, F.J., Könneke, M., Lipp, J.S., Becker, K.W., Gagen, E.J., Hinrichs, K.-U., 2014. Effects of growth phase on the membrane lipid composition of the thaumarchaeon Nitrosopumilus maritimus and their implications for archaeal lipid distributions in the marine environment. Geochim. Cosmochim. Acta.

Emiliani, C., 1955. Pleistocene Temperatures. J. Geol. 63, 538–578.

Epstein, S., Sharp, R.P., Gow, A.J., 1970. Antarctic Ice Sheet: Stable Isotope Analyses of Byrd Station Cores and Interhemispheric Climatic Implications. Science, New Series 168, 1570–1572.

Ericson, D.B., Wollin, G., 1956. Correlation of six cores from the equatorial Atlantic and the Caribbean. Deep Sea Res. 1953 3, 104–125.

Ernst, N., Peterse, F., Breitenbach, S.F.M., Syiemlieh, H.J., Eglinton, T.I., 2013. Biomarkers record environmental changes along an altitudinal transect in the wettest place on Earth. Org. Geochem.

Estep, M., Hoering, T., 1980. Biogeochemistry of the stable hydrogen isotopes. Geochim. Cosmochim. Acta 44, 1197-1206

Feakins, S.J., Sessions, A.L., 2010. Controls on the D/H ratios of plant leaf waxes in an arid ecosystem. Geochim. Cosmochim. Acta 74, 2128–2141.

Ficken, K.., Li, B., Swain, D.., Eglinton, G., 2000. An *n*-alkane proxy for the sedimentary input of submerged/floating freshwater aquatic macrophytes. Org. Geochem. 31, 745–749.

Fontijn, K., Williamson, D., Mbede, E., Ernst, G.G.J., 2012. The Rungwe Volcanic Province, Tanzania – A volcanological review. J. Afr. Earth Sci. 63, 12–31.

Gagosian, R.B., Peltzer, E.T., 1986. The importance of atmospheric input of terrestrial organic material to deep sea sediments. Org. Geochem. 10, 661–669.

Gao, L., Hou, J., Toney, J., MacDonald, D., Huang, Y., 2011. Mathematical modeling of the aquatic macrophyte inputs of mid-chain n-alkyl lipids to lake sediments: Implications for interpreting compound specific hydrogen isotopic records. Geochim. Cosmochim. Acta 75, 3781–3791.

Gao, L., Nie, J., Clemens, S., Liu, W., Sun, J., Zech, R., Huang, Y., 2012. The importance of solar insolation on the temperature variations for the past 110 kyr on the Chinese Loess Plateau. Palaeogeogr. Palaeoclimatol. Palaeoecol. 317–318, 128–133.

Garcin, Y., Williamson, D., Taieb, M., Vincens, A., Mathé, P.-E., Majule, A., 2006. Centennial to millennial changes in maar-lake deposition during the last 45,000 years in tropical Southern Africa (Lake Masoko, Tanzania). Palaeogeogr. Palaeoclimatol. Palaeoecol. 239, 334–354.

Garcin, Y., Williamson, D., Bergonzini, L., Radakovitch, O., Vincens, A., Buchet, G., Guiot, J., Brewer, S., Mathé, P.-E., Majule, A., 2007. Solar and anthropogenic imprints on Lake Masoko (southern Tanzania) during the last 500 years. J. Paleolimnol. 37, 475–490.

Garcin, Y., Melnick, D., Strecker, M.R., Olago, D., Tiercelin, J.-J., 2012a. East African mid-Holocene wet–dry transition recorded in palaeo-shorelines of Lake Turkana, northern Kenya Rift. Earth Planet. Sci. Lett. 331–332, 322–334.

Garcin, Y., Schwab, V.F., Gleixner, G., Kahmen, A., Todou, G., Séné, O., Onana, J.-M., Achoundong, G., Sachse, D., 2012b. Hydrogen isotope ratios of lacustrine sedimentary n-alkanes as proxies of tropical African hydrology: Insights from a calibration transect across Cameroon. Geochim. Cosmochim. Acta 79, 106–126.

Gasse, F., 2000. Hydrological changes in the African tropics since the Last Glacial Maximum. Quat. Sci. Rev. 19, 189–211.

Gelorini, V., Verbeken, A., van Geel, B., Cocquyt, C., Verschuren, D., 2011. Modern non-pollen palynomorphs from East African lake sediments. Rev. Palaeobot. Palynol. 164, 143–173.

Gliozzi, A., Paoli, G., De Rosa, M., Gambacorta, A., 1983. Effect of isoprenoid cyclization on the transition temperature of lipids in thermophilic archaebacteria. Biochim. Biophys. Acta BBA - Biomembr. 735, 234–242.

Gocke, M., Hambach, U., Eckmeier, E., Schwark, L., Zöller, L., Fuchs, M., Löscher, M., Wiesenberg, G.L.B., 2014. Introducing an improved multi-proxy approach for paleoenvironmental reconstruction of loess–paleosol archives applied on the Late Pleistocene Nussloch sequence (SW Germany). Palaeogeogr. Palaeoclimatol. Palaeoecol. 410, 300–315.

Godard, A., Tabeaud, M., 2009. Les Climats - mécanismes, variabilités, répartition, 4e edition. ed, Cursus, série géographie. Armand Colin, Paris.

Gornitz, V., 2009. Encyclopedia of Paleoclimatology and Ancient Environments, Springer. ed, Encyclopedia of Earth Sciences Series.

Gosling, W.D., Miller, C.S., Livingstone, D.A., 2013. Atlas of the tropical West African pollen flora. Rev. Palaeobot. Palynol., Palynology of tropical Africa 199, 1–135.

Gow, A.J., Ueda, H.T., Garfield, D.E., 1968. Antarctic Ice Sheet: Preliminary Results of First Core Hole to Bedrock. Science, New Series 161, 1011–1013.

Graz, Y., Di-Giovanni, C., Copard, Y., Laggoun-Défarge, F., Boussafir, M., Lallier-Vergès, E., Baillif, P., Perdereau, L., Simonneau, A., 2010. Quantitative palynofacies analysis as a new tool to study transfers of fossil organic matter in recent terrestrial environments. Int. J. Coal Geol. 84, 49–62.

Gunstone, F.D., Harwood, J.L., Padley, F.B., 1994. The lipid handbook, Chapman and Hall. ed. London New York.

Han, D., Ha, H.K., Hwang, C.Y., Lee, B.Y., Hur, H.-G., Lee, Y.K., 1968. Bacterial distribution along stratified water Columns in the pacific sector of the Arctic ocean. Deep Sea Res. Part II Top. Stud. Oceanogr.

Hanisch, S., Ariztegui, D., Püttmann, W., 2003. The biomarker record of Lake Albano, central Italy—implications for Holocene aquatic system response to environmental change. Org. Geochem. 34, 1223–1235.

Harkin, D.A., 1960. The Rungwe volcanics at the Northern end of lake Nyasa, Government Printer. ed.

Harvey, H.R., Fallon, R.D., Patton, J.S., 1986. The effect of organic matter and oxygen on the degradation of bacterial membrane lipids in marine sediments. Geochim. Cosmochim. Acta 50, 795–804.

Hatté, C., Antoine, P., Fontugne, M., Lang, A., Rousseau, D.-D., Zöller, L., 2001. $\delta^{13}C$ of loess organic matter as a potential proxy for paleoprecipitation. Quat. Res. 55, 33–38.

Hatté, C., Rousseau, D.-D., 2013. Interface air-sol : les séquences loessiques, marqueurs de la circulation atmosphérique, in: Paleoclimatologie Trouver, Dater et Interpréter Les Indices (Tome I). Les Ulis et Paris (France).

Hemp, A., 2006. Vegetation of Kilimanjaro: hidden endemics and missing bamboo. Afr. J. Ecol. 44, 305–328.

Herbert, T.D., 2003. 6.15 - Alkenone Paleotemperature Determinations, in: Turekian, H.D.H.K. (Ed.), Treatise on Geochemistry. Pergamon, Oxford, pp. 391–432.

Herfort, L., Schouten, S., Boon, J.P., Woltering, M., Baas, M., Weijers, J.W.H., Damsté, J.S.S., 2006. Characterization of Transport and Deposition of Terrestrial Organic Matter in the Southern North Sea Using the BIT Index. Limnol. Oceanogr. 51, 2196–2205.

Herndl, G.J., Reinthaler, T., Teira, E., Aken, H. van, Veth, C., Pernthaler, A., Pernthaler, J., 2005. Contribution of Archaea to Total Prokaryotic Production in the Deep Atlantic Ocean. Appl. Environ. Microbiol. 71, 2303–2309.

Hogg, A.G., Hua, Q., Blackwell, P.G., Niu, M., Buck, C.E., Guilderson, T.P., Heaton, T.J., Palmer, J.G., Reimer, P.J., Reimer, R.W., Turney, C.S.M., Zimmerman, S.R.H., 2013. SHCal13 Southern Hemisphere Calibration, 0–50,000 Years cal BP. Radiocarbon 55, 1889–1903.

Hopmans, E.C., Schouten, S., Pancost, R.D., van der Meer, M.T.J., Sinninghe Damsté, J.S., 2000. Analysis of intact tetraether lipids in archaeal cell material and sediments by high performance liquid chromatography/atmospheric pressure chemical ionization mass spectrometry. Rapid Commun. Mass Spectrom. 14, 585–589.

Hopmans, E.C., Weijers, J.W.., Schefuß, E., Herfort, L., Sinninghe Damsté, J.S., Schouten, S., 2004. A novel proxy for terrestrial organic matter in sediments based on branched and isoprenoid tetraether lipids. Earth Planet. Sci. Lett. 224, 107–116.

Hou, J., D'Andrea, W.J., MacDonald, D., Huang, Y., 2007. Hydrogen isotopic variability in leaf waxes among terrestrial and aquatic plants around Blood Pond, Massachusetts (USA). Org. Geochem. 38, 977–984.

Hou, J., D'Andrea, W.J., Huang, Y., 2008. Can sedimentary leaf waxes record D/H ratios of continental precipitation? Field, model, and experimental assessments. Geochim. Cosmochim. Acta 72, 3503–3517.

Hren, M.T., Pagani, M., Erwin, D.M., Brandon, M., 2010. Biomarker reconstruction of the early Eocene paleotopography and paleoclimate of the northern Sierra Nevada. Geology 38, 7–10.

Huang, Y., Shuman, B., Wang, Y., Webb, T., 2004. Hydrogen isotope ratios of individual lipids in lake sediments as novel tracers of climatic and environmental change: a surface sediment test. J. Paleolimnol. 31, 363–375.

Huguet, A., Fosse, C., Laggoun-Défarge, F., Toussaint, M.-L., Derenne, S., 2010a. Occurrence and distribution of glycerol dialkyl glycerol tetraethers in a French peat bog. Org. Geochem. 41, 559–572.

Huguet, A., Fosse, C., Metzger, P., Fritsch, E., Derenne, S., 2010b. Occurrence and distribution of non-extractable glycerol dialkyl glycerol tetraethers in temperate and tropical podzol profiles. Org. Geochem. 41, 833–844.

Huguet, A., Wiesenberg, G.L.B., Gocke, M., Fosse, C., Derenne, S., 2012. Branched tetraether membrane lipids associated with rhizoliths in loess: Rhizomicrobial overprinting of initial biomarker record. Org. Geochem. 43, 12–19.

Huguet, A., Fosse, C., Laggoun-Défarge, F., Delarue, F., Derenne, S., 2013a. Effects of a short-term experimental microclimate warming on the abundance and distribution of branched GDGTs in a French peatland. Geochim. Cosmochim. Acta 105, 294–315.

Huguet, A., Gocke, M., Derenne, S., Fosse, C., Wiesenberg, G.L.B., 2013b. Root-associated branched tetraether source microorganisms may reduce estimated paleotemperatures in subsoil. Chem. Geol. 356, 1–10.

Huguet, A., Francez, A.-J., Jusselme, M.D., Fosse, C., Derenne, S., 2014. A climatic chamber experiment to test the short term effect of increasing temperature on branched GDGT distribution in Sphagnum peat. Org. Geochem. 73, 109–112.

Huguet, C., Kim, J.-H., Sinninghe Damsté, J.S., Schouten, S., 2006. Reconstruction of sea surface temperature variations in the Arabian Sea over the last 23 kyr using organic proxies (TEX_{86} and $U_{37}^{K'}$). Paleoceanography 21, PA3003.

Huguet, C., Martens-Habbena, W., Urakawa, H., Stahl, D.A., Ingalls, A.E., 2010. Comparison of extraction methods for quantitative analysis of core and intact polar glycerol dialkyl glycerol tetraethers (GDGTs) in environmental samples. Limnol. Oceanogr. Methods 8, 127–145.

IPCC, (Intergovernmental Panel on Climate Change), 2013. Climate Change 2013: the Physical Science Basis. Contribution of Working Group I to the Fifth Assessment Report of the Intergovernmental Panel on Climate Change, Cambridge University Press. ed. Cambridge and New York.

Jacob, J., Disnar, J.-R., Arnaud, F., Chapron, E., Debret, M., Lallier-Vergès, E., Desmet, M., Revel-Rolland, M., 2008. Millet cultivation history in the French Alps as evidenced by a sedimentary molecule. J. Archaeol. Sci. 35, 814–820.

Jenkyns, H.C., Schouten-Huibers, L., Schouten, S., Sinninghe Damsté, J.S., 2012. Warm Middle Jurassic–Early Cretaceous high-latitude sea-surface temperatures from the Southern Ocean. Clim Past 8, 215–226.

Jia, G., Wei, K., Chen, F., Peng, P., 2008. Soil *n*-alkane δD vs. altitude gradients along Mount Gongga, China. Geochim. Cosmochim. Acta 72, 5165–5174.

Jia, G., Rao, Z., Zhang, J., Li, Z., Chen, F., 2013. Tetraether biomarker records from a loess-paleosol sequence in the western Chinese Loess Plateau. Front. Microbiol. 4.

Juggins, S., 2007. C2 Version 1.5 User guide. Software for ecological and palaeoecological data analysis and visualisation.

Jung, S., Lowe, S.E., Hollingsworth, R.I., Zeikus, J.G., 1993. Sarcina ventriculi synthesizes very long chain dicarboxylic acids in response to different forms of environmental stress. J. Biol. Chem. 268, 2828–2835.

Kahmen, A., Schefuß, E., Sachse, D., 2013a. Leaf water deuterium enrichment shapes leaf wax *n*-alkane δD values of angiosperm plants I: Experimental evidence and mechanistic insights. Geochim. Cosmochim. Acta, Hydrogen Isotopes 111, 39–49.

Kahmen, A., Hoffmann, B., Schefuß, E., Arndt, S.K., Cernusak, L.A., West, J.B., Sachse, D., 2013b. Leaf water deuterium enrichment shapes leaf wax *n*-alkane δD values of angiosperm plants II: Observational evidence and global implications. Geochim. Cosmochim. Acta, Hydrogen Isotopes 111, 50–63.

Karner, M.B., DeLong, E.F., Karl, D.M., 2001. Archaeal dominance in the mesopelagic zone of the Pacific Ocean. Nature 409, 507–510.

Kayvantash, D., 2012. Le régime thermique du lac Masoko et son influence sur l'hydrochimique du lac (rapport de master 1 Sciences de la Terre). Université Paris-Sud, Orsay.

Killops, V., Killops, S., 2005. Introduction to organic geochemistry 2d edition. Blackwel Publishing Ltd.

Kim, J.-H., Schouten, S., Buscail, R., Ludwig, W., Bonnin, J., Sinninghe Damsté, J.S., Bourrin, F., 2006. Origin and distribution of terrestrial organic matter in the NW Mediterranean (Gulf of Lions): Exploring the newly developed BIT index. Geochem. Geophys. Geosystems 7, Q11017.

Kim, J.-H., Ludwig, W., Schouten, S., Kerhervé, P., Herfort, L., Bonnin, J., Sinninghe Damsté, J.S., 2007. Impact of flood events on the transport of terrestrial organic matter to the ocean: A study of the Têt River (SW France) using the BIT index. Org. Geochem. 38, 1593–1606.

Kim, J.-H., Schouten, S., Hopmans, E.C., Donner, B., Sinninghe Damsté, J.S., 2008. Global sediment core-top calibration of the TEX_{86} paleothermometer in the ocean. Geochim. Cosmochim. Acta 72, 1154–1173.

Kim, J.-H., van der Meer, J., Schouten, S., Helmke, P., Willmott, V., Sangiorgi, F., Koç, N., Hopmans, E.C., Damsté, J.S.S., 2010. New indices and calibrations derived from the distribution of crenarchaeal isoprenoid tetraether lipids: Implications for past sea surface temperature reconstructions. Geochim. Cosmochim. Acta 74, 4639–4654.

Kim, J.-H., Zell, C., Moreira-Turcq, P., Pérez, M.A.P., Abril, G., Mortillaro, J.-M., Weijers, J.W.H., Meziane, T., Sinninghe Damsté, J.S., 2012. Tracing soil organic carbon in the lower Amazon River and its tributaries using GDGT distributions and bulk organic matter properties. Geochim. Cosmochim. Acta 90, 163–180.

Knappy, C.S., Keely, B.J., 2011. Novel glycerol dialkanol triols in sediments: transformation products of glycerol dibiphytanyl glycerol tetraether lipids or biosynthetic intermediates? Chem. Commun. 48, 841–843.

Koga, Y., Kyuragi, T., Nishihara, M., Sone, N., 1998. Did Archaeal and Bacterial Cells Arise Independently from Noncellular Precursors? A Hypothesis Stating That the Advent of Membrane Phospholipid with Enantiomeric Glycerophosphate Backbones Caused the Separation of the Two Lines of Descent. J. Mol. Evol. 46, 54–63.

Koga, Y., Morii, H., 2007. Biosynthesis of Ether-Type Polar Lipids in Archaea and Evolutionary Considerations. Microbiol. Mol. Biol. Rev. 71, 97–120.

Kotsyurbenko, O.R., Chin, K.-J., Glagolev, M.V., Stubner, S., Simankova, M.V., Nozhevnikova, A.N., Conrad, R., 2004. Acetoclastic and hydrogenotrophic methane production and methanogenic populations in an acidic West-Siberian peat bog. Environ. Microbiol. 6, 1159–1173.

Kratz, T.K., DeWitt, C.B., 1986. Internal Factors Controlling Peatland-Lake Ecosystem Development. Ecology 67, 100–107.

Laggoun-Défarge, F., Gilbert, D., Buttler, A., Epron, D., Francez, A.-J., Grasset, L., Mitchell, E.A.D., Guimbaud, C., Roy, J.-C., 2008a. Effects of experimental warming on carbon sink function of a temperate pristine mire : the PEATWARM project., in: International Peat Society Congress. Tullamore, Irlande.

Laggoun-Défarge, F., Mitchell, E., Gilbert, D., Disnar, J.-R., Comont, L., Warner, B.G., Buttler, A., 2008b. Cut-over Peatland Regeneration Assessment Using Organic Matter and Microbial Indicators (Bacteria and Testate Amoebae). J. Appl. Ecol. 45, 716–727.

Langworthy, T.A., Smith, P.F., Mayberry, W.R., 1972. Lipids of Thermoplasma acidophilum. J. Bacteriol. 112, 1193–1200.

Langworthy, T.A., 1977. Long-chain diglycerol tetraethers from Thermoplasma acidophilum. Biochim. Biophys. Acta BBA - Lipids Lipid Metab. 487, 37–50.

Lear, C.H., Elderfield, H., Wilson, P.A., 2000. Cenozoic Deep-Sea Temperatures and Global Ice Volumes from Mg/Ca in Benthic Foraminiferal Calcite. Science 287, 269–272.

Lincoln, S.A., Wai, B., Eppley, J.M., Church, M.J., Summons, R.E., DeLong, E.F., 2014. Planktonic Euryarchaeota are a significant source of archaeal tetraether lipids in the ocean. Proc. Natl. Acad. Sci. 111, 9858–9863.

Lipp, J.S., Hinrichs, K.-U., 2009. Structural diversity and fate of intact polar lipids in marine sediments. Geochim. Cosmochim. Acta 73, 6816–6833.

Liu, W., Huang, Y., 2005. Compound specific D/H ratios and molecular distributions of higher plant leaf waxes as novel paleoenvironmental indicators in the Chinese Loess Plateau. Org. Geochem. 36, 851–860.

Liu, W., Wang, H., Zhang, C.L., Liu, Z., He, Y., 2013. Distribution of glycerol dialkyl glycerol tetraether lipids along an altitudinal transect on Mt. Xiangpi, NE Qinghai-Tibetan Plateau, China. Org. Geochem. 57, 76–83.

Liu, X.-L., Leider, A., Gillespie, A., Gröger, J., Versteegh, G.J.M., Hinrichs, K.-U., 2010. Identification of polar lipid precursors of the ubiquitous branched GDGT orphan lipids in a peat bog in Northern Germany. Org. Geochem. 41, 653–660.

Liu, X.-L, Lipp, J.S., Hinrichs, K.-U., 2011. Distribution of intact and core GDGTs in marine sediments. Org. Geochem. 42, 368–375.

Liu, X.-L., Lipp, J.S., Schröder, J.M., Summons, R.E., Hinrichs, K.-U., 2012a. Isoprenoid glycerol dialkanol diethers: A series of novel archaeal lipids in marine sediments. Org. Geochem. 43, 50–55.

Liu, X.-L., Lipp, J.S., Simpson, J.H., Lin, Y.-S., Summons, R.E., Hinrichs, K.-U., 2012b. Mono- and dihydroxyl glycerol dibiphytanyl glycerol tetraethers in marine sediments: Identification of both core and intact polar lipid forms. Geochim. Cosmochim. Acta 89, 102–115.

Liu, X.-L., Summons, R.E., Hinrichs, K.-U., 2012c. Extending the known range of glycerol ether lipids in the environment: structural assignments based on tandem mass spectral fragmentation patterns. Rapid Commun. Mass Spectrom. 26, 2295–2302.

Lliros, M., Gich, F., Plasencia, A., Auguet, J.-C., Darchambeau, F., Casamayor, E.O., Descy, J.-P., Borrego, C., 2010. Vertical Distribution of Ammonia-Oxidizing Crenarchaeota and Methanogens in the Epipelagic Waters of Lake Kivu (Rwanda-Democratic Republic of the Congo). Appl. Environ. Microbiol. 76, 6853–6863.

Logemann, J., Graue, J., Köster, J., Engelen, B., Rullkötter, J., Cypionka, H., 2011. A laboratory experiment of intact polar lipid degradation in sandy sediments. Biogeosciences 8, 2547–2560.

Loisel, J., Yu, Z., 2013. Surface vegetation patterning controls carbon accumulation in peatlands. Geophys. Res. Lett. 40, 5508–5513.

Loomis, S.E., Russell, J.M., Sinninghe Damsté, J.S., 2011. Distributions of branched GDGTs in soils and lake sediments from western Uganda: Implications for a lacustrine paleothermometer. Org. Geochem. 42, 739–751.

Loomis, S.E., Russell, J.M., Ladd, B., Street-Perrott, F.A., Sinninghe Damsté, J.S., 2012. Calibration and application of the branched GDGT temperature proxy on East African lake sediments. Earth Planet. Sci. Lett. 357–358, 277–288.

Loomis, S.E., Russell, J.M., Eggermont, H., Verschuren, D., Sinninghe Damsté, J.S., 2014a. Effects of temperature, pH and nutrient concentration on branched GDGT distributions in East African lakes: Implications for paleoenvironmental reconstruction. Org. Geochem. 66, 25–37.

Loomis, S.E., Russell, J.M., Heureux, A.M., D'Andrea, W.J., Damste, J.S.S., 2014b. Seasonal variability of branched glycerol dialkyl glycerol tetraethers (brGDGTs) in a temperate lake system. Geochim. Cosmochim. Acta 144, 173–187.

Luo, P., Peng, P. 'an, Gleixner, G., Zheng, Z., Pang, Z., Ding, Z., 2011. Empirical relationship between leaf wax *n*-alkane δD and altitude in the Wuyi, Shennongjia and Tianshan Mountains, China: Implications for paleoaltimetry. Earth Planet. Sci. Lett. 301, 285–296.

Macalady, J.L., Vestling, M.M., Baumler, D., Boekelheide, N., Kaspar, C.W., Banfield, J.F., 2004. Tetraether-linked membrane monolayers in Ferroplasma spp: a key to survival in acid. Extremophiles 8, 411–419.

Marlowe, I., Green, J., Neal, A., Brassell, S., Eglinton, G., Course, P., 1984. Long-Chain (n-C37-C39) Alkenones in the Prymnesiophyceae - Distribution. Br. Phycol. J. 19, 203–216.

Mayewski, P.A., Rohling, E.E., Curt Stager, J., Karlén, W., Maasch, K.A., David Meeker, L., Meyerson, E.A., Gasse, F., van Kreveld, S., Holmgren, K., Lee-Thorp, J., Rosqvist, G., Rack, F., Staubwasser, M., Schneider, R.R., Steig, E.J., 2004. Holocene climate variability. Quat. Res. 62, 243–255.

McGregor, G.R., Nieuwolt, S., 1998. Tropical Climatology, 2d edition. ed. Wiley, New York.

Meador, T.B., Zhu, C., Elling, F.J., Könneke, M., Hinrichs, K.-U., 2014. Identification of isoprenoid glycosidic glycerol dibiphytanol diethers and indications for their biosynthetic origin. Org. Geochem. 69, 70-75.

Menges, J., Huguet, C., Alcañiz, J.M., Fietz, S., Sachse, D., Rosell-Melé, A., 2013. Water availability determines branched glycerol dialkyl glycerol tetraether distributions in soils of the Iberian Peninsula. Biogeosciences Discuss 10, 9043–9068.

Meyers, P.A., 1997. Organic geochemical proxies of paleoceanographic, paleolimnologic, and paleoclimatic processes. Org. Geochem. 27, 213–250.

Meyers, P.A., 2003. Applications of organic geochemistry to paleolimnological reconstructions: a summary of examples from the Laurentian Great Lakes. Org. Geochem. 34, 261–289.

Mills, K., Ryves, D.B., Anderson, N.J., Bryant, C.L., Tyler, J.J., 2014. Expressions of climate perturbations in western Ugandan crater lake sediment records during the last 1000 years. Clim Past 10, 1581–1601.

Miola, A., 2012. Tools for Non-Pollen Palynomorphs (NPPs) analysis: A list of Quaternary NPP types and reference literature in English language (1972–2011). Rev. Palaeobot. Palynol., Non-pollen Palynomorphs as Relevant indicators in Palaeoecology and Archaeobotany 186, 142–161.

Mügler, I., Sachse, D., Werner, M., Xu, B., Wu, G., Yao, T., Gleixner, G., 2008. Effect of lake evaporation on δD values of lacustrine n-alkanes: A comparison of Nam Co (Tibetan Plateau) and Holzmaar (Germany). Org. Geochem. 39, 711–729.

Nguyen Tu, T.T., Derenne, S., Largeau, C., Mariotti, A., Bocherens, H., Pons, D., 2000. Effects of fungal infection on lipid extract composition of higher plant remains: comparison of shoots of a Cenomanian conifer, uninfected and infected by extinct fungi. Org. Geochem. 31, 1743–1754.

Nguyen Tu, T.T., Derenne, S., Largeau, C., Bardoux, G., Mariotti, A., 2004. Diagenesis effects on specific carbon isotope composition of plant n-alkanes. Org. Geochem., Selected papers from the Eleventh International Humic Substances Society Conference 35, 317–329.

Nguyen Tu, T.T., Egasse, C., Zeller, B., Bardoux, G., Biron, P., Ponge, J.-F., David, B., Derenne, S., 2011. Early degradation of plant alkanes in soils: A litterbag experiment using 13C-labelled leaves. Soil Biol. Biochem. 43, 2222–2228.

Nichols, J.E., Booth, R.K., Jackson, S.T., Pendall, E.G., Huang, Y., 2006. Paleohydrologic reconstruction based on n-alkane distributions in ombrotrophic peat. Org. Geochem. 37, 1505–1513.

Nichols, J., Booth, R.K., Jackson, S.T., Pendall, E.G., Huang, Y., 2010. Differential hydrogen isotopic ratios of Sphagnum and vascular plant biomarkers in ombrotrophic peatlands as a quantitative proxy for precipitation—evaporation balance. Geochim. Cosmochim. Acta 74, 1407–1416.

Nichols, J.E., Peteet, D.M., Moy, C.M., Castañeda, I.S., McGeachy, A., Perez, M., 2014. Impacts of climate and vegetation change on carbon accumulation in a south-central Alaskan peatland assessed with novel organic geochemical techniques. The Holocene 24, 1146–1155.

Nishihara, M., Koga, Y., 1987a. Extraction and Composition of Polar Lipids from the Archaebacterium, Methanobacterium thermoautotrophicum: Effective Extraction of Tetraether Lipids by an Acidified Solvent. J. Biochem. (Tokyo) 101, 997–1005.

Nishihara, M., Morii, H., Koga, Y., 1987b. Structure Determination of a Quartet of Novel Tetraether Lipids from Methanobacterium thermoautotrophicum. J. Biochem. (Tokyo) 101, 1007–1015.

Nott, C.J., Xie, S., Avsejs, L.A., Maddy, D., Chambers, F.M., Evershed, R.P., 2000. *n*-Alkane distributions in ombrotrophic mires as indicators of vegetation change related to climatic variation. Org. Geochem. 31, 231–235.

Nürnberg, D., Bijma, J., Hemleben, C., 1996. Assessing the reliability of magnesium in foraminiferal calcite as a proxy for water mass temperatures. Geochim. Cosmochim. Acta 60, 803–814.

Pancost, R.D., Geel, B. van, Baas, M., Damsté, J.S.S., 2000. $\delta^{13}C$ values and radiocarbon dates of microbial biomarkers as tracers for carbon recycling in peat deposits. Geology 28, 663–666.

Pancost, R.D., Baas, M., van Geel, B., Sinninghe Damsté, J.S., 2002. Biomarkers as proxies for plant inputs to peats: an example from a sub-boreal ombrotrophic bog. Org. Geochem. 33, 675–690.

Pancost, R.D., Pressley, S., Coleman, J.M., Talbot, H.M., Kelly, S.P., Farrimond, P., Schouten, S., Benning, L., Mountain, B.W., 2006. Composition and implications of diverse lipids in New Zealand Geothermal sinters. Geobiology 4, 71–92.

Pearson, A., Ingalls, A.E., 2013. Assessing the Use of Archaeal Lipids as Marine Environmental Proxies. Annu. Rev. Earth Planet. Sci. 41, 359–384.

Pearson, E.J., Juggins, S., Talbot, H.M., Weckström, J., Rosén, P., Ryves, D.B., Roberts, S.J., Schmidt, R., 2011. A lacustrine GDGT-temperature calibration from the Scandinavian Arctic to Antarctic: Renewed potential for the application of GDGT-paleothermometry in lakes. Geochim. Cosmochim. Acta 75, 6225–6238.

Pécsi, M., 1990. Loess is not just the accumulation of dust. Quat. Int. 7–8, 1–21.

Pedentchouk, N., Sumner, W., Tipple, B., Pagani, M., 2008. $\delta^{13}C$ and δD compositions of *n*-alkanes from modern angiosperms and conifers: An experimental set up in central Washington State, USA. Org. Geochem., Advances in Organic Geochemistry 2007 Proceedings of the 23rd International Meeting on Organic Geochemistry 39, 1066–1071.

Pesaro, M., Widmer, F., 2002. Identification of novel Crenarchaeota and Euryarchaeota clusters associated with different depth layers of a forest soil. FEMS Microbiol. Ecol. 42, 89–98.

Peterse, F., van der Meer, M.T.J., Schouten, S., Jia, G., Ossebaar, J., Blokker, J., Damste, J.S.S., 2009. Assessment of soil n-alkane delta D and branched tetraether membrane lipid distributions as tools for paleoelevation reconstruction. Biogeosciences 6, 2799–2807.

Peterse, F., Prins, M.A., Beets, C.J., Troelstra, S.R., Zheng, H., Gu, Z., Schouten, S., Damsté, J.S.S., 2011. Decoupled warming and monsoon precipitation in East Asia over the last deglaciation. Earth Planet. Sci. Lett. 301, 256–264.

Peterse, F., van der Meer, J., Schouten, S., Weijers, J.W.H., Fierer, N., Jackson, R.B., Kim, J.-H., Sinninghe Damsté, J.S., 2012. Revised calibration of the MBT–CBT paleotemperature proxy based on branched tetraether membrane lipids in surface soils. Geochim. Cosmochim. Acta 96, 215–229.

Peterse, F., Martinez-Garcia, A., Zhou, B., Beets, C.J., Prins, M.A., Zheng, H., Eglinton, T.I., 2014. Molecular records of continental air temperature and monsoon precipitation variability in East Asia spanning the past 130,000 years. Quat. Sci. Rev. 83, 76–82.

Pitcher, A., Wuchter, C., Siedenberg, K., Schouten, S., Sinninghe Damsté, J.S., 2011. Crenarchaeol tracks winter blooms of ammonia-oxidizing Thaumarchaeota in the coastal North Sea. Limnol. Oceanogr. 56, 2308–2318.

Polissar, P.J., Freeman, K.H., Rowley, D.B., McInerney, F.A., Currie, B.S., 2009. Paleoaltimetry of the Tibetan Plateau from D/H ratios of lipid biomarkers. Earth Planet. Sci. Lett. 287, 64–76.

Pouliot, J., Galand, P.E., Lovejoy, C., Vincent, W.F., 2009. Vertical structure of archaeal communities and the distribution of ammonia monooxygenase A gene variants in two meromictic High Arctic lakes. Environ. Microbiol. 11, 687–699.

Powers, L.A., Werne, J.P., Johnson, T.C., Hopmans, E.C., Sinninghe Damsté, J.S., Schouten, S., 2004. Crenarchaeotal membrane lipids in lake sediments: A new paleotemperature proxy for continental paleoclimate reconstruction? Geology 32, 613.

Powers, L.A., Johnson, T.C., Werne, J.P., Castanada, I.S., Hopmans, E.C., Damste, J.S.S., Schouten, S., 2005. Large temperature variability in the southern African tropics since the Last Glacial Maximum. Geophys. Res. Lett. 32.

Powers, L., Werne, J.P., Vanderwoude, A.J., Sinninghe Damsté, J.S., Hopmans, E.C., Schouten, S., 2010. Applicability and calibration of the TEX_{86} paleothermometer in lakes. Org. Geochem. 41, 404–413.

Powers, L.A., Johnson, T.C., Werne, J.P., Castañeda, I.S., Hopmans, E.C., Sinninghe Damsté, J.S., Schouten, S., 2011. Organic geochemical records of environmental variability in Lake Malawi during the last 700 years, Part I: The TEX_{86} temperature record. Palaeogeogr. Palaeoclimatol. Palaeoecol., Southern hemisphere tropical climate over the past 145ka: Results of the Lake Malawi Scientific Drilling Project, East Africa 303, 133–139.

Prado, A., Da Costa, M.S., Madeira, V.M., 1988. Effect of Growth Temperature on the Lipid Composition of two Strains of Thermus sp. J. Gen. Microbiol. 134, 1653–1660.

Prahl, F.G., Muehlhausen, L.A., Zahnle, D.L., 1988. Further evaluation of long-chain alkenones as indicators of paleoceanographic conditions. Geochim. Cosmochim. Acta 52, 2303–2310.

Rampen, S.W., Schouten, S., Sinninghe Damsté, J.S., 2011. Occurrence of long chain 1,14-diols in Apedinella radians. Org. Geochem. 42, 572–574.

Rampen, S.W., Willmott, V., Kim, J.-H., Uliana, E., Mollenhauer, G., Schefuß, E., Sinninghe Damsté, J.S., Schouten, S., 2012. Long chain 1,13- and 1,15-diols as a potential proxy for palaeotemperature reconstruction. Geochim. Cosmochim. Acta 84, 204–216.

Rampen, S.W., Willmott, V., Kim, J.-H., Rodrigo-Gámiz, M., Uliana, E., Mollenhauer, G., Schefuß, E., Sinninghe Damsté, J.S., Schouten, S., 2014. Evaluation of long chain 1,14-alkyl diols in marine sediments as indicators for upwelling and temperature. Org. Geochem. 76, 39–47.

Ramsey, C.B., 2008. Deposition models for chronological records. Quat. Sci. Rev., INTegration of Ice-core, Marine and Terrestrial records (INTIMATE): Refining the record of the Last Glacial-Interglacial Transition 27, 42–60.

Rao, Z., Jia, G., Qiang, M., Zhao, Y., 2014. Assessment of the difference between mid- and long chain compound specific δD *n*-alkanes values in lacustrine sediments as a paleoclimatic indicator. Org. Geochem. 76, 104–117.

R Core Team, 2013. R: A language and environment for statistical computing.

Reizer, J., Grossowicz, N., Barenholz, Y., 1985. The effect of growth temperature on the thermotropic behavior of the membranes of a thermophilic Bacillus. Composition-structure-function relationships. Biochim. Biophys. Acta 815, 268–280.

Ring, M.W., Schwär, G., Thiel, V., Dickschat, J.S., Kroppenstedt, R.M., Schulz, S., Bode, H.B., 2006. Novel Iso-branched Ether Lipids as Specific Markers of Developmental Sporulation in the Myxobacterium Myxococcus xanthus. J. Biol. Chem. 281, 36691–36700.

Rommerskirchen, F., Eglinton, G., Dupont, L., Güntner, U., Wenzel, C., Rullkötter, J., 2003. A north to south transect of Holocene southeast Atlantic continental margin sediments: Relationship between aerosol transport and compound-specific $\delta^{13}C$ land plant biomarker and pollen records. Geochem. Geophys. Geosystems 4, 1101.

Rommerskirchen, F., Plader, A., Eglinton, G., Chikaraishi, Y., Rullkötter, J., 2006. Chemotaxonomic significance of distribution and stable carbon isotopic composition of long-chain alkanes and alkan-1-ols in C4 grass waxes. Org. Geochem., Stable Isotopes in Biogeosciences 37, 1303–1332.

Russell, J.M., Johnson, T.C., 2005. A high-resolution geochemical record from Lake Edward, Uganda Congo and the timing and causes of tropical African drought during the late Holocene. Quat. Sci. Rev. 24, 1375–1389.

Sachse, D., Radke, J., Gleixner, G., 2004. Hydrogen isotope ratios of recent lacustrine sedimentary *n*-alkanes record modern climate variability. Geochim. Cosmochim. Acta 68, 4877–4889.

Sachse, D., Radke, J., Gleixner, G., 2006. δD values of individual *n*-alkanes from terrestrial plants along a climatic gradient – Implications for the sedimentary biomarker record. Org. Geochem. 37, 469–483.

Sachse, D., Billault, I., Bowen, G.J., Chikaraishi, Y., Dawson, T.E., Feakins, S.J., Freeman, K.H., Magill, C.R., McInerney, F.A., van der Meer, M.T.J., Polissar, P., Robins, R.J., Sachs, J.P., Schmidt, H.-L., Sessions, A.L., White, J.W.C., West, J.B., Kahmen, A., 2012. Molecular Paleohydrology: Interpreting the Hydrogen-Isotopic Composition of Lipid Biomarkers from Photosynthesizing Organisms. Annu. Rev. Earth Planet. Sci. 40, 221–249.

Sauer, P.E., Eglinton, T.I., Hayes, J.M., Schimmelmann, A., Sessions, A.L., 2001. Compound-specific D/H ratios of lipid biomarkers from sediments as a proxy for environmental and climatic conditions. Geochim. Cosmochim. Acta 65, 213–222.

Schefuß, E., Schouten, S., Jansen, J.H.F., Sinninghe Damsté, J.S., 2003. African vegetation controlled by tropical sea surface temperatures in the mid-Pleistocene period. Nature 422, 418–421.

Schefuß, E., Schouten, S., Schneider, R.R., 2005. Climatic controls on central African hydrology during the past 20,000 years. Nature 437, 1003–1006.

Schouten, S., Hopmans, E.C., Schefuß, E., Sinninghe Damsté, J.S., 2002. Distributional variations in marine crenarchaeotal membrane lipids: a new tool for

reconstructing ancient sea water temperatures? Earth Planet. Sci. Lett. 204, 265–274.

Schouten, S., Hopmans, E.C., Baas, M., Boumann, H., Standfest, S., Könneke, M., Stahl, D.A., Damsté, J.S.S., 2008. Intact Membrane Lipids of "Candidatus Nitrosopumilus maritimus," a Cultivated Representative of the Cosmopolitan Mesophilic Group I Crenarchaeota. Appl. Environ. Microbiol. 74, 2433–2440.

Schouten, S., Rijpstra, W.I.C., Durisch-Kaiser, E., Schubert, C.J., Sinninghe Damsté, J.S., 2012. Distribution of glycerol dialkyl glycerol tetraether lipids in the water column of Lake Tanganyika. Org. Geochem. 53, 34–37.

Schouten, S., Hopmans, E.C., Sinninghe Damsté, J.S., 2013. The organic geochemistry of glycerol dialkyl glycerol tetraether lipids: A review. Org. Geochem. 54, 19–61.

Schwark, L., Zink, K., Lechterbeck, J., 2002. Reconstruction of postglacial to early Holocene vegetation history in terrestrial Central Europe via cuticular lipid biomarkers and pollen records from lake sediments. Geology 30, 463–466.

Scrimgeour, C.M., Begley, I.S., Thomason, M.L., 1999. Measurement of deuterium incorporation into fatty acids by gas chromatography/isotope ratio mass spectrometry. Rapid Commun. Mass Spectrom. 13, 271–274.

Seki, O., Meyers, P.A., Kawamura, K., Zheng, Y., Zhou, W., 2009. Hydrogen isotopic ratios of plant wax *n*-alkanes in a peat bog deposited in northeast China during the last 16 kyr. Org. Geochem. 40, 671–677.

Sessions, A.L., Burgoyne, T.W., Schimmelmann, A., Hayes, J.M., 1999. Fractionation of hydrogen isotopes in lipid biosynthesis. Org. Geochem. 30, 1193–1200.

Shanahan, T.M., McKay, N., Overpeck, J.T., Peck, J.A., Scholz, C., Heil Jr., C.W., King, J., 2013. Spatial and temporal variability in sedimentological and geochemical properties of sediments from an anoxic crater lake in West Africa: Implications for paleoenvironmental reconstructions. Palaeogeogr. Palaeoclimatol. Palaeoecol. 374, 96–109.

Shevenell, A.E., Ingalls, A.E., Domack, E.W., Kelly, C., 2011. Holocene Southern Ocean surface temperature variability west of the Antarctic Peninsula. Nature 470, 250–254.

Shintani, T., Yamamoto, M., Chen, M.-T., 2011. Paleoenvironmental changes in the northern South China Sea over the past 28,000 years: A study of TEX_{86}-derived sea surface temperatures and terrestrial biomarkers. J. Asian Earth Sci. 40, 1221–1229.

Sinninghe Damsté, J.S., Hopmans, E.C., Pancost, R.D., Schouten, S., Geenevasen, J.A.J., 2000. Newly discovered non-isoprenoid glycerol dialkyl glycerol tetraether lipids in sediments. Chem. Commun. 1683–1684.

Sinninghe Damsté, J.S., Rampen, S., Irene, W., Rijpstra, C., Abbas, B., Muyzer, G., Schouten, S., 2003. A diatomaceous origin for long-chain diols and mid-chain hydroxy methyl alkanoates widely occurring in quaternary marine sediments: indicators for high-nutrient conditions. Geochim. Cosmochim. Acta 67, 1339–1348.

Sinninghe Damsté, J.S., Ossebaar, J., Schouten, S., Verschuren, D., 2008. Altitudinal shifts in the branched tetraether lipid distribution in soil from Mt. Kilimanjaro (Tanzania): Implications for the MBT/CBT continental palaeothermometer. Org. Geochem. 39, 1072–1076.

Sinninghe Damsté, J.S., Ossebaar, J., Abbas, B., Schouten, S., Verschuren, D., 2009. Fluxes and distribution of tetraether lipids in an equatorial African lake:

Constraints on the application of the TEX_{86} palaeothermometer and BIT index in lacustrine settings. Geochim. Cosmochim. Acta 73, 4232–4249.

Sinninghe Damsté, J.S., Rijpstra, W.I.C., Hopmans, E.C., Weijers, J.W.H., Foesel, B.U., Overmann, J., Dedysh, S.N., 2011. 13,16-Dimethyl Octacosanedioic Acid (iso-Diabolic Acid), a Common Membrane-Spanning Lipid of Acidobacteria Subdivisions 1 and 3. Appl. Environ. Microbiol. 77, 4147–4154.

Sinninghe Damsté, J.S., Ossebaar, J., Schouten, S., Verschuren, D., 2012a. Distribution of tetraether lipids in the 25-ka sedimentary record of Lake Challa: extracting reliable TEX_{86} and MBT/CBT palaeotemperatures from an equatorial African lake. Quat. Sci. Rev. 50, 43–54.

Sinninghe Damsté, J.S., Rijpstra, W.I.C., Hopmans, E.C., Jung, M.-Y., Kim, J.-G., Rhee, S.-K., Stieglmeier, M., Schleper, C., 2012b. Intact Polar and Core Glycerol Dibiphytanyl Glycerol Tetraether Lipids of Group I.1a and I.1b Thaumarchaeota in Soil. Appl. Environ. Microbiol. 78, 6866–6874.

Sinninghe Damsté, J.S., Rijpstra, W.I.C., Hopmans, E.C., Foesel, B.U., Wüst, P.K., Overmann, J., Tank, M., Bryant, D.A., Dunfield, P.F., Houghton, K., Stott, M.B., 2014. Ether- and Ester-Bound iso-Diabolic Acid and Other Lipids in Members of Acidobacteria Subdivision 4. Appl. Environ. Microbiol. 80, 5207–5218.

Standley, L.J., Simoneit, B.R.T., 1987. Characterization of extractable plant wax, resin, and thermally matured components in smoke particles from prescribed burns. Environ. Sci. Technol. 21, 163–169.

Stockmarr, J., 1971. Tablets with spores used in absolute pollen analysis. Pollen Spores 13, 615–621.

Sun, Q., Chu, G., Liu, M., Xie, M., Li, S., Ling, Y., Wang, X., Shi, L., Jia, G., Lü, H., 2011. Distributions and temperature dependence of branched glycerol dialkyl glycerol tetraethers in recent lacustrine sediments from China and Nepal. J. Geophys. Res. 116, G01008.

Suutari, M., Laakso, S., 1992. Changes in fatty acid branching and unsaturation of Streptomyces griseus and Brevibacterium fermentans as a response to growth temperature. Appl. Environ. Microbiol. 58, 2338–2340.

Swan, J.M.A., Gill, A.M., 1970. The Origins, Spread, and Consolidation of a Floating Bog in Harvard Pond, Petersham, Massachusetts. Ecology 51, 829–840.

Takano, Y., Chikaraishi, Y., Ogawa, N.O., Nomaki, H., Morono, Y., Inagaki, F., Kitazato, H., Hinrichs, K.-U., Ohkouchi, N., 2010. Sedimentary membrane lipids recycled by deep-sea benthic archaea. Nat. Geosci. 3, 858–861.

Talbot, H.M., Watson, D.F., Murrell, J.C., Carter, J.F., Farrimond, P., 2001. Analysis of intact bacteriohopanepolyols from methanotrophic bacteria by reversed-phase high-performance liquid chromatography–atmospheric pressure chemical ionisation mass spectrometry. J. Chromatogr. A 921, 175–185.

Talling, J.F., Lemoalle, J., ORSTOM, 1998. Ecological Dynamics of Tropical Inland Waters, Cambridge University Press. ed. United Kingdom.

Taylor, K.W.R., Huber, M., Hollis, C.J., Hernandez-Sanchez, M.T., Pancost, R.D., 2013. Re-evaluating modern and Palaeogene GDGT distributions: Implications for SST reconstructions. Glob. Planet. Change 108, 158–174.

Thevenon, F., Williamson, D., Vincens, A., Taieb, M., Merdaci, O., Decobert, M., Buchet, G., 2003. A late-Holocene charcoal record from Lake Masoko, SW Tanzania: climatic and anthropologic implications. The Holocene 13, 785–792.

Thevenon, F., Williamson, D., Bard, E., Anselmetti, F.S., Beaufort, L., Cachier, H., 2010. Combining charcoal and elemental black carbon analysis in sedimentary

archives: Implications for past fire regimes, the pyrogenic carbon cycle, and the human-climate interactions. Glob. Planet. Change 72, 381–389.

Tierney, J.E., Russell, J.M., Huang, Y., Damsté, J.S.S., Hopmans, E.C., Cohen, A.S., 2008. Northern Hemisphere Controls on Tropical Southeast African Climate During the Past 60,000 Years. Science 322, 252–255.

Tierney, J.E., Russell, J.M., 2009. Distributions of branched GDGTs in a tropical lake system: implications for lacustrine application of the MBT/CBT paleoproxy. Org. Geochem. 40, 1032–1036.

Tierney, J.E., Russell, J.M., Eggermont, H., Hopmans, E.C., Verschuren, D., Sinninghe Damsté, J.S., 2010. Environmental controls on branched tetraether lipid distributions in tropical East African lake sediments. Geochim. Cosmochim. Acta 74, 4902–4918.

Tierney, J.E., Russell, J.M., Sinninghe Damsté, J.S., Huang, Y., Verschuren, D., 2011. Late Quaternary behavior of the East African monsoon and the importance of the Congo Air Boundary. Quat. Sci. Rev. 30, 798–807.

Tierney, J.E., Schouten, S., Pitcher, A., Hopmans, E.C., Sinninghe Damsté, J.S., 2012. Core and intact polar glycerol dialkyl glycerol tetraethers (GDGTs) in Sand Pond, Warwick, Rhode Island (USA): Insights into the origin of lacustrine GDGTs. Geochim. Cosmochim. Acta 77, 561–581.

Tierney, J.E., Tingley, M.P., 2014. A Bayesian, spatially-varying calibration model for the TEX_{86} proxy. Geochim. Cosmochim. Acta 127, 83–106.

Timonen, S., Bomberg, M., 2009. Archaea in dry soil environments. Phytochem. Rev. 8, 505–518.

Turich, C., Freeman, K.H., Bruns, M.A., Conte, M., Jones, A.D., Wakeham, S.G., 2007. Lipids of marine Archaea: Patterns and provenance in the water-column and sediments. Geochim. Cosmochim. Acta 71, 3272–3291.

Tyler, J.J., Nederbragt, A.J., Jones, V.J., Thurow, J.W., 2010. Assessing past temperature and soil pH estimates from bacterial tetraether membrane lipids: Evidence from the recent lake sediments of Lochnagar, Scotland. J. Geophys. Res. Biogeosciences 115, G01015.

Uda, I., Sugai, A., Itoh, Y.H., Itoh, T., 2001. Variation in molecular species of polar lipids from Thermoplasma acidophilum depends on growth temperature. Lipids 36, 103–105.

van der Ent, R.J., Savenije, H.H.G., 2013. Oceanic sources of continental precipitation and the correlation with sea surface temperature. Water Resour. Res. 49, 3993–4004.

van Geel, B., 1978. A palaoeoecological study of Holocene peat bog sections in Germany and the Netherlands. Rev. Palaeobot. Palynol. 25.

van Geel, B., Gelorini, V., Lyaruu, A., Aptroot, A., Rucina, S., Marchant, R., Damsté, J.S.S., Verschuren, D., 2011. Diversity and ecology of tropical African fungal spores from a 25,000-year palaeoenvironmental record in southeastern Kenya. Rev. Palaeobot. Palynol. 164, 174–190.

Velichkevich, F.Y., Zastawniak, E., 2006. Atlas of the Pleistocene vascular plant macrofossils of Central and Eastern Europe. Part 1-Pteridophytes and monocotyledons. W. Szafer Institute of Botany, Polish Academy of Sciences, Krakow, Poland.

Velichkevich, F.Y., Zastawniak, E., 2009. Atlas of the Pleistocene vascular plant macrofossils of Central and Eastern Europe. Part 2-Herbaceous dicotyledons. W. Szafer Institute of Botany, Polish Academy of Sciences, Krakow, Poland.

Verschuren, D., Laird, K.R., Cumming, B.F., 2000. Rainfall and drought in equatorial east Africa during the past 1,100 years. Nature 403, 410–414.

Verschuren, D., 2003. Lake-based climate reconstruction in Africa: progress and challenges. Hydrobiologia 500, 315–330.

Verschuren, D., Sinninghe Damsté, J.S., Moernaut, J., Kristen, I., Blaauw, M., Fagot, M., Haug, G.H., Geel, B. van, Batist, M.D., Barker, P., Vuille, M., Conley, D.J., Olago, D.O., Milne, I., Plessen, B., Eggermont, H., Wolff, C., Hurrell, E., Ossebaar, J., Lyaruu, A., Plicht, J. van der, Cumming, B.F., Brauer, A., Rucina, S.M., Russell, J.M., Keppens, E., Hus, J., Bradley, R.S., Leng, M., Mingram, J., Nowaczyk, N.R., 2009. Half-precessional dynamics of monsoon rainfall near the East African Equator. Nature 462, 637–641.

Villanueva, L., Damsté, J.S.S., Schouten, S., 2014. A re-evaluation of the archaeal membrane lipid biosynthetic pathway. Nat. Rev. Microbiol. 12, 438–448.

Vincens, A., Williamson, D., Thevenon, F., Taieb, M., Buchet, G., Decobert, M., Thouveny, N., 2003. Pollen-based vegetation changes in southern Tanzania during the last 4200 years: climate change and/or human impact. Palaeogeogr. Palaeoclimatol. Palaeoecol. 198, 321–334.

Vincens, A., Lézine, A.-M., Buchet, G., Lewden, D., Le Thomas, A., 2007. African pollen database inventory of tree and shrub pollen types. Rev. Palaeobot. Palynol. 145, 135–141.

Volkman, J.K., Eglinton, G., Corner, E.D.S., Forsberg, T.E.V., 1980. Long-chain alkenes and alkenones in the marine coccolithophorid Emiliania huxleyi. Phytochemistry 19, 2619–2622.

Volkman, J.K., Barrett, S.M., Dunstan, G.A., Jeffrey, S.W., 1992. C_{30}-C_{32} alkyl diols and unsaturated alcohols in microalgae of the class Eustigmatophyceae. Org. Geochem. 18, 131–138.

Volkman, J.K., Barrett, S.M., Blackburn, S.I., 1999. Eustigmatophyte microalgae are potential sources of C_{29} sterols, C_{22}–C_{28} *n*-alcohols and C_{28}–C_{32} *n*-alkyl diols in freshwater environments. Org. Geochem. 30, 307–318.

Wang, H., Liu, W., Zhang, C.L., Wang, Z., Wang, J., Liu, Z., Dong, H., 2012. Distribution of glycerol dialkyl glycerol tetraethers in surface sediments of Lake Qinghai and surrounding soil. Org. Geochem. 47, 78–87.

Wang, H., Liu, W., Zhang, C.L., Liu, Z., He, Y., 2013. Branched and isoprenoid tetraether (BIT) index traces water content along two marsh-soil transects surrounding Lake Qinghai: Implications for paleo-humidity variation. Org. Geochem. 59, 75–81.

Wanner, H., Solomina, O., Grosjean, M., Ritz, S.P., Jetel, M., 2011. Structure and origin of Holocene cold events. Quat. Sci. Rev. 30, 3109–3123.

Ward, D.M., Brassell, S.C., Eglinton, G., 1985. Archaebacterial lipids in hot-spring microbial mats. Nature 318, 656–659.

Weijers, J.W.H., Schouten, S., van der Linden, M., van Geel, B., Sinninghe Damsté, J.S., 2004. Water table related variations in the abundance of intact archaeal membrane lipids in a Swedish peat bog. FEMS Microbiol. Lett. 239, 51–56.

Weijers, J.W.H., Schouten, S., Hopmans, E.C., Geenevasen, J.A.J., David, O.R.P., Coleman, J.M., Pancost, R.D., Sinninghe Damsté, J.S., 2006a. Membrane lipids of mesophilic anaerobic bacteria thriving in peats have typical archaeal traits. Environ. Microbiol. 8, 648–657.

Weijers, J.W.H., Schouten, S., Spaargaren, O.C., Sinninghe Damsté, J.S., 2006b. Occurrence and distribution of tetraether membrane lipids in soils: Implications

for the use of the TEX_{86} proxy and the BIT index. Org. Geochem. 37, 1680–1693.

Weijers, J.W.H., Schouten, S., van den Donker, J.C., Hopmans, E.C., Sinninghe Damsté, J.S., 2007. Environmental controls on bacterial tetraether membrane lipid distribution in soils. Geochim. Cosmochim. Acta 71, 703–713.

Weijers, J.W.H., Panoto, E., van Bleijswijk, J., Schouten, S., Rijpstra, W.I.C., Balk, M., Stams, A.J.M., Damsté, J.S.S., 2009. Constraints on the Biological Source(s) of the Orphan Branched Tetraether Membrane Lipids. Geomicrobiol. J. 26, 402–414.

Weijers, J.W.H., Steinmann, P., Hopmans, E.C., Schouten, S., Sinninghe Damsté, J.S., 2011. Bacterial tetraether membrane lipids in peat and coal: Testing the MBT–CBT temperature proxy for climate reconstruction. Org. Geochem. 42, 477–486.

White, D.C., Davis, W.M., Nickels, J.S., King, J.D., Bobbie, R.J., 1979. Determination of the sedimentary microbial biomass by extractible lipid phosphate. Oecologia 40, 51–62.

White, F., 1983. Vegetation of Africa - a descriptive memoir to accompany the Unesco/AETFAT/UNSO vegetation map of Africa.

White, G.F., Russell, N.J., Tidswell, E.C., 1996. Bacterial scission of ether bonds. Microbiol. Rev. 60, 216–232.

Williamson, D., Jelinowska, A., Kissel, C., Tucholka, P., Gibert, E., Gasse, F., Massault, M., Taieb, M., Van Campo, E., Wieckowski, K., 1998. Mineral-magnetic proxies of erosion/oxidation cycles in tropical maar-lake sediments (Lake Tritrivakely, Madagascar): paleoenvironmental implications. Earth Planet. Sci. Lett. 155, 205–219.

Williamson, D., Jackson, M.J., Banerjee, S.K., Marvin, J., Merdaci, O., Thouveny, N., Decobert, M., Gibert-Massault, E., Massault, M., Mazaudier, D., Taieb, M., 1999. Magnetic signatures of hydrological change in a tropical maar-lake (Lake Massoko, Tanzania): Preliminary results. Phys. Chem. Earth Part Solid Earth Geod. 24, 799–803.

Williamson, D., 2013. Interface air-sols: les traceurs sédimentologique des lacs tropicaux, in: Paleoclimatologie Trouver, Dater et Interpréter Les Indices (Tome I), Savoirs Actuels. Les Ulis et Paris (France).

Williamson, D., Majule, A., Delalande, M., Mwakisunga, B., Mathé, P.-E., Gwambene, B., Bergonzini, L., 2014. A potential feedback between landuse and climate in the Rungwe tropical highland stresses a critical environmental research challenge. Curr. Opin. Environ. Sustain., Sustainability challenges 6, 116–122.

Williams, R.S., Ferrigno, J.G., 2012. A-2 Glaciers, in: State of the Earth's Cryosphere at the Begining of the 21st Century: Glaciers, Global Snow Cover, Floating Ice, and Permafrost and Periglacial Environments. U.S. Department of the Interior, Washington D.C.

Woese, C.R., Fox, G.E., 1977. Phylogenetic structure of the prokaryotic domain: The primary kingdoms. Proc. Natl. Acad. Sci. 74, 5088–5090.

Woltering, M., Werne, J.P., Kish, J.L., Hicks, R., Damste, J.S.S., Schouten, S., 2012. Vertical and temporal variability in concentration and distribution of thaumarchaeotal tetraether lipids in Lake Superior and the implications for the application of the TEX_{86} temperature proxy. Geochim. Cosmochim. Acta 87, 136–153.

Wuchter, C., Schouten, S., Wakeham, S.G., Sinninghe Damsté, J.S., 2006. Archaeal tetraether membrane lipid fluxes in the northeastern Pacific and the Arabian Sea: Implications for TEX_{86} paleothermometry. Paleoceanography 21, PA4208.

Xie, S., Lipp, J.S., Wegener, G., Ferdelman, T.G., Hinrichs, K.-U., 2013. Turnover of microbial lipids in the deep biosphere and growth of benthic archaeal populations. Proc. Natl. Acad. Sci. 110, 6010–6014.

Xie, S., Nott, C.J., Avsejs, L.A., Volders, F., Maddy, D., Chambers, F.M., Gledhill, A., Carter, J.F., Evershed, R.P., 2000. Palaeoclimate records in compound-specific δD values of a lipid biomarker in ombrotrophic peat. Org. Geochem. 31, 1053–1057.

Xie, S., Nott, C.J., Avsejs, L.A., Maddy, D., Chambers, F.M., Evershed, R.P., 2004. Molecular and isotopic stratigraphy in an ombrotrophic mire for paleoclimate reconstruction. Geochim. Cosmochim. Acta 68, 2849–2862.

Xie, S., Pancost, R.D., Chen, L., Evershed, R.P., Yang, H., Zhang, K., Huang, J., Xu, Y., 2012. Microbial lipid records of highly alkaline deposits and enhanced aridity associated with significant uplift of the Tibetan Plateau in the Late Miocene. Geology 40, 291–294.

Yakir, D., DeNiro, M.J., 1990. Oxygen and Hydrogen Isotope Fractionation during Cellulose Metabolism in Lemna gibba L. Plant Physiol. 93, 325–332.

Yang, H., Ding, W., Zhang, C.L., Wu, X., Ma, X., He, G., Huang, J., Xie, S., 2011. Occurrence of tetraether lipids in stalagmites: Implications for sources and GDGT-based proxies. Org. Geochem. 42, 108–115.

Yang, H., Ding, W., Wang, J., Jin, C., He, G., Qin, Y., Xie, S., 2012. Soil pH impact on microbial tetraether lipids and terrestrial input index (BIT) in China. Sci. China Earth Sci. 55, 236–245.

Yang, H., Pancost, R.D., Dang, X., Zhou, X., Evershed, R.P., Xiao, G., Tang, C., Gao, L., Guo, Z., Xie, S., 2014a. Correlations between microbial tetraether lipids and environmental variables in Chinese soils: Optimizing the paleo-reconstructions in semi-arid and arid regions. Geochim. Cosmochim. Acta 126, 49–69.

Yang, H., Pancost, R.D., Tang, C., Ding, W., Dang, X., Xie, S., 2014b. Distributions of isoprenoid and branched glycerol dialkanol diethers in Chinese surface soils and a loess–paleosol sequence: Implications for the degradation of tetraether lipids. Org. Geochem. 66, 70–79.

Yang, H., Xiao, W., Jia, C., Xie, S., 2014c. Paleoaltimetry proxies based on bacterial branched tetraether membrane lipids in soils. Front. Earth Sci. 9, 13–25.

Yang H.Y., Ding W., He G., Xie S., 2012. Archaeal and bacterial tetraether membrane lipids in soils of varied altitudes in Mt. Jianfengling in South China. J. Earth Sci. 21, 277–280.

Zachos, J.C., Schouten, S., Bohaty, S., Quattlebaum, T., Sluijs, A., Brinkhuis, H., Gibbs, S.J., Bralower, T.J., 2006. Extreme warming of mid-latitude coastal ocean during the Paleocene-Eocene Thermal Maximum: Inferences from TEX_{86} and isotope data. Geology 34, 737–740.

Zech, M., Pedentchouk, N., Buggle, B., Leiber, K., Kalbitz, K., Marković, S.B., Glaser, B., 2011. Effect of leaf litter degradation and seasonality on D/H isotope ratios of *n*-alkane biomarkers. Geochim. Cosmochim. Acta 75, 4917–4928.

Zech, R., Gao, L., Tarozo, R., Huang, Y., 2012. Branched glycerol dialkyl glycerol tetraethers in Pleistocene loess-paleosol sequences: Three case studies. Org. Geochem., Advances in Organic Geochemistry 2011: Proceedings of the 25th International Meeting on Organic Geochemistry 53, 38–44.

Zell, C., Kim, J.-H., Balsinha, M., Dorhout, D., Fernandes, C., Baas, M., Sinninghe Damsté, J.S., 2014. Transport of branched tetraether lipids from the Tagus River basin to the coastal ocean of the Portuguese margin: consequences for the

interpretation of the MBT'/CBT paleothermometer. Biogeosciences 11, 5637–5655.

Zhang, Z., Zhao, M., Eglinton, G., Lu, H., Huang, C.-Y., 2006. Leaf wax lipids as paleovegetational and paleoenvironmental proxies for the Chinese Loess Plateau over the last 170 kyr. Quat. Sci. Rev. 25, 575–594.

Zhou, W., Xie, S., Meyers, P.A., Zheng, Y., 2005. Reconstruction of late glacial and Holocene climate evolution in southern China from geolipids and pollen in the Dingnan peat sequence. Org. Geochem. 36, 1272–1284.

Zhou, W., Zheng, Y., Meyers, P.A., Jull, A.J.T., Xie, S., 2010. Postglacial climate-change record in biomarker lipid compositions of the Hani peat sequence, Northeastern China. Earth Planet. Sci. Lett. 294, 37–46.

Zhuang, G., Pagani, M., Chamberlin, C., Strong, D., Vandergoes, M., 2015. Altitudinal shift in stable hydrogen isotopes and microbial tetraether distribution in soils from the Southern Alps, NZ: Implications for paleoclimatology and paleoaltimetry. Org. Geochem. 79, 56–64.

Zhu, C., Meador, T.B., Dummann, W., Hinrichs, K.-U., 2014a. Identification of unusual butanetriol dialkyl glycerol tetraether and pentanetriol dialkyl glycerol tetraether lipids in marine sediments. Rapid Commun. Mass Spectrom. 28, 332–338.

Zhu, C., Yoshinaga, M.Y., Peters, C.A., Liu, X.-L., Elvert, M., Hinrichs, K.-U., 2014b. Identification and significance of unsaturated archaeal tetraether lipids in marine sediments: Unsaturated archaeal tetraether lipids. Rapid Commun. Mass Spectrom. 28, 1144–1152.

Zink, K.-G., Vandergoes, M.J., Mangelsdorf, K., Dieffenbacher-Krall, A.C., Schwark, L., 2010. Application of bacterial glycerol dialkyl glycerol tetraethers (GDGTs) to develop modern and past temperature estimates from New Zealand lakes. Org. Geochem., Advances in Organic Geochemistry 2009 Proceedings of the 24th International Meeting on Organic Geochemistry 41, 1060–1066.

Zocatelli, R., Turcq, B., Boussafir, M., Cordeiro, R.C., Disnar, J.R., Costa, R.L., Sifeddine, A., Albuquerque, A.L.S., Bernardes, M.C., Jacob, J., 2012. Late Holocene paleoenvironmental changes in Northeast Brazil recorded by organic matter in lacustrine sediments of Lake Boqueirão. Palaeogeogr. Palaeoclimatol. Palaeoecol. 363–364, 127–134.

Appendices

Appendix 1: Sample information (date of sampling, coordinates, altitude)

A. Soil and sediment samples

Sample type	Sample	Altitude (m)	Coordinates	Sampling dates
Surface soil	1	520	S 09.40492° E 33.90782°	04/2012
along	2	520	S 09.40492° E 33.90782°	04/2012
Mt.	3	529	S 09.40842° E 33.917284°	04/2012
Rungwe	4	640	S 09.37025° E33.79949°	04/2012
	5	692	S 09.35699° E 33.79721°	04/2012
	6	826	S 09.35270° E 33.82296°	04/2012
	7	869	S 09.33008° E 33.75884°	04/2012
	8	869	S 09.33008° E 33.75884°	04/2012
	9	994	S 09.33470° E 33.81031°	04/2012
	10	1092	S 09.32068° E 33.80958°	04/2012
	11	1211	S 09.30013° E 33.80783°	04/2012
	12	1374	S 09.28262° E 33.81349°	04/2012
	13	1550	S 09.26021 E 33.820295°	04/2012
	14	1680	S 09.23784° E 33.81677°	04/2012
	15	1702	S 09.35993° E 33.81637°	04/2012
	16	1846	S 09.22716° E 33.81249°	04/2012
	17	2020	S 09.02202° E 33.56576°	04/2012
	18	2055	S 09.02124° E 33.56478°	04/2012
	19	2080	S 09.07322° E 33.40782°	04/2012
	20	2200	S 09.15288° E 33.43117°	12/2012
	21	2800	S 09.13715° E 33.94668°	12/2012
	22	537	S 09.41600° E 33.85702°	07/2014
	23	565	S 09.41337° E 33.82782°	07/2014
	24	700	S 09.34422° E 33.78682°	07/2014
	25	873	S 09.33243° E 33.79362°	07/2014
	26	911	S 09.33178° E 33.75133°	07/2014
	27	1013	S 09.31867° E 33.79822°	07/2014
	28	1164	S 09.30667° E 33.80592°	07/2014
	29	1412	S 09.27702° E 33.81220°	07/2014
	30	1493	S 09.26383° E 33.79052°	07/2014
	31	1600	S 09.25233° E 33.77098°	07/2014
	32	1699	S 09.12733° E 33.82943°	07/2014
	33	1700	S 09.24097° E 33.76847°	07/2014
	34	1913	S 09.11998° E 33.84292°	07/2014
	35	1960	S 09.11813° E 33.84347°	07/2014
	36	2008	S 09.02525° E 33.56698°	07/2014
	37	2212	S 09.01672° E 33.56090°	07/2014
	38	2080	S 09.05166° E 33.76778°	07/2014
	39	2021	S 09. 26194° E 33. 64722°	07/2014
	40	1979	S 09. 20083° E 33. 73750°	07/2014
	41	3160	S 0° 0' 26.77" E 37° 25' 27.87"	2013
	42	3119	S 0° 2' 26.59" E 37° 27' 43.91"	2013

Surface soil	43	3119	S 0° 2' 24.91" E 37° 27' 28.39"	2013
along	44	3119	S 0° 2' 24.91" E 37° 27' 28.39"	2013
Mt.	45	3268	S 0° 2' 6.79" E 37° 26' 6.81"	2013
Kenya	46	3047	N 0° 1' 8.29" E 37° 25' 13.19"	2013
	47	2924	N 0° 2' 43.19" E 37° 26' 1.14"	2013
	48	2846	N 0° 2' 59.48"E 37° 26' 46.61"	2013
	49	2705	N 0° 3' 28.17" E 37° 27' 35.25"	2013
	50	2642	N 0° 3' 35.15" E 37° 28' 2.59"	2013
	51	2500	N 0° 4' 55.13" E 37° 28' 52.35"	2013
	52	2323	N 0° 7' 15.32" E 37° 26' 48.95"	2013
	53	2189	N 0° 7' 48.96" E 37° 27' 39.11"	2013
	54	2097	N 0° 8' 11.54" E 37° 28' 6.78"	2013
	55	2052	N 0° 8' 26.50" E 37° 28' 44.63"	2013
	56	1897	N 0° 2' 10.29" E 37° 36' 5.43"	2013
	57	2027	N 0° 2' 9.60" E 37° 34' 36.59"	2013
	58	2130	N 0° 2' 29.77" E 37° 33' 44.23"	2013
	59	2258	N 0° 2' 5.45" E 37° 32' 45.06"	2013
	60	2318	N 0° 2' 28.85" E 37° 32' 33.91"	2013
Lake	Soil 1	840 m.a.s.l.	S 9°20.0’ E 33°45.3	07/2014
Masoko	Soil 2			07/2014
	Soil 3			07/2014
	Soil 4			07/2014
	Sed. 1		Edge	07/2014
	Sed. 2		Edge	07/2014
	Sed. 3		Edge	07/2014
	Sed 4		Edge	07/2014
	Sed. 5		Bottom	12/2013
	Sed. 6		Bottom	07/2014
	POM	5m		12/2012
	POM	18 m		12/2012
	POM	33 m		12/2012
	POM	5m		04/2013
	POM	18 m		04/2013
	POM	33 m		04/2013
	POM	18 m		12/2013
	POM	33 m		12/2013
	core	2.70 m		2007
Kyambangunguru	Soil 1	660 m.a.s.l.	S 9°22’ E 33°47’	04/2012
marsh	Soil 2			04/2012
	Soil 3			04/2012
	Soil 4			04/2013
	Soil 5			04/2013
	Core	4 m long		12/2012

B. Vegetation samples collected in 07/2014

Location	Altitude (m)	Coordinates	*Persea Americana*	*Arundinaria tesselata*
Mt. Rungwe slopes	873	S 09.33243° E 33.79362°	x	x
	1013	S 09.31867° E 33.79822°	x	x
	1164	S 09.30667° E 33.80592°	x	x
	1412	S 09.27702° E 33.81220°	x	x
	1493	S 09.26383° E 33.79052°	x	x
	1600	S 09.25233° E 33.77098°	x	x
	1700	S 09.24097° E 33.76847°	x	
	700	S 09.34422° E 33.78682°	x	x
	911	S 09.33178° E 33.75133°	x	x
	1699	S 09.12733° E 33.82943°	x	
	1913	S 09.11998° E 33.84292°	x	x
	2008	S 09.02525° E 33.56698°	x	x
	2212	S 09.01672° E 33.56090°	x	x
	2021	S 09. 26194° E 33. 64722°	x	
	537	S 09.41600° E 33.85702°	x	
	565	S 09.41337° E 33.82782°	x	
	690	S 9°22′ E 33°47′		x
	1913	S 09.11998° E 33.84292°		x
	1960	S 09.11813° E 33.84347°		x
	1979	S 09. 20083° E 33. 73750°		x

Location	taxon	slope vs. marsh
Kyambangunguru marsh	*Brachystegia*	slope
	Melia Exelsa	slope
	Persea Americana	slope
	Syzigium	slope
	Rubiaceae	slope
	Fern	slope
	Uapaca	slope
	Nymphea	marsh
	Reed	marsh
	Cyperus	marsh

Appendix 2: Section 4.1 supplementary table

Relative abundances of the different branched and isoprenoid GDGTs in all the soil samples collected along Mt. Rungwe in 2012. (n.d., not detected.)

ample	Altitude (m)	Isoprenoid GDGTs (%)							Branched GDGTs (%)								
		I	II	III	IV	V	VI	VI'	VIIa	VIIb	VIIc	VIIIa	VIIIb	VIIIc	IXa	IXb	IXc
1	520	25.5	n.d.	7.0	6.6	n.d.	53.3	7.6	3.1	n.d.	n.d.	19.7	8.7	n.d.	30.2	32.8	5.6
2	520	20.6	n.d.	11.9	n.d.	n.d.	59.6	7.8	2.0	n.d.	n.d.	18.4	6.0	n.d.	39.3	28.7	5.6
3	529	25.8	n.d.	n.d.	n.d.	n.d.	74.2	n.d.	n.d.	n.d.	n.d.	28.3	0.1	n.d.	21.8	41.1	8.6
4	640	12.2	3.9	12.2	8.6	n.d.	55.5	7.6	2.9	n.d.	n.d.	22.9	11.0	n.d.	38.5	20.1	4.5
5	692	10.5	3.4	8.0	7.1	n.d.	63.7	7.3	2.4	n.d.	n.d.	18.3	10.3	n.d.	35.3	26.8	7
6	826	62.4	3.1	5.6	n.d.	n.d.	25.1	3.8	5.4	n.d.	n.d.	25.6	7.6	n.d.	42.6	16.1	2.7
7	869	10.5	39.6	22.9	n.d.	n.d.	27.0	n.d.	2.1	n.d.	n.d.	20.9	7.8	n.d.	50.0	15.9	3.5
8	869	7.2	10.2	16.1	17.3	n.d.	45.2	4.0	n.d.	n.d.	n.d.	15.2	5.9	n.d.	64.5	10.8	3.7
9	994	4.3	5.7	10.4	13.8	n.d.	55.8	10.0	3.2	n.d.	n.d.	24.2	5.8	0.7	37.8	23.5	4.8
10	1092	3.0	13.9	20.3	9.4	n.d.	50.6	2.9	2.1	n.d.	n.d.	26.4	5.7	n.d.	49.6	14.0	2.3
11	1211	21.1	n.d.	n.d.	n.d.	n.d.	79	n.d.	1.4	n.d.	n.d.	22.1	1.1	n.d.	59.0	14.1	2.4
12	1374	11.0	23.4	24.8	12	n.d.	25.6	3.2	0.8	n.d.	n.d.	13.5	2.1	1.9	65.7	11.1	4.9
13	1550	12.3	9.6	17.8	5.1	n.d.	52.7	2.5	3.1	n.d.	n.d.	27.9	3.6	n.d.	58.8	4.8	1.9
14	1680	24.2	8.2	9.7	6.7	n.d.	51.2	3.8	2.4	n.d.	n.d.	33.7	5.7	1.0	38.8	15.6	2.8
15	1702	6.3	11.9	14.9	8.9	n.d.	52.7	5.3	3.1	n.d.	n.d.	28.0	3.5	n.d.	51.4	13.0	1.0
16	1846	5.2	19.2	18.8	7.9	n.d.	46.0	3.0	4.6	n.d.	n.d.	30.5	6.2	0.9	40.3	12.8	4.8
17	2020	3.7	12.3	14.6	10.8	8.2	45.2	5.1	6.0	1.6	n.d.	33.0	8.3	2.8	33.7	9.8	4.9
18	2055	2.3	9.4	14.3	11.6	5.3	49.9	7.2	0.8	0.1	n.d.	36.3	14.9	3.8	25.0	13.1	4.0
19	2080	14.3	20.1	13.7	13.3	n.d.	37.1	1.6	3.7	n.d.	n.d.	31.4	4.2	n.d.	50.3	7.5	2.9
20	2200	4.9	10.3	9.0	5.1	n.d.	62.9	7.8	4.9	n.d.	n.d.	32.5	4.9	n.d.	50.3	5.6	1.9
21	2800	21.5	52.8	25.7	n.d.	n.d.	n.d.	n.d.	4.5	n.d.	n.d.	32.4	5.1	n.d.	48.7	6.5	2.9

Appendix 3: Section 4.2 supplementary table

Relative abundances of the different branched GDGTs in all the soil samples collected along Mt. Rungwe in 2014. (n.d., not detected.)

sample	altitude (m.a.s.l.)	concentration (ng/g soil)	br GDGTs (%)								
			VIIa	VIIb	VIIc	VIIIa	VIIIb	VIIIc	IXa	IXb	IXc
22	537	1604.8	1.5	0.2	0.1	16.4	4.0	0.5	55.5	17.3	4.6
23	565	1303.6	0.9	0.1	0.1	15.0	1.0	0.1	76.5	5.4	0.9
24	700	4004.7	2.4	0.6	0.1	15.9	9.3	0.7	36.8	28.1	6.2
25	873	905.1	1.4	0.1	0.2	17.9	2.3	n.d.	67.2	9.3	1.6
26	911	593.5	0.8	n.d.	n.d.	13.4	1.2	0.3	76.8	6.7	0.8
27	1013	1083.2	1.3	0.2	0.2	18.3	2.5	0.2	65.4	10.3	1.6
28	1164	1297.0	0.9	n.d.	0.1	15.5	1.0	0.2	76.8	4.7	0.8
29	1412	3129.7	3.7	0.3	0.1	28.2	6.1	0.5	48.6	11.0	1.5
30	1493	967.6	2.1	0.3	0.3	24.5	2.9	0.5	61.4	6.6	1.3
31	1600	1886.2	2.6	0.2	0.1	27.4	3.6	0.3	56.0	8.2	1.6
32	1699	555.0	2.5	0.1	0.1	26.0	2.6	0.2	60.1	6.9	1.5
33	1700	1125.9	2.9	0.2	0.3	28.9	3.8	0.8	54.6	7.0	1.6
34	1913	6821.3	7.1	0.7	0.1	34.9	11.3	1.3	26.7	13.7	4.2
35	1960	8165.9	6.7	0.6	0.1	34.3	9.7	0.9	31.3	12.9	3.6
36	2008	4440.8	6.6	0.6	0.1	35.6	10.8	0.8	30.7	12.1	2.7
37	2212	3675.4	3.4	0.1	n.d.	30.2	2.0	0.2	60.5	2.8	0.7

Appendix 4: Section 5.1. supplementary table

Relative abundances of the different branched and isoprenoid GDGTs and GDDs (br GDD, iso GDD) along the Kyambangunguru peat core (n.d.. not detected).

	CLs							
	Relative br GDGT abundance (%)			*Total br GDGT concentration (µg/g C_{org})*	*Relative br GDD abundance (%)*			*Total br GDD concentration (µg/g C_{org})*
Depth (cm)	f(IXa)	f(VIIIa)	f(VIIa)		f(IXa)	f(VIIIa)	f(VIIa)	
1.5	80.6	17.9	1.5	274.1	72.2	25.9	2.0	6.1
15	78.0	22.0	n.d.	232.0	70.0	30.0	n.d.	12.6
30	73.1	24.2	2.7	207.2	63.2	33.3	3.5	7.1
45	85.3	13.5	1.2	234.0	78.2	20.1	1.7	7.7
60	89.5	9.9	0.6	251.9	86.7	12.5	0.7	7.1
74	88.7	10.7	0.6	349.9	82.4	16.8	0.8	18.8
105	87.2	12.0	0.8	462.3	80.7	18.0	1.3	22.1
120	88.9	10.6	0.5	372.4	83.4	15.5	1.1	5.5
135	89.2	9.9	0.9	537.4	84.6	14.1	1.3	26.2
150	90.5	9.2	0.3	633.0	85.8	13.1	1.1	12.5
165	89.0	10.1	0.9	261.2	86.0	12.9	1.1	9.7
180	86.3	12.8	0.9	357.3	80.6	17.8	1.6	8.3
210	77.6	20.3	2.1	185.2	71.1	27.0	2.0	5.8
225	77.1	20.7	2.1	296.2	68.8	28.0	3.2	11.0
240	72.8	24.6	2.6	167.6	64.5	32.5	3.0	6.4
255	72.5	24.7	2.8	217.4	62.0	34.5	3.5	10.7
270	75.9	24.1	n.d.	164.4	66.0	33.9	n.d.	6.1
285	72.5	24.8	2.8	176.6	66.1	31.3	2.6	9.6
300	72.2	25.1	2.7	117.0	64.4	32.5	3.1	3.7
315	74.4	23.4	2.2	157.4	64.7	32.4	2.9	8.2
360	79.0	19.3	1.6	189.2	67.5	30.0	2.5	5.4
375	79.1	19.3	1.6	153.0	70.3	27.8	1.8	7.1
390	80.1	18.2	1.7	143.9	71.1	26.9	2.0	5.4
405	77.7	20.4	1.8	61.4	68.3	29.6	2.1	3.40

	CLs											
	Relative iso GDGT abundance (%)					*Total iso GDGT concentration (µg/g C_{org})*	*Relative iso GDD abundance (%)*					*Total iso GDD concentration (µg/g C_{org})*
Depth (cm)	f(VI)	f(IV)	f(III)	f(II)	f(I)		f(VI)	f(IV)	f(III)	f(II)	f(I)	
1.5	n.d.	2.1	8.5	7.3	82.0	41.3	3.2	1.1	10.4	9.5	75.8	1.4
15	1.0	3.6	11.9	9.8	73.7	60.7	9.2	1.3	7.1	9.3	73.2	3.0
30	1.1	3.1	11.4	10.7	73.7	68.1	1.3	0.4	6.2	9.7	82.4	1.6
45	2.2	4.9	12.7	8.5	71.8	59.0	2.7	1.3	9.6	11.4	75.1	1.4
60	1.7	6.8	10.6	8.3	72.6	115.0	2.8	5.4	12.1	8.2	71.5	3.1
74	1.8	7.4	9.0	7.5	74.3	146.5	2.0	6.8	14.7	11.2	65.3	7.8
105	n.d.	6.3	10.2	6.4	77.0	158.5	n.d.	16.5	13.3	33.4	36.9	9.2
120	1.5	8.2	7.0	6.1	77.1	147.8	2.3	23.3	14.4	4.5	55.5	2.7
135	1.5	10.2	10.6	8.2	69.6	194.1	1.8	17.5	23.2	n.d.	57.5	10.3
150	3.3	9.6	6.3	4.6	76.3	235.5	3.3	26.3	18.4	3.7	48.3	6.9
165	3.0	6.0	5.4	3.5	82.1	107.7	2.6	38.3	23.9	1.6	33.6	7.3
180	2.1	6.6	7.8	5.4	78.1	142.1	4.5	20.1	14.7	6.9	53.7	3.8
210	n.d.	4.6	12.8	9.2	73.5	74.6	n.d.	7.8	9.9	9.5	72.8	2.1
225	n.d.	3.3	11.0	9.3	76.3	121.6	n.d.	5.1	9.1	12.5	73.3	3.4
240	n.d.	2.9	10.9	10.7	75.5	77.2	n.d.	4.7	9.5	11.3	74.5	2.0
255	n.d.	3.5	10.6	9.8	76.2	84.2	n.d.	3.6	7.1	11.4	77.9	2.8
270	n.d.	3.0	9.8	9.4	77.8	63.8	n.d.	1.8	6.3	13.0	78.9	1.6
285	n.d.	n.d.	11.5	10.3	78.2	61.4	n.d.	n.d.	6.9	13.6	79.5	1.8
300	n.d.	3.4	11.3	8.7	76.5	49.3	n.d.	2.6	8.9	11.9	76.6	1.0
315	n.d.	n.d.	11.8	9.8	78.3	62.3	n.d.	n.d.	6.2	10.7	83.1	2.0
360	n.d.	2.7	8.2	7.0	82.1	72.3	n.d.	2.3	6.7	9.3	81.7	1.4
375	0.1	n.d.	9.6	8.8	81.4	49.5	n.d.	n.d.	6.9	14.2	78.9	1.4
390	n.d.	2.7	8.1	10.2	79.0	48.0	n.d.	1.3	7.4	12.6	78.7	1.2
405	n.d.	n.d.	n.d.	16.2	83.8	18.3	n.d.	n.d.	n.d.	11.6	88.4	0.5

	IPLs							
	Relative br GDGT abundance (%)			*Total br GDGT concentration (µg/g C_{org})*	*Relative br GDD abundance (%)*			*Total br GDD concentration (µg/g C_{org})*
Depth (cm)	f(IXa)	f(VIIIa)	f(VIIa)		f(IXa)	f(VIIIa)	f(VIIa)	
1.5	76.2	21.7	2.1	36.2	69.2	28.5	2.3	1.3
15	75.3	22.7	2.0	31.3	64.5	33.1	2.4	1.1
30	71.6	25.5	2.8	25.5	58.5	37.6	3.9	0.9
45	81.3	17.3	1.4	26.4	72.1	26.0	2.0	0.8
60	83.0	13.3	3.7	21.2	79.3	17.2	3.5	0.5
74	86.2	13.8	n.d.	36.5	79.1	20.9	n.d.	1.0
105	86.1	12.7	1.2	63.7	79.3	19.1	1.6	1.2
120	86.1	13.4	0.5	54.7	80.4	17.8	1.8	1.2
135	84.6	13.6	1.9	42.8	71.8	19.3	8.9	0.6
150	88.3	11.1	0.6	40.0	84.6	14.2	1.1	0.7
165	89.2	10.1	0.7	38.3	76.1	12.4	11.4	0.7
180	85.6	13.4	1.0	75.5	82.0	16.9	1.1	1.1
210	76.7	20.9	2.4	43.9	66.3	29.6	4.1	1.1
225	75.2	22.2	2.5	30.1	65.8	31.0	3.2	0.6
240	73.5	22.9	3.7	12.0	57.1	38.5	4.3	0.5
255	69.3	26.7	4.0	14.2	57.9	36.7	5.4	0.6
270	65.4	30.9	3.6	23.1	57.8	38.1	4.0	1.3
285	69.6	27.2	3.2	26.7	58.1	38.2	3.7	0.9
300	67.8	28.3	3.9	14.6	57.7	37.6	4.7	0.6
315	68.8	27.9	3.3	11.5	58.6	36.6	4.8	0.4
360	71.0	26.4	2.6	18.4	61.0	36.1	2.9	1.0
375	71.7	25.3	3.0	7.5	59.3	35.4	5.3	0.3
390	73.3	23.3	3.5	8.5	61.0	33.6	5.4	0.7
405	70.8	25.7	3.5	2.7	58.9	41.1	n.d.	0.2

	IPLs											
	Relative iso GDGT abundance (%)					*Total iso GDGT concentration (µg/g C_{org})*	*Relative iso GDD abundances(%)*					*Total iso GDD concentration (µg/g C_{org})*
Depth (cm)	f(VI)	f(IV)	f(III)	f(II)	f(I)		f(VI)	f(IV)	f(III)	f(II)	f(I)	
1.5	0.4	3.5	15.0	11.1	70.0	47.4	0.8	3.3	16.0	14.1	65.8	0.9
15	0.2	3.3	14.1	10.3	72.1	30.9	n.d.	1.1	17.6	11.0	70.3	0.6
30	0.2	2.8	13.5	10.0	73.4	33.8	0.3	0.6	15.9	13.2	70.0	0.6
45	0.4	5.4	15.8	8.7	69.7	26.4	1.4	3.2	18.1	19.9	57.4	0.5
60	6.5	8.4	13.8	9.2	62.1	30.3	0.9	5.9	17.9	14.1	61.2	0.4
74	n.d.	12.2	14.8	8.7	64.3	39.9	n.d.	9.8	17.1	12.4	60.6	0.9
105	n.d.	10.9	12.7	6.9	69.4	39.6	n.d.	6.2	16.6	15.5	61.7	0.6
120	0.4	17.4	10.1	7.0	65.0	46.4	1.0	19.5	13.9	7.8	57.9	0.8
135	n.d.	19.3	14.8	10.5	55.4	45.8	n.d.	15.3	17.7	12.9	54.1	0.7
150	0.1	15.0	11.0	7.5	66.4	20.5	2.8	20.1	14.6	8.0	54.6	0.4
165	0.9	5.6	8.8	7.2	77.5	13.4	3.3	9.5	14.5	6.4	66.3	0.3
180	0.5	7.0	11.6	8.0	72.9	34.1	2.5	5.1	18.2	10.2	64.0	0.4
210	n.d.	4.9	15.3	7.6	72.2	39.6	n.d.	2.3	15.9	13.7	68.1	0.8
225	n.d.	n.d.	15.3	8.6	76.1	31.2	n.d.	n.d.	15.9	11.8	72.3	0.4
240	n.d.	2.6	11.4	8.6	77.4	19.7	n.d.	1.2	12.6	10.9	75.4	0.4
255	n.d.	n.d.	11.6	9.7	78.7	24.5	n.d.	n.d.	9.9	12.5	77.7	0.5
270	n.d.	2.7	10.4	8.5	78.4	35.3	n.d.	2.9	9.8	7.1	80.2	1.0
285	n.d.	n.d.	10.0	8.9	81.1	37.2	n.d.	n.d.	11.6	12.2	76.2	0.8
300	n.d.	2.6	10.7	8.3	78.4	24.9	n.d.	1.4	13.6	11.2	73.8	0.5
315	n.d.	2.4	9.5	7.8	80.2	19.3	n.d.	n.d.	12.5	10.4	77.1	0.4
360	n.d.	2.1	8.5	7.4	82.1	29.7	n.d.	1.3	14.8	11.1	72.8	0.9
375	n.d.	n.d.	10.2	9.1	80.7	15.6	n.d.	n.d.	n.d.	16.4	83.6	0.3
390	n.d.	2.4	8.5	8.8	80.3	23.7	n.d.	2.1	17.4	13.1	67.4	0.7
405	n.d.	n.d.	11.3	10.8	77.8	7.2	n.d.	n.d.	15.9	34.9	49.2	0.2

Appendix 5: Section 5.1. supplementary figures

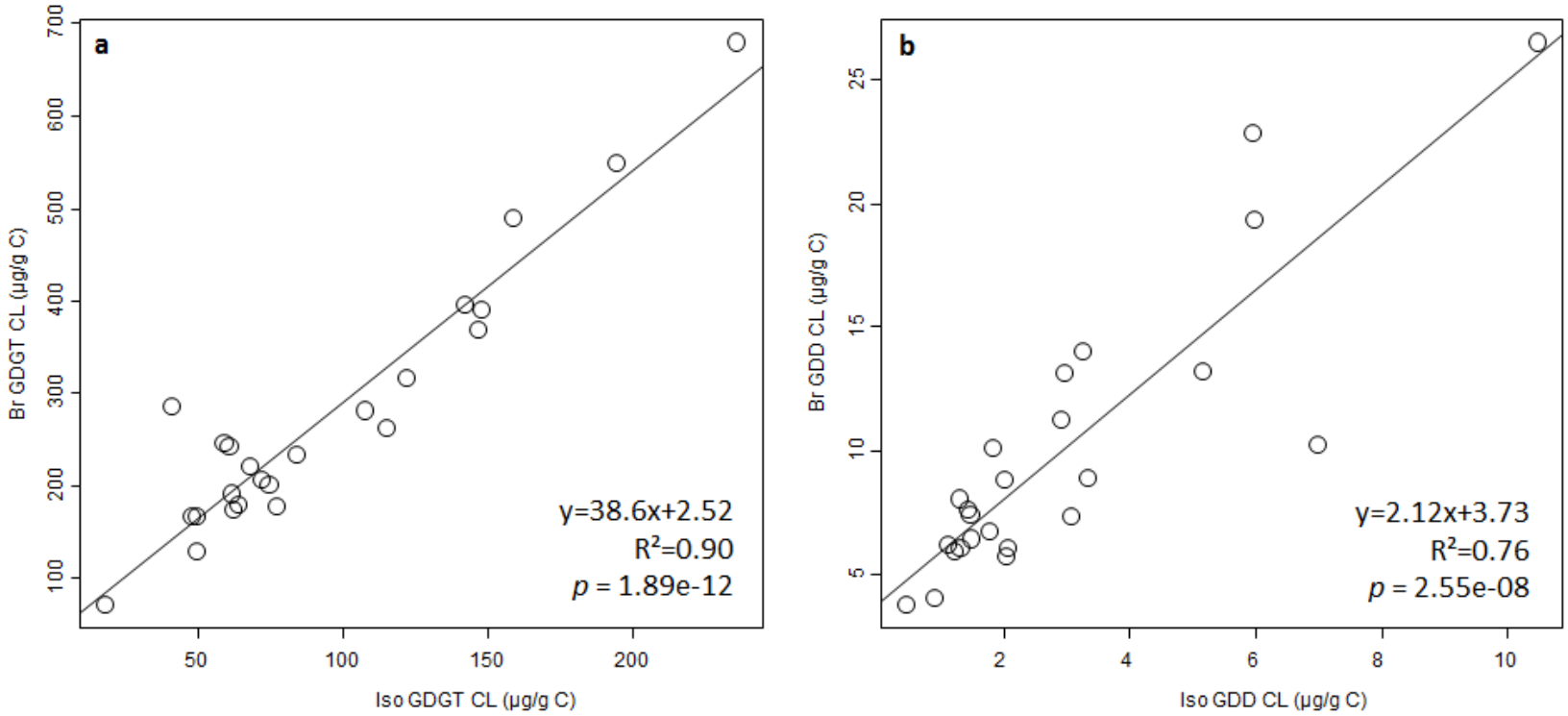

A. Relationship between br and iso GDGT CLs (a) and between br and iso GDD CLs (b).

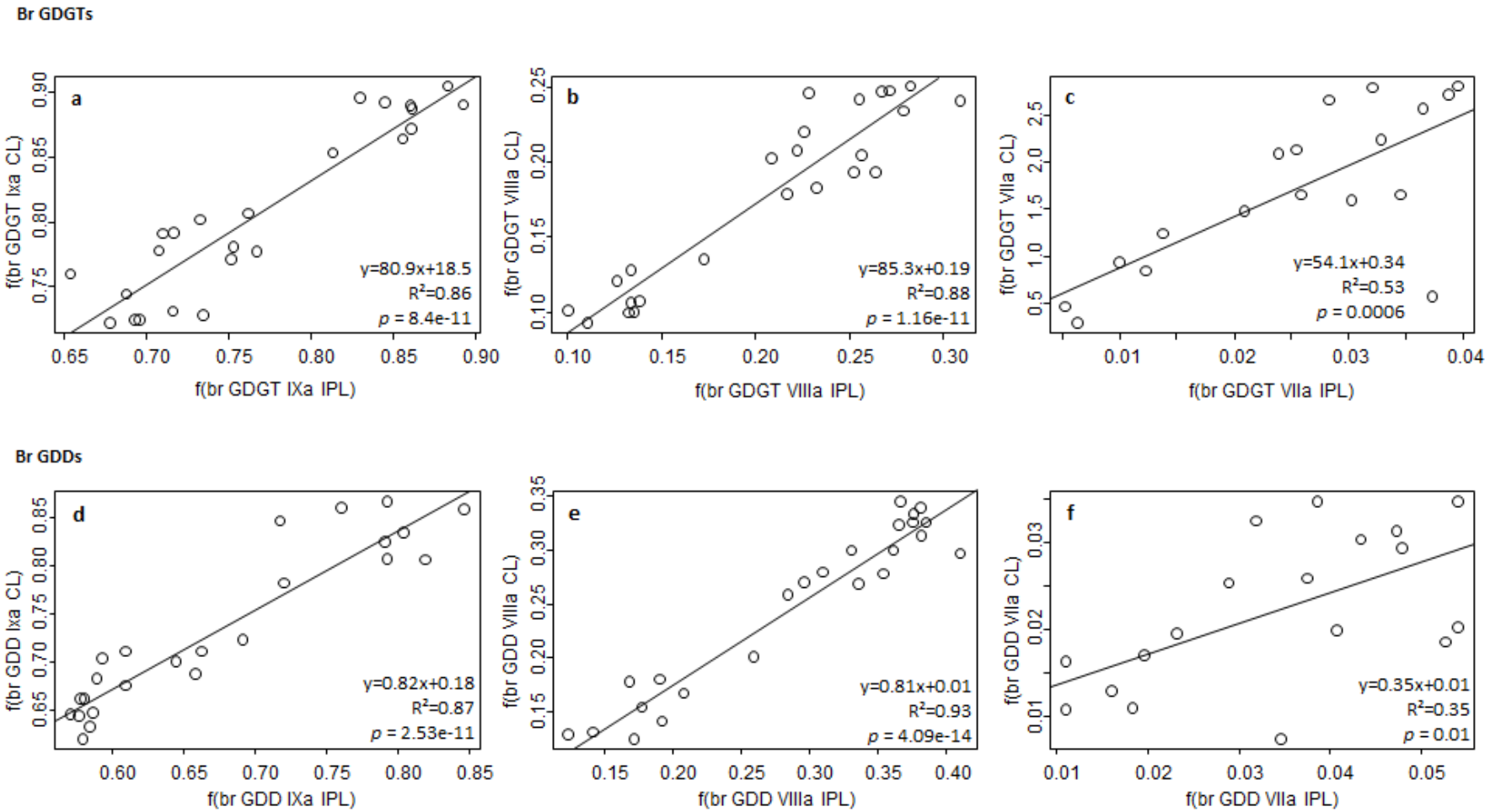

B. Relationship between fractional abundance of compounds IXa, VIIIa and VIIa in the CL and in the IPL pool for GDGTs (a, b, c) and for GDDs (d, e, f).

Appendix 6: Section 5.2. supplementary table

Relative abundances of the different branched GDGTs along the Kyambangunguru peat core (n.d.. not detected).

Depth (cm)	*Relative br GDGT abundance (%)*									Total concentration (µg/g dry wt. peat)
	f(IXa)	f(IXb)	f(IXc)	f(VIIIa)	f(VIIIb)	f(VIIIc)	f(VIIa)	f(VIIb)	f(VIIc)	
1.5	75.5	2.3	0.8	16.6	0.6	0.1	4.0	n.d.	n.d.	127.9
12	73.3	2.6	0.9	18.8	0.6	0.1	3.7	n.d.	n.d.	56.0
15	73.4	2.5	0.8	20.6	0.8	0.1	4.7	n.d.	n.d.	116.6
22	68.0	3.4	0.9	21.6	1.2	0.1	4.5	n.d.	n.d.	61.2
30	66.4	3.3	0.7	22.0	1.6	0.1	5.8	n.d.	n.d.	115.7
37	69.4	2.4	0.6	22.0	n.d.	0.1	4.9	n.d.	n.d.	59.1
45	77.1	3.4	0.9	14.0	n.d.	0.1	4.0	n.d.	n.d.	99.3
57	79.6	2.3	1.2	13.0	n.d.	0.1	3.3	n.d.	n.d.	10.8
60	86.5	1.8	1.5	9.1	n.d.	0.1	3.1	n.d.	n.d.	95.8
73	84.4	2.3	2.0	10.2	n.d.	0.2	2.8	n.d.	n.d.	186.4
90	87.2	1.6	1.9	8.4	n.d.	0.1	2.3	n.d.	n.d.	113.4
105	80.6	2.1	2.7	11.1	n.d.	0.2	2.9	n.d.	n.d.	278.0
120	82.5	1.7	2.4	9.8	n.d.	0.2	3.0	n.d.	n.d.	216.7
135	85.0	1.8	2.4	9.5	n.d.	0.1	2.4	n.d.	n.d.	306.7
150	84.2	2.2	4.1	8.6	n.d.	0.2	2.3	n.d.	n.d.	389.1
165	82.6	2.3	4.3	9.3	n.d.	0.2	2.5	n.d.	n.d.	164.2
180	78.0	3.1	5.7	11.5	n.d.	0.3	2.9	n.d.	n.d.	223.1
196	72.4	3.4	4.6	13.8	0.6	0.3	4.9	n.d.	n.d.	170.3
201	68.8	3.3	3.3	18.5	0.8	0.3	4.9	n.d.	n.d.	75.3
210	71.6	3.7	2.8	18.7	1.0	0.3	5.7	n.d.	n.d.	114.7

225	72.2	3.4	1.6	19.4	1.2	0.2	5.5	n.d.	n.d.	179.4
240	65.2	3.3	0.9	22.0	1.2	0.2	7.2	n.d.	n.d.	103.7
255	67.4	4.2	1.0	23.0	1.5	0.2	6.7	n.d.	n.d.	80.1
270	68.0	4.8	1.0	21.5	1.9	0.2	7.2	n.d.	n.d.	100.2
285	66.8	4.8	0.9	22.8	1.9	0.1	6.8	n.d.	n.d.	104.7
300	65.4	5.8	1.1	22.7	2.2	0.2	6.9	n.d.	n.d.	70.4
315	67.0	5.8	1.2	21.1	2.5	0.2	6.3	n.d.	n.d.	92.0
330	65.7	5.1	0.9	23.3	2.4	0.2	6.3	n.d.	n.d.	109.4
337	59.8	5.7	1.0	25.0	2.6	0.2	5.5	n.d.	n.d.	47.7
345	71.4	4.8	0.6	19.2	2.1	0.1	5.1	n.d.	n.d.	104.0
360	72.3	5.3	0.8	17.7	2.2	0.1	5.0	n.d.	n.d.	108.7
375	72.4	5.2	0.9	17.7	2.1	0.2	4.5	n.d.	n.d.	83.1
390	68.9	9.5	1.8	15.7	2.5	0.2	5.1	n.d.	n.d.	72.1
405	67.4	8.2	2.0	17.7	2.9	0.3	5.1	n.d.	n.d.	7.1
417	49.8	13.7	4.8	20.9	7.1	0.4	7.4	n.d.	n.d.	8.9

Appendix 7: Section 5.2. supplementary figure

***n*-Alkane distribution and δ^2H_{wax} in leaf samples collected in and around Kyambangunguru marsh**

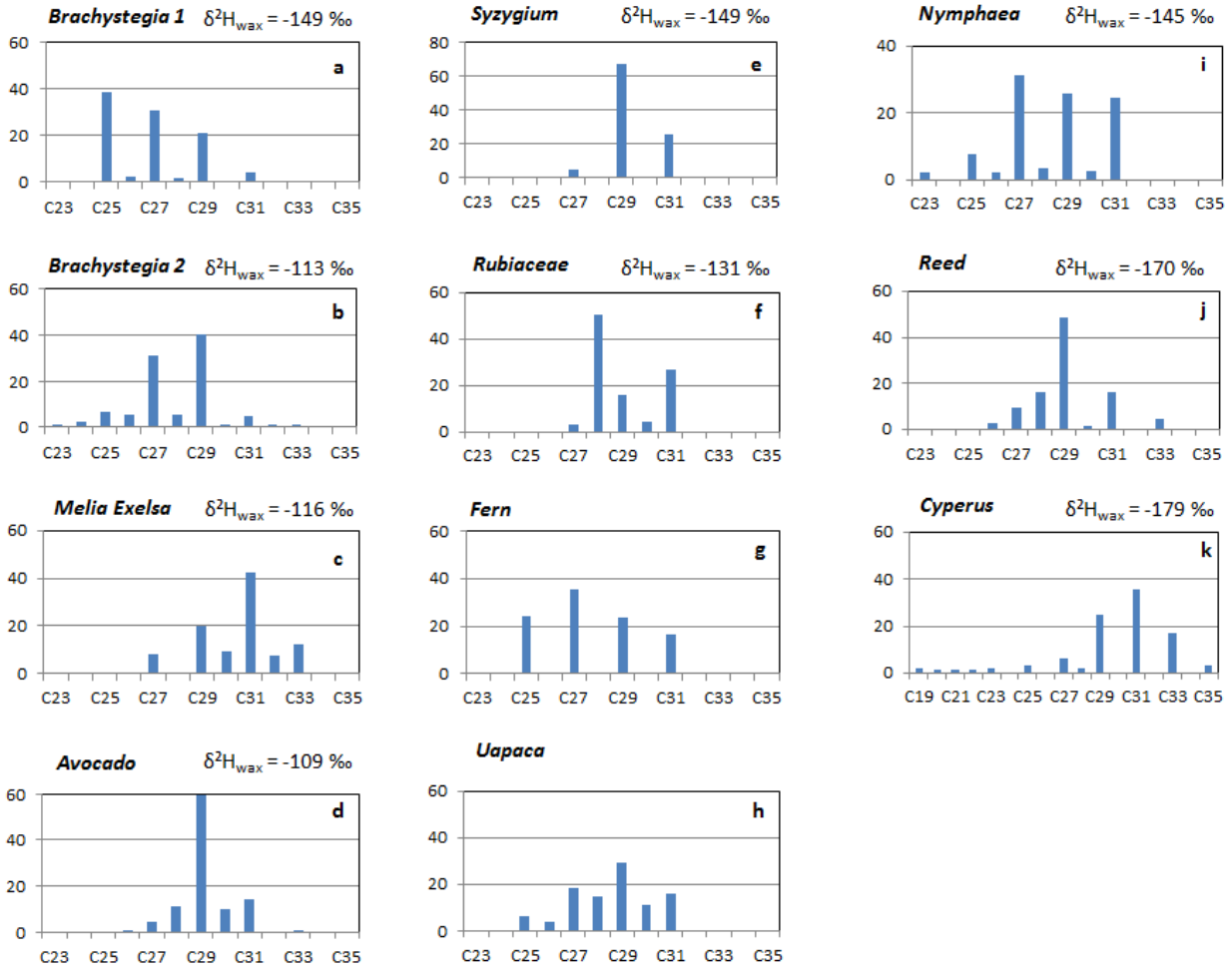

Appendix 8: Section 6.2. supplementary table

Relative abundances of the different isoprenoid and branched GDGTs along Lake Masoko sediment core (n.d.. not detected).

Profondeur	Relative abundance iso GDGTs (%)							Concentration
(cm)	I	II	III	IV	V	VI	VI'	(ng/g sed.)
0.5	16.6	7.6	9.2	9.0	2.9	53.1	1.7	21
2.5	16.2	8.4	10.0	9.7	2.9	51.5	1.3	16
6.5	15.5	8.3	10.3	9.7	2.2	52.4	1.7	20
10.5	17.2	8.9	11.3	10.3	1.5	49.1	1.7	22
12.5	15.1	8.5	11.1	10.3	2.0	51.3	1.7	22
16.5	17.0	8.5	10.4	9.4	1.5	51.5	1.7	24
20.5	16.0	8.7	10.7	10.0	1.7	51.3	1.6	31
22.5	14.7	7.9	9.9	9.5	1.5	54.6	1.9	22
26.5	18.0	7.9	10.0	8.5	1.3	52.9	1.5	33
30.5	27.9	6.3	8.2	7.7	2.4	45.8	1.7	25
32.5	23.4	6.4	8.4	8.2	2.1	49.6	1.9	22
36.5	14.5	6.8	9.3	9.2	1.5	56.7	2.1	30
40.5	21.4	7.3	9.9	8.4	1.5	49.8	1.7	33
46.5	17.1	7.9	10.4	9.7	1.8	51.2	1.8	32
50.5	23.4	7.0	9.5	8.8	1.3	48.2	1.8	25
56.5	18.7	7.5	9.7	8.7	2.4	51.1	1.8	19
60.5	18.3	6.9	9.7	8.9	1.5	52.8	1.9	42
66.5	16.0	7.3	9.7	9.0	2.3	53.7	2.1	30
70.5	24.9	7.1	9.6	8.9	1.7	46.2	1.8	33
76.5	35.2	6.1	8.3	6.6	1.7	40.8	1.4	26
80.5	35.8	9.8	10.1	5.0	1.7	36.1	1.5	2
126.5	24.1	8.0	10.5	7.6	1.9	46.4	1.5	32
129.5	20.4	7.5	9.3	8.4	3.5	49.0	1.8	45
136	20.7	8.8	10.9	8.8	1.8	47.2	1.6	40
140	27.3	10.7	11.5	6.4	2.8	40.0	1.3	6
146	31.2	9.9	9.8	6.7	3.3	38.1	1.1	11
150	33.5	7.6	9.0	7.4	1.3	39.9	1.3	51
156	65.3	5.9	5.5	3.8	1.0	18.1	0.5	50
160	52.8	8.4	8.4	5.5	0.7	23.5	0.7	26
166	52.1	7.6	7.2	5.4	0.8	26.3	0.7	26
170	46.9	8.3	8.6	6.9	0.8	27.9	0.7	36
176	44.1	7.4	8.1	7.3	2.0	30.2	0.9	39
180	39.3	9.3	9.3	6.3	2.2	32.7	0.8	24
186	39.8	8.7	9.3	7.2	1.6	32.5	0.8	32
190	37.6	8.0	9.2	7.3	1.7	35.1	1.1	30
196	47.9	7.9	8.7	6.8	1.9	26.0	0.6	24
200	41.2	7.3	8.6	7.9	2.3	31.7	0.9	27
206	53.3	7.0	6.9	5.2	1.0	25.8	0.9	46
210	46.1	7.2	8.1	6.3	1.4	30.0	0.9	80
216	70.0	4.2	4.4	3.0	0.7	17.2	0.5	195

220	57.9	5.2	6.1	4.3	1.1	24.8	0.7	98
226	42.6	8.2	8.5	5.7	2.0	31.8	1.2	41
230	46.8	10.0	9.5	5.7	0.7	26.3	0.8	16
236	43.3	6.5	8.1	6.8	0.9	33.3	1.1	86
240	35.6	7.4	8.9	7.4	1.2	38.4	1.2	64
246	41.9	11.7	11.6	5.7	0.9	27.5	0.6	15
250	38.9	11.2	10.2	6.2	1.0	31.4	1.0	18
256	40.1	10.4	10.1	6.4	1.2	30.8	0.9	19
260	42.4	6.9	8.1	6.2	1.4	34.2	0.9	51
266	47.2	7.0	7.9	5.5	1.4	30.1	0.9	99

Profondeur	Relative abundance br GDGTs (%)									Concentration
(cm)	VIIa	VIIb	VIIc	VIIIa	VIIIb	VIIIc	IXa	IXb	IXc	(ng/g sed.)
0.5	11.0	1.0	0.1	28.5	6.9	0.8	40.6	11.2	0.0	114
2.5	10.5	0.9	0.1	28.5	7.0	0.9	41.2	10.8	0.0	82
6.5	10.5	0.8	0.1	29.7	6.7	0.9	40.5	10.8	0.0	87
10.5	10.8	1.1	0.1	30.1	6.4	0.9	40.1	10.3	0.0	88
12.5	10.7	1.2	0.1	29.7	6.5	0.9	40.5	10.4	0.0	78
16.5	10.0	1.0	0.2	29.1	6.9	0.9	41.2	10.7	0.0	85
20.5	10.2	1.1	0.1	28.4	6.7	0.9	42.1	10.4	0.0	97
22.5	10.4	1.0	0.1	29.2	6.7	0.8	41.4	10.4	0.0	78
26.5	9.9	1.2	0.1	30.4	6.2	0.8	42.0	9.4	0.0	88
30.5	9.2	0.8	0.1	31.3	6.3	0.7	42.3	9.2	0.0	73
32.5	9.7	1.2	0.1	29.4	7.1	0.7	42.2	9.6	0.0	53
36.5	9.7	0.9	0.1	29.0	6.8	0.9	42.8	9.8	0.0	58
40.5	9.8	1.1	0.1	29.1	7.4	0.8	41.8	9.9	0.0	75
46.5	9.9	1.0	0.1	29.4	8.0	0.7	40.4	10.6	0.0	80
50.5	9.6	0.9	0.1	30.9	7.5	0.7	40.5	9.9	0.0	76
56.5	8.4	0.7	0.1	28.0	7.9	0.9	42.0	12.0	0.0	67
60.5	10.0	0.9	0.2	29.6	7.5	0.9	41.4	9.5	0.0	96
66.5	9.6	0.9	0.1	29.0	7.5	0.8	41.1	11.0	0.0	75
70.5	8.8	0.7	0.1	31.0	6.9	0.6	41.4	10.4	0.0	168
76.5	8.7	0.9	0.1	27.4	7.1	0.6	44.8	10.3	0.0	99
80.5	7.8	0.6	0.3	24.3	6.7	0.8	46.5	13.0	0.0	7
126.5	9.5	1.0	0.1	27.9	7.4	0.6	43.2	10.2	0.0	140
129.5	9.6	1.0	0.1	28.7	7.6	0.7	42.3	10.0	0.0	136
136	10.2	1.0	0.1	28.4	8.0	0.7	41.8	9.9	0.0	82
140	8.1	0.5	0.1	25.5	6.7	0.8	46.5	11.8	0.0	32
146	8.2	0.8	0.1	25.7	7.2	0.7	45.8	11.4	0.0	61
150	9.5	1.0	0.1	28.1	6.9	0.6	44.3	9.5	0.0	200
156	9.7	1.0	0.1	27.9	6.7	0.8	42.7	11.1	0.0	224
160	9.0	0.8	0.1	28.3	6.8	0.8	42.7	11.5	0.0	140
166	9.2	0.8	0.1	28.0	6.4	0.9	43.2	11.5	0.0	128

170	8.8	0.7	0.1	26.0	5.4	0.7	47.3	11.0	0.0	232
176	8.3	0.9	0.1	26.8	6.4	0.7	45.9	11.0	0.0	200
180	8.2	0.7	0.1	25.8	6.5	0.7	46.4	11.4	0.0	126
186	8.1	0.8	0.1	26.3	6.7	0.8	45.5	11.8	0.0	212
190	8.4	0.7	0.1	25.8	6.0	0.7	47.9	10.5	0.0	116
196	7.8	0.7	0.1	25.5	6.4	0.8	47.7	11.0	0.0	176
200	8.0	0.6	0.1	25.8	5.7	0.8	48.6	10.5	0.0	167
206	7.7	0.7	0.1	25.2	6.2	0.7	48.1	11.3	0.0	198
210	8.1	0.9	0.1	26.2	6.3	0.6	47.0	10.7	0.0	283
216	7.9	0.7	0.1	26.6	6.4	0.7	46.1	11.5	0.0	358
220	8.0	0.7	0.1	25.6	6.3	0.7	47.0	11.6	0.0	206
226	8.0	0.6	0.1	25.2	5.4	0.6	49.7	10.4	0.0	77
230	7.1	0.6	0.1	24.5	6.1	0.7	49.4	11.5	0.0	49
236	8.0	0.6	0.1	26.3	6.2	0.8	47.6	10.4	0.0	207
240	7.6	0.7	0.1	25.6	6.5	0.8	47.2	11.6	0.0	199
246	6.7	0.4	0.1	23.8	4.9	0.5	54.1	9.5	0.0	64
250	6.8	0.6	0.1	24.0	5.3	0.6	52.7	10.0	0.0	69
256	7.0	0.5	0.1	24.2	5.0	0.6	53.0	9.6	0.0	72
260	7.8	0.7	0.1	26.2	6.5	0.8	47.4	10.5	0.0	132
266	7.8	0.7	0.1	25.7	6.8	1.0	46.9	11.0	0.0	263

Appendix 9: List of publications and communications in relation with the thesis

PUBLICATIONS:

1. Coffinet S., Huguet A., Williamson D., Bergonzini L., Anquetil C., Majule A., Derenne S., (2015). **Occurrence and distribution of glycerol dialkanol diethers and glycerol dialkyl glycerol tetraethers in a peat core from SW Tanzania**, Organic Geochemistry 83-84. pp.170-177.
   Full manuscript can be found at the end of this thesis.
2. Coffinet S., Huguet A., Williamson D., Fosse C., Derenne S., (2014). **Potential of GDGTs as a temperature proxy along an altitudinal transect in Mount Rungwe (Tanzania)**, Organic Geochemistry, p.82-89.
   Full manuscript can be found at the end of this thesis.

COMMUNICATIONS:

Orals

1. **27th International Meeting in Organic Geochemistry (IMOG), 2015**, Prague, Czech Republic, September:
Multi-proxy record of past environmental changes from a tropical peatland (Kyambangunguru, Tanzania), Coffinet S., Huguet A., Pedentchouk P., Anquetil A., Kolaczek P., Williamson D., Bergonzini L., Majule A., Laggoun-Défarge F., Wagner T. and Derenne S..

2. **Tropical Deserts and Lakes through time - Symposium in memory of Françoise Gasse, 2015,** Aix-en-Provence, France, July:
RESON: A 4000 yr ecosystem multi-proxy record from the Kyambangunguru crater marsh (Rungwe volcanic province, Tanzania), Huguet A., Coffinet S., Pedentchouk N., Williamson D., Bergonzini L., Mathé P.-E., Laggoun-Défarge F., Boucher H., Majule A., Masao C., Wagner T. and Derenne S..

3. **European Geoscience Union (EGU) General Assembly 2015,** Vienna, Austria, April-May:
Multi-proxy record of past environmental changes from a tropical peatland (Kyambangunguru, Tanzania), Coffinet S. , Huguet A., Pedentchouk N., Anquetil C., Williamson D., Bergonzini L., Majule A., Laggoun-Défarge F., Derenne S.

4. **24th Earth Sciences Meeting (RST) 2014,** Pau, France, October:
Multi-proxy record of past environmental changes from a tropical peatland (Kyambangunguru, Tanzania), Coffinet S. , Huguet A., Anquetil C., Williamson D., Bergonzini L., Majule A., Derenne S.

5. **1st Scientific Conference of UMR METIS 2014**, Paris, France, September:
Multi-proxy record of past environmental changes from a tropical peatland (Kyambangunguru, Tanzania), Coffinet S. , Huguet A., Anquetil C., Williamson D., Bergonzini L., Majule A., Derenne S.

6. **European Geoscience Union (EGU) General Assembly 2014,** Vienna, Austria, April-May:
Potential of GDGTs as temperature proxies along altitudinal transects in East Africa, Coffinet S., Huguet A., Omuombo C., Williamson D., Fosse C., Anquetil C., Derenne S.

Posters

1. **27th International Meeting in Organic Geochemistry (IMOG), 2015,** Prague, Czech Republic, September:
Potential of GDGTs and δ^2H of soil n-alkanes as paleoaltitude proxies in East Africa, Coffinet S., Huguet A., Pedentchouk N., Omuombo T., Williamson D., Bergonzini L., Majule A., Wagner T. and Derenne S..

Occurrence and distribution of glycerol dialkanol diethers and glycerol dialkyl glycerol tetraethers in a peat core from SW Tanzania. Coffinet S., Huguet A., Williamson D., Bergonzini L., Anquetil C., Derenne S.

2. **European Geoscience Union (EGU) General Assembly 2015,** Vienna, Austria, April-May:
$^2H/^1H$ composition of SOIL n-alkanes along two altitudinal transects in East Africa, Coffinet S., Huguet A., Pedentchouk N., Omuombo C., Williamson D., Bergonzini L., Wagner T. and Derenne S.

3. **24th Earth Sciences Meeting (RST) 2014,** Pau, France, October:
Potential of GDGTs as temperature proxies along altitudinal transects in East Africa, Coffinet S., Huguet A., Omuombo A., Williamson D., Fosse C., Anquetil C. and Derenne S.

4. **1st Scientific Conference of UMR METIS 2014**, Paris, France, September:
Potential of GDGTs as temperature proxies along altitudinal transects in East Africa, Coffinet S., Huguet A., Omuombo A., Williamson D., Fosse C., Anquetil C. and Derenne S.

5. **Goldshmidt conference 2014**, Sacramento, California, USA, 8-13 June:
Potential of GDGTs as temperature proxies along altitudinal transects in East Africa, Coffinet S., Huguet A., Omuombo A., Williamson D., Fosse C., Anquetil C. and Derenne S.

6. **4th Conference of the Eastern Quaternary Research Association 2013,** Nanyuki, Kenya, July:
Exploring the applicability of GDGTs as temperature proxies along an altitudinal transect in Mt. Rungwe, Coffinet S., Huguet A., Williamson D., Fosse C., Majule A., Derenne S.

7. **Workshop GDGT-based proxies**, Texel, the Netherlands, April:
Potential of GDGTs as temperature proxies along an altitudinal transect in Mt. Rungwe (Tanzania), Coffinet S., Huguet A., Williamson D., Fosse C, Majule A., Derenne S.

8. **26th International Meeting in Organic Geochemistry (IMOG), 2013,** Tenerife, Spain, September:
Exploring the applicability of GDGTs as temperature proxies along an altitudinal transect in Mt. Rungwe, Coffinet S., Huguet A., Williamson D., Fosse C., Majule A., Derenne S.

Appendix 10: Résumé long en français

Université Pierre et Marie Curie

Ecole doctorale des Sciences de l'Environnement d'Ile-de-France

UMR 7619 METIS / Département biogéochimie

Validation et application de biomarqueurs lipidiques pour la reconstruction des changements environnementaux en Afrique de l'Est

Résumé en français de la thèse de doctorat de Sarah Coffinet

Sous la direction de Sylvie Derenne et Arnaud Huguet

Introduction

Comprendre et anticiper la variabilité climatique a toujours été un enjeu central des civilisations. Des calendriers solaires développés pour planifier les périodes de semences à l'émergence d'une institution scientifique internationale, le GIEC (groupe d'experts intergouvernemental sur l'évolution du climat), ayant pour objectif de prévoir et quantifier les dérèglements climatiques à venir, les sociétés humaines ont toujours tenté de rationaliser et prévoir la variabilité climatique, car celle-ci conditionne notre existence sur Terre. Au XX^{e} siècle nous avons collectivement pris conscience que nous ne faisions pas que subir le climat mais que, de par nos activités quotidiennes, nous contribuions aussi à sa variabilité. Une augmentation de la température de la Terre a en effet été observée depuis la moitié du XIX^{e} siècle et les émissions de gaz à effet de serre, notamment le CO_2, dans l'atmosphère en sont la cause principale (Fig. 1). Ces observations font l'objet d'un large consensus scientifique (IPCC, 2013). Connaître les amplitudes climatiques passées et comprendre leurs interactions avec la biosphère et la géosphère sont essentiels pour appréhender les changements climatiques à venir. Ne disposant pas de mesures directes des conditions environnementales antérieures au XIX^{e} siècle, il nous faut réussir à les lire dans les fossiles, témoins des temps géologiques passés.

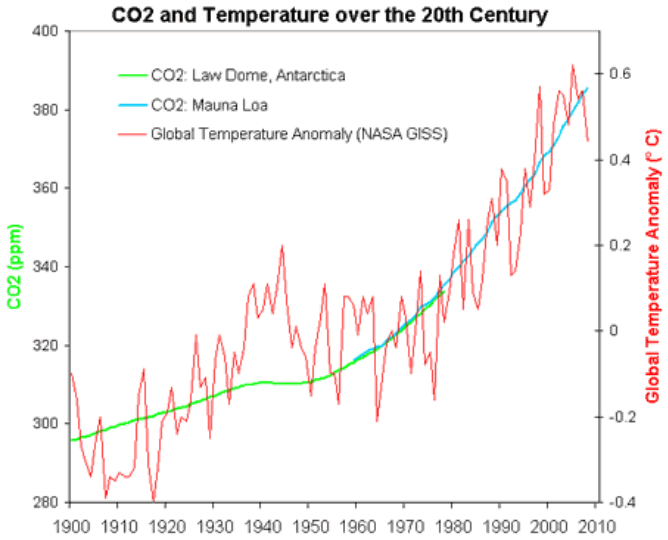

Figure 1 : Evolution des anomalies de températures à l'échelle globale (en rouge) et de la concentration en CO_2 de l'atmosphère d'après (i) l'analyse de carottes de glace extraites à Law Dome, Antarctique Est (en vert), (ii) des mesures effectuées à Mauna Loa, Hawaii (NOAA ; en bleu). *Source : Réseau Action Climat (RAC – France)*

L'objet de cette thèse est de tester l'utilisation de lipides – molécules synthétisées par tous les organismes vivants et dont la stabilité de la structure chimique, composée de chaînes carbonées, assure leur préservation à l'échelle des temps géologiques – comme « enregistreurs », appelés biomarqueurs, des conditions environnementales en Afrique de

l'Est. Nous nous sommes intéressés à deux classes de lipides : les alkyl tetraéthers de glycérol (que nous nommerons tetraéthers dans la suite de ce document) et les *n*-alcanes à moyennes et longues chaînes (C_{23} – C_{31}). Les premiers sont produits par des microorganismes, d'origine archéenne et bactérienne, tandis que les seconds constituent la cire épicuticulaire recouvrant les organes externes des plantes, plus particulièrement leurs feuilles. Ces deux familles de composés ont été détectées dans tous types d'environnements marins et continentaux. Alors que les premières études paléoclimatiques se sont appuyées sur l'étude des carottes glaciaires puis des carottes sédimentaires marines - dont la composition et le mécanisme de formation est simple - l'enjeu est aujourd'hui de développer des reconstitutions du climat continental afin d'améliorer notre compréhension du climat mondial passé mais aussi parce que les surfaces continentales, de par leur hétérogénéité de forme et de matière (forêts, lacs, villes, relief …), perturbent la circulation atmosphérique. Nous nous sommes donc intéressés à l'applicabilité de ces biomarqueurs dans des archives continentales en Afrique de l'Est. L'Afrique de l'Est est située à une position clé pour la compréhension de la circulation atmosphérique. Les tropiques sont parfois surnommés « la machine à chaleur » de la Terre (Verschuren, 2003) parce qu'ils reçoivent le maximum d'énergie solaire du fait de leur position autour de l'équateur tandis que les pôles sont, eux, largement déficitaires (Fig. 2).

a

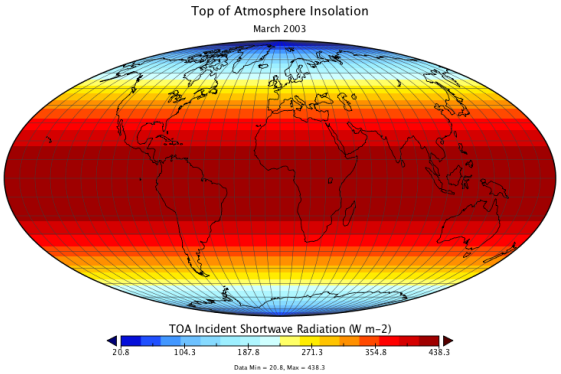

b

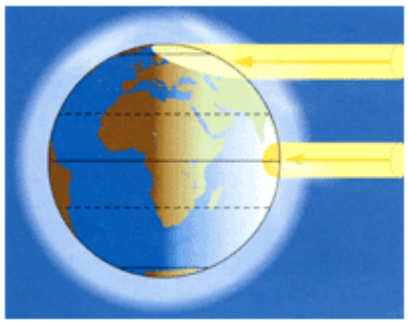

Figure 2 : L'incidence du rayonnement solaire est plus forte à l'équateur qu'aux pôles (a) (échelle 20.8 W/m² en bleu à 438.3 W/m² en rouge) du fait de la courbure terrestre (b). *Source : sites internet du département de géosciences de Penn State (2a) et de l'académie d'Amiens (2b).*

La circulation atmosphérique compense ce déséquilibre en redistribuant cette chaleur vers les pôles via des cellules de convection méridionales (Fig. 3). L'Afrique de l'Est se situe dans la zone de convergence de la cellule de Hadley (Fig. 3) et son climat est contrôlé par le déplacement annuel de l'équateur météorologique, aussi appelé zone de convergence intertropicale (ZCIT). Il s'agit d'une zone de basses pressions où les alizées de chaque hémisphère, saturés en eau, convergent, provoquant de fortes précipitations saisonnières.

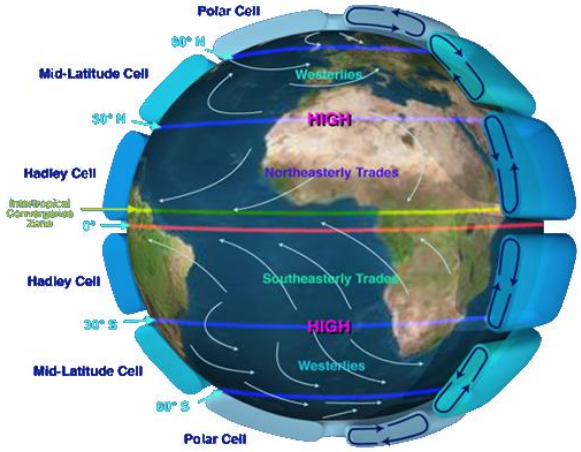

Figure 3 : Position des cellules méridionales de convection, des principaux courants atmosphériques et de l'équateur météorologique (ZCIT), en partie responsables du transport du surplus énergétiques de l'équateur vers les pôles. *Source : site internet du consortium universitaire américain pour la recherche atmosphérique (UCAR)*

Cette thèse présente l'étude de trois types d'archives continentales : sols, marécage tourbeux et lac, tous collectés dans la province volcanique du Rungwe (PVR) au sud-ouest de la Tanzanie, à l'extrémité sud de la branche ouest du rift est-africain (Fig. 4a). Cette région a été choisie car elle donne accès aux trois types d'archives continentales sus-citées dans un espace délimité commun soumis aux mêmes paramètres extérieurs (climat, tectonique, forçage anthropique …). Par ailleurs, cette région a fait l'objet d'importantes recherches depuis plus de dix ans, dans le cadre du RESON (Rungwe Environmental Science Observatory Network), notamment au niveau hydrologique (Bergonzini et al., 2001; Delalande et al., 2005), biogéochimique (de Mesmay, 2008) et géologique (Williamson et al., 2014). Des reconstitutions paléoclimatiques ont aussi déjà été effectuées dans la région, essentiellement à partir d'archives du lac Masoko (Barker et al., 2000; Vincens et al., 2003; Garcin et al., 2006, 2007). Ces données nous ont ainsi permis de contraindre l'impact de facteurs environnementaux autres que climatiques sur les biomarqueurs étudiés.

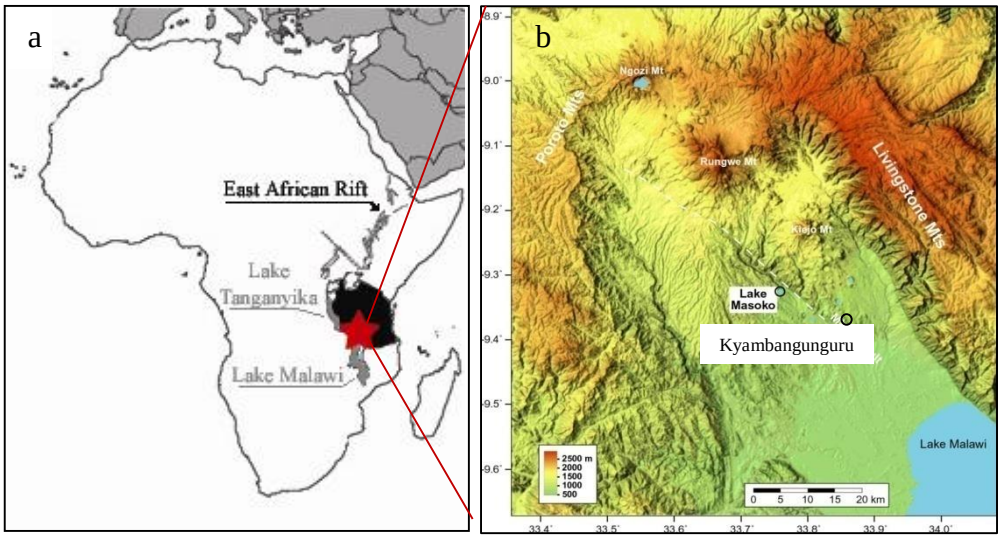

Figure 4 : Localisation de la province volcanique du Rungwe à l'extrémité du Rift est africain (a ; d'après Delalande, 2008) et modèle numérique de terrain (b ; MNT d'après Garcin et al., 2006) présentant le relief de la région et les différents sites étudiés.

Le présent document résume les principaux résultats obtenus pour partie dans le cadre du projet *Etude de lipides complexes (alkyl tetraéthers de glycérol) et de leurs microorganismes sources en milieu lacustre : cas du lac Masoko (Tanzanie)* coordonné par A. Huguet et financé par le programme national de l'INSU (Institut National des Sciences de l'Univers du CNRS) « EC2CO » (2012-2013). Ce projet a servi de base à ma thèse de doctorat intitulée *Validation et application de biomarqueurs lipidiques pour la reconstruction des changements environnementaux en Afrique de l'Est.* Cette thèse a été financée par le ministère de l'Education Nationale (2012-2015) et a également bénéficié d'une bourse de l'association des géochimistes organiciens européens (EAOG) pour financer l'analyse, au Royaume-Uni, du rapport isotopique de l'hydrogène des *n*-alcanes (δ^2H_{wax}) ainsi que d'une bourse de l'association française d'étude des sols (AFES) pour financer la présentation de premiers résultats au 26^e congrès international des géochimistes organiciens (IMOG) à Tenerife (Espagne) en septembre 2013. Après une présentation des biomarqueurs étudiés, nous résumerons les résultats issus (i) de l'étude de sols de surface collectés le long de transects altitudinaux le long du Mt. Rungwe et d'autres sites est africains, (ii) de l'analyse d'une carotte de tourbe prélevée dans le marécage tourbeux de Kyambangunguru (Fig. 4b) et (iii) de l'étude de la colonne d'eau et des sédiments, y compris une carotte sédimentaire, du lac Masoko (Fig. 4b).

Chapitre 1. Les alkyl tetraéthers de glycerol et les *n*-alcanes : biomarqueurs lipidiques

Au cours du XX^{e} siècle, des molécules d'origine biologique ont démontré leur capacité à (i) enregistrer les variations de l'environnement dans lequel elles ont été produites et à (ii) être préservées dans les archives géologiques (sédiments, roches pétrolifères …). Ces molécules sont appelées biomarqueurs. Dans le cadre de cette thèse, nous nous sommes intéressés à deux types de biomarqueurs : les alkyl tetraéthers de glycérol (nommés tetraéthers ci-après) et les *n*-alcanes.

Les tetraéthers sont des lipides membranaires produits par la plupart des communautés archéennes et par certaines bactéries encore non identifiées. Ces molécules présentent une diversité de structures (Fig. 5). Tout d'abord deux grands types peuvent être distingués : les tetraéthers à chaînes alkyles isopréniques, d'origine archéenne (Derosa and Gambacorta, 1988), et les tetraéthers à chaînes alkyles ramifiées, d'origine bactérienne (Weijers et al., 2006). Notons aussi que ces composés sont présents dans le milieu naturel sous deux formes : (i) le lipide intact, tel qu'il compose les membranes des microorganismes vivants, qui possède une tête polaire (sucre ou phosphate) lié à un ou deux glycérol et (ii) le lipide de cœur tel qu'il est représenté dans la figure 5 est qui est la forme majoritairement conservée dans les archives géologiques après la lyse des cellules de microorganismes. Les structures des tetraéthers varient par le nombre de cyclopentanes contenus dans leurs chaînes alkyles et, pour les tetraéthers ramifiés, par le nombre de groupements méthyles. L'analyse de sédiments (Schouten et al., 2002) prélevés dans le monde entier a montré que le nombre de cycles pentane des tetraéthers isopréniques était corrélé à la température de surface des mers. Des calibrations permettant la reconstruction quantitative des températures de surface des mers à partir de la distribution de ces composés dans les sédiments marins ont été établies (Schouten et al., 2002; Kim et al., 2008, 2010) et par la suite étendues à la reconstruction des températures de surface des lacs (Powers et al., 2010, 2005). De même, l'analyse statistique de la distribution des tetraéthers ramifiés dans plus de 130 sols répartis mondialement a démontré que leur nombre de cycles pentanes était corrélé au pH du sol étudié et que leur nombre de groupements méthyles était corrélé à la température moyenne annuelle de l'air (TMAA) et, dans une moindre mesure, au pH (Weijers et al., 2007). Ces corrélations ont été converties en calibration permettant la reconstruction quantitative des TMAA et du pH du sol

à partir de l'analyse des tetraéthers ramifiés. Cette calibration a récemment été étendue à un échantillonnage plus large de sols (plus de 200) par Peterse et al. (2012).

La deuxième famille de biomarqueurs étudiée dans le cadre de ma thèse est les *n*-alcanes, qui sont des lipides simples constitués d'une chaîne carbonée plus ou moins longue et produits par une large gamme d'organismes. Leur analyse dans un grande variété d'échantillons naturels et dans des organismes isolés a permis d'établir la typologie suivante : les *n*-alcanes à courtes chaînes, paires et impaires (< C_{21}), sont essentiellement synthétisés par des cyanobactéries et des organismes aquatiques (micro et macro algues ; Han et al., 1968), les *n*-alcanes à longueur de chaîne moyenne et impaire (C_{21} –C_{25}) sont majoritairement produits par des macrophytes flottants ou immergés (Ficken et al., 2000) tandis que les *n*-alcanes à plus longues chaînes (> C_{25}) sont principalement produits par les végétaux supérieurs terrestres (Eglinton and Hamilton, 1967). L'analyse de l'évolution de la distribution de ces différents *n*-alcanes permet donc de reconstruire les changements de végétation d'un site. Par ailleurs, le rapport isotopique de l'hydrogène de ces *n*-alcanes (δ^2H_{wax}) est corrélé au rapport isotopique de l'hydrogène des précipitations météoriques, qui sont la principale source d'hydrogène des plantes (Sessions et al., 1999; Sauer et al., 2001). L'analyse du δ^2H_{wax} peut donc informer sur les variations hydrologiques passées d'un site.

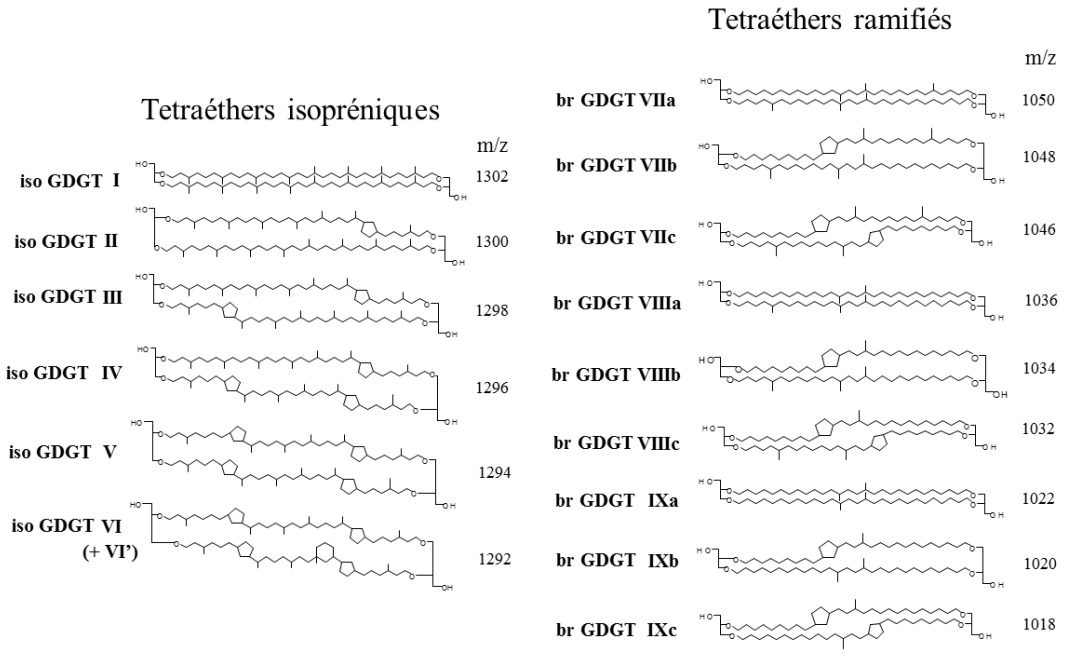

Figure 5 : Structures des principaux tetraéthers isopréniques (à gauche) et ramifiés (à droite) accompagnées de leur rapport m/z équivalent à leur masse molaire.

Chapitre 2. Applicabilité de biomarqueurs de température dans les sols d'après l'étude de transects altitudinaux est-africains.

Ce chapitre présente les résultats d'une étude méthodologique portant sur le potentiel des tetraéthers et du δ^2H_{wax} à enregistrer les changements de TMAA dans les sols et paléosols à partir de l'étude de sols de surface, supposés modernes, le long de transects altitudinaux. Une étude préliminaire de l'effet des changements de température liés à l'altitude sur la distribution des tetraéthers (ramifiés et archéens) a été effectuée le long du Rungwe et a fait l'objet d'une publication dans Organic Geochemistry (Coffinet et al., 2014). Une synthèse des études de transects altitudinaux dans la région a ensuite été effectuée pour les tetraéthers ramifiés et le δ^2H_{wax} et a conduit à l'établissement d'une calibration régionale des tetraéthers ramifiés. Cette étude sera prochainement soumise dans Earth and Planetary Science Letters.

2.1. Potentiel des tetraéthers comme biomarqueurs de température le long d'un transect altitudinal du Mt. Rungwe (Tanzanie) :

L'analyse des tetraéthers ramifiés dans des sols d'altitudes variables a déjà été réalisée le long du Mt. Kilimanjaro (Tanzanie ; Sinninghe Damsté et al., 2008), en Inde (Mt. Meghalaya ; Ernst et al., 2013), en Chine (Mts. Gongga, Peterse et al., 2009b ; Jianfengling, Huan et al., 2012 ; Xiangpi, Liu et al., 2013 ; Shennongjia, Yang et al., 2014c) et en Colombie (Cordillière Est, Anderson et al., 2014). Ces études ont toutes observées une corrélation entre la distribution des tetraéthers ramifiés et l'altitude. Le long du Mt. Rungwe, cette corrélation a aussi été observée (Fig. 6) et les TMAA reconstruites à partir des indices MBT et CBT sont similaires à celles mesurées par des stations météorologiques situées à 540 m, 920 m et 1720 m (Fig. 6). Le gradient de température reconstruit (0,7 °C/100 m) est également identique à celui reconstruit par (Sinninghe Damsté et al., 2008) le long du Mt. Kilimanjaro (nord Tanzanie). Ces résultats confirment que les tetraéthers ramifiés sont un biomarqueur adéquat pour la reconstruction des variations de température de l'air en Afrique de l'Est.

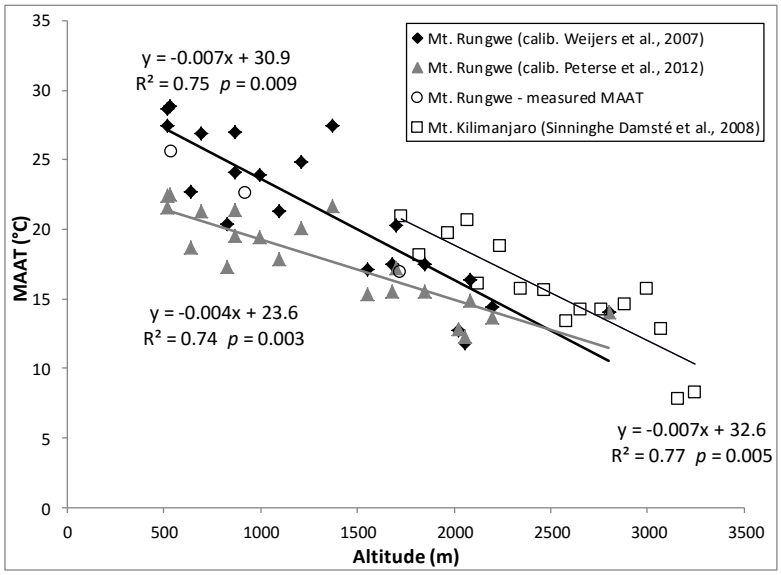

Figure 57 : Corrélation entre l'altitude et la TMAA reconstruite à partir de la distribution des tetraéthers ramifiés (les losanges correspondant à la calibration de Weijers et al. (2007) et les triangles à celle de Peterse et al. (2012)). Pour comparaison les TMAA mesurées par des stations météorologiques sur le site sont représentées par les cercles blancs et le gradient altitudinal reconstruit par Sinninghe Damsté et al. (2008) le long du Mt. Kilimanjaro est représenté par des carrés blancs.

Par ailleurs les tetraéthers isopréniques, majoritairement étudiés dans les archives aquatiques (marines et lacustres), ont été détectés dans tous les échantillons analysés le long du Rungwe avec une forte prédominance du crénarchaeol (GDGT-VI ; Fig. 4) ce qui indique que les Thaumarchées (groupe d'archées biosynthétisant spécifiquement ce composé) sont les principaux producteurs de tetraéthers isopréniques dans ces sols. Le TEX_{86}, indiquant le degré moyen de cyclisation des tetraéthers isopréniques, a ainsi pu être calculé. Une corrélation statistiquement significative a alors été observée entre le TEX_{86} et l'altitude (Fig. 7a). Seuls Liu et al. (2013) avaient déjà observé une corrélation entre le TEX_{86} et l'altitude le long du Mt. Xiangpi (Chine). Comme le TEX_{86} varie essentiellement en fonction des variations de température de l'eau dans les milieux aquatiques, on peut supposer que de la même façon, le long de ces gradients altitudinaux, ce sont les variations de température de l'air avec l'altitude qui sont à l'origine des corrélations observées. Cette hypothèse nécessite cependant d'être validée par des études intégrant un plus grand nombre d'échantillons et de sites répartis dans les différentes régions du globe. Les calibrations marines (Kim et al., 2010) et lacustres (Powers et al., 2010) développées pour reconstruire les températures de surface de l'eau à partir des variations de TEX_{86} ont été utilisées pour reconstruire les températures de l'air le long du Mt. Rungwe. Les températures obtenues sont plus élevées que les températures mesurées sur le site (18 °C et 7 °C respectivement ; Fig. 7b) ce qui indique que le

développement d'une calibration spécifique aux sols est nécessaire pour pouvoir utiliser les tetraéthers isopréniques dans les sols pour reconstruire les variations de TMAA.

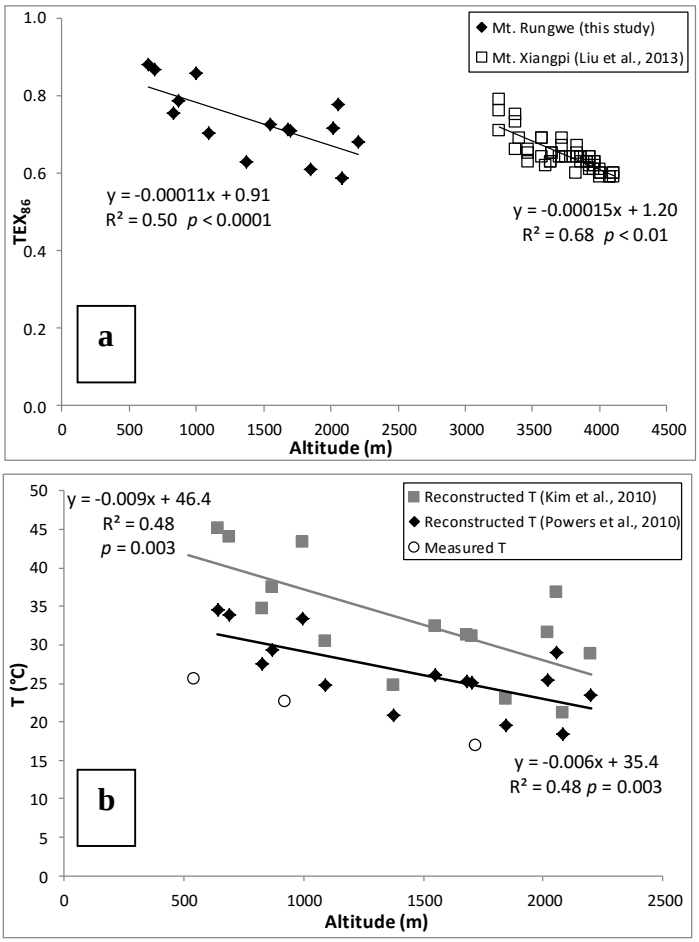

Figure 7 : (a) Variation du TEX_{86} en fonction de l'altitude le long du Mt. Rungwe (losanges) et le long du Mt. Xiangpi (carrés ; Liu et al., 2013) et (b) comparaison des reconstructions de la température de l'air le long du gradient altitudinal du Rungwe à partir de la calibration marine de Kim et al. (2010 ; carrés) et de la calibration lacustre de Powers et al. (2010 ; losanges) avec les TMAA mesurées sur le site par des stations météorologiques fixes (cercles).

2.2. Applicabilité du δ^2H_{wax}et des tetraéthers ramifiés à l'échelle régionale :

Le rapport isotopique de l'hydrogène des *n*-alcanes (δ^2H_{wax}) a été déterminé le long du Mt. Rungwe (40 échantillons de sol de surface) et le long du Mt. Kenya (Kenya ; 20 échantillons de sol de surface). Pour ce dernier, une tendance significative à la diminution du δ^2H_{wax} avec l'altitude a été observée (Fig. 8a), qui confirme que le δ^2H_{wax} enregistre l'appauvrissement en deutérium des précipitations avec l'altitude comme cela a été suggéré par (Jia et al., 2008). Cependant, aucune relation entre l'altitude et le δ^2H_{wax} n'a été observée le long du Mt. Rungwe (Fig. 8b). Peterse et al. (2009) avait analysé le δ^2H_{wax} le long du Mt. Kilimanjaro et n'avait pas non plus observé de relation entre altitude et le δ^2H_{wax}. Les raisons

pour lesquelles une relation est observée le long de certains montagnes mais pas le long d'autres restent peu comprises, notamment parce que de nombreux facteurs, climatiques mais aussi liés à la biosynthèse des *n*-alcanes, peuvent jouer sur le δ^2H_{wax}. Cette étude montre que l'application du δ^2H_{wax} à l'échelle régionale en Afrique de l'Est est compliquée et invite à la prudence avant l'application de ce biomarqueur pour des reconstructions paléoclimatiques dans la région.

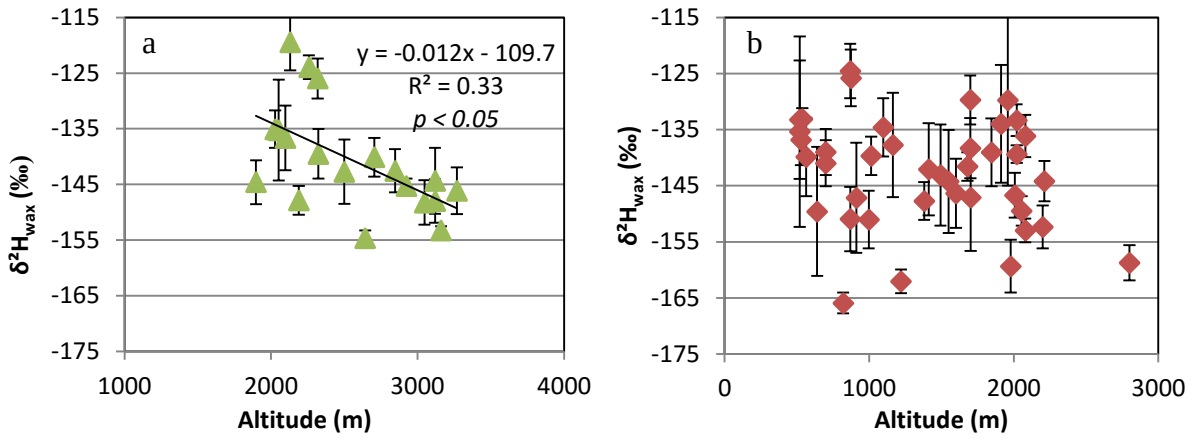

Figure 8 : Variation du δ²Hwax en fonction de l'altitude (a) le long du Mt. Kenya (Kenya) et (b) le long du Mt. Rungwe (Tanzanie). Les barres d'erreur représentent l'erreur analytique pour chaque échantillon.

Les tetraéthers ramifiés ont, quant à eux, montré leur potentiel comme marqueur de température le long de plusieurs montagnes d'Afrique de l'Est (Sinninghe Damsté et al., 2008 ; Coffinet et al., 2014). Nous avons donc combiné les valeurs de MBT' et CBT de ces précédentes études avec celles obtenues après l'analyse des sols de surface supplémentaires, prélevés le long des monts Rungwe et Kenya. Cela nous a permis de déterminer une calibration régionale entre la TMAA et la distribution des tetraéthers ramifiés :

$$TMAA = -8.17 * CBT + 25.39 * MBT' + 9.1$$

Cette calibration régionale est-africaine permet de reconstruire des TMAA plus précise (déterminé par l'erreur quadratique moyenne, RMSE = 2,4 °C) et plus justes (déterminé par le coefficient de détermination de la corrélation entre TMAA mesurées et reconstruites, R^2 = 0,75 ; Fig. 9a) que la calibration globale des sols appliquée aux sols est-africains (RMSE = 5,0 °C, R^2=0,61 ; Fig. 9b, Peterse et al., 2012). L'amélioration observée indique que des paramètres environnementaux régionaux tels que le régime hydrologique ou la physico-chimie des sols impactent aussi la distribution des tetraéthers ramifiés, comme

suggéré dans de précédentes études des tetraéthers ramifiés dans les sols (Dirghangi et al., 2013), et peut être à l'origine de la dispersion observée sur la calibration globale des sols (Peterse et al., 2012). Le développement de calibrations régionales telle que celle développée ici permet donc de s'affranchir du biais lié à l'influence de ces paramètres additionnels. Cette calibration régionale doit maintenant être testée sur des paléosols. Il serait aussi intéressant d'utiliser cette calibration régionale sur des sols d'autres zones tropicales pour déterminer si ces paramètres environnementaux supplémentaires sont communs à toutes les zones tropicales.

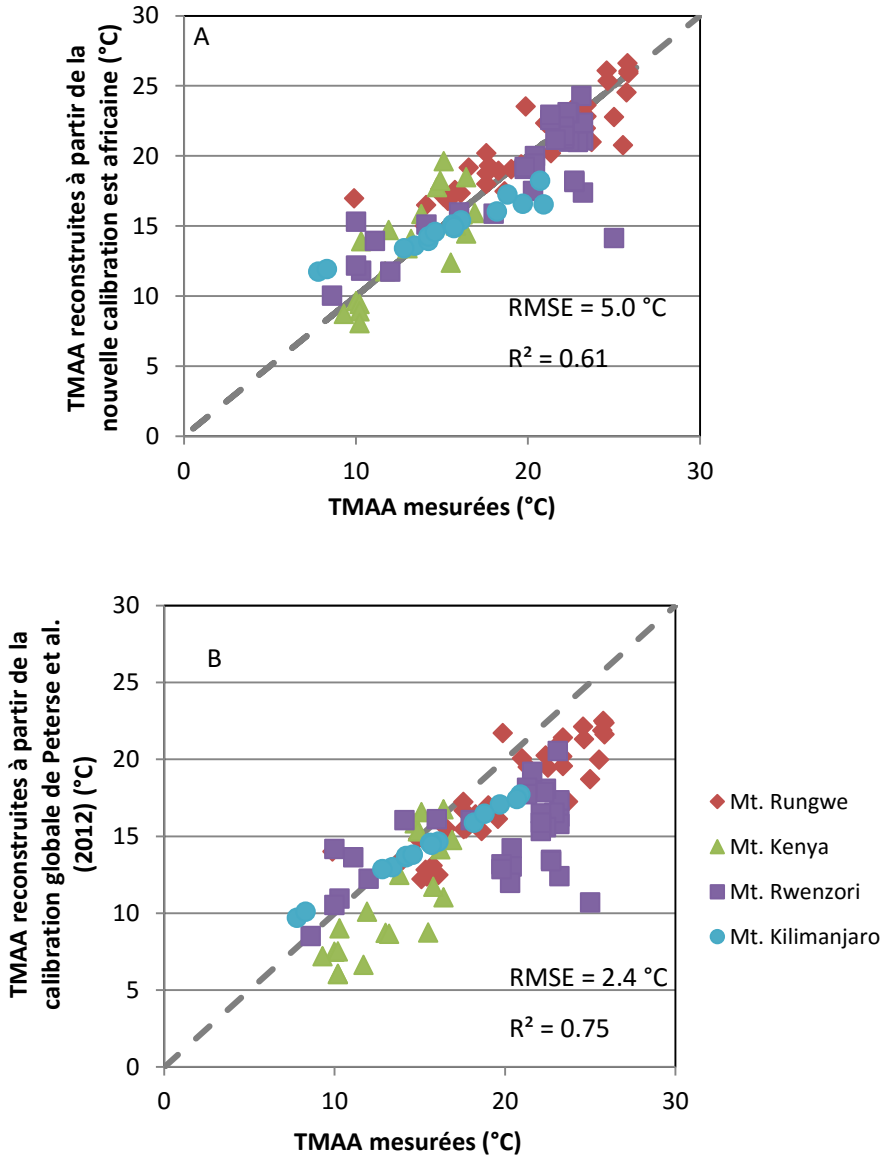

Figure 9 : Comparaison des TMAA mesurées avec les TMAA reconstruites à partir de (a) la calibration est-africaine de cette étude et de (b) la calibration globale de Peterse et al. (2012) le long des 4 monts étudiés (Rungwe, Kenya (cette étude), Rwenzori (Loomis et al., 2011) et Kilimanjaro (Sinninghe Damsté et al., 2008)

Chapitre 3. Le marécage tourbeux de Kyambangunguru : prospection des voies biosynthétiques des tetraéthers et reconstitution multi-proxy des changements environnementaux

Le marécage tourbeux de Kyambangunguru se situe au centre d'un cratère à 660 m d'altitude dans la région du Rungwe (Fig. 4). Les pentes du cratère sont escarpées et recouvertes d'une végétation dense de type Miombo tandis que le marécage tourbeux est colonisée par des macrophytes émergés de la famille des *Cypéracées* et des macrophytes immergés et flottants, notamment du genre *Nymphea*. Le faciès du site varie beaucoup au cours de l'année, d'un marécage tourbeux saturé en eau pendant la saison sèche à un lac peu profond (1,50 m maximum) à la fin de la saison des pluies. Une carotte de 4 m, représentant les 4000 dernières années (d'après des datations au ^{14}C), a été prélevée en décembre 2012 à Kyambangunguru et les résultats de son étude sont résumés dans ce chapitre. Dans un premier temps, nous présenterons une étude méthodologique combinant l'analyse des tetraéthers et de composés analogues, les alkanol diéthers de glycérol, dont l'origine et la fonction sont à ce jour inconnues. Cette étude a fait l'objet d'une publication dans Organic Geochemistry (Coffinet et al., 2015). La deuxième partie de ce chapitre, quant à elle, présente la reconstitution des changements environnementaux à Kyambangunguru depuis 4000 ans, grâce à l'étude couplée de marqueurs microscopiques (macro- et micro-fossiles, palynofaciès), élémentaires (teneur en carbone organique (C_{org}) et en azote total), moléculaires (tetraéthers et *n*-alcanes) et isotopiques (δ^2H_{wax}). Cette étude sera prochainement soumise à Quaternary Science Reviews.

3.1. Détection et distribution des alkanol diéthers de glycérol et des alkyl tetraéthers de glycérol dans une tourbière du sud-ouest de la Tanzanie

Les alkanol diéthers de glycérol (Fig. 10) ont été détectés récemment dans des sédiments, des sols et de la tourbe (Knappy and Keely, 2011; Liu et al., 2012, 2013; Becker et al., 2013; Meador et al., 2014; Yang et al., 2014a). Ils présentent une série de composés isopréniques et une autre de composés ramifiés, et la diversité de leurs chaînes carbonées est analogue à celles des tetraéthers, ce qui laisse penser que les diéthers isopréniques sont d'origine archéenne et les diéthers ramifiés d'origine bactérienne. Des études précédentes ont émis deux hypothèses quant à leur source et fonction : (i) intermédiaires de biosynthèse ou (ii) produits de dégradation des tetraéthers (Liu et al., 2012c; Meador et al., 2014; Yang et al.,

2014c). Nous avons apprécié ces deux hypothèses au regard de l'analyse des deux formes (dérivé du lipide intact et lipide de cœur) de ces diéthers et des tetraéthers dans la carotte de tourbe prélevée à Kyambangunguru.

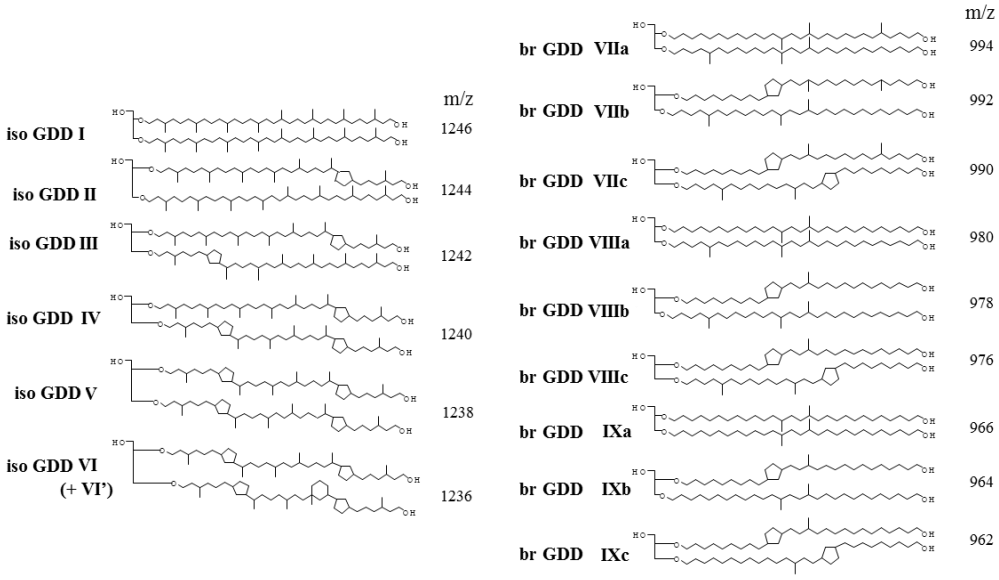

Figure 10 : Structures des alkanol diéthers de glycérol de type isopréniques (à gauche) et ramifiés (à droite) et leurs rapports m/z équivalents à leur masse molaire.

Les alkanol diéthers de glycérol isopréniques ont déjà été détectés sous forme de lipides intacts dans des échantillons naturels et dans une culture de *Nitrosopumilus maritimus* (Meador et al., 2014). Nous avons cependant détecté pour la première fois des dérivés de la forme intacte des alkanol diéthers de glycérol ramifiés le long de la carotte de Kyambangunguru, ce qui suggère que ces composés sont d'origine biosynthétique. Nous avons par ailleurs observé que la concentration en alkanol diéthers était corrélée à celle en tetraéthers pour chaque sous-famille de composés – les composés isopréniques de cœur et intacts et les composés ramifiés de cœur et intacts – dans l'ensemble des échantillons. De plus, l'abondance relative de chaque alkanol diéther est globalement corrélée à celle du tetraéther correspondant (Fig. 11). Nous avons cependant observé des paires où l'abondance relative en diéthers était plus grande que le tetraéthers correspondant (Fig. 12 c-d ; couple GDD/GDGT III et IV) ce qui est un argument supplémentaire pour une origine biosynthétique des alkanol diéthers.

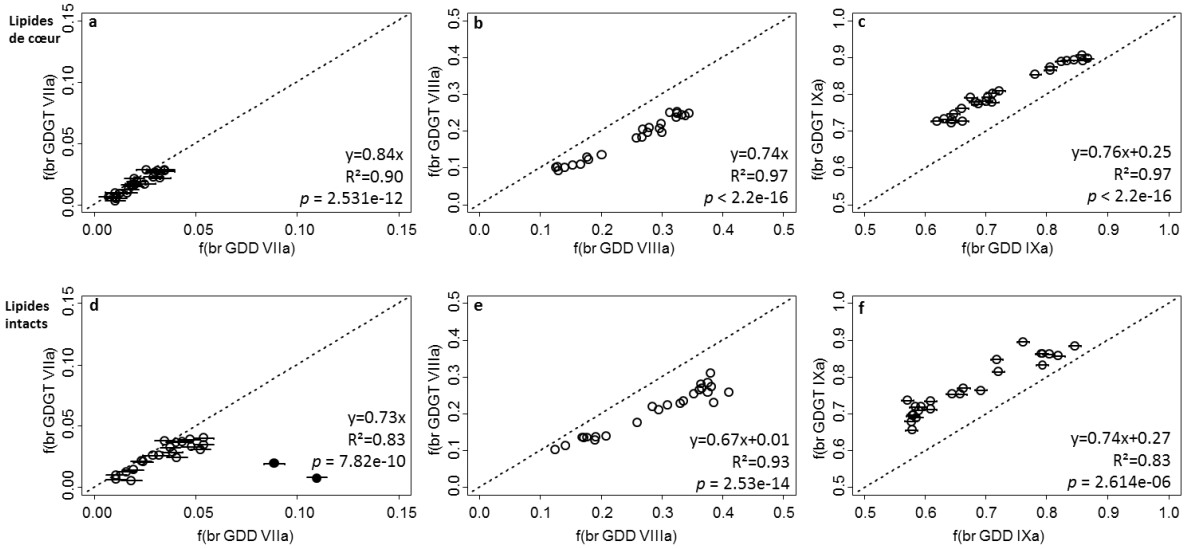

Figure 11 : Corrélation entre l'abondance relative de chaque alkanol diéther avec le tetraéther correspondant pour les composés d'origine bactérienne, sous forme de lipide de cœur (a-c) et lipide intact (d-f). La ligne 1:1 est représentée en pointillés

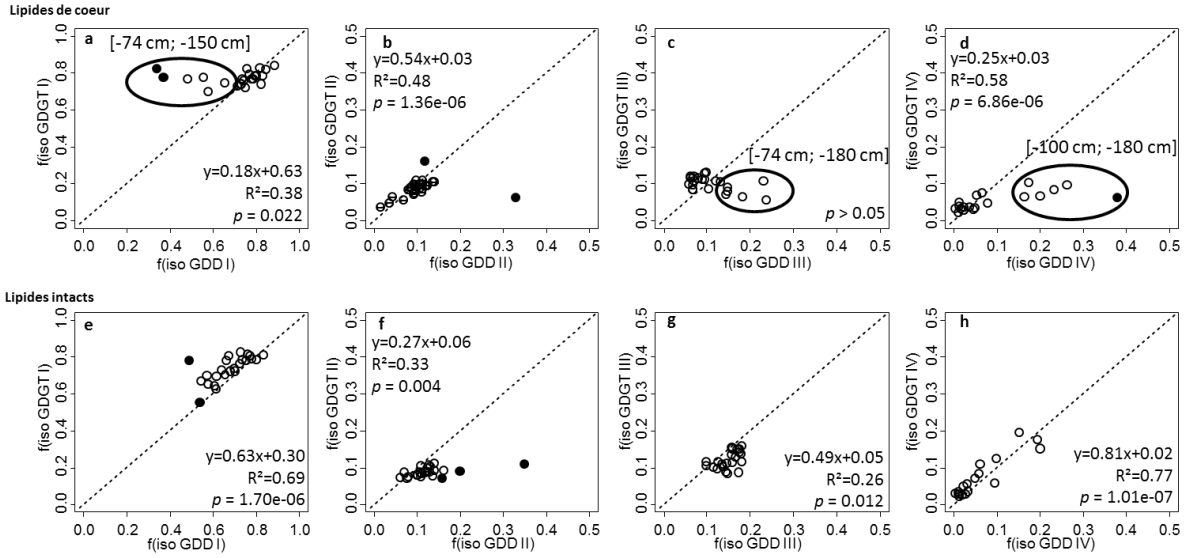

Figure 12 : Corrélation entre l'abondance relative de chaque alkanol diéther avec le tetraéther correspondant pour les composés d'origine bactérienne, sous forme de lipide de cœur (a-d) et lipide intact (e-h). La ligne 1:1 est représentée en pointillés.

3.2. Reconstruction multi-proxies des changements environnementaux des 4000 dernières années dans le marécage tourbeux de Kyambangunguru

La combinaison de marqueurs de végétations (macro- et micro-restes, pollens), de pH (tetraéthers ramifiés) et d'origine de la matière organique (C/N, palynofaciès) a permis de distinguer la succession de trois écosystèmes lors des 4000 dernières années à Kyambangunguru (Fig. 13) : une première phase lacustre de 4040 an BP à 2150 an BP avec le développement de micro (phytoplancton) et macro algues ainsi que de macrophytes flottants. Ces espèces disparaissent brutalement à 2150 an BP. Cette disparition est accompagnée (i) d'une augmentation du rapport C/N, (ii) d'une acidification du milieu d'après l'analyse des tetraéthers et (iii) de l'apparition de mycélium de champignons terrestres, ce qui indique le passage à un écosystème tourbeux qui persiste jusqu'à 860 an BP. La dernière phase correspond aux conditions actuelles, c'est-à-dire l'alternance d'un lac peu profond en saison des pluies et d'un marécage à zones tourbeuses en saison sèche. Cette dualité est visible dans la carotte où nous avons pu observer des marqueurs lacustres (restes phytoplanctoniques et de macrophytes flottants du genre *Nymphea*) et des marqueurs de tourbe/marécage (végétation caractéristique des zones tourbeuse comme les *Carex*).

En parallèle, l'analyse des tetraéthers ramifiés et du δ^2H_{wax} le long de la carotte a permis de reconstruire les variations climatiques en terme de température et de régime des pluies des 4000 dernières années (Fig. 13). Il apparaît que les variations de température ont été plus importantes que celles du régime des pluies avec une augmentation des températures d'environ 1 °C entre 2150 et 640 an BP (Fig. 13), synchrone à la transition d'un lac à une tourbière. Le régime des pluies, tel qu'enregistré par le δ^2H_{wax}, semble peu varier au cours des 4000 dernières années bien qu'un enrichissement en ^2H soit observé autour de 1500 an BP (Fig. 13) ce qui pourrait indiquer une saison sèche plus marquée. En conclusion, il semble que la transition d'un lac à une tourbière, observée il y a 2150 an BP dans le lac, soit principalement liée à une succession hydrosérale, c'est-à-dire à la colonisation naturelle et progressive d'un plan d'eau par des macrophytes conduisant à son étouffement. Cette colonisation a pu être favorisée par l'augmentation des températures à la même période entraînant une évaporation accrue à la surface du lac.

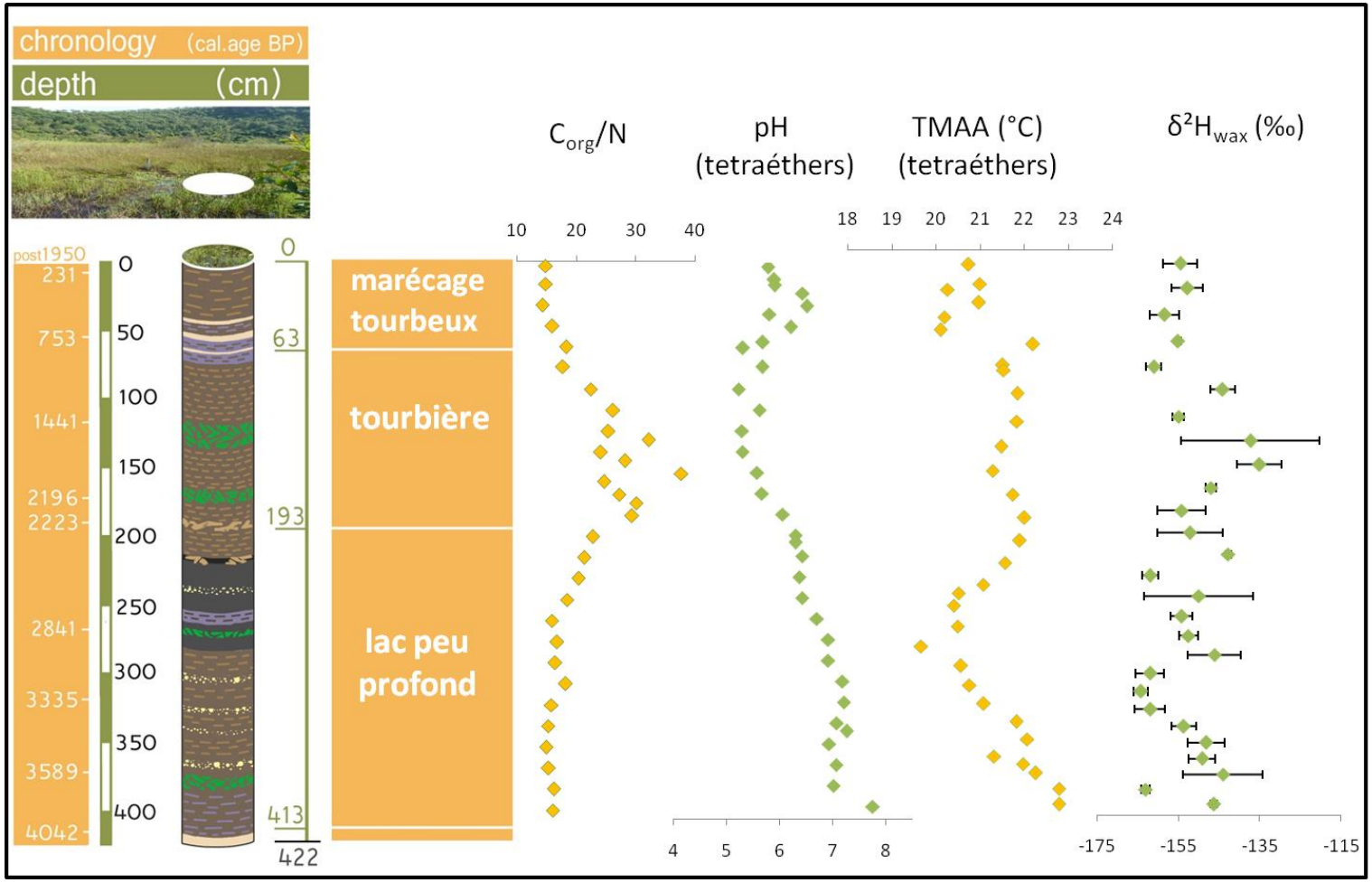

Figure 13 : L'évolution du rapport C/N et du pH (reconstruit à partir des tetraéthers ramifiés) ont permis de distinguer trois zones le long de la carotte. Les variations de température et d'humidité ont été reconstruites à partir des tetraéthers ramifiés et du δ^2H_{wax} respectivement.

Chapitre 4. Lac Masoko : origine des tetraéthers lacustres et reconstitution des variations climatiques de l'Holocène tardif

Le lac Masoko est un lac de cratère situé à 840 m d'altitude dans la province volcanique du Rungwe. Il a déjà fait l'objet de nombreuses études (Williamson et al., 1999 ; Delalande et al., 2005; de Mesmay, 2008), notamment des études paléoenvironnementales sur les 4000 dernières années (Barker et al., 2000; Thevenon et al., 2003; Vincens et al., 2003). Ces études ont observé de fortes variations du niveau du lac au cours de ces 4000 dernières années qui indiqueraient un régime des pluies instable au cours de l'Holocène tardif. Ils ont aussi noté une augmentation du nombre de feux de forêts (d'après l'étude des charbons fossilisés, Thevenon et al., 2003) et des pollens, Vincens et al., 2003). Cependant, l'Holocène tardif marque aussi la colonisation de la région par l'Homme, aussi cette augmentation des feux de forêt peut-elle avoir une origine climatique ou/et anthropique. Ce chapitre présente les premiers résultats de l'analyse des tetraéthers et des *n*-alcanes sur une carotte prélevée à Masoko en 2007 et couvrant la même période que les articles sus-cités (Holocène tardif, 4000 dernières années), l'objectif étant, en utilisant ces biomarqueurs, de déconvoluer le signal climatique du signal anthropique dans l'archive sédimentaire de Masoko.

4.1. Origine des tetraéthers ramifiés du lac Masoko et implications pour les reconstructions climatiques

Un piège à sédiments avec 3 profondeurs de collecte (5 m, 18 m et 33 m) a été installé au centre du lac Masoko en avril 2012 afin de suivre l'évolution de la distribution et de la concentration des tetraéthers ramifiés le long de la colonne d'eau. Des sols et sédiments au bord du lac ont aussi été échantillonnés afin de comparer leur concentration et distribution en tetraéthers ramifiés. En effet plusieurs études (e.g. Tierney and Russell, 2009; Blaga et al., 2010, 2009; Buckles et al., 2014) ont montré que selon les lacs, les tetraéthers ramifiés détectés dans le sédiment pouvait être produits (i) dans les sols du bassin versant ou/et (ii) dans la colonne d'eau. Cette multiplication des lieux de production complique l'utilisation des tetraéthers ramifiés comme marqueurs de température dans les lacs car, selon le lac, le signal analysé pourra être (i) essentiellement terrigène, (ii) essentiellement lacustre ou bien (iii) un mélange des deux ce qui biaisera la température reconstruite (dans les études sus-citées, un biais vers des températures plus froides qu'attendues a été observé). Des calibrations spécifiques aux lacs, mondiales (Pearson et al., 2011) et régionales (e.g. Zink et al., 2010 ;

Sun et al., 2011; Loomis et al., 2012) ont été établies pour prendre en compte l'effet de ces sources multiples sur les températures reconstruites.

A Masoko, la comparaison de la distribution en tetraéthers ramifiés (degré de méthylation moyen : MBT' ; degré de cyclisation moyen : CBT) dans les sols, sédiments bordant le lac et sédiments de surface au centre du lac (Fig. 14) montre que cette dernière est significativement ($p < 0.05$) différente dans les sédiments par rapport aux sols environnants. Par ailleurs les concentrations en tetaéthers ramifiés dans les sédiments est presque 10 fois plus importante que dans les sols (377.2 µg/g C_{org} vs. 49.0 µg/g C_{org}). Ces deux observations suggèrent que la majorité des tetraéthers ramifiés détectés dans le sédiment sont produits *in situ*, i.e. dans la colonne d'eau et/ou le sédiment. L'utilisation d'une calibration spécifique aux lacs tenant compte de cette production *in situ* est donc nécessaire pour reconstruire les TMAA à partir des tetraéthers ramifiés dans l'archive sédimentaire de Masoko (cf. paragraphe 4.2.)

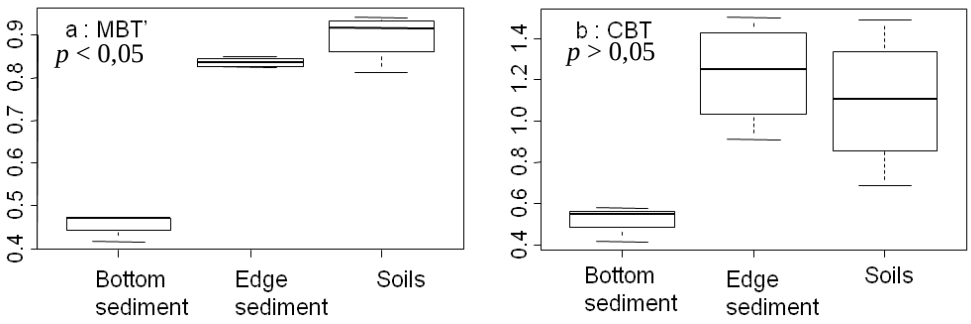

Figure 14 : Box plot de la comparaison des (a) MBT' et (b) CBT déterminés pour (i) les sédiments de surface au fond du lac (appelés *fond*), (ii) les sédiments de bord du lac (appelés *sédiment*) et (iii) les sols autour du lac (appelés *sol*).

Par ailleurs, nous avons pu effectuer un suivi temporel de la distribution des tetraéthers ramifiés le long de la colonne d'eau en collectant des échantillons dans des pièges à sédiments pendant 1,5 an (Fig. 15). Nous observons que les TMAA reconstruites à 5 m de profondeur sont différentes des TMAA reconstruites dans les sols et dans le sédiment de surface (au fond du lac), tandis que les TMAA reconstruites à 33 m de profondeur sont similaires à celles du sédiment de surface. Les TMAA reconstruites à 18 m, quant à elles, semblent intermédiaires entre celles reconstruites à 5 m et à 33 m. Ces résultats suggèrent que les tetraéthers ramifiés détectés dans l'archive sédimentaire du lac sont produits tout le long de la colonne d'eau.

Buckles et al. (2014) ont observé la même distribution des zones de production dans le Lac Challa situé sur les flancs du Mt. Kilimanjaro (Kenya).

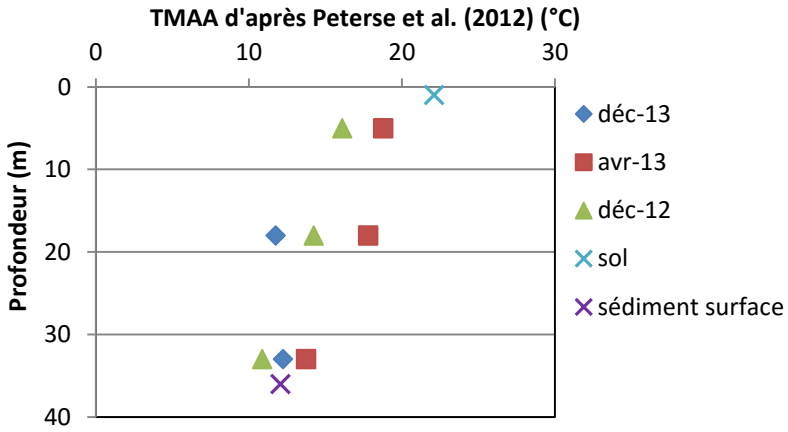

Figure 15 : Reconstruction des TMAA d'après la calibration globale des sols (Peterse et al., 2012) en fonction de la profondeur et comparaison avec les TMAA reconstruite dans les sols environnants et dans les sédiments de surface au fond du lac.

4.2. Reconstruction des changements environnementaux des 4000 dernières années

Les tetraéthers ramifiés et isopréniques ainsi que les *n*-alcanes ont été analysés le long d'une carotte sédimentaire de 2,70 m de long couvrant les 4000 dernières années. Nous ne disposons pas encore de modèle d'âge pour cette archive. Cependant la présence de deux tephras (couche de cendres volcaniques) à 2,70 m et de 1,20 à 0,80 m nous permet de borner cet enregistrement. En effet, l'analyse de précédentes carottes prélevées à Masoko (Barker and Gasse, 2003 ; Garcin et al., 2006) a montré que le tephra à 2,70 m s'est déposé il y a 4000 ans BP et celui entre 1,20 et 0,80 m, il y a 1100 ans BP.

Les températures de surface du lac et les TMAA reconstruites à partir des 10 premiers cm de sédiments de la carotte sont cohérentes avec les températures actuelles mesurées sur le site : température de surface reconstruite = 26 ± 0.4 °C, températures de surface mesurées = 28 °C ; TMAA reconstruite = 21 ± 0.4 °C, TMAA mesurées = 22.3 °C) ce qui confirme la fiabilité des tetraéthers pour reconstruire les températures de l'air et du lac. Les températures à la surface du lac, reconstruites à partir de tetraéthers isopréniques, montrent une tendance à l'augmentation depuis 4000 ans (Fig. 16a). Cependant les températures reconstruites dans la partie inférieure de la carotte (de 2,70 m à 1,20 m) sont très dispersées ce qui limite leur interprétation en terme de variations climatiques. Cette dispersion est peut-être liée à des processus physiques et/ou biologique de perturbation de la sédimentation (turbidites,

bioturbation) mais peut aussi être liée à une production, dans les sédiments profonds, de tetraéthers isopréniques.

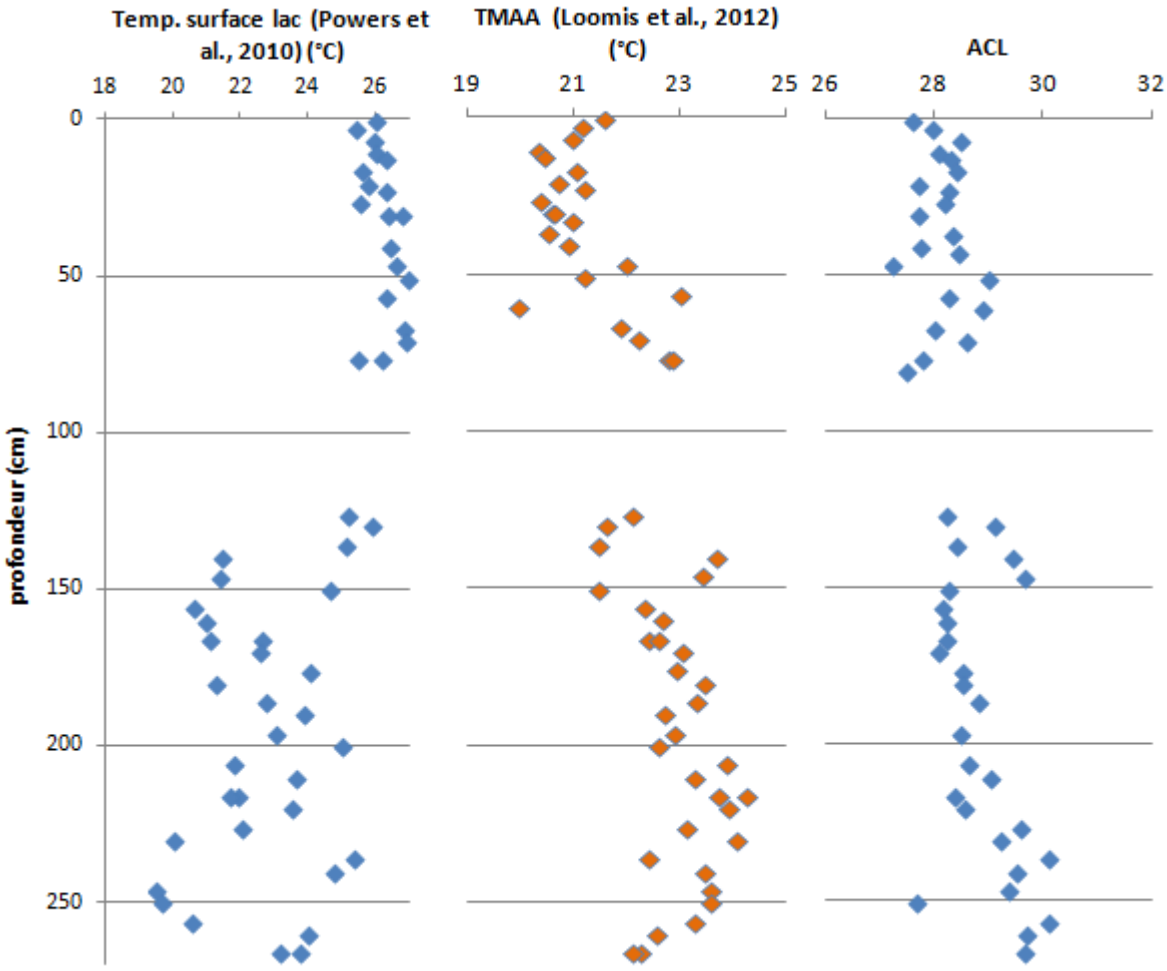

Figure 16 : Evolution des températures à la surface du lac reconstruites à partir des tetraéthers isopréniques (à gauche), des TMAA reconstruites à partir des tetraéthers ramifiés (milieu) et de l'ACL des n-alcanes le long de la carotte (à droite). La discontinuité entre 120 et 80 cm correspond à la couche de tephra non échantillonnée.

Les TMAA reconstruites le long de la carotte à partir des tetraéthers bactériens montrent une diminution relative de la température d'environ 2,5 °C de 2,50 m à 1,50 m suivie par une période plus chaude entre 1,20 m et 0,50 m (Fig. 16b). Les 50 derniers cm présentent des températures stables. L'évolution de la longueur moyenne de chaîne des *n*-alcanes (ACL ; Fig. 16c) montre une diminution de 30 à 28 dans la partie inférieure de la carotte (2,70 m à 1,20) qui peut-être lié à un remplacement des espèces herbacées du bassin versant par des arbres. Ce passage d'une végétation herbacée à une végétation boisée est caractéristique de conditions plus humides. Bien que nous ne disposions que de deux bornes

temporelles, cette reconstruction climatique préliminaire est cohérente avec (i) les variations observées dans la tourbière de Kyambangunguru (cf. Chapitre 3) et avec (ii) de précédentes études effectuées dans la région (Tierney et al., 2008; Powers et al., 2011; Sinninghe Damsté et al., 2012).

Ces résultats sont préliminaires à une étude plus détaillée de l'archive sédimentaire de Masoko. L'analyse élémentaire en C_{org} et N total ainsi que celle du rapport isotopique du carbone ($\delta^{13}C$) et de l'azote ($\delta^{15}N$) de la matière organique totale sont notamment en cours. Plusieurs échantillons de sédiment seront également datés au ^{14}C. L'ensemble de ces résultats seront comparés à ceux obtenus à partir de précédentes carottes sédimentaires prélevées à Masoko (Barker et al., 2000; Thevenon et al., 2003; Vincens et al., 2003). L'analyse d'autres biomarqueurs, notamment les diols à longues chaînes, pourra, quant à elle, préciser les variations de températures obtenues lors de cette étude préliminaire.

Conclusion

Cette étude a permis de valider l'applicabilité des biomarqueurs lipidiques, les alkyl tetraéthers de glycérol et les *n*-alcanes, en Afrique de l'Est, région clé pour la compréhension de la circulation atmosphérique mondiale. Nous avons montré que les alkyl tetraéthers de glycérol analysés dans des sols de surface de la région donnent un signal robuste et fiable de la température. Nous avons pu appliquer avec succès ces deux familles de biomarqueurs lipidiques à l'étude de deux archives continentales - une carotte de tourbe et une carotte de sédiment lacustre - permettant ainsi la reconstruction des changements climatiques (température et hydrologie) et environnementaux (notamment les changements de végétation) dans la région. Une hausse de la température, synchrones aux deux archives, il y a 1500 ans BP a été observée. De plus, le long de la carotte de tourbe, l'analyse de ces biomarqueurs, couplée à l'observation au microscope optique des macro- et micro-restes, a permis de reconstruire l'histoire écologique du site de Kyambangunguru, notamment sa conversion d'un lac peu profond à une tourbière. Des composés analogues aux tetraéthers, les alkanol diéthers de glycérol, ont été détectés le long de cette carotte et leur concentration et distribution suggèrent qu'ils soient des intermédiaires de biosynthèse des tetraéthers. L'étude de l'applicabilité du rapport isotopique de l'hydrogène dans les *n*-alcanes (δ^2H_{wax}) comme marqueur de température le long de 2 monts est-africains a cependant montré que ce dernier pouvait également être influencé par d'autres facteurs, d'origine climatique et/ou biologique, compliquant son utilisation à l'échelle régionale. Au final, les résultats obtenus au cours de cette thèse montrent que les alkyl tetraéthers de glycérol et les *n*-alcanes sont des outils très prometteurs pour la reconstruction des changements environnementaux, mais que l'obtention de résultats fiables nécessitent l'utilisation de marqueurs complémentaires à ces derniers dans le cadre d'approches multi-proxies.

List of Figures:

List of Tables:

Validation et application de biomarqueurs lipidiques pour la reconstruction des changements environnementaux en Afrique de l'Est

Résumé :

La Province Volcanique du Rungwe (PVR) en Afrique de l'Est abrite diverses archives continentales (séquence de loess-paléosols, tourbières, lacs) permettant d'étudier les changements environnementaux passés des zones tropicales continentales. Ce travail s'est intéressé à l'applicabilité des alkyl tetraéthers de glycérol (tetraéthers) et des *n*-alcanes comme biomarqueurs de ces changements passés. Leur analyse le long de transects altitudinaux a permis de rendre compte de la capacité des tetraéthers à enregistrer de faibles changements de température de l'air dans la région. En conséquence, une calibration régionale a été établie afin d'améliorer les reconstructions de température de l'air en Afrique de l'Est. Au contraire, il est apparu que la composition isotopique de l'hydrogène des *n*-alcanes (δ^2H_{wax}) était impactée par des paramètres physiques et biologiques supplémentaires ce qui complique son utilisation pour suivre les changements de température à l'échelle régionale. L'étude des variations de ces deux biomarqueurs le long d'une carotte de tourbe et d'une carotte de sédiment lacustre prélevées dans la PVR a révélé l'existence synchrone d'une période climatique plus chaude au cours de l'Holocène tardif. Par ailleurs, il a été observé dans la carotte de tourbe une transition d'un lac à une tourbière il y a ca. 2000 ans BP. Le présent travail démontre donc que les tetraéthers et les *n*-alcanes sont des biomarqueurs prometteurs, notamment parce qu'ils sont sensibles à de faibles variation climatiques ; cependant, afin de les interpréter correctement, il est nécessaire d'adopter une approche multi-marqueurs.

Mots clés : Tropiques, Afrique de l'Est, alkyl tetraéthers de glycérol (tetraéthers), *n*-alkanes, δ^2H_{wax}, Holocène tardif, transects altitudinaux, tourbière, lac.

Validation and application of lipid biomarkers to reconstruct environmental changes in East Africa

Abstract :

The Rungwe Volcanic Province (RVP) in East Africa offers a wide diversity of continental archives (loess-paleosols sequences, peatlands, lakes), allowing the investigation of past environmental changes in tropical continents. This work focused on the validation of glycerol dialkyl glycerol tetraether- (GDGT) and *n*-alkane-derived proxies. Analyses of these two biomarkers along altitudinal transects allowed assessing their ability to record temperature changes in the region. GDGTs were found to be robust temperature proxies in East Africa, and a regional calibration was established to improve temperature reconstructions from soil archives. In contrast, investigation of *n*-alkane hydrogen isotopic composition (δ^2H_{wax}) in surface soils revealed that its variations seemed to be impacted by additional biological and physical parameters than temperature, preventing its generalization at a regional scale. Application of GDGT and *n*-alkane proxies to continental archives revealed past environmental changes over the Late Holocene in the RVP. A late Holocene synchronous temperature maximum was especially observed in a peat core and sediment core from two sites of the RVP. A multi-proxy approach was applied to the peat core, revealing that an ecosystem change from a lake to a peatland occurred ca. 2000 yrs BP ago. The present work showed that GDGTs and *n*-alkanes are promising biomarkers because of their sensitivity to slight climate variations, but that they need to be combined with other proxies to accurately reconstruct environmental changes.

Keywords: Tropics, East Africa, glycerol dialkyl glycerol tetraethers (GDGTs), *n*-alkanes, δ^2H_{wax}, Late Holocene, altitudinal transects, peatland, lake.